



University of Zagreb
FACULTY OF SCIENCE
DEPARTMENT OF BIOLOGY

Marija Pinterić

**THE ROLE OF SIRTUIN 3 PROTEIN IN
ESTROGEN-MEDIATED CELL
RESPONSE MECHANISMS IN
PHYSIOLOGICAL AND
PATHOPHYSIOLOGICAL CONDITIONS**

DOCTORAL DISSERTATION

Zagreb, 2021



Sveučilište u Zagrebu

PRIRODOSLOVNO-MATEMATIČKI FAKULTET

BIOLOŠKI ODSJEK

Marija Pinterić

**ULOGA PROTEINA SIRTUINA 3 U
MEHANIZMIMA STANIČNOG
ODGOVORA KOJI SU POSREDOVANI
ESTROGENOM U FIZIOLOŠKIM I
PATO FIZIOLOŠKIM UVJETIMA**

DOKTORSKI RAD

Zagreb, 2021

The work presented in this doctoral thesis was performed at Ruđer Bošković Institute, Zagreb, Croatia under the supervision of senior scientist Tihomir Balog, PhD, as a part of the postgraduate doctoral programme in Biology at the Department of Biology, Faculty of Science, University of Zagreb.

Ovaj je doktorski rad izrađen u Institutu Ruđer Bošković, Zagreb, Hrvatska, pod vodstvom dr. sc. Tihomira Baloga, znanstvenog savjetnika u trajnom zvanju, u sklopu Sveučilišnog poslijediplomskog dokorskog studija Biologije pri Biološkom odsjeku Prirodoslovno-matematičkog fakulteta Sveučilišta u Zagrebu.

Supervisor curriculum vitae

Tihomir Balog, PhD

EDUCATION:

1999. PhD in the field of pharmacy, Faculty of Pharmacy and Biochemistry, University of Zagreb

1996. Mr.sc. in the field of biology and immunology, Faculty of Science, University of Zagreb

1990. Dipl.ing. medical biochemistry, Faculty of Pharmacy and Biochemistry, University of Zagreb

EMPLOYMENT

2016- now Head of the Department of Molecular Medicine of the RBI,

2012- now Head of the Laboratory for Mitochondrial Bioenergetics and Diabetes, ZMM, RBI

2006-2012: Senior Research Associate ZMM, RBI

2003-2006: Research Associate ZMM, RBI

1999-2003: Postdoctoral Researcher ZMM, RBI

1992-1999: Research Fellow, Department of Experimental Biology and Medicine, RBI

PROJECTS:

2015.-2020. Project supported by Croatian Science Foundation HRZZ No 4533 "Sirtuin3 as a mediator of mitochondrial function in estrogen-dependent resistance to hyperoxia and high-fat diet", project PI

2016.-2018. EU-Operational Program Cohesion Competitiveness, IRI-Project „Cedevita Healthy OTG“, project PI

2011.-2013. Project supported by Ministry of science RH "Cytochrome P 450 monooxygenase and tumor appearance in aging and oxidative stress " project PI

1998.-2000. Project supported by Ministry of Science RH "Binding of enkephalin to human neutrophils and modulation of their functions", project PI.

SUPERVISION OF DOCTORAL STUDENTS: From 2009 to 2021 under his supervision three PhD students defended their doctoral thesis.

TEACHING:

2009- University of Rijeka, Biotechnology and Pharmaceutical Research, undergraduate study, associate prof

1997-2008: University of Zagreb, Faculty of Science, postgraduate study

1997-2008: University of Zagreb, School of Medicine, postgraduate study

MEMBERSHIP IN SCIENCE ORGANIZATIONS AND ORGANIZATIONAL SKILLS

Member of national and international scientific organizations and member of the scientific and organizing committee of eleven congress meetings.

SCIENTIFIC ACHIEVEMENTS:

63 peer-reviewed original scientific publications; total citation according to Scopus/WoS of all published papers is 820, h-index is 13; the average IF of published papers is 3.2;

Reviewer in four scientific journals; Reviewer of competitive scientific projects, etc.

Acknowledgements

First and foremost, thanks to my Lab, the best lab in the world, Laboratory for mitochondrial bioenergetics and diabetes, for being there for me in this important phase of my life. To dr.sc Sandra Sobočanec and dr.sc. Iva Škrinjar, thank you for your guidance, patience and help. With your professional and friendly advice, you have made the challenges of this doctorate easier to overcome. Thank you to dr.sc. Marijana Popović-Hadžija for all the assistance in developing new methods - you are the most patient person in the world. You are the one who could always calm me down, cheer me up and encourage me to continue with my work. To Iva Pešun Međimorec, our lab manager, thank you for everything you have taught me, for your organization and calmness during these years. Without you, all of this would be impossible. To Marina Marš, thank you for your support, for driving me to work and for listening to me early in the morning. Finally, to my mentor, dr. sc. Tihomir Balog, thank you for your support, guidance and help.

Special thanks to “my morning coffee family” for starting every day with a smile on my face and ready for new challenges. To Marija Mioč and Lea Vidatić, thank you for your advice, support, help and for listening when it was hard. To our new lab member and colleague, dr.sc. Mladen Paradžik, thank you for teaching me flow cytometry and help with the project. To dr.sc. Ana Tadijan, thank you for all your support and collaboration. To dr.sc. Vedrana Filić Mileta and dr.sc. Maja Marinović, thank you for all the hours we spent on the confocal microscope.

To all the students that passed through our lab for the past four years: Grazia Malovan, Denis Pleše, Ivan Ciganek, Dora Marčinko, Ivana Kučar, thank you for choosing us and being part of our lab and for all the good moments we shared.

To all of my colleagues from the Division of Molecular Medicine and the Division of Molecular Biology, thanks for all the support, experiment counselling and help.

Special thanks to Kristina, a longtime colleague and a great friend, for being there for me from the day one of university. Everything went easier with you by my side and together we went through some of the most difficult periods in life.

To my girls from Rijeka, MMA, MMe, Vedrana, and Kiki, thank you for all your love and support.

Finally, special thanks to my family, for unconditional love and support.

Ivan, thank you for sharing this journey with me, love you.

Looking forward to the next chapter of my life.

**THE ROLE OF SIRTUIN 3 PROTEIN IN ESTROGEN-MEDIATED CELL
RESPONSE MECHANISMS IN PHYSIOLOGICAL AND PATHOPHYSIOLOGICAL
CONDITIONS**

Marija Pinterić

Ruđer Bošković Institute, Bijenička cesta 54, Zagreb, Croatia

The relationship between Sirtuin 3 (Sirt3) and estrogen (E2) in physiological and pathophysiological conditions was studied using pharmacological, dietary and genetic approaches *in vitro* and *in vivo*. This thesis shows that both Sirt3 and hyperoxia act as a tumor-suppressors of MCF-7 breast cancer cells' malignant properties, which is observed through their reduced proliferation, survival and mitochondrial dysfunction. Furthermore, Sirt3 negatively affects the proliferative effect of E2 causing the reduction of cells' response to E2. Additionally, it affects p53 by disrupting the ER α -p53 interaction, inhibits cells' clonogenic capacity and lowers their migration capacity. The studies on Sirt3 WT and KO male and female mice upon high-fat diet (HFD) show sex-specific effects of HFD through reduced Sirt3 expression only in male WT mice, alleviated lipid accumulation and reduced glucose uptake in male KO mice, pointing towards a higher reliance of males on the protective effect of Sirt3 against HFD-induced metabolic dysregulation. Moreover, HFD in combination with ovariectomy and Sirt3 depletion increases body weight gain, impairs the response of an antioxidative system, upregulates the expression of oxidative stress-inducing genes, making these females more prone to NAFLD. Overall, studies on mice highlight the importance of preclinical biomedical research on both sexes and the influence of sex hormones and Sirt3 on metabolic homeostasis.

(40 pages, 3 figures, 164 references, original in English)

Keywords: Sirtuin 3, estrogen, MCF-7 breast cancer cells, hyperoxia, mice, high-fat diet, sex differences

Supervisor: Tihomir Balog, PhD

Reviewers: Maja Herak Bosnar, PhD

Bato Korać, PhD

Domagoj Đikić, PhD

**ULOGA PROTEINA SIRTUINA 3 U MEHANIZMIMA STANIČNOG ODGOVORA
KOJI SU POSREDOVANI ESTROGENOM U FIZIOLOŠKIM I
PATOLOGIJSKIM UVJETIMA**

Marija Pinterić

Institut Ruđer Bošković, Bijenička cesta 54, Zagreb, Hrvatska

Za istraživanje povezanosti Sirtuina 3 (Sirt3) i estrogena (E2) u fiziološkim i patofiziološkim uvjetima korišteni su farmakološki, prehrambeni i genetički pristupi na *in vitro* i *in vivo* modelima. U ovom doktorskom radu pokazano je da Sirt3 i hiperoksija djeluju kao tumorski supresori malignih svojstava stanica raka dojke MCF-7, smanjujući njihovu proliferaciju i preživljenje te potičući ekspresiju glavnog tumorskog supresorskog proteina p53 i mitohondrijsku disfunkciju. Nadalje, Sirt3 negativno djeluje na proliferativni učinak E2 uzrokujući smanjenje odgovora stanica na E2, utječe na p53 narušavajući interakciju ER α -p53 te smanjuje sposobnost formiranja kolonija i migraciju. Istraživanja na muškim i ženskim Sirt3 WT i KO miševima pokazuju spolne razlike u utjecaju prehrane s visokim udjelom masti (engl. *high-fat diet*, HFD) koja, za razliku od ženki, uzrokuje smanjenu ekspresiju Sirt3 samo u mužjaka WT, dok u mužjaka KO rezultira smanjenim unosom glukoze u jetru i posljedično manjim nakupljanjem lipida. Navedeni rezultati ukazuju na veću ovisnost mužjaka o zaštitnom učinku Sirt3 protiv metaboličke disregulacije izazvane HFD-om. Nadalje, HFD u kombinaciji s ovarijektomijom i nedostatkom Sirt3 povećava prirast tjelesne težine, oslabljuje odgovor antioksidativnog sustava te povećava ekspresiju gena koji izazivaju oksidativni stres, ukazujući na zaštitni učinak ženskih spolnih hormona i Sirt3. Sveukupno, istraživanja na miševima ističu važnost pretkliničkih biomedicinskih istraživanja na oba spola te ukazuju na značaj spolnih hormona i Sirt3 u održavanju metaboličke homeostaze.

(40 stranica, 3 slike, 164 literaturnih navoda, jezik izvornika: engleski)

Ključne riječi: Sirtuin 3, estrogen, stanice raka dojke MCF-7, hiperoksija, miševi, prehrana s visokim udjelom masti, spolne razlike

Mentor: Dr.sc. Tihomir Balog

Ocjenjivači: Dr.sc. Maja Herak Bosnar

Dr.sc. Bato Korać

Dr.sc. Domagoj Đikić

Sažetak

Sirt3 je glavna mitohondrijska deacetilaza ovisna o NAD^+ , koja regulira mnoge stanične procese, uključujući glavne metaboličke puteve i proizvodnju energije. Sirt3 učinkovito balansira između pretvorbe stanične energije i neželjenih nuspojava mitohondrijskih procesa, poput stvaranja reaktivnih kisikovih vrsta. Estrogen je ženski steroidni hormon koji regulira rast, diferencijaciju i funkciju velikog broja ciljanih tkiva u ljudskom tijelu. Također, estrogen koordinira i integrira stanični metabolizam i aktivnost mitohondrija izravnim i neizravnim mehanizmima posredovanim diferencijalnom ekspresijom i smještajem estrogenskih receptora (ER) ovisno o vrsti stanice.

Iako estrogen ima citoprotektivnu ulogu u uvjetima oksidativnog i metaboličkog stresa, ima i štetan učinak u nekim patološkim stanjima, poput raka dojke. Rak dojke je najčešći rak među ženama, a 70% svih oblika raka dojke pozitivno je na ER. Dosadašnja istraživanja pokazala su da je niska ekspresija proteina Sirt3 povezana sa smanjenim preživljavanjem kod svih vrsta raka dojke, ističući njegovu ulogu biomarkera i potencijalne terapijske molekule. Međutim, točan mehanizam njegova djelovanja još nije razjašnjen. Više od desetljeća hiperoksija (izlaganje visokoj koncentraciji kisika) se koristi kao uspješno liječenje niza bolesti i stanja čija je zajednička značajka nedostatak kisika, odnosno hipoksija. Cilj ovog doktorskog rada bio je razjasniti ulogu proteina Sirt3 u stanicama raka dojke MCF-7, kao potencijalne farmakološke molekule od interesa, u uvjetima oksidativnog stresa uzrokovanog hiperoksijom. Osim toga, cilj je bio pokazati mehanizme utjecaja Sirt3 na proliferacijsku ulogu estrogena u ovom patofiziološkom stanju.

U ovom doktorskome radu pokazano je da Sirt3 i hiperoksija djeluju kao tumorski supresori malignih svojstava stanica raka dojke MCF-7, smanjujući njihovu proliferaciju i preživljavanje te potičući ekspresiju glavnog tumorskog supresorskog proteina p53 i mitohondrijsku disfunkciju. Nadalje, Sirt3 negativno djeluje na proliferativni učinak estrogena uzrokujući smanjenje odgovora stanica na estrogen, utječe na p53 narušavajući interakciju $\text{ER}\alpha$ -p53 te smanjuje sposobnost formiranja kolonija i migraciju. Stoga, ova disertacija pokazuje da Sirtuin 3 i hiperoksija, osobito u kombinaciji, imaju potencijal negativno modulirati tumorska svojstva stanica raka dojke pozitivnih na ER i proliferativni učinak estrogena, što bi se trebalo dodatno istražiti *in vitro*, a osobito *in vivo*, kao potencijalnu terapiju u liječenju raka dojke ovisnih o estrogenu.

U današnje vrijeme neuravnotežena prehrana bogata mastima u kombinaciji sa sjedilačkim načinom života dovodi do pretilosti i metaboličkog sindroma, što pridonosi razvoju kroničnih bolesti, dijabetesa tipa 2, kardiovaskularnih bolesti i raka. Ženski spolni hormoni, naročito estrogen, imaju ključnu ulogu u regulaciji metabolizma, unosa hrane i tjelesne težine kod žena. Nadalje, učestalost metaboličkih poremećaja dramatično raste nakon menopauze što ukazuje na značajan utjecaj ženskih spolnih hormona na raspodjelu masnog tkiva i učestalost metaboličkog sindroma. Sirt3 regulira metabolizam nutrijenata, ravnotežu ATP-a, antioksidativnog sustava i ostalih mehanizama ključnih za mitohondrije i homeostazu stanice. Nadalje, i Sirt3 i estrogen imaju dobro utvrđenu ulogu u zaštiti od metaboličke disfunkcije. Postoje izražene spolne razlike u osjetljivosti na metabolički stres koji prethodi pretilosti i razvoju metaboličkog sindroma, a opisane su i kod miševa i kod ljudi te ističu važnost takvih istraživanja na oba spola. Unatoč opsežnim istraživanjima o Sirt3 i estrogenu pojedinačno, veza između estrogena i Sirt3 u odgovoru na metabolički stres uzrokovan prehranom sa visokim udjelom masti (engl. *high-fat diet*, HFD) još nije dokazana. Cilj ove doktorske disertacije bio je pojašnjenje uloge Sirt3 i estrogena u miševa oba spola hranjenih HFD-om.

U ovom doktorskom radu pokazano je da nutritivni stres u obliku HFD-a, za razliku od ženki, smanjuje ekspresiju proteina Sirt3 u mužjaka WT, dok u mužjaka KO rezultira smanjenim unosom glukoze u jetru i posljedično manjim nakupljanjem lipida. Navedeni rezultati ukazuju na veću ovisnost mužjaka o zaštitnom učinku Sirt3 protiv metaboličke disregulacije izazvane HFD-om. Ženke imaju veću ekspresiju gena uključenih u homeostazu lipida, a HFD ili nedostatak proteina Sirt3 ugrožava mitohondrijsku respiraciju i povećava oksidativno oštećenje proteina. Ovarijsktomija kod ženki WT rezultira povećanom ekspresijom Sirt3 koja je popraćena održavanjem mitohondrijske funkcije i smanjenom razinom lipidnih hidroperoksida, dok kombinacija ovarijsktomije i nedostatka Sirt3 dovodi do poremećaja u metabolizmu lipida i povećanog oksidativnog oštećenja lipida. HFD u kombinaciji s ovarijsktomijom i nedostatkom Sirt3 uzrokuje povećanje tjelesne težine, oslabljuje odgovor antioksidativnog sustava i povećava ekspresiju gena koji izazivaju oksidativni stres i oštećenja jetre čineći ovarijsktomizirane ženke KO sklonije razvoju metaboličkog sindroma. Sveukupno, istraživanja na miševima pridonose karakterizaciji spolnih razlika u razvoju metaboličkih bolesti i ističu važnost prekliničkih biomedicinskih istraživanja na oba spola te ukazuju na značaj spolnih hormona i Sirt3 u održavanju metaboličke homeostaze.

Table of contents

INTRODUCTION	1
Sirtuin family	1
Sirtuin 3	2
Mitochondria and Sirtuin 3	4
Estrogen	6
Sirtuin 3, estrogen and breast cancer	8
Sirtuin 3 and estrogen in metabolism.....	10
Research problem and scope of the thesis	12
LIST OF PUBLICATIONS	14
DISCUSSION	15
Tumor-suppressive effect of Sirtuin 3 in MCF-7 breast cancer cells is enhanced upon hyperoxic treatment and mediated by the attenuated response to estrogen.....	15
Relationship of sex and Sirtuin 3 in response to high-fat diet in 129S mice.....	19
CONCLUSIONS	24
REFERENCES	26
CURRICULUM VITAE.....	40

INTRODUCTION

Sirtuin family

Sirtuins are evolutionarily conserved nicotinamide adenine dinucleotide (NAD⁺)-dependent lysine deacetylases or ADP-ribosyltransferases. The mammalian sirtuin (Sirt) family consists of seven members, Sirt1–7, that differ in their subcellular localization (Figure 1)¹. The first identified Sirt, *SIR2* from *Saccharomyces cerevisiae*, was originally named *MAR1* (for mating-type regulator 1) since a mutation in this gene caused sterility by relieving silencing at the mating-type loci HMR and HML². The name “sirtuin” (from Silent Information Regulator) came after the discovery of additional genes with the same features, putting MAR nomenclature behind³. *SIR2* homologs have been found in organisms ranging from bacteria to plants and mammals, demonstrating that *SIR2* is a member of a large and ancient family of genes we now refer to as ‘sirtuins’. Almost all of the mammalian sirtuins have now been described and their functions ascribed⁴, while their biological roles are intensively studied.

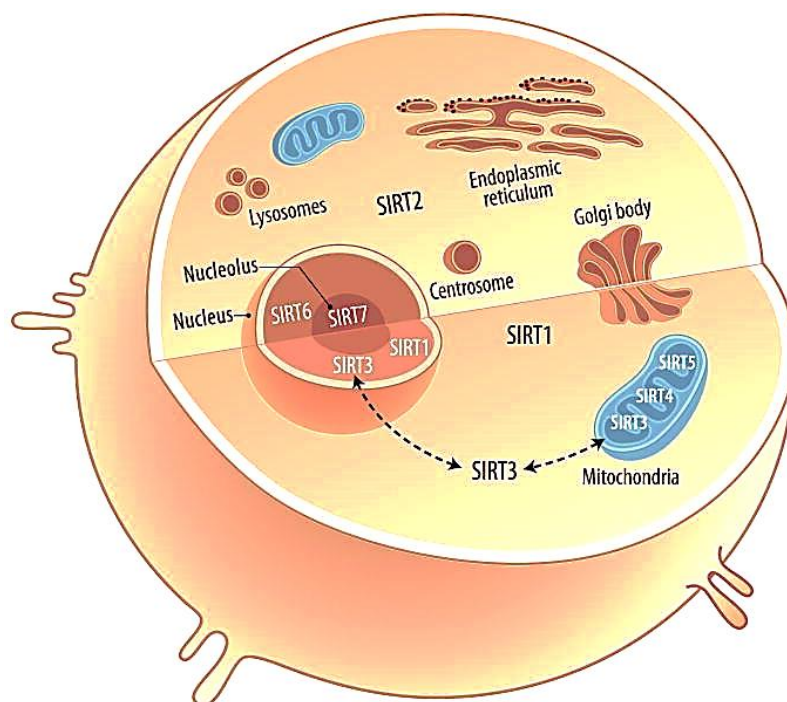


Figure 1. Sirtuins’ subcellular localization. Sirt1 is predominantly located in the nucleus, and also in the cytoplasm. Sirt2 is localized in the cytosol. Sirt3, Sirt4, and Sirt5 are mitochondrial sirtuins, but Sirt3 may also be found in the nucleus and cytoplasm under different cellular events. Sirt6 and Sirt7 are localized in the nucleus and nucleolus, respectively. Adapted from⁵.

Sirtuins are members of the class III deacetylases that differ in subcellular localization, enzymatic activity and targets¹. Sirt1, Sirt6 and Sirt7 are predominately in the nucleus, Sirt2 resides in the cytoplasm, and Sirt3, Sirt4 and Sirt5 have been described as mitochondrial sirtuins⁴. Sirtuins are protein deacetylases and ADP-ribosyltransferases that couple the deacetylation of lysine to the hydrolysis of NAD⁺ by transferring the acetyl group to the ADP-ribose moiety to form O-acetyl-ADP-ribose, releasing free nicotinamide⁶. All sirtuins possess a conserved catalytic NAD⁺-binding domain, consisting of about 275 amino acids, which is flanked by the N- and C-terminal sequences of variable lengths⁷. Although the sirtuins were originally thought to mainly catalyse lysine deacetylation⁸, more recent studies have revealed a much broader range of activities, including several different lysine deacetylation reactions⁹, removal of lipid modifications¹⁰ and ADP-ribosylation¹¹. These protein modifications are significant additional layers that can drastically affect the target protein function; therefore, both the expression and the activity of sirtuins themselves need to be regulated. The requirement for NAD⁺ as a co-substrate suggests that the sirtuins might have evolved as sensors of cellular energy and redox states coupled with the metabolic status of the cell. Additionally, the sirtuins are extensively regulated by numerous other mechanisms, including transcriptional and post-transcriptional regulation of expression⁴. They play an important role in the regulation of cellular homeostasis, in particular metabolism¹², inflammation¹³, oxidative stress¹⁴, and senescence¹⁵. Dysregulation of sirtuins by metabolic stress induced by overfeeding and an unhealthy diet can take part in the pathogenesis of metabolic diseases by disrupting the basic metabolic pathways and by compromising the defence against oxidative stress¹⁶.

Sirtuin 3

Sirtuin 3 (Sirt3) is a major mitochondrial NAD⁺ dependent deacetylase¹⁷, with a fundamental role in maintaining mitochondrial and cellular homeostasis. Sirt3 is first expressed in the cytoplasm as a 399-amino acid (44 kDa) inactive precursor, subsequently targeted to the mitochondria, where it is cleaved at the N-terminus by the mitochondrial matrix processing peptidase protein (MPP) to generate a mature 28 kDa protein (Figure 2)¹⁷. It is the only member of the Sirt family linked to longevity in humans¹⁸. In addition, Sirt3 modulates important cellular functions, such as nutrient metabolism, ATP balance, reactive oxygen species (ROS) generation and antioxidant machinery, as well as other mechanisms fundamental to mitochondria¹⁹.

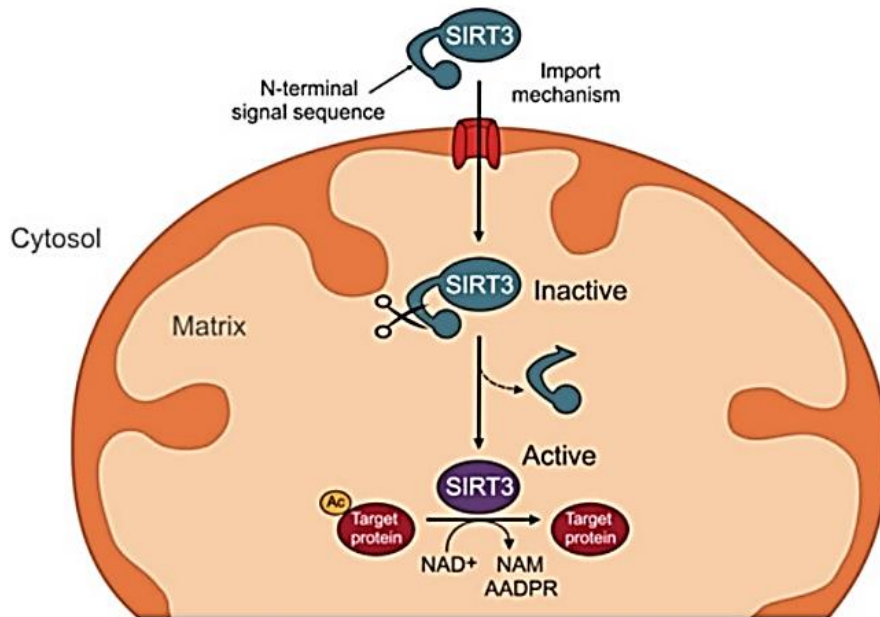


Figure 2. Sirtuin 3 processing. Sirt3 is encoded by the nuclear genome and translated in the cytoplasm as a longer, enzymatically inactive precursor (44 kDa) that is imported into the mitochondrial matrix by an N-terminal targeting sequence. Following the import, the targeting sequence is cleaved by a mitochondrial protein peptidase (MMP) forming the enzymatically active protein (28 kDa). Adapted from²⁰.

Although Sirt4 and Sirt5 are also present in the mitochondria, Sirt3 is considered the main mitochondrial deacetylase because only Sirt3 KO mice show hyperacetylation of mitochondrial proteins²¹. Localized in the mitochondrial matrix, Sirt3 is involved in the regulation of all mitochondrial functions, including the tricarboxylic acid (TCA), the urea cycle, amino acid metabolism, fatty acid oxidation (FAO), oxidative phosphorylation (OXPHOS), ROS detoxification, mitochondrial dynamics and the mitochondrial unfolded protein response (UPR)²². Sirt3 is highly expressed in tissues with high metabolic demands such as heart, liver, kidney, brain, brown adipose tissue, and skeletal muscles²³. This suggests that Sirt3 has an important role in maintaining mitochondrial homeostasis in these metabolically demanding tissues that are also more exposed to stress conditions, where modulation of Sirt3 expression and activity contributes to maintaining cellular and mitochondrial function upon stress exposure. Given the crucial role in mitochondria, Sirt3 has been implicated in the regulation of aging, neurodegeneration, cardiovascular diseases, liver and kidney diseases, cancer and other metabolic diseases.

Mitochondria and Sirtuin 3

Mitochondria are cellular organelles of proteobacterial origin that carry out a range of core metabolic processes and are involved in the regulation of apoptosis and the process of ageing. They have a small genome in the form of mitochondrial DNA (mtDNA) encoding only a few of the mitochondrial proteins, specifically, 13 in humans. These mtDNA-encoded proteins are key parts of the OXPHOS complexes, but the majority of them, more than 1,000 are encoded in the nucleus and need to be imported into mitochondria after translation in the cytosol. This is the reason why the mitochondrial gene expression system needs to interconnect with the cell nucleus and cytosol to ensure mitochondrial function²⁴.

Mitochondria are involved in all aspects of cell metabolism (TCA cycle, β -oxidation of fatty acids, but also in producing fatty acids, amino acids, nucleotides, etc.) and Sirt3 coordinates changes in nutrient metabolism by regulating the activity of diverse enzymes involved in these distinct metabolic pathways. In carbohydrate metabolism, Sirt3 deacetylates and inactivates cyclophilin D (CyP-D), resulting in the dissociation of hexokinase 2 (HK2) from the mitochondrial outer membrane and the subsequent inhibition of glycolysis²⁵. Sirt3 can also block the malate-aspartate shuttle by inhibiting glutamate oxaloacetate transaminase 2 (GOT2)²⁶. Acetyl-CoA is a primary entry point in the TCA cycle and Sirt3 can deacetylate and activate acetyl-CoA synthetase 2 (AceCS2)²⁷ but also increase acetyl-CoA levels by deacetylating the upstream enzymes responsible for activating the pyruvate dehydrogenase complex (PDC)²⁸. In addition, as mentioned above, it accelerates the oxidation of isocitrate by targeting isocitrate dehydrogenase 2 (IDH2)²⁹ and coordinates the TCA cycle and the electron transport chain (ETC) by activating complex II e.g., the flavoprotein subunit of succinate dehydrogenase (SDH)^{30,31}. Sirt3 participates in amino acid metabolism by increasing the enzymatic activity of glutamate dehydrogenase (GDH)³², a key enzyme involved in amino acid oxidation, and in the urea cycle by deacetylating ornithine transcarbamylase (OTC), thereby increasing urea cycle flux during energy restriction³³. Finally, Sirt3 accelerates the process of FAO by modulating the activity of long-chain acyl-CoA dehydrogenase (LCAD)³⁴ and also enhances the enzymatic activity of 3-hydroxy-3-methylglutaryl CoA synthase 2 (HMGCS2) to promote the synthesis of the ketone body, β -hydroxybutyrate³⁵. By regulating the activity of these enzymes involved in various metabolic pathways that occur in mitochondria, Sirt3 orchestrates global shifts in nutrient metabolism under physiological conditions, with potential implications in disease, especially cancer.

Since mitochondria are considered to be a major source of ROS, the regulation of mitochondrial function is crucial for cellular viability. Various endogenous and exogenous stresses can perturb mitochondrial function, inducing a rise in mitochondrial ROS levels³⁶. ROS that are physiologically produced in mitochondria participate in important signaling pathways to mediate adaptive responses and regulate diverse biological processes including cell growth and differentiation. High levels of ROS that exceed physiological levels cause oxidative stress, leading to mitochondrial dysfunction and cellular damage. Therefore, a rise in intracellular oxidant levels has two possible effects: oxidative damage to various cell macromolecules (DNA, proteins, lipids, etc.) and/or triggering the activation of specific signaling pathways³⁷. Therefore, the impairment of these important organelles is one of the central features of aging and age-related diseases. The production of mitochondrial superoxide radicals occurs primarily at two points in the ETC, namely at the complex I (NADH dehydrogenase) and at complex III (ubiquinone-cytochrome c reductase), the latter being the main site of ROS production³⁸. Sirt3 regulates proteins of the mitochondrial electron transport chain such as complex I³⁹, SDH-A of complex II^{30,31}, and ATP synthase (complex V)⁴⁰, and increases ATP production³⁹. Basal levels of ATP in the liver are reduced by 50% in mice lacking Sirt3³⁹. Sirt3 has an important role in mitochondrial biogenesis and specifically regulates the production of ROS at the ETC, and their detoxification through direct deacetylation and activation of major mitochondrial antioxidant enzyme, superoxide dismutase 2 (SOD2)⁴¹. Moreover, SIRT3 activates IDH2, a crucial enzyme that plays a vital role in glutathione antioxidant systems by generating NADPH and improves antioxidant capability²⁹. Thus, Sirt3 integrates cellular energy metabolism and different mitochondrial processes, including ROS generation.

Estrogen

Estrogens are steroid hormones that regulate growth, differentiation, and function in a broad range of target tissues in the human body. There are three main naturally occurring estrogens: estrone (E1), estradiol (E2, or 17 β -estradiol) and estriol (E3). E1 and E3 were first isolated in the 1930s, while the third estrogen, E2, was isolated later by Edward E. Doisy⁴². The most potent and dominant estrogen in humans is E2 with the highest affinity for estrogen receptor α (ER α)⁴³ and is the predominant estrogen in premenopausal women. Estrogens are produced primarily in the ovaries, but small amounts can also be produced by non-reproductive tissue, such as the liver, heart, skin and brain, but also the adipose tissue⁴⁴.

Estrogen signaling pathways are mainly ER-dependent, but there are also ER-independent pathways. ER-dependent pathways are interrelated and classified as either “genomic” or “non-genomic”, based on whether the end result is regulation of transcription (Figure 3). In the classical, “genomic” pathway estrogen binds to ER α and/or ER β , followed by its activation and binding to DNA or binding of this estrogen-ER complex to other nuclear-receptors coactivators or corepressors⁴⁵. The molecular mechanisms underlying the non-genomic actions of estrogens are specific for a certain cell type and are usually initiated through the interaction of ERs (ER α and/or ER β) or G-protein coupled ER (GPER)⁴⁶, with membrane-associated signaling proteins resulting in activation of intracellular signaling cascade⁴⁵. In ER-independent pathways, estrogen can regulate enzymatic activities or interact with other proteins to protect against cell damage^{47,48}.

The major effects of estrogen are mediated by its interaction with the nuclear receptors ER α and ER β , which have a high identity within DNA-binding and ligand-binding domains, but differ in the amino acid composition of N-terminus⁴⁹. These receptors act as ligand-activated transcription factors, with ER α being essential for pro-proliferative signaling in both normal and breast cancer⁵⁰. The classical mechanism of ER action involves estrogen binding to receptors (predominantly ER α) in the nucleus, after which the receptors dimerize and bind to specific response elements known as estrogen response elements (EREs) located in the promoters of target genes⁵¹. At the same time, E2 binding triggers ER α proteasomal degradation which is required for the cellular response to environmental estrogen levels⁵². However, a small portion of ER α and ER β interacts with plasma membrane-associated signaling proteins to activate intracellular signaling cascades that ultimately alter transcriptional responses, including mitochondrial morphology and function⁵³. In addition to the full-length ER α and

ER β , each subtype has numerous splice variants⁵⁴. Moreover, these receptors are structurally and functionally distinct in their response to estrogens in many aspects: ligand recognition, receptor activation, recruitment of co-regulators and target genes they regulate in a time and tissue-dependent manner⁵¹.

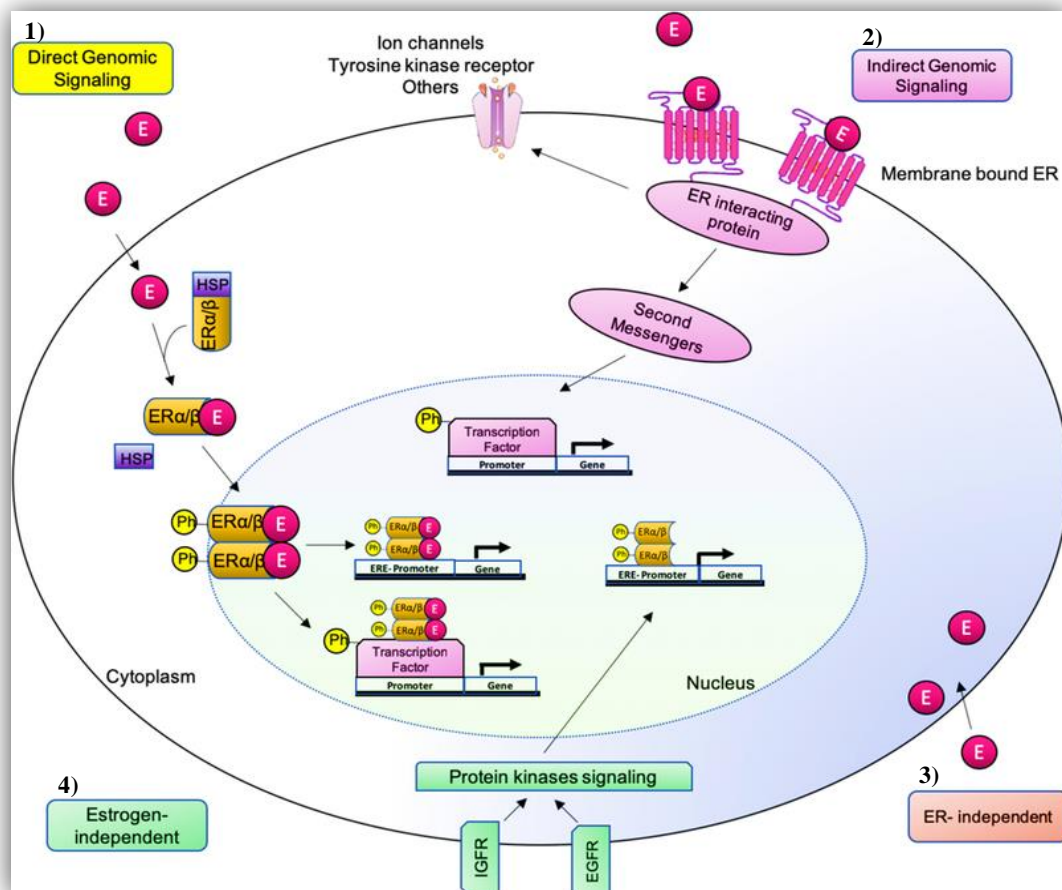


Figure 3. Genomic and non-genomic estrogen signaling pathways. There are different estrogen-mediated signaling mechanisms. 1) Direct genomic signaling: estrogen binds to ERs causing complex dimerization and translocation to the nucleus where it causes transcriptional changes in estrogen-responsive genes with or without EREs. 2) Indirect genomic signaling: the membrane-bound receptor induces cytoplasmic events. 3) ER-independent: estrogen exerts antioxidant effects in an ER-independent manner. 4) Estrogen-independent: ligand-independent genomic events. Adapted from⁵⁵.

E2's physiological functions range from the regulation of the menstrual cycle and reproduction to modulation of bone density, brain function, and cholesterol mobilization. In addition, estrogens and their receptors play key roles in regulating body weight, energy and metabolic homeostasis. E2 deficiency and disruptive mutation in the ER genes promote metabolic

dysfunction leading to obesity, metabolic syndrome, and type 2 diabetes⁵⁶. Considering the importance of E2 in these physiological functions and its role in preventing metabolic diseases, it is important to clarify the role of E2 and its receptors in these signaling pathways with a focus on tissue-specific effects in metabolism that will contribute to better understanding and improvement of targeted therapies.

Sirtuin 3, estrogen and breast cancer

Cancer is the second leading cause of death globally and about 16% of deaths worldwide are due to cancer⁵⁷. Carcinogenesis, also called oncogenesis or tumorigenesis, is characterized by the enrichment of cells displaying phenotypes that result in excessive proliferation, resistance to apoptosis, and metabolic dysregulation whereby normal cells are transformed into cancer cells⁵⁸. Although these cellular events have been extensively investigated, much still remains unclear. However, it is known that post-translational modification of proteins (like lysine acetylation) is one of the mechanisms responsible for fine-tuning intracellular signaling and metabolic pathways that can either promote or prevent tumorigenesis¹⁹.

Sirt3 has a dual role in cancer, acting as an oncogenic or tumor suppressor protein depending on the type of cancer and the context of intracellular signaling pathways¹⁹. Also, Sirt3 plays conflicting roles in malignancies originating from the same type of tissue, like gastric cancer^{59,60}, lung cancer^{61,62}, breast cancer^{63,64}, etc. Breast cancer is now the most frequent cancer worldwide, with an increased mortality rate but still ranks as the fifth cause of death by cancer⁵⁷. Tumorigenic properties of Sirt3 in breast cancer have been reported through its deacetylation activity of mitochondrial proteins such as SOD2, IDH2, and FOXO3a, inhibition of mitochondrial ROS production and an increase in cell proliferation⁶⁵. On the other hand, many other reports indicate that the tumor-suppressive role of Sirt3 in breast cancer is achieved through inhibition of glycolysis and metabolic reprogramming in different breast cancer lines^{25,66}. More importantly, Sirt3 KO mice spontaneously develop ER/PR-positive mammary tumors⁶⁷, while decreased Sirt3 protein expression has been observed in tumor compared to normal human breast epithelium, including normal epithelium adjacent to tumors⁶⁴. In addition, one *sirt3* allele is deleted in roughly 40% of human breast cancer samples⁶⁶ and low Sirt3 expression is associated with poor outcome in all breast cancers⁶⁴. Even though there is growing evidence that Sirt3 is a tumor suppressor in breast cancer, the exact mechanism by which Sirt3 exerts this action is not fully understood.

Despite the beneficial actions of E2, numerous studies have demonstrated the association of E2 with the development and/or progression of various types of cancer, including breast, endometrium, ovary, prostate, lung, and colon cancer^{68,69}. E2 is a major risk factor for initiation and progression of malignancy in ER-positive breast cancers⁷⁰. ER α is a key transcription factor in breast cancer and the binding of E2 promotes cellular proliferation through the upregulation of cell cycle-regulating genes. Furthermore, mitochondria are also affected by E2 and the cross-talk between nucleus and mitochondria appears to control E2-induced signaling involved in apoptosis, proliferation and differentiation of both normal and malignant cells. Mitochondria may transduce signals to the nucleus through its interaction with the cytoskeleton, exported signaling peptides, and/or generation of ROS that activate transcription factors AP-1, NF- κ B, and CREB involved in the cell cycle and proliferation^{71,72}. In addition, studies have shown that by controlling mitochondrial biogenesis it is possible to inhibit breast tumor growth⁷³. Cancer cells exhibit aberrant ROS production and mitochondrial ROS production contributes to a high degree of genomic instability in cancer¹⁸. It is evident that E2 has either a protective or a detrimental effect, depending on the context, although the molecular mechanisms underlying these effects is still not fully understood. In addition, it is not clear whether Sirt3 as a pivotal factor regulating cellular metabolic homeostasis, participates in these events and further investigations could give a new insight into the potential mechanistic connection between mitochondrial function, Sirt3 and E2 in breast cancer.

Hyperoxia, the exposure to high levels of oxygen, is often used to treat individuals with respiratory distress⁷⁴ and non-healing wounds in diabetes⁷⁵, yet prolonged hyperoxia causes mitochondrial dysfunction and excessive ROS production that cause oxidative damage to DNA, proteins and lipids⁷⁴. Tumor hypoxia plays a major role in cell survival, angiogenesis, glycolytic metabolism and metastasis and the hypoxic environment encourages cancer cells to acquire stemness and become resistant to chemotherapeutic drugs. Today both normobaric and hyperbaric oxygen therapy are used as adjuvant therapy in attenuating the effects of hypoxia by enhancing the effects of chemotherapy and radiotherapy via increasing oxygen delivery to the tissue^{76,77}. Oxygen therapy has now been used alongside chemotherapy in breast cancer patients and it has been shown that oxygen therapy improved chemotherapy and reduction in cancer volume⁷⁸. Considering the tumor-suppressive role of Sirt3 in carcinogenesis, especially in breast cancer, and the negative impact of hyperoxia on tumorigenic properties of tumor hypoxia, one would expect that Sirt3 expression would negatively impact breast cancer cells, especially in combination with hyperoxic treatment.

Sirtuin 3 and estrogen in metabolism

Unbalanced nutrition with an increase in caloric food intake or consumption of diets high in both fat and carbohydrates along with physical inactivity leads to increased obesity, a key factor in the development of metabolic syndrome. The metabolic syndrome represents a cluster of risk factors characterized by abdominal obesity, insulin resistance, hypertension, and hyperlipidemia that contribute to the development of chronic diseases such as type 2 diabetes (T2D), cardiovascular diseases, and several cancers, but also inflammation, atherosclerosis, renal, liver and respiratory disease, cancer, and premature aging^{79,80}. More and more research is showing that there is a significant difference between men and women in developing metabolic syndrome and this difference is largely related to hormonal regulation of body fat distribution and concomitant metabolic dysregulation.

Body fat distribution is different in men and women, with men having less total body fat but more intra-abdominal visceral adipose tissue (VAT), whereas women tend to have more total fat and subcutaneous adipose tissue (SAT) in the gluteal/femoral area⁸¹. After menopause, women tend to have fat distribution more similar to that of men⁸². Body adipose tissue tends to expand through hyperplasia in women and hypertrophy in men⁸³. In addition, compared with age-matched men, premenopausal women have enhanced insulin sensitivity⁸⁴, but also store more fat while men tend to have a higher rate of lipid oxidation⁸⁵. These sex differences in body fat distribution and energy metabolism are the consequence of the action of sex chromosomes and sex-specific hormones, including estrogens and progesterone in females and androgens in males⁸⁶. Moreover, sex differences have a high impact on health and disease and more studies on both sexes are essential to explain the molecular mechanisms underlying these differences.

Sex-based differences in diseases are caused in part by endogenous sex steroid hormones, which regulate mitochondrial metabolism. In addition, there is increasing evidence that estrogens and their receptors play key roles in regulating body weight, energy expenditure, and metabolic homeostasis. Investigations on premenopausal/postmenopausal women and ER KO mice demonstrate that both E2 and ER downregulation result in alterations in metabolic homeostasis such as glucose intolerance, hyperinsulinemia, and dyslipidemia⁵⁶. More specifically, E2 signaling promotes FAO along with changes in the expression of several genes involved in OXPHOS⁸⁷. In addition, E2 has been shown to suppress several key lipogenic genes, such as transcription factor *srebp1-c* and its target genes *scd-1* and *fas* in white adipose tissue (WAT) of female mice⁸⁸. These studies show that E2 has a major role in maintaining normal

physiological conditions and is involved in the prevention of obesity and metabolic syndrome. In addition, E2 production as well as ER expression differ depending on the cell type or tissue, thus, it is important to understand the tissue-specific roles of E2 and ER in these processes.

The effects of an unbalanced diet and overnutrition on human health and the development of metabolic diseases can be effectively mimicked in rodent models using dietary intervention, such as high-fat diets (HFDs)⁸⁹. The nutrient overload generated by a HFD in mice leads to a chronic increase in ROS production, which leads to oxidative stress⁸⁰. Oxidative stress is associated with the metabolic syndrome, but whether it is the cause or the consequence is a matter of debate. Nevertheless, a HFD is capable of functioning as a metabolic stressor causing mitochondria dysfunction and other metabolic changes that contribute to diverse pathological states⁸⁹.

Sirt3 plays a role in the prevention of the metabolic syndrome⁹⁰, although it is not clear whether this protection is accomplished *via* alleviation of oxidative stress, metabolic reprogramming, or modification of other signaling pathways. Sirt3 mediates oxidative stress suppression during caloric restriction⁹¹, but its role on oxidative stress during excessive caloric intake in the form of a HFD remains to be elucidated. As already mentioned, many metabolic pathways take place in mitochondria, and proteins involved in these pathways are targets for deacetylation and activity modulation by Sirt3, including proteins associated with oxidative phosphorylation, FAO, and TCA cycle^{27,30,34}. Moreover, it is shown that Sirt3 deficiency in mice has detrimental effects upon HFD^{90,92,93}. Currently, little is known about Sirt3 expression in the context of sex-related differences in the development of the metabolic syndrome. The understanding of sex differences in physiology and disease is of fundamental importance with regard to preventing metabolic diseases.

Research problem and scope of the thesis

The focus of the research is the Sirt3 protein, a major mitochondrial NAD⁺-dependent deacetylase, which regulates many cellular processes, including main metabolic pathways and energy production. Sirt3 effectively balances between cellular energy conversion and undesirable side effects of mitochondrial processes, such as the formation of ROS.

E2 is a female steroid hormone that coordinates and integrates cellular metabolism and mitochondrial activity by direct and indirect mechanisms. Although E2 has a cytoprotective role under conditions of oxidative and metabolic stress, it also has a detrimental effect in some pathological conditions, such as breast cancer. Breast cancer is the most common cancer among women, and 70% of all breast cancers are ER-positive. Studies to date have shown that low Sirt3 expression correlates with reduced survival in all types of breast cancers, highlighting its role as a biomarker and a potential therapeutic molecule. However, the exact mechanism of its action has not yet been elucidated. For more than a decade hyperoxia has been used as a successful treatment of a number of diseases and conditions whose common feature is lack of oxygen, i.e. hypoxia. This research contributes to the understanding of the role of Sirt3 protein in breast cancer cells, as a potential pharmacological molecule of interest, upon hyperoxia-induced oxidative stress. In addition, this research clarifies the role of Sirt3 in ER-positive MCF-7 breast cancer cells and shows how it affects the proliferative role of E2 in this pathophysiological condition.

Nowadays, an unbalanced diet rich in fats in combination with a sedentary lifestyle leads to obesity and metabolic syndrome, which contributes to the development of chronic diseases, T2D, cardiovascular diseases and cancer. In females, ovarian hormones have a key role in the regulation of metabolism, food intake, and body weight. Furthermore, the prevalence of metabolic disorders increases drastically after menopause indicating the influence of sex hormones on body adiposity and metabolic syndrome incidence. Sirt3 regulates many cellular processes, including the activity of enzymes involved in major metabolic pathways and energy production. Furthermore, both Sirt3 and E2 have a well-established role in protecting against metabolic dysfunction. There are pronounced sex differences in susceptibility to metabolic stress that precedes obesity and the development of metabolic syndrome, and they have been described in both mice and humans, highlighting the importance of such research on both sexes. Despite extensive research on Sirt3 and E2 individually, the link between E2 and Sirt3 in response to metabolic stress caused by HFD has not yet been demonstrated. Clarifying the role

of Sirt3 and E2 in mice of both sexes fed a HFD will contribute to the characterization of sex-related differences in the development of metabolic diseases as well as potential targets that would contribute to their prevention and/or treatment.

LIST OF PUBLICATIONS

1. Pinterić, M.; Podgorski, I.I.; Sobočanec, S.; Popović Hadžija, M.; Paradžik, M.; Dekanić, A.; Marinović, M.; Halasz, M.; Belužić, R.; Davidović, G.; Ambriović Ristov, A.; Balog T. *De novo* expression of transfected sirtuin 3 enhances susceptibility of human MCF-7 breast cancer cells to hyperoxia treatment. *Free Radical Research* **2018**, 52, 672–684. <https://doi.org/10.1080/10715762.2018.1462495>
2. Pinterić, M.; Podgorski, I.I.; Popović Hadžija, M.; Filić, V.; Paradžik, M.; Proust, B.L.J.; Dekanić, A.; Ciganek, I.; Pleše, D.; Marčinko, D.; Balog, T.; Sobočanec, S. Sirt3 exerts its tumor-suppressive role by increasing p53 and attenuating response to estrogen in MCF-7 cells. *Antioxidants* **2020**, 9, 294. <https://doi.org/10.3390/antiox9040294>
3. Pinterić, M.; Podgorski, I.I.; Popović Hadžija, M.; Tartaro Bujak, I.; Dekanić, A.; Bagarić, R.; Farkaš, V.; Sobočanec, S.; Balog, T. Role of Sirt3 in differential sex-related responses to a high-fat diet in mice. *Antioxidants* **2020**, 9, 174. <https://doi.org/10.3390/antiox9020174>
4. Pinterić, M.; Podgorski, I.I.; Popović Hadžija, M.; Tartaro Bujak, I.; Tadijan, A.; Balog, T.; Sobočanec, S. Chronic high fat diet intake impairs hepatic metabolic parameters in ovariectomized Sirt3 KO mice. *International Journal of Molecular Sciences* **2021**, 22, 4277. <https://doi.org/10.3390/ijms22084277>

DISCUSSION

Tumor-suppressive effect of Sirtuin 3 in MCF-7 breast cancer cells is enhanced upon hyperoxic treatment and mediated by the attenuated response to estrogen

Breast cancer is the most common cancer worldwide and the leading cause of death in women. The significance of Sirt3 in breast cancer lies in the fact that most of the normal breast tissue is positive and most of the breast cancers are negative for Sirt3 expression. Furthermore, low Sirt3 expression is associated with poor outcomes in multiple subtypes of breast cancers⁶⁴. Numerous cell lines are widely used as an *in vitro* model of cancer research and the MCF-7 breast cancer cell line is mostly used in research of ER-positive breast cancers and has so far produced more data of practical knowledge for patient care than any other breast cancer cell line⁹⁴. Hyperoxia suppresses the growth of breast cancer cells⁹⁵ but also improves chemotherapy and reduces the cancer volume in breast cancer patients⁷⁸, which indicates the therapeutic effect of hyperoxia on tumor growth and proliferation.

This study shows that after 44h of treatment with hyperoxia (95% O₂) Sirt3 is upregulated in MCF-7 breast cancer cells, which is consistent with the study showing its upregulation after oxidative stress treatment⁹⁶. In addition, the combined effect of Sirt3 and hyperoxia downregulates genes involved in angiogenesis (*vegfr-1* and *vegfr-2*)⁹⁷, and two markers of EMT, *vimentin* and *slug*⁹⁸, indicating that Sirt3 and hyperoxia both act as suppressors of the EMT transition and malignant properties of the MCF-7 cells. This is in accordance with previous studies showing that downregulation of Vegf-A, but also vimentin, is enough for the inhibition of Vegf-A-associated angiogenesis and EMT in breast cancer^{99,100}.

A number of breast cancer cell lines, particularly MCF-7, depend on a mixture of glycolysis and OXPHOS to support their proliferation¹⁰¹. This study shows that Sirt3 might induce the metabolic shift from glycolysis to OXPHOS¹⁰² through upregulation of Sirt1/Pgc-1 α ¹⁰³ along with downregulation of glycolysis marker LdhA¹⁰¹, thus confirming previous reports that metabolic reprogramming mediated by Sirt3 contributes to its tumor-suppressive role in human breast cancer cell lines⁶⁶.

Treatment with elevated levels of O₂ (i.e. hyperoxia) causes an increase in cellular ROS levels, a property often used in anticancer therapy since some molecularly targeted drugs and chemotherapeutic agents effectively kill cancer cells by inducing ROS generation¹⁰⁴. Hyperoxia

has a major impact on the mitochondrial function of MCF-7 cells, as indicated by high mitochondrial mass and potential, but also by decreased mitochondrial respiration, which led to mitochondrial dysfunction, elevated ROS production, and impairment of antioxidative defense. This finding implies that the tumor-suppressive effect of hyperoxia may be partially achieved through mitochondrial dysfunction that is shown to prevent breast cancer tumor growth¹⁰⁵ and is nowadays recognized as a powerful tool for the development of mitochondrial-targeted therapies in cancer treatment¹⁰⁶.

A major tumor suppressor p53, often mutated or deregulated in many human cancers¹⁰⁷, was significantly upregulated in Sirt3-overexpressing cells and this effect was further enhanced upon hyperoxia. The upregulation of p53 upon hyperoxia is accompanied by an increase in DNA damage, along with diminished cell proliferation, metabolic rate and clonogenic capacity. Although one would expect that cells with a lot of DNA damage would undergo the apoptosis pathway, MCF-7 cells rather become senescent than enter apoptosis, probably due to the lack of functional caspase 3 expression¹⁰⁸. This was also shown in previous studies where hyperbaric oxygen treatment lowered proliferation but did not induce apoptosis in MCF-7 cells¹⁰⁹. Collectively and in agreement with the previous studies^{106,109,110}, these results show that hyperoxia inhibits proliferation and survival of cancer cells through the mitochondrial dysfunction and activation of p53 upon DNA damage and induction of senescence. The majority of the observed negative effects of hyperoxia (compromised antioxidative defense, enhanced ROS production, DNA damage and p53 expression, as well as lower proliferation) were even more pronounced upon Sirt3 expression. Thus, the mitigation of tumorigenic properties and enhanced susceptibility of the MCF-7 breast cancer cells to the hyperoxic treatment upon the *de novo* Sirt3 expression, indicates that both Sirt3 and hyperoxia, especially combined, have a potential to negatively modulate the properties of cancer cells and should, therefore, be further explored *in vitro*, and particularly *in vivo*, as an adjuvant tumor therapy in breast cancer malignancies.

17 β -estradiol (E2) is a master regulator of human physiology both in males and in females. By binding to ER α , E2 promotes cell proliferation through upregulation of cell cycle-regulating genes, and simultaneously triggers ER-proteasomal degradation that is required for normal response to environmental E2 levels⁵². Since 70% of all breast cancers are ER α -positive, E2 is also a major risk factor for initiation and progression of malignancy in ER-positive breast cancers and is often followed by estrogen receptor alpha (*esr1*) gene amplification⁷⁰. ER α expression in breast cancer is dynamic, reversible, and regulated by different cellular factors

and mechanisms¹¹¹. This study shows that the overexpression of Sirt3 is followed by upregulation of ER α gene and protein expression while the silencing of Sirt3 causes downregulation of ER α protein, thus pointing towards the involvement of Sirt3 in ER α expression. However, since no ER α was present in mitochondria, but only in the nucleus and cytoplasm, Sirt3 probably indirectly regulates the expression of ER α in MCF-7 breast cancer cells.

Estrogens regulate transcription and cell signaling pathways that affect mitochondrial function, including mitochondrial bioenergetics and biogenesis, calcium homeostasis, and antioxidant defense¹¹². Therefore, the role of Sirt3 in E2-mediated response on mitochondrial function in MCF-7 cells was explored. This study shows that Sirt3 induced protein expression of OXPHOS complex I (NDUFA9), II (SDH-A), and III (UQCRC2) and consequently elevated mitochondrial potential, which is consistent with its role in maintaining mitochondrial potential and homeostasis by affecting various OXPHOS complexes and proteins¹¹³. In addition, Sirt3 potentiated the inducing effect of E2 on metabolic activity, probably as a result of elevated SDH-A expression¹¹⁴ upon E2 stimulation. By treatment with ICI (ER-antagonist), the metabolic activity along with SDH-A expression was lowered to control level indicating for the first time that this effect is mediated through the E2-ER α axis.

Mitochondria of tumor cells exhibit aberrant ROS that account for the high degree of genomic instability in cancer cells¹⁸, while Sirt3 mediates mitochondrial oxidative pathways and regulates the production of ROS. Therefore, the role of Sirt3 in E2-mediated ROS production and antioxidative defense was explored. Sirt3 boosts the antioxidative system through the upregulation of Nrf2 and Cat protein expression accompanied by higher MnSOD and CuZnSOD activities. Furthermore, following the E2 treatment both cytosolic and mitochondrial ROS were reduced in Sirt3-overexpressing cells. This could be the result of a more efficient antioxidant enzyme system induced by Sirt3 upon E2 treatment as shown by its role in ROS scavenging following E2 treatment¹¹⁵. Since other studies have shown that ROS generated after exposure to E2 contributes to the development of human breast cancer^{66,116}, these findings suggest that Sirt3 can function as a tumor suppressor by activating antioxidative enzymes and attenuating the E2-induced ROS levels from both cytosolic and mitochondrial compartments.

Although Sirt3-overexpressing MCF-7 cells demonstrated improved mitochondrial function and antioxidative enzyme system response, the opposite effect was observed on their proliferation and migration. The Sirt3-mediated inhibitory effect on E2-induced proliferation

was shown through a significant decrease in the colony-forming ability of the MCF-7 cells in red DMEM and an almost complete absence of colonies in white DMEM. The mechanism by which Sirt3 causes reduction of the clonogenic capacity is still not clear but probably involves DNA damage accumulation observed as an increase in γ H2AX phosphorylation, followed by an increase in expression of p53. The increased DNA damage was accompanied by a higher frequency of micronucleated cells which has been shown to cause growth inhibition in MCF-7 cells¹¹⁷. In addition, the Sirt3-overexpressing cells also showed lower migration capacity which complies with the downregulation of metastatic genes *vegfa*, *vegfr1*, *vimentin* and *slug*. Breast cancer cells usually have functional p53, although its activity is altered by various mechanisms¹¹⁸. The abrogation of the p53 signaling pathway is a major event towards cancer progression in ER α -positive breast cancer cells, where p53 is functionally repressed by interaction with ER α ¹¹⁹. Sirt3-overexpressing cells show disruption of ER α -p53 interaction and since ER α binding to p53 results in inactivation of p53, disruption of this interaction by Sirt3 indicates the possible mechanism of the tumor-suppressive role of Sirt3 in MCF-7 breast cancer cells.

In conclusion, this study shows that Sirt3, despite improving the mitochondrial function of MCF-7 breast cancer cells, reduces their response to E2, affects p53 by disruption of the ER α -p53 interaction, inhibits clonogenic cell growth and lowers migration capacity. Collectively, these studies highlight the mitochondrial fidelity protein Sirt3 as a tumor suppressor and potential therapeutic target in ER α -positive breast cancers.

Relationship of sex and Sirtuin 3 in response to high-fat diet in 129S mice

The prevalence of individual risk factors that contribute to metabolic syndrome differs within sex and understanding how and why metabolic processes differ will enable targeted and personalized therapies based on sex. Only a few studies focus on these important differences between males and females, and in fact, most biomedical research is conducted on males¹²⁰. In females, ovarian hormones play a pivotal role in metabolic, food intake, and body weight regulation¹²¹. Moreover, premenopausal women have fewer obesity-related metabolic disorders, but their prevalence increases dramatically after menopause indicating the influence of sex hormones on body adiposity and the metabolic syndrome incidence¹²². HFD is an important factor in the development of many metabolic diseases, with the liver as a metabolic center being highly exposed to its influence⁸⁹. Estrogens regulate liver lipogenesis and insulin sensitivity, and both clinical and experimental studies show that E2 through ER α has a protective effect by improving insulin sensitivity and glucose homeostasis, enhancing FAO, and reducing hepatic lipogenesis (reviewed in^{56,123}). Sirt3 regulates mitochondrial FAO by reversible enzyme deacetylation³⁴ and maintains mitochondrial metabolic and redox homeostasis, with a prominent role in protection from metabolic syndrome and non-alcoholic fatty liver disease (NAFLD)^{90,124}. Furthermore, Sirt3 plays a role in preventing metabolic syndrome⁹⁰, but its role in the context of sex-related differences in the development of metabolic syndrome is still unknown. Ovariectomy, surgical removal of the ovaries, is the most frequently used model for studies of female sex hormones (mostly estrogen) on different physiological parameters¹²⁵. Ovariectomy in combination with HFD results in obesity, insulin resistance and glucose intolerance^{121,126}, disturbs adipose tissue immune homeostasis¹²⁷ and makes these rodents more susceptible to subcutaneous tumor growth¹²⁸. However, the combination of both Sirt3 and ovary hormones deficiency in regulating metabolic stress *in vivo* has not yet been investigated. For this purpose, the effect of HFD on sex-related differences in physiological and metabolic parameters in the liver of Sirt3 WT and KO male and female mice, and sham-operated and ovariectomized (ovx) female mice was investigated.

Sirt3 expression is differentially regulated in dietary interventions, showing upregulation during caloric restriction⁹¹ and downregulation after chronic exposure to HFD in male mice⁹⁰. Moreover, Sirt3 deficiency is associated with the accelerated development of metabolic syndrome⁹⁰. In this study Sirt3 expression was also downregulated in male mice upon HFD, however, the diet did not influence Sirt3 expression in females, but ovary hormone depletion did. Ovariectomy induced transcriptional coactivator *pgc1- α* and its downstream target Sirt3

irrespective of diet as a possible compensatory response to stress caused by ovary hormone deprivation¹²⁹. This suggests that sex-related changes in Sirt3 expression following HFD and upon ovary hormone depletion may contribute to the observed sex differences in the development of metabolic dysregulation as it has also been shown for other proteins¹³⁰.

Dysregulation in glucose homeostasis is one of the main features of metabolic syndrome¹³¹, but there was no effect of Sirt3, ovx or HFD on glucose levels, only the effect of sex, where females had lower glucose than males, indicating better glucose homeostasis and insulin sensitivity in females⁸⁶. Even though HFD usually causes increased body weight gain¹³², in this study only a combination of a HFD with ovariectomy and Sirt3 depletion had such an effect. The reason for this is that this particular mouse strain, 129S, is not prone to the development of obesity and hyperglycemia following HFD. However, these mice still develop the features of metabolic syndrome but with lower severity compared to some other strains^{133–136}. Although the animals were not obese, all groups had an excessive accumulation of fat in the liver and developed hepatic steatosis following ten weeks of HFD. Interestingly, Sirt3 deficiency reduces FAO which results in higher lipid accumulation in SFD-fed KO male mice¹³⁷, as also shown in males in this study. However, the opposite effect was present in SFD-fed ovx KO females, suggesting that both Sirt3 and ovary hormones have an important role in the maintenance of lipid homeostasis in SFD conditions. In addition, following HFD, KO males had the lowest hepatic liver accumulation along with the lowest hepatic glucose uptake, indicating that HFD, in the absence of Sirt3, caused impaired hepatic glucose uptake and increased reliance on fatty acids. This was also shown in the skeletal muscles of KO male mice¹³⁸. The same effect was present in HFD-fed ovx WT and KO females, suggesting the important role of ovary hormones in these processes. Finally, the observed differences in glucose uptake and lipid accumulation present only in KO males and ovx females highlight the importance of both Sirt3 and ovary hormones in metabolic homeostasis in both SFD and HFD conditions.

The liver is a major metabolic organ where fatty acids, triglycerides, and cholesterol metabolism are coordinated to meet metabolic needs in normal physiology. The capacity for the β -oxidation of fatty acids, the major lipid catabolic pathway, is regulated at the gene expression level in response to various physiological stimuli, and these genes are regulated differentially between sexes, as shown in different animal models¹²³. NAFLD includes a spectrum of liver disorders characterized by increased hepatic fat accumulation, inflammation, and hepatocyte dysfunction¹³⁹, and is a common result in mice fed with HFD¹⁴⁰. Genes involved in hepatic lipid homeostasis under HFD conditions are *hnf4a*¹⁴¹, *ppara*¹⁴² and *ppary*¹⁴³, and

cytochrome P450 (*cyp*) enzymes, the majority of which are regulated in a sex-dependent manner¹⁴⁴. WT females had higher expression of both *hnf4a* and *ppara* than males, while ovx in WT females and HFD generally caused upregulation of *ppara*, thus indicating the better response of females' lipid metabolism following HFD¹⁴². On the other hand, *cyp* showed altered expression with respect to Sirt3, ovx and/or HFD. In females, all three *cyp* transcripts, *cyp2e1*, *cyp2a4*, and *cyp4a14*, were upregulated following HFD, while males and ovx females had a different response to the HFD with respect to Sirt3. Only *cyp4a14* showed strong upregulation following HFD in both WT and KO males, while *cyp2a4* and *cyp2e1* were upregulated only in HFD-fed KO males. Since Cyp2e1 and Cyp4a14 have a role in FAO¹⁴⁵ and were known to be upregulated following HFD¹⁴⁶, their upregulation suggests a higher FAO rate in association with lower accumulation of total lipids in the liver of KO males. Furthermore, depletion of either ovary hormones or both ovary hormones and Sirt3 changed the expression of *cyp2e1* and *cyp4a14*, genes involved in the development of non-alcoholic steatohepatitis (NASH)¹⁴⁵, a disease that is a part of NAFLD¹³⁹. Higher expression of either of these genes indicates that these mice are prone to NAFLD with an increase in ROS and oxidative stress^{145,147}. Furthermore, Cyp4a14 was shown to be more involved in the induction of NAFLD¹⁴⁸, while Cyp2e1 is more involved in the development of alcoholic hepatitis¹⁴⁹. This may be the reason why *cyp4a14* has higher expression upon HFD in all groups and highest in the ovx KO group in either SFD or HFD conditions. Interestingly, the expression of the *ho-1* gene, which has been reported to attenuate oxidative stress and prevent NASH¹⁵⁰, is upregulated in WT and decreased in ovx KO females. This indicates that, upon HFD-induced nutritional stress, Sirt3 may protect ovx females from NAFLD by upregulation of *ho-1*, while in the absence of Sirt3 the expression of *ho-1* is abolished, making these females more susceptible to the development of NAFLD. Overall, despite lower hepatic lipid accumulation, ovary hormone depletion, especially in combination with Sirt3 depletion makes these mice more prone to NAFLD, with increased weight gain leading to obesity.

Studies have shown that HFD leads to increased ROS production, followed by increased lipid peroxidation, protein carbonylation, and decreased antioxidant defense which indicates that oxidative imbalance occurs in HFD-fed animals⁸⁹. Sensitivity towards oxidative stress is sex-related as well¹⁵¹, and the role of Sirt3 in these sex-related differences upon nutritional stress is unknown. Sirt3 has an important role in metabolic stress and mitochondrial lipid metabolism, but it also regulates ROS production and clearance¹⁶. This study shows that in WT mice, HFD induces oxidative damage of proteins only in females (as seen through higher PC levels and

HO-1, an indicator of the oxidative stress presence¹⁵²), making them more susceptible towards oxidative stress upon HFD as a possible consequence of ROS generated by higher lipid metabolism^{145,153}. Furthermore, Sirt3 deficiency increases susceptibility to protein oxidative damage equally in both sexes, indicating that Sirt3 is an important factor in protection against oxidative damage as previously reported^{67,154,155}. Interestingly, since ovx caused upregulation of *pgc1-α* and its downstream target Sirt3 in SFD-fed WT females, these females had lower levels of lipid oxidative damage and higher MnSOD activity proving again the protective role of Sirt3 against oxidative damage^{154–156}. On the contrary, ovx KO females had the highest lipid oxidative damage in SFD conditions, despite high MnSOD activity, due to the highest upregulation of *cyp4a14* since it was shown that its upregulation causes increased lipid peroxidation in murine liver¹⁴⁵.

It is widely accepted that the mitochondrial dysfunction contributes to the development of metabolic diseases. Accumulation of lipids in the hepatocytes impairs the oxidative capacity of mitochondria, increasing the reduced state of the ETC complexes, and stimulating peroxisomal and microsomal FAO pathways followed by increased ROS production^{157,158}. Nonetheless, fatty acids are metabolic fuels and β-oxidation represents their main degradation pathway in mitochondria¹⁵⁹. This research shows that WT females have a higher CI-driven respiration than WT males on SFD, but decreased CI-driven respiration following HFD, with no effect on respiration in males. This suggests that in conditions of nutritive excess, more efficient lipid metabolism in WT females may cause higher oxidative stress followed by increased protein oxidative damage that is in association with reduced mitochondrial function. Furthermore, in accordance with other studies^{90,138,160}, KO mice display decreased CI-driven respiration. However, despite reduced respiration in KO mice, this study shows, for the first time, that KO females have higher respiration than KO males, indicating a possible beneficial effect of female sex hormones on mitochondrial function. Surprisingly, following HFD, KO males had increased respiration compared to WT males, as a possible consequence of impaired glucose uptake and increased reliance on fatty acids to provide substrates for the respiratory chain. This is consistent with the results showing that mitochondrial function is unaffected or even improved by HFD feeding in male rodents^{161,162} and that impairment of glucose homeostasis precedes HFD-induced mitochondrial dysfunction¹⁶³. Interestingly, ovx females maintained both CI and CII-driven respiration following HFD possibly due to increased palmitoleic and vaccenic acids, monounsaturated fatty acids that are known for enhancing mitochondrial β-oxidation and ATP production¹⁶⁴. Furthermore, HFD-fed ovx females had lower Cat activity

than sham mice, which might imply that they rely more on mitochondrial β -oxidation than peroxisomal β -oxidation. On the contrary, HFD-fed sham females had lower mitochondrial CII-driven respiration as well as higher Cat activity, which might indicate that these females depended more on peroxisomal β -oxidation. Collectively, these results show that the CI and CII-driven respiration displays sex-specific effect concerning both HFD and Sirt3.

Sexual dimorphism exists in various physiological processes, which also includes sex-related prevalence towards metabolic dysregulation. This study shows significant sex differences at the level of metabolic, oxidative, and mitochondrial parameters, with different roles of Sirt3 in males and females following nutritional stress in the form of a HFD. Furthermore, this research adds to the previous studies and confirms the hypothesis that protection against harmful effects of HFD in female mice is attributed to the combined effect of female sex hormones and Sirt3. Nevertheless, further studies are necessary in order to prevent metabolic dysfunction, improve preclinical research, and enable the development of sex-related therapeutic agents for obesity and metabolic diseases. Moreover, these studies emphasize the key role of mitochondrial fidelity protein Sirt3 in mitochondrial processes, which extend beyond mitochondria and affects whole-body homeostasis.

CONCLUSIONS

- Sirt3 and hyperoxia both act as tumor suppressors of MCF-7 breast cancer cells' malignant properties, which is observed through their reduced survival, proliferation and mitochondrial dysfunction, as well as the upregulation of cellular growth suppressors and activation of p53 upon DNA damage and induction of senescence.
- Sirt3 induces the metabolic shift from glycolysis to OXPHOS, through upregulation of Sirt1/Pgc-1 α along with downregulation of glycolysis marker LdhA, thus confirming previous reports that metabolic reprogramming mediated by Sirt3 contributes to its tumor-suppressive role in human breast cancer cell lines.
- Despite improving the mitochondrial function of MCF-7 breast cancer cells, Sirt3 reduces their response to E2, positively affects p53 by disruption of the ER α -p53 interaction, inhibits clonogenic cell growth and lowers their migration capacity.
- Collectively, studies on MCF-7 breast cancer cells show that Sirt3 and hyperoxia both act as a tumor suppressors of MCF-7 breast cancer cells' malignant properties and that Sirt3 negatively affects the proliferative effect of E2, thus, highlighting the mitochondrial fidelity protein Sirt3 as a tumor suppressor and potential therapeutic target in ER α -positive breast cancers.
- Nutritional stress in form of a HFD reduces Sirt3 expression only in WT males, and results in alleviated lipid accumulation accompanied by reduced glucose uptake in the liver of KO males, pointing towards a higher reliance of males on the protective effect of Sirt3 against HFD-induced metabolic dysregulation.
- Females generally have a higher expression of genes involved in lipid homeostasis, and either HFD or Sirt3 depletion compromises mitochondrial respiration and increases oxidative damage of protein.
- Ovariectomy in WT females results in an increased Sirt3 expression that is followed by maintained mitochondrial function and decreased levels of lipid hydroperoxides in SFD conditions. The combination of ovariectomy and Sirt3 depletion dysregulates lipid metabolism and increases lipid oxidative damage in SFD conditions.
- HFD in combination with ovariectomy and Sirt3 depletion results in increased body weight gain, higher expression of NAFLD- and oxidative stress-inducing genes, and impaired

response of antioxidative system suggesting that protection against harmful effects of HFD in female mice is attributed to the combined effect of female sex hormones and Sirt3

- Collectively, studies in mice emphasize the importance of preclinical biomedical research in both males and females and the influence of sex hormones and mitochondrial fidelity protein Sirt3 on metabolic homeostasis, which, when disrupted, leads to disease.

REFERENCES

1. Kupis, W., Pałyga, J., Tomal, E. & Niewiadomska, E. The role of sirtuins in cellular homeostasis. *J. Physiol. Biochem.* **72**, 371–380 (2016).
2. Klar, A. J. S., Fogel, S. & Macleod, K. MAR1—a regulator of the HMa and HMα loci in *Sachharomyces cervisiae*. *Genetics* **93**, 37–50 (1979).
3. Rine, J. & Herskowitz, I. Four genes responsible for a position effect on expression from HML and HMR in *Saccharomyces cerevisiae*. *Genetics* **116**, 9–22 (1987).
4. Michan, S. & Sinclair, D. Sirtuins in mammals: insights into their biological function. *Biochem. J.* **404**, 1–13 (2007).
5. Alhazzazi, T. Y., Kamarajan, P., Verdin, E. & Kapila, Y. L. SIRT3 and cancer: Tumor promoter or suppressor? *Biochim. Biophys. Acta - Rev. Cancer* **1816**, 80–88 (2011).
6. Dang, W. The controversial world of sirtuins. *Drug Discov. Today Technol.* **12**, e9–e17 (2014).
7. Sanders, B. D., Jackson, B. & Marmorstein, R. Structural basis for sirtuin function: what we know and what we don't. *Biochim. Biophys. Acta - Proteins Proteomics* **1804**, 1604–1616 (2010).
8. Imai, S. I., Armstrong, C. M., Kaeberlein, M. & Guarente, L. Transcriptional silencing and longevity protein Sir2 is an NAD-dependent histone deacetylase. *Nature* **403**, 795–800 (2000).
9. Du, J. *et al.* Sirt5 is a NAD-dependent protein lysine demalonylase and desuccinylase. *Science* **334**, 806–809 (2011).
10. Mathias, R. A. *et al.* Sirtuin 4 is a lipoamidase regulating pyruvate dehydrogenase complex activity. *Cell* **159**, 1615–1625 (2014).
11. Liszt, G., Ford, E., Kurtev, M. & Guarente, L. Mouse Sir2 homolog SIRT6 is a nuclear ADP-ribosyltransferase. *J. Biol. Chem.* **280**, 21313–21320 (2005).
12. Houtkooper, R. H., Pirinen, E. & Auwerx, J. Sirtuins as regulators of metabolism and healthspan. *Nat. Rev. Mol. Cell Biol.* **13**, 225–238 (2012).
13. Haigis, M. C. & Sinclair, D. A. Mammalian sirtuins: biological insights and disease

- relevance. *Annu. Rev. Pathol. Mech. Dis.* **5**, 253–295 (2010).
14. Singh, C. K. *et al.* The role of sirtuins in antioxidant and redox signaling. *Antioxid. Redox Signal.* **28**, 643–661 (2018).
 15. Sack, M. N. & Finkel, T. Mitochondrial metabolism, sirtuins, and aging. *Cold Spring Harb. Perspect. Biol.* **4**, a013102 (2012).
 16. Elkhwanky, M.-S. & Hakkola, J. Extranuclear sirtuins and metabolic stress. *Antioxid. Redox Signal.* **28**, 662–676 (2017).
 17. Schwer, B., North, B. J., Frye, R. A., Ott, M. & Verdin, E. The human silent information regulator (Sir)2 homologue hSIRT3 is a mitochondrial nicotinamide adenine dinucleotide-dependent deacetylase. *J. Cell Biol.* **158**, 647–657 (2002).
 18. Park, S. H. *et al.* Sirt3, mitochondrial ROS, ageing, and carcinogenesis. *Int. J. Mol. Sci.* **12**, 6226–6239 (2011).
 19. Xiong, Y. *et al.* Sirtuin 3: A Janus face in cancer (Review). *Int. J. Oncol.* **49**, 2227–2235 (2016).
 20. Giralt, A. & Villarroja, F. SIRT3, a pivotal actor in mitochondrial functions: metabolism, cell death and aging. *Biochem. J.* **444**, 1–10 (2012).
 21. Lombard, D. B. *et al.* Mammalian Sir2 homolog SIRT3 regulates global mitochondrial lysine acetylation. *Mol. Cell. Biol.* **27**, 8807–8814 (2007).
 22. Zhang, J. *et al.* Mitochondrial Sirtuin 3: New emerging biological function and therapeutic target. *Theranostics* **10**, 8315–8342 (2020).
 23. Jin, L. *et al.* Biochemical characterization, localization, and tissue distribution of the longer form of mouse SIRT3. *Protein Sci.* **18**, 514–525 (2009).
 24. Kummer, E. & Ban, N. Mechanisms and regulation of protein synthesis in mitochondria. *Nat. Rev. Mol. Cell Biol.* **22**, 307–325 (2021).
 25. Wei, L. *et al.* Oroxylin A induces dissociation of hexokinase II from the mitochondria and inhibits glycolysis by SIRT3-mediated deacetylation of cyclophilin D in breast carcinoma. *Cell Death Dis.* **4**, e601 (2013).
 26. Yang, H. *et al.* SIRT 3-dependent GOT 2 acetylation status affects the malate–aspartate NADH shuttle activity and pancreatic tumor growth. *EMBO J.* **34**, 1110–1125 (2015).

27. Schwer, B., Bunkenborg, J., Verdin, R. O., Andersen, J. S. & Verdin, E. Reversible lysine acetylation controls the activity of the mitochondrial enzyme acetyl-CoA synthetase 2. *Proc. Natl. Acad. Sci. U. S. A.* **103**, 10224–10229 (2006).
28. Fan, J. *et al.* Tyr phosphorylation of PDP1 toggles recruitment between ACAT1 and SIRT3 to regulate the pyruvate dehydrogenase complex. *Mol. Cell* **53**, 534–548 (2014).
29. Yu, W., Dittenhafer-Reed, K. E. & Denu, J. M. SIRT3 protein deacetylates isocitrate dehydrogenase 2 (IDH2) and regulates mitochondrial redox status. *J. Biol. Chem.* **287**, 14078–14086 (2012).
30. Cimen, H. *et al.* Regulation of succinate dehydrogenase activity by SIRT3 in mammalian mitochondria. *Biochemistry* **49**, 304–311 (2010).
31. Finley, L. W. S. *et al.* Succinate dehydrogenase is a direct target of sirtuin 3 deacetylase activity. *PLoS One* **6**, e23295 (2011).
32. Schlicker, C. *et al.* Substrates and regulation mechanisms for the human mitochondrial sirtuins Sirt3 and Sirt5. **382**, 790–801 (2008).
33. Hallows, W. C. *et al.* Sirt3 promotes the urea cycle and fatty acid oxidation during dietary restriction. *Mol. Cell* **41**, 139–149 (2011).
34. Hirschey, M. D. *et al.* SIRT3 regulates mitochondrial fatty-acid oxidation by reversible enzyme deacetylation. *Nature* **464**, 121–125 (2010).
35. Shimazu, T. *et al.* SIRT3 deacetylates mitochondrial 3-hydroxy-3-methylglutaryl CoA synthase 2 and regulates ketone body production. *Cell Metab.* **12**, 654–661 (2010).
36. Bause, A. S. & Haigis, M. C. SIRT3 regulation of mitochondrial oxidative stress. *Exp. Gerontol.* **48**, 634–639 (2013).
37. Finkel, T. & Holbrook, N. J. Oxidants, oxidative stress and the biology of ageing. *Nature* **408**, 239–247 (2000).
38. Dröse, S. & Brandt, U. Molecular mechanisms of superoxide production by the mitochondrial respiratory chain. *Adv. Exp. Med. Biol.* **748**, 145–169 (2012).
39. Ahn, B. H. *et al.* A role for the mitochondrial deacetylase Sirt3 in regulating energy homeostasis. *Proc. Natl. Acad. Sci. U. S. A.* **105**, 14447–14452 (2008).
40. Vassilopoulos, A. *et al.* SIRT3 deacetylates ATP synthase F1 complex proteins in

- response to nutrient-and exercise-induced stress. *Antioxid. Redox Signal.* **21**, 551–564 (2014).
41. Zhong, L. & Mostoslavsky, R. Fine tuning our cellular factories: sirtuins in mitochondrial biology. *Cell Metab.* **13**, 621–626 (2011).
 42. Simoni, R. D., Hill, R. L. & Vaughan, M. The discovery of estrone, estriol, and estradiol and the biochemical study of reproduction. The work of Edward Adelbert Doisy. *J. Biol. Chem.* **277**, e1–e2 (2002).
 43. Kuiper, G. G. J. M. *et al.* Comparison of the ligand binding specificity and transcript tissue distribution of estrogen receptors α and β . *Endocrinology* **138**, 863–870 (1997).
 44. Cui, J., Shen, Y. & Li, R. Estrogen synthesis and signaling pathways during ageing: from periphery to brain. *Trends Mol. Med.* **19**, 197–209 (2013).
 45. Björnström, L. & Sjöberg, M. Mechanisms of estrogen receptor signaling: convergence of genomic and nongenomic actions on target genes. *Mol. Endocrinol.* **19**, 833–842 (2005).
 46. Gaudet, H. M., Cheng, S. B., Christensen, E. M. & Filardo, E. J. The G-protein coupled estrogen receptor, GPER: The inside and inside-out story. *Mol. Cell. Endocrinol.* **418**, 207–219 (2015).
 47. Yue, W. *et al.* Effects of estrogen on breast cancer development: role of estrogen receptor independent mechanisms. *Int. J. cancer.* **127**, 1748–1757 (2010).
 48. Richardson, T. E., Yu, A. E., Wen, Y., Yang, S.-H. & Simpkins, J. W. Estrogen prevents oxidative damage to the mitochondria in Friedreich’s ataxia skin fibroblasts. *PLoS One* **7**, e34600 (2012).
 49. Gustafsson, J. A. Historical overview of nuclear receptors. *J. Steroid Biochem. Mol. Biol.* **157**, 3–6 (2016).
 50. Musgrove, E. A. & Sutherland, R. L. Biological determinants of endocrine resistance in breast cancer. *Nat. Rev. Cancer* **9**, 631–643 (2009).
 51. Nilsson, S. *et al.* Mechanisms of estrogen action. *Physiol. Rev.* **81**, 1535–1565 (2001).
 52. Reid, G. *et al.* Cyclic, proteasome-mediated turnover of unliganded and liganded ER α on responsive promoters is an integral feature of estrogen signaling. *Mol. Cell* **11**, 695–

707 (2003).

53. Klinge, C. M. Estrogenic control of mitochondrial function. *Redox Biol.* **31**, 101435 (2020).
54. Yaşar, P., Ayaz, G., User, S. D., Güpür, G. & Muyan, M. Molecular mechanism of estrogen-estrogen receptor signaling. *Reprod. Med. Biol.* **16**, 4–20 (2017).
55. Fuentes, N. & Silveyra, P. Estrogen receptor signaling mechanisms. *Adv. Protein Chem. Struct. Biol.* **116**, 135–170 (2019).
56. Mauvais-Jarvis, F., Clegg, D. J. & Hevener, A. L. The role of estrogens in control of energy balance and glucose homeostasis. *Endocr. Rev.* **34**, 309–338 (2013).
57. Sung, H. *et al.* Global cancer statistics 2020: GLOBOCAN estimates of incidence and mortality worldwide for 36 cancers in 185 countries. *CA. Cancer J. Clin.* **71**, 209–249 (2021).
58. Hanahan, D. & Weinberg, R. A. Hallmarks of cancer: The next generation. *Cell* **144**, 646–674 (2011).
59. Yang, B., Fu, X., Shao, L., Ding, Y. & Zeng, D. Aberrant expression of SIRT3 is conversely correlated with the progression and prognosis of human gastric cancer. *Biochem. Biophys. Res. Commun.* **443**, 156–160 (2014).
60. Cui, Y. *et al.* SIRT3 enhances glycolysis and proliferation in SIRT3-expressing gastric cancer cells. *PLoS One* **10**, e0129834 (2015).
61. Li, H. *et al.* SIRT3 regulates cell proliferation and apoptosis related to energy metabolism in non-small cell lung cancer cells through deacetylation of NMNAT2. *Int. J. Oncol.* **43**, 1420–1430 (2013).
62. Xiao, K. *et al.* Sirt3 is a tumor suppressor in lung adenocarcinoma cells. *Oncol. Rep.* **30**, 1323–1328 (2013).
63. Ashraf, N. *et al.* Altered sirtuin expression is associated with node-positive breast cancer. *Br. J. Cancer* **95**, 1056–1061 (2006).
64. Desouki, M. M., Doubinskaia, I., Gius, D. & Abdulkadir, S. A. Decreased mitochondrial SIRT3 expression is a potential molecular biomarker associated with poor outcome in breast cancer. *Hum. Pathol.* **45**, 1071–1077 (2014).

65. Torrens-Mas, M., Pons, D. G., Sastre-Serra, J., Oliver, J. & Roca, P. SIRT3 silencing sensitizes breast cancer cells to cytotoxic treatments through an increment in ROS production. *J. Cell. Biochem.* **118**, 397–406 (2016).
66. Finley, L. W. S. *et al.* SIRT3 opposes reprogramming of cancer cell metabolism through HIF1 α destabilization. *Cancer Cell* **19**, 416–428 (2011).
67. Kim, H.-S. S. *et al.* SIRT3 is a mitochondria-localized tumor suppressor required for maintenance of mitochondrial integrity and metabolism during stress. *Cancer Cell* **17**, 41–52 (2010).
68. Shang, Y. Hormones and cancer. *Cell Res.* **17**, 277–279 (2007).
69. Folkerd, E. J. & Dowsett, M. Influence of sex hormones on cancer progression. *J. Clin. Oncol.* **28**, 4038–4044 (2010).
70. Holst, F. *et al.* Estrogen receptor alpha (ESR1) gene amplification is frequent in breast cancer. *Nat. Genet.* **39**, 655–660 (2007).
71. Felty, Q. & Roy, D. Estrogen, mitochondria, and growth of cancer and non-cancer cells. *J. Carcinog.* **4**, 1 (2005).
72. Gabriela, V., Arciuch, A., Elguero, M. E., Poderoso, J. J. & Carreras, M. C. Mitochondrial regulation of cell cycle and proliferation. *Antioxid. Redox Signal.* **16**, 1150–1180 (2012).
73. Salem, A. F., Whitaker-Menezes, D., Howell, A., Sotgia, F. & Lisanti, M. P. Mitochondrial biogenesis in epithelial cancer cells promotes breast cancer tumor growth and confers autophagy resistance. *Cell Cycle* **11**, 4174–4180 (2012).
74. Resseguie, E. A., Staversky, R. J., Brookes, P. S. & O'Reilly, M. A. Hyperoxia activates ATM independent from mitochondrial ROS and dysfunction. *Redox Biol.* **5**, 176–185 (2015).
75. Liu, Z.-J. & Velazquez, O. C. Hyperoxia, endothelial progenitor cell mobilization, and diabetic wound healing. *Antioxid. Redox Signal.* **10**, 1869–1882 (2008).
76. Kim, S. W. *et al.* Normobaric hyperoxia inhibits the progression of lung cancer by inducing apoptosis. *Exp. Biol. Med.* **243**, 739–748 (2018).
77. Stępień, K., Ostrowski, R. P. & Matyja, E. Hyperbaric oxygen as an adjunctive therapy

- in treatment of malignancies, including brain tumours. *Med. Oncol.* **33**, 101 (2016).
78. Aphale, R. & Shah, S. M. A randomised clinical trial to compare the efficacy of hyperbaric oxygen therapy with neoadjuvant chemotherapy with neoadjuvant chemotherapy alone for carcinoma breast: a pilot Study. *Indian J. Surg.* (2020). doi:10.1007/s12262-020-02601-4
 79. Cornier, M. A. *et al.* The metabolic syndrome. *Endocr. Rev.* **29**, 777–822 (2008).
 80. Bonomini, F., Rodella, L. F. & Rezzani, R. Metabolic syndrome, aging and involvement of oxidative stress. *Aging Dis.* **6**, 109–120 (2015).
 81. Enzi, G. *et al.* Subcutaneous and visceral fat distribution according to sex, age, and overweight, evaluated by computed tomography. *Am. J. Clin. Nutr.* **44**, 739–746 (1986).
 82. Lovejoy, J. C., Champagne, C. M., De Jonge, L., Xie, H. & Smith, S. R. Increased visceral fat and decreased energy expenditure during the menopausal transition. *Int. J. Obes.* **32**, 949–958 (2008).
 83. Tchoukalova, Y. D. *et al.* Subcutaneous adipocyte size and body fat distribution. *Am. J. Clin. Nutr.* **87**, 56–63 (2008).
 84. Yki-Järvinen, H. Sex and insulin sensitivity. *Metabolism* **33**, 1011–1015 (1984).
 85. Uranga, A. P., Levine, J. & Jensen, M. Isotope tracer measures of meal fatty acid metabolism: Reproducibility and effects of the menstrual cycle. *Am. J. Physiol. - Endocrinol. Metab.* **288**, 547–555 (2005).
 86. Varlamov, O., Bethea, C. L. & Roberts, C. T. Sex-specific differences in lipid and glucose metabolism. *Front. Endocrinol.* **5**, 241 (2015).
 87. Torres, M. J. *et al.* 17 β -Estradiol directly lowers mitochondrial membrane microviscosity and improves bioenergetic function in skeletal muscle. *Cell Metab.* **27**, 167–179 (2018).
 88. Bryzgalova, G. *et al.* Mechanisms of antidiabetogenic and body weight-lowering effects of estrogen in high-fat diet-fed mice. *Am. J. Physiol. - Endocrinol. Metab.* **295**, 904–912 (2008).
 89. Kakimoto, P. A. & Kowaltowski, A. J. Effects of high fat diets on rodent liver bioenergetics and oxidative imbalance. *Redox Biol.* **8**, 216–225 (2016).

90. Hirschey, M. D. *et al.* SIRT3 deficiency and mitochondrial protein hyperacetylation accelerate the development of the metabolic syndrome. *Mol. Cell* **44**, 177–190 (2011).
91. Qiu, X., Brown, K., Hirschey, M. D., Verdin, E. & Chen, D. Calorie restriction reduces oxidative stress by SIRT3-mediated SOD2 activation. *Cell Metab.* **12**, 662–667 (2010).
92. Nassir, F., Arndt, J. J., Johnson, S. A. & Ibdah, J. A. Regulation of mitochondrial trifunctional protein modulates nonalcoholic fatty liver disease in mice. *J. Lipid Res.* **59**, 967–973 (2018).
93. Chen, M. *et al.* SIRT3 deficiency promotes high-fat diet-induced nonalcoholic fatty liver disease in correlation with impaired intestinal permeability through gut microbial dysbiosis. *Mol. Nutr. Food Res.* **63**, 1800612 (2019).
94. Comşa, Ş., Cîmpean, A. M. & Raica, M. The story of MCF-7 breast cancer cell line: 40 years of experience in research. *Anticancer Res.* **35**, 3147–3154 (2015).
95. Moen, I. & Stuhr, L. E. B. Hyperbaric oxygen therapy and cancer - a review. *Target. Oncol.* **7**, 233–242 (2012).
96. Dai, S. H. *et al.* Sirt3 attenuates hydrogen peroxide-induced oxidative stress through the preservation of mitochondrial function in HT22 cells. *Int. J. Mol. Med.* **34**, 1159–1168 (2014).
97. Ceci, C., Atzori, M. G., Lacal, P. M. & Graziani, G. Role of VEGFs/VEGFR-1 signaling and its inhibition in modulating tumor invasion: Experimental evidence in different metastatic cancer models. *Int. J. Mol. Sci.* **21**, 1388 (2020).
98. Liu, C. Y., Lin, H. H., Tang, M. J. & Wang, Y. K. Vimentin contributes to epithelial-mesenchymal transition cancer cell mechanics by mediating cytoskeletal organization and focal adhesion maturation. *Oncotarget* **6**, 15966–15983 (2015).
99. Li, C., Wang, Q., Shen, S., Wei, X. & Li, G. Oridonin inhibits vegf-a-associated angiogenesis and epithelial-mesenchymal transition of breast cancer in vitro and in vivo. *Oncol. Lett.* **16**, 2289–2298 (2018).
100. Luo, M. *et al.* VEGF/NRP-1 axis promotes progression of breast cancer via enhancement of epithelial-mesenchymal transition and activation of NF- κ B and β -catenin. *Cancer Lett.* **373**, 1–11 (2016).

101. Zheng, J. Energy metabolism of cancer: Glycolysis versus oxidative phosphorylation (review). *Oncol. Lett.* **4**, 1151–1157 (2012).
102. Vellinga, T. T. *et al.* SIRT1/PGC1 α -dependent increase in oxidative phosphorylation supports chemotherapy resistance of colon cancer. *Clin. Cancer Res.* **21**, 2870–2879 (2015).
103. Fernandez-Marcos, P. J. & Auwerx, J. Regulation of PGC-1 α , a nodal regulator of mitochondrial biogenesis. *Am. J. Clin. Nutr.* **93**, 884S–890S (2011).
104. Zou, Z., Chang, H., Li, H. & Wang, S. Induction of reactive oxygen species: an emerging approach for cancer therapy. *Apoptosis* **22**, 1321–1335 (2017).
105. Sanchez-Alvarez, R. *et al.* Mitochondrial dysfunction in breast cancer cells prevents tumor growth: understanding chemoprevention with metformin. *Cell Cycle* **12**, 172–182 (2013).
106. Chiu, H. Y., Tay, E. X. Y., Ong, D. S. T. & Taneja, R. Mitochondrial dysfunction at the center of cancer Therapy. *Antioxid. Redox Signal.* **32**, 309–330 (2020).
107. Herrero, A. B., Rojas, E. A., Misiewicz-Krzeminska, I., Krzeminski, P. & Gutiérrez, N. C. Molecular mechanisms of p53 deregulation in cancer: an overview in multiple myeloma. *Int. J. Mol. Sci.* **17**, 2003 (2016).
108. Wang, S. *et al.* Cell-in-cell death is not restricted by caspase-3 deficiency in MCF-7 cells. *J. Breast Cancer* **19**, 231–241 (2016).
109. Granowitz, E. V. *et al.* Hyperbaric oxygen inhibits benign and malignant human mammary epithelial cell proliferation. *Anticancer Res.* **25**, 3833–3842 (2005).
110. Marinello, P. C. *et al.* Mechanism of metformin action in MCF-7 and MDA-MB-231 human breast cancer cells involves oxidative stress generation, DNA damage, and transforming growth factor β 1 induction. *Tumor Biol.* **37**, 5337–5346 (2016).
111. Hua, H., Zhang, H., Kong, Q. & Jiang, Y. Mechanisms for estrogen receptor expression in human cancer. *Exp. Hematol. Oncol.* **7**, 24 (2018).
112. Klinge, C. M. Estrogens regulate life and death in mitochondria. *J. Bioenerg. Biomembr.* **49**, 307–324 (2017).
113. Yang, W. *et al.* Mitochondrial sirtuin network reveals dynamic SIRT3-dependent

- deacetylation in response to membrane depolarization. *Cell* **167**, 985–1000 (2016).
114. Rai, Y. *et al.* Mitochondrial biogenesis and metabolic hyperactivation limits the application of MTT assay in the estimation of radiation induced growth inhibition. *Sci. Rep.* **8**, 1531 (2018).
 115. Oh, J. Y. *et al.* 17 β -Estradiol protects mesenchymal stem cells against high glucose-induced mitochondrial oxidants production via Nrf2/Sirt3/MnSOD signaling. *Free Radic. Biol. Med.* **130**, 328–342 (2019).
 116. Okoh, V. O. *et al.* Redox signalling to nuclear regulatory proteins by reactive oxygen species contributes to oestrogen-induced growth of breast cancer cells. *Br. J. Cancer* **112**, 1687–1702 (2015).
 117. Otto, A. M., Paddenbergh, R., Schubert, S. & Mannherz, H. G. Cell cycle arrest, micronucleus formation, and cell death in growth inhibition of MCF-7 breast cancer cells by tamoxifen and cisplatin. *J. Cancer Res. Clin. Oncol.* **122**, 603–612 (1996).
 118. Gasco, M., Shami, S. & Crook, T. The p53 pathway in breast cancer. *Breast Cancer Res.* **4**, 70–76 (2002).
 119. Liu, W. *et al.* Estrogen receptor- α binds p53 tumor suppressor protein directly and represses its function. *J. Biol. Chem.* **281**, 9837–9840 (2006).
 120. Beery, A. K. & Zucker, I. Sex bias in neuroscience and biomedical research. *Neurosci. Biobehav. Rev.* **35**, 565–572 (2011).
 121. Iwasa, T., Matsuzaki, T., Yano, K. & Irahara, M. The effects of ovariectomy and lifelong high-fat diet consumption on body weight, appetite, and lifespan in female rats. *Horm. Behav.* **97**, 25–30 (2018).
 122. Carr, M. C. The emergence of the metabolic syndrome with menopause. *J. Clin. Endocrinol. Metab.* **88**, 2404–2411 (2003).
 123. Salvoza, N. C., Giraudi, P. J., Tiribelli, C. & Rosso, N. Sex differences in non-alcoholic fatty liver disease: hints for future management of the disease. *Explor. Med.* **1**, 51–74 (2020).
 124. Cho, E.-H. SIRT3 as a regulator of non-alcoholic fatty liver disease. *J. Lifestyle Med.* **4**, 80–85 (2014).

125. Koebele, S. V. & Bimonte-Nelson, H. A. Modeling menopause: the utility of rodents in translational behavioral endocrinology research. *Maturitas* **87**, 5–17 (2016).
126. Riant, E. *et al.* Estrogens protect against high-fat diet-induced insulin resistance and glucose intolerance in mice. *Endocrinology* **150**, 2109–2117 (2009).
127. Pae, M., Baek, Y., Lee, S. & Wu, D. Loss of ovarian function in association with a high-fat diet promotes insulin resistance and disturbs adipose tissue immune homeostasis. *J. Nutr. Biochem.* **57**, 93–102 (2018).
128. Bader, J. *et al.* High-fat diet-fed ovariectomized mice are susceptible to accelerated subcutaneous tumor growth potentially through adipose tissue inflammation, local insulin-like growth factor release, and tumor associated macrophages. *Oncotarget* **11**, 4554–4569 (2020).
129. Muthusami, S. *et al.* Ovariectomy induces oxidative stress and impairs bone antioxidant system in adult rats. *Clin. Chim. Acta* **360**, 81–86 (2005).
130. Ganz, M., Csak, T. & Szabo, G. High fat diet feeding results in gender specific steatohepatitis and inflammasome activation. *World J. Gastroenterol.* **20**, 8525–8534 (2014).
131. Mauvais-Jarvis, F. Gender differences in glucose homeostasis and diabetes. *Physiol. Behav.* **187**, 20–23 (2018).
132. Hariri, N. & Thibault, L. High-fat diet-induced obesity in animal models. *Nutr. Res. Rev.* **23**, 270–299 (2010).
133. Biddinger, S. B. *et al.* Effects of diet and genetic background on sterol regulatory element-binding protein-1c, stearoyl-CoA desaturase 1, and the development of the metabolic syndrome. *Diabetes* **54**, 1314–1323 (2005).
134. Almind, K. & Kahn, C. R. Genetic determinants of energy expenditure and insulin resistance in diet-induced obesity in mice. *Diabetes* **53**, 3274–3285 (2004).
135. Asgharpour, A. *et al.* A diet-induced animal model of non-alcoholic fatty liver disease and hepatocellular cancer. *J. Hepatol.* **65**, 579–588 (2016).
136. Ussar, S. *et al.* Interactions between gut microbiota, host genetics and diet modulate the predisposition to obesity and metabolic syndrome. *Cell Metab.* **22**, 516–530 (2015).

137. Chen, T. *et al.* Mouse SIRT3 attenuates hypertrophy-related lipid accumulation in the heart through the deacetylation of LCAD. *PLoS One* **10**, e0118909 (2015).
138. Lantier, L. *et al.* SIRT3 is crucial for maintaining skeletal muscle insulin action and protects against severe insulin resistance in high-fat-fed mice. *Diabetes* **64**, 3081–3092 (2015).
139. Haas, J. T., Francque, S. & Staels, B. Pathophysiology and mechanisms of nonalcoholic fatty liver disease. *Annu. Rev. Physiol.* **78**, 181–205 (2016).
140. Zhong, F., Zhou, X., Xu, J. & Gao, L. Rodent models of nonalcoholic fatty liver disease. *Digestion* **101**, 522–535 (2020).
141. Yu, D. *et al.* High fat diet-induced oxidative stress blocks hepatocyte nuclear factor 4 α and leads to hepatic steatosis in mice. *J. Cell. Physiol.* **233**, 4770–4782 (2018).
142. Patsouris, D., Reddy, J. K., Müller, M. & Kersten, S. Peroxisome proliferator-activated receptor α mediates the effects of high-fat diet on hepatic gene expression. *Endocrinology* **147**, 1508–1516 (2006).
143. Inoue, M. *et al.* Increased expression of PPAR γ in high fat diet-induced liver steatosis in mice. *Biochem. Biophys. Res. Commun.* **336**, 215–222 (2005).
144. Waxman, D. J. & Holloway, M. G. Sex differences in the expression of hepatic drug metabolizing enzymes. *Mol. Pharmacol.* **76**, 215–228 (2009).
145. Leclercq, I. A. *et al.* CYP2E1 and CYP4A as microsomal catalysts of lipid peroxides in murine nonalcoholic steatohepatitis. *J. Clin. Invest.* **105**, 1067–1075 (2000).
146. Osabe, M. *et al.* Expression of hepatic UDP-glucuronosyltransferase 1A1 and 1A6 correlated with increased expression of the nuclear constitutive androstane receptor and peroxisome proliferator-activated receptor α in male rats fed a high-fat and high-sucrose diet. *Drug Metab. Dispos.* **36**, 294–302 (2008).
147. Abdelmegeed, M. A. *et al.* Critical role of cytochrome P450 2E1 (CYP2E1) in the development of high fat-induced non-alcoholic steatohepatitis. *J. Hepatol.* **57**, 860–866 (2012).
148. Zhang, X. *et al.* Ablation of cytochrome P450 omega-hydroxylase 4A14 gene attenuates hepatic steatosis and fibrosis. *Proc. Natl. Acad. Sci. U. S. A.* **114**, 3181–3185 (2017).

149. Leung, T. M. & Nieto, N. CYP2E1 and oxidant stress in alcoholic and non-alcoholic fatty liver disease. *J. Hepatol.* **58**, 395–398 (2013).
150. Nan, Y. *et al.* Heme oxygenase-1 prevents non-alcoholic steatohepatitis through suppressing hepatocyte apoptosis in mice. *Lipids Health Dis.* **9**, 124 (2010).
151. Kander, M. C., Cui, Y. & Liu, Z. Gender difference in oxidative stress: a new look at the mechanisms for cardiovascular diseases. *J. Cell. Mol. Med.* **21**, 1024–1032 (2017).
152. Kamalvand, G., Pinard, G. & Ali-Khan, Z. Heme-oxygenase-1 response, a marker of oxidative stress, in a mouse model of AA amyloidosis. *Amyloid* **10**, 151–159 (2003).
153. Chen, Q. *et al.* Oxidative stress mediated by lipid metabolism contributes to high glucose-induced senescence in retinal pigment epithelium. *Free Radic. Biol. Med.* **130**, 48–58 (2019).
154. Kong, X. *et al.* Sirtuin 3, a new target of PGC-1 α , plays an important role in the suppression of ROS and mitochondrial biogenesis. *PLoS One* **5**, e11707 (2010).
155. Liu, J. *et al.* SIRT3 protects hepatocytes from oxidative injury by enhancing ROS scavenging and mitochondrial integrity. *Cell Death Dis.* **8**, e3158 (2017).
156. Zheng, J. *et al.* Sirt3 ameliorates oxidative stress and mitochondrial dysfunction after intracerebral hemorrhage in diabetic rats. *Front. Neurosci.* **12**, 414 (2018).
157. Bhatti, J. S., Bhatti, G. K. & Reddy, P. H. Mitochondrial dysfunction and oxidative stress in metabolic disorders — A step towards mitochondria based therapeutic strategies. *Biochim. Biophys. Acta - Mol. Basis Dis.* **1863**, 1066–1077 (2017).
158. Rolo, A. P., Teodoro, J. S. & Palmeira, C. M. Role of oxidative stress in the pathogenesis of nonalcoholic steatohepatitis. *Free Radic. Biol. Med.* **52**, 59–69 (2012).
159. Aon, M. A., Bhatt, N. & Cortassa, S. Mitochondrial and cellular mechanisms for managing lipid excess. *Front. Physiol.* **31**, 282 (2014).
160. Tyagi, A. *et al.* SIRT3 deficiency-induced mitochondrial dysfunction and inflammasome formation in the brain. *Sci. Rep.* **8**, 17547 (2018).
161. Hoeks, J. *et al.* Mitochondrial function, content and ROS production in rat skeletal muscle: Effect of high-fat feeding. *FEBS Lett.* **582**, 510–516 (2008).
162. Turner, N. *et al.* Excess lipid availability increases mitochondrial fatty acid oxidative

- capacity in muscle. *Diabetes* **56**, 2085–2092 (2007).
163. Bonnard, C. *et al.* Mitochondrial dysfunction results from oxidative stress in the skeletal muscle of diet-induced insulin-resistant mice. *J. Clin. Invest.* **118**, 789–800 (2008).
164. Cruz, M. M. *et al.* Palmitoleic acid (16:1n7) increases oxygen consumption, fatty acid oxidation and ATP content in white adipocytes. *Lipids Health Dis.* **17**, 55 (2018).

CURRICULUM VITAE

Marija Pinterić was born in Rijeka (Croatia) on the 8th July 1989 where she finished elementary school and Gymnasium Andrija Mohorovičić. She graduated from the Department of Biology, Faculty of Science, University of Zagreb in 2014 and obtained a Master's degree in Molecular Biology. During her studies, she was a student assistant at the Division of Animal Physiology and participated in science dissemination activities.

After finishing her Master's, she worked for two years in the Microbiology laboratory in the pharmaceutical company Jadran Galenski Laboratorij. Since 2017, she has been employed as an assistant in the Laboratory for mitochondrial bioenergetics and diabetes of the Division of Molecular Medicine at the Ruđer Bošković Institute. In November 2017 she enrolled in the postgraduate doctoral programme in Biology at the Department of Biology, Faculty of Science, University of Zagreb.

Marija Pinterić published six peer-reviewed scientific articles in journals cited by the SCI database, five as the first author. She was awarded five different grants and participated in numerous national and international conferences, meetings and workshops, as well as in science dissemination activities. She is an active member of several international and national scientific organizations and a member of the board for young scientists of the Croatian Society of Biochemistry and Molecular Biology (HDBMB).



De novo expression of transfected sirtuin 3 enhances susceptibility of human MCF-7 breast cancer cells to hyperoxia treatment

Marija Pinterić, Iva I. Podgorski, Sandra Sobočanec, Marijana Popović Hadžija, Mladen Paradžik, Ana Dekanić, Maja Marinović, Mirna Halasz, Robert Belužić, Grazia Davidović, Andreja Ambriović Ristov & Tihomir Balog

To cite this article: Marija Pinterić, Iva I. Podgorski, Sandra Sobočanec, Marijana Popović Hadžija, Mladen Paradžik, Ana Dekanić, Maja Marinović, Mirna Halasz, Robert Belužić, Grazia Davidović, Andreja Ambriović Ristov & Tihomir Balog (2018): De novo expression of transfected sirtuin 3 enhances susceptibility of human MCF-7 breast cancer cells to hyperoxia treatment, Free Radical Research, DOI: [10.1080/10715762.2018.1462495](https://doi.org/10.1080/10715762.2018.1462495)

To link to this article: <https://doi.org/10.1080/10715762.2018.1462495>



Published online: 23 Apr 2018.



Submit your article to this journal [↗](#)



View related articles [↗](#)



View Crossmark data [↗](#)

ORIGINAL ARTICLE



De novo expression of transfected sirtuin 3 enhances susceptibility of human MCF-7 breast cancer cells to hyperoxia treatment

Marija Pinterić*, Iva I. Podgorski*, Sandra Sobočanec*, Marijana Popović Hadžija, Mladen Paradžik, Ana Dekanić, Maja Marinović, Mirna Halasz, Robert Belužić, Grazia Davidović, Andreja Ambriović Ristov and Tihomir Balog

Division of Molecular Medicine, Ruđer Bošković Institute, Zagreb, Croatia

ABSTRACT

Sirtuin 3 (Sirt3) has a promising role in cancer tumourigenesis and treatment, but there have been controversies about its role as oncogene or tumour suppressor in different types of cancer. Changes in its expression are associated with the excessive production of reactive oxygen species (ROS), thus contributing to mitochondrial dysfunction and age-related pathologies. Hyperoxic treatment (i.e. generator of ROS) was shown to support some tumourigenic properties, but finally suppresses growth of certain mammary carcinoma cells. Due to strikingly reduced Sirt3 level in many breast cancer cell lines, we aimed to clarify the effect of *de novo* Sirt3 expression upon hyperoxic treatment in the human MCF-7 breast cancer cells. *De novo* expression of Sirt3 decreased metabolic activity and cellular growth of MCF-7 cells, reduced expression of proangiogenic and epithelial mesenchymal transition genes, induced metabolic switch from glycolysis to oxidative phosphorylation, and decreased abundance of senescent cells. These effects were enhanced upon hyperoxic treatment: induction of DNA damage and upregulation of p53, with an increase of ROS levels followed by mitochondrial and antioxidant dysfunction, resulted in additional reduction of metabolic activity and inhibition of cellular growth and survival. The mitigation of tumorigenic properties and enhancement of the susceptibility of the MCF-7 breast cancer cells to the hyperoxic treatment upon *de novo* Sirt3 expression indicates that these factors, individually and in combination, should be further explored *in vitro* and particularly *in vivo*, as an adjuvant tumour therapy in breast cancer malignancies.

ARTICLE HISTORY

Received 20 February 2018
Revised 26 March 2018
Accepted 4 April 2018



KEYWORDS

Hyperoxia; MCF-7;
mitochondrial function;
ROS; sirtuin 3

Introduction

Sirtuin 3 (Sirt3) is a major mitochondrial NAD⁺-dependent deacetylase that plays critical role in activation of mitochondrial proteins involved in energy metabolism, ATP production and mitochondrial biogenesis [1]. Longer, enzymatically inactive form of Sirt3 (44 kDa) is imported into mitochondria by the N-terminal mitochondrial localisation sequence (MLS). Following the import, the MLS is proteolytically cleaved, resulting in catalytically active, short form of Sirt3 (28 kDa) which is able to deacetylate target mitochondrial proteins [2]. Sirt3 is the only member of sirtuin family that is linked with prolonged lifespan. Therefore, the control of enzymes involved in energy metabolism by Sirt3 is in accordance with the overall protection against pathological conditions and aging itself [3]. However, there have been controversies about the role of Sirt3 in different types of cancer [4].

Cancer cells exhibit prominent genetic, metabolic and bioenergetic differences when compared to normal cells: high rate of glycolysis, lactate production along with the absence of respiration, despite the presence of oxygen thus characterising the phenomenon known as Warburg effect [5]. Because of rapid proliferation, cancer cells quickly exhaust nutrients and oxygen supply, making tumour microenvironment hypoxic. Under hypoxia, tumour's surroundings become acidic as a result of increased lactate production and excretion, thus contributing to the malignant phenotype of the cancer [6]. However, although tumour cells often live in hypoxic conditions due to metabolic and structural abnormalities, their angiogenesis, growth and survival depend on the sufficient supply of oxygen and nutrients. Therefore, one would expect that enhanced oxygenation (hyperoxia) would act as a tumour-promoting effect. On the other hand, several reports demonstrate growth

CONTACT Tihomir Balog,  tihomir.balog@irb.hr  Division of Molecular Medicine, Ruđer Bošković Institute, Zagreb, Croatia

*These authors contributed equally to this work.

suppression of mammary carcinoma cells upon hyperoxic treatment [7], thus pointing out the therapeutic effect of hyperoxia on tumour growth and proliferation.

The excessive production of reactive oxygen species (ROS) leads to oxidative stress, a crucial event that contributes to mitochondrial dysfunction and age-related pathologies [8]. It has been shown that irregular ROS production or scavenging is associated with changes in Sirt3 expression [9]. Recent data report the association between Sirt3 levels and cancer progression, with either oncogenic or tumour-suppressive role of Sirt3 in cancer [4,10]. Several studies described a prosurvival role of Sirt3 in certain cancer cell lines, thus supporting its oncogenic role in cancer, although the exact mechanism by which Sirt3 exerts its action is not fully understood. On the other hand, Sirt3 is recognised as a fidelity protein that repairs cellular molecules and is involved in metabolic reprogramming of some breast cancer cell lines towards oxidative phosphorylation (OXPHOS) [11], and as such may be considered as a tumour suppressor. Therefore, the loss of function of Sirt3 may contribute to a more aggressive phenotype in some types of cancers [1].

Although hyperoxic treatment is clinically important for treatment of hypoxia, it is known that exposure to the increased oxygen concentrations causes impaired energy metabolism that results in dysfunction of normal cells [12]. Since hypoxia is a hallmark of various tumours, we hypothesised that hyperoxia would have negative impact on cancer cells, thus providing therapeutic strategy against their tumourigenic properties. In addition, considering tumour suppressive role of Sirt3 in carcinogenesis, we hypothesised that Sirt3 expression would also negatively impact the cancerous cells, especially in combination with hyperoxic treatment.

Breast cancer is the most frequent cancer among women, and ranks as the fifth cause of cancer death worldwide [13]. Sirtuin family of genes shows differential expressions in breast cancer cells, which is often different from the expression in the breast cancer tissues [14]. Since breast cancer cells have strikingly reduced Sirt3 level, and even 20% of them have almost no detectable Sirt3 protein [15], we wanted to examine the effect of *de novo* Sirt3 expression upon hyperoxic treatment in human MCF-7 breast cancer cells model. This setting of *de novo* expression is advantageous because it is the only changing factor in the control and transfected cells under the same treatment, thus providing a model which avoids any possible phenotypic distinctions in the cells caused by other factors.

Therefore, in this study, we have developed human MCF-7 breast cancer cells transfectants expressing the Sirt3 protein in order to test its potential in affecting

the response of these cells upon the hyperoxic treatment, i.e. to clarify whether it sensitises or makes these cancer cells more resistant to oxidative stress.

Materials and methods

Cell lines, plasmids and transfection

MCF-7 cell line, obtained from the ECACC (Cat. no. 86012803, Public Health England), was grown in Dulbecco's Modified Eagle Medium with high glucose (DMEM, Sigma Aldrich, St. Louis, MO) with 10% foetal bovine serum (FBS, Invitrogen/Life Technologies, Carlsbad, CA), 2 mM L-glutamine (Sigma Aldrich, St. Louis, MO), 1% nonessential amino acids and antibiotic/antimycotic solution GA-1000 (Lonza, Allendale, NJ), at 37 °C with 5% CO₂ in a humidified atmosphere. pcDNA3.1+ plasmid with Flag-tagged Sirt3 (Cat. no. 13814), purchased from Addgene, Cambridge, MA [16], was amplified in *Escherichia coli* strain dh5 α and purified with PureYield™ Plasmid Midiprep System (Promega, Madison, WI) according to the manufacturer's protocol. pcDNA3.1+ (given by courtesy of dr.sc. Grbeša) was used as a control plasmid. The MCF-7 cells were transfected with the Flag-tagged Sirt3 or empty pcDNA3.1+ plasmid using Lipofectamine 2000 (Thermo Fisher Scientific, Waltham, MA), according to the manufacturer's protocol. In brief, 1.5×10^5 cells were seeded on 24-well plate in growth medium and 24 h later transfected and incubated for additional 24 h. The cells were then split into selective growth medium containing 200- μ g/ml G418 antibiotic (Sigma Aldrich, St. Louis, MO). Colonies of stable Sirt3 transfectants were selected, expanded in the growth media containing G418 antibiotic, and cryogenically stored at -80 °C.

Normoxic and hyperoxic conditions

Cells were exposed to hyperoxia (95% O₂) for 44 h in a gas-tight modular incubator chamber (StemCell™ Technology Inc, Vancouver, BC, Canada) at 37 °C in order to establish hyperoxia-treated groups, while the normoxic groups were exposed to normal growth conditions.

Immunofluorescence and confocal microscopy

Immunofluorescence analysis was performed as described previously [17]. In brief, cells were labelled with 200 nM MitoTracker Deep Red (Thermo Fisher Scientific, Waltham, MA), fixed with 2% paraformaldehyde, incubated with anti-Sirt3 primary monoclonal antibody (dilution 1:100, Santa Cruz Technologies, Santa

Cruz, CA), followed by FITC-labeled Goat anti-mouse IgG secondary antibody (dilution 1:100, Proteintech, Chicago, IL). Dapi (4,6-diamidino-2-phenylindol, Sigma Aldrich, St. Louis, MO) was used for nuclear staining. Confocal imaging was performed by sequential scanning using Leica TCS SP8 X laser scanning microscope (Leica Microsystems, Wetzlar, Germany), equipped with a HC PL APO CS2 63×/1.40 oil immersion objective and a white light laser (Leica Microsystems, Wetzlar, Germany). The excitation wavelengths and emission detection ranges used were 405 nm and 420–477 nm for DAPI, 490 nm and 500–600 nm for FITC, 644 nm and 665–780 nm for MitoTracker Deep Red.

RNA isolation, reverse transcription and qPCR analysis

Total RNA was isolated from 10^6 cells using Trizol reagent (Invitrogen, Carlsbad, CA) according to the manufacturer's instructions. Relative gene expression of *sirt3*, *sirt1*, superoxide dismutase two (*sod2*), catalase (*cat*), mitochondrial NADH dehydrogenase subunit 1 (*mtND1*), vascular endothelial growth factor A (*vegfa*), vascular endothelial growth factor receptor 1 (*vegfr1*), *vimentin* and *slug* were quantified by reverse transcription of total RNA and real-time quantitative PCR (qPCR) analysis as described previously [18]. Assays and primers used in this study are listed in Table 1. Data were analysed using the $2^{-\Delta\Delta Ct}$ method and presented as the fold-change in gene expression normalised to endogenous reference gene (β -actin) and relative to the control. All reactions were carried out in triplicate.

SDS-PAGE and western blot analysis

For western blot analysis, proteins were isolated using Trizol reagent (Invitrogen, Carlsbad, CA) according to the manufacturer's instructions. Protein pellets were dissolved in 1% SDS in the presence of protease inhibitors (Roche, Pasadena, CA). Total cellular proteins (20 μ g per lane) were resolved by SDS-PAGE and transferred onto a PVDF membrane (Bio-Rad, Hercules, CA). Membranes were blocked in 5% non-fat dry milk in TN buffer (50 mM TRIS, 150 mM NaCl, pH 7.4) for 1 h at 37 °C and incubated overnight at 4 °C with primary polyclonal or monoclonal antibodies, followed by incubation with a horseradish peroxidase-conjugated secondary antibody for 1 h at room temperature. Primary and secondary antibodies used in this study are listed in Table 2. To confirm equal loading and normalise the bands, AmidoBlack (Sigma Aldrich, St. Louis, MO) was used. The chemiluminescence signals were detected and

Table 1. Assays and primers used for real time quantitative PCR analyses.

Gene	Assay ID ^a /primers ^b	Product size (bp)
β -actin	Hs01060665_g1	63
<i>mtND1</i>	Hs02596873_s1	143
<i>sod2</i>	Hs01553554_m1	69
<i>cat</i>	Hs00156308_m1	68
<i>sirt1</i>	Hs01009005_m1	94
<i>sirt3</i>	Hs00953477_m1	83
<i>vegfa</i>	Hs00900058_m1	81
<i>vegfr1</i>	Hs01052936_m1	72
<i>vimentin</i>	5'-CGTGATGCTGAGAAGTTTCGTTGA-3' 5'-CCAACTTTTCCTCCCTGAACC-3	142
<i>slug</i>	5'-GAGGAGAAAATGCCTTTG-3' 5'-ATGAGCAATCTGGCTGCT-3'	119

^aTaqman[®] Applied Biosystems, Cheshire, UK.

^bPower SYBR[™] Green PCR Master Mix, Applied Biosystems, Cheshire, UK.

Table 2. Primary and secondary antibodies used for Western blot analyses.

	Dilution	Manufacturer
Primary antibody		
Anti-Sirt3	1:400	Cell Signaling Technology, Boston, MA
Anti-LdhA	1:200	Santa Cruz Biotechnology, Santa Cruz, CA
Anti-Sod2	1:2000	Abcam, Cambridge, UK
Anti-Sirt1	1:300	Santa Cruz Biotechnology, Santa Cruz, CA
Anti-PGC1 α	1:1000	Novus Biologicals, Littleton, CO
Anti-Cat	1:500	Abcam, Cambridge, UK
Anti-gammaH2AX	1:2000	Abcam, Cambridge, UK
Anti-p53 (DO-1)	1:2000	Santa Cruz Biotechnology, Santa Cruz, CA
Secondary antibody		
Anti- rabbit IgG HRP linked	1:4000	GE Healthcare, Chalfont St Giles, UK
Antimouse IgG HRP linked	1:2000	Santa Cruz Biotechnology, Santa Cruz, CA

analysed with the Alliance 4.7 Imaging System (UVITEC, Cambridge, UK).

MTT, growth curves and CFU assays

For the MTT assay, 7×10^3 cells were seeded in 96-well plate and 24 h later treated with hyperoxia. After that, growth medium was removed and $1 \times$ MTT was added and cells were incubated for 4 h in the growth conditions, followed by addition of dimethyl sulphoxide and 20-min incubation with gentle mixing. The absorbance was measured at $\lambda = 570$ nm on ELISA microplate reader (LabSystem Multiskan MS, Artisan Technology Group, Champaign, IL). The same assay was used for determination of cellular growth after 7 d of growing in high-glucose medium in normoxic conditions. For the CFU assay, 2×10^3 cells were seeded in 5-cm Petri dishes and 24 h later treated with hyperoxia. After that, the growth medium was replaced with new one and the

cells were incubated for 14 d until the visible colonies were observed. Cells were fixed with methanol for 10 min, followed by 30 min drying at room temperature. Giemsa dye was added and incubated for 30 min, washed by reH₂O and cells were dried. Colonies were counted and the cell viability was determined in comparison with the control cells from normoxia.

Flow cytometry

Flow cytometry was performed using a Becton Dickinson FACSCalibur model equipped with a 488-nm argon laser and a 635-nm red diode laser. Cytoplasmic ROS production was measured with 2',7'-dichlorofluorescein diacetate (H2DCFDA, Sigma Aldrich, St. Louis, MO), mitochondrial superoxide production with MitoSOX Red reagent (Thermo Fisher Scientific, Waltham, MA), variations in the mitochondrial transmembrane potential ($\Delta\Psi$ m) with 3,3'-dihexyloxycarbocyanine iodide (DiOC(6(3))), Enzo Life Science, East Farmingdale, NY SAD), and 10-N-nonyl acridine orange (NAO, Invitrogen, Carlsbad, CA, SAD) was used for measurement of mitochondrial mass. In a 6 well plate, 1.5×10^5 cells were seeded and 24 h later treated with hyperoxia. After that, cells were washed with PBS and incubated with specific dye prepared in the growth medium (40 nM DiOC(6(3))), 50 nM NAO, 5 μ M H2DCFDA and 3 μ M MitoSOX Red) for 30 min in the growth conditions. Cells were washed, collected in PBS, and minimum of 10,000 events were acquired. For discrimination of dead cells, propidium iodide (10 μ M) was used. The collected data were analysed using FCS Express software version 3 (SPSS, Chicago, IL).

Determination of mtDNA/nDNA ratio

Total DNA was isolated from MCF-7 cell culture pellets containing $2\text{--}5 \times 10^5$ cells, using AccuPrepR Genomic DNA extraction kit (Bioneer, Inc, Alameda, CA), following the manufacturer's protocol. DNA samples were fragmented to approximately 1000 bp in size by using Bioruptor[®] sonication system (Diagenode, Liège, Belgium). Mitochondrial DNA (mtDNA) copy number was determined by qPCR of the mitochondrial *mtND1* gene relative to the nuclear β -actin housekeeping gene (Taqman[®] Gene Expression Assays, Applied Biosystems, Cheshire, UK; nDNA). The standard mode thermal cycling conditions were used on ABI PRISM Sequence Analyzer 7300 (Applied Biosystems, Cheshire, UK). All experiments were repeated in at least three independent biological replicates. MtDNA copy number was determined for each sample using mtDNA/nDNA ratio. Average C_T values were calculated from technical

replicates for both mtDNA and nDNA. Relative mtDNA content was calculated as described previously [19], using the formula: $2 \times 2^{(\Delta C_T)}$, where ΔC_T equalled the difference between β -actin gene and *mtnd1* gene C_T values (nDNA C_T – mtDNA C_T).

Mitochondrial oxygen consumption

Oxygen consumption by the cells (10^7 cells from each clone in respiration buffer: 20 mM HEPES pH = 7.4, 10 mM MgCl₂ and 250 mM sucrose dissolved in reH₂O) was determined polarographically by the Clark type electrode (Oxygraph, Hansatech, Norfolk, UK) in an airtight 1.5 ml chamber at 35 °C. After measurement of basal state respiration, the complex III inhibitor antimycin A (2.5 μ M) was added to inhibit the cellular respiration. Oxygen consumption was calculated in pmol/min/ 10^6 cells and normalised to the normoxic control group.

Senescence-associated beta-galactosidase (SA- β -Gal) activity assay

Cells (4×10^5 cells per well) were seeded into 24-well plate and 24 h later treated with hyperoxia. After that, SA- β -Gal staining was performed: cells were fixed for 10 min in 1% glutaraldehyde in DMEM, washed twice with PBS and incubated at 37 °C with X-gal (1 mg/ml), dissolved and incubated for 16 h in a solution containing 40 mM citric acid/Na phosphate buffer pH 6.0, 5-mM potassium ferrocyanide, 5-mM potassium ferricyanide, 150 mM NaCl and 2 mM MgCl₂. Senescent cells were evaluated using an Olympus 1 \times 50 microscope (Olympus, Tokyo, Japan) under a \times 20 lens. Cells were photographed and the percentage of SA- β -Gal-positive cells was calculated.

Statistical analysis

Statistical analysis of data was performed using R v2.15.3 (CRAN) and RStudio for Windows, v1.1.423 [20]. Before all analyses, samples were tested for normality of distribution using Shapiro–Wilk test. Since all experiments data followed normal distribution, parametric tests for multiple comparisons of the samples were performed: two-way ANOVA was used for all analyses.

Results

Characterisation of stable Sirt3 overexpressing MCF-7 clones in normoxia and hyperoxia

Given the fact that breast cancer cell line MCF-7 has reduced expression of Sirt3, which was shown to act as

either tumour suppressor or a tumour promotor in different types of cancer [4], we have generated stable Sirt3 overexpressing clones to explore its role in this cell model. Briefly, MCF-7 cells were stably transfected with empty pcDNA3.1+ plasmid or pcDNA3.1+ plasmid with Flag-tagged Sirt3, and were labelled as MCF-7C or MCF-7S3, respectively. Stable expression of catalytically active Sirt3 (28 kDa) in MCF-7S3 was determined with qPCR and western blot analysis. qPCR analysis showed 23-fold increase in Sirt3 gene expression level in MCF-7S3 compared with MCF-7C, and 43-fold increase in hyperoxia (Figure 1(A)). Western blot analysis confirmed that the specific signal for Sirt3 protein was absent from MCF-7C, while MCF-7S3 expressed high levels of Sirt3 equivalent to molecular weight of 28 kDa, as detected by anti-Sirt3 monoclonal antibody, and this expression was additionally increased upon hyperoxia (Figure 1(B,C)).

De novo Sirt3 expression is enriched upon hyperoxia and colocalises with mitochondria

Next we wanted to determine the expression and localisation of Sirt3 protein in MCF-7C and MCF-7S3 cells. No signal for Sirt3 was detected in MCF-7C, whereas clear signal was observed in MCF-7S3, and was even stronger upon hyperoxic treatment. These results confirm *de novo* expression of Sirt3 protein in MCF-7S3 cells, as expected, in both normoxia and hyperoxia, with stronger signal per cell in hyperoxia-treated cells (Figure 1(D,E)). Next, we wanted to analyse whether Sirt3 might be localised in mitochondria. The confocal microscopy analysis of Sirt3 (green) and costaining with MitoTracker Deep Red, which specifically dyes mitochondria (red), revealed overlapping of the two signals (yellow) confirming localisation of Sirt3 in mitochondria. Also, we found that hyperoxia induced mitochondrial signal intensity in both clones. These data demonstrate that hyperoxia induced increase in

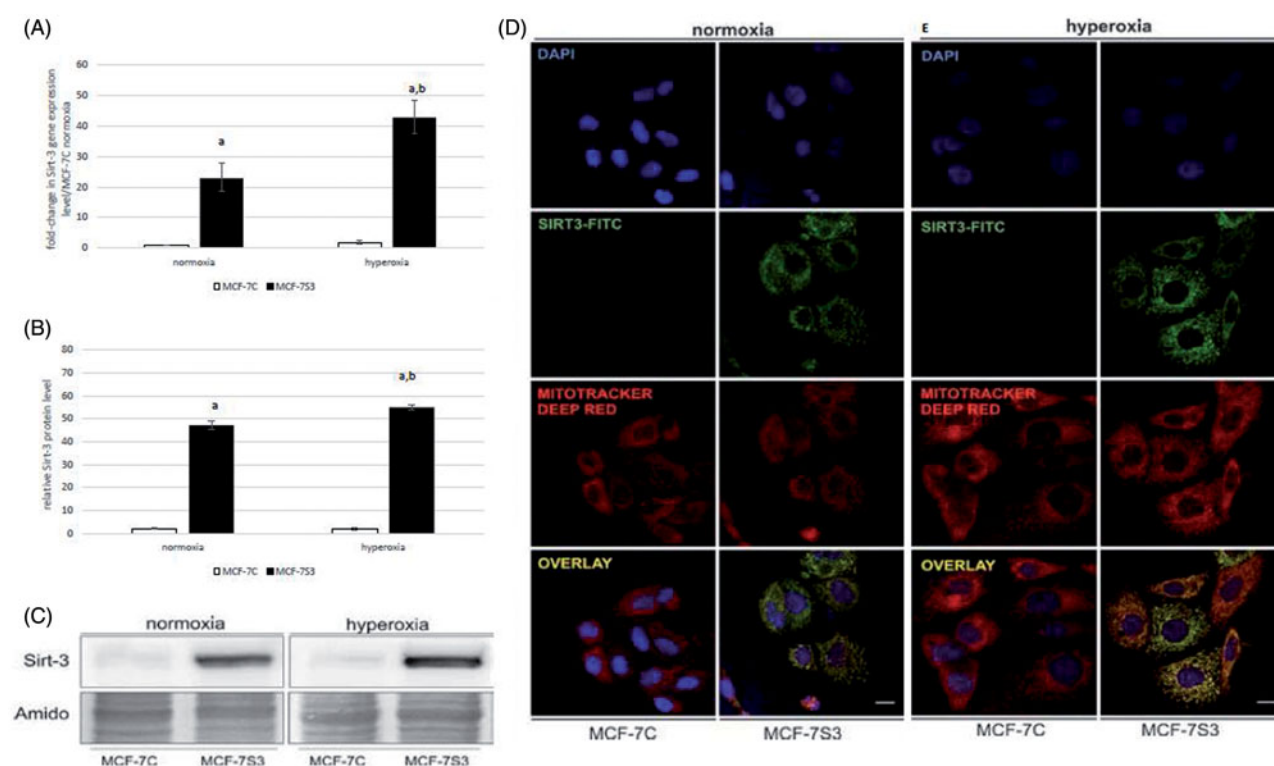


Figure 1. Characterisation of MCF-7C and MCF-7S3 cells. (A) Real-time qPCR analysis of sirt3 gene expression level in MCF-7C and MCF-7S3 cells in normoxia and hyperoxia. Significant increase in sirt3 expression was observed in normoxia (^a $p < .001$), hyperoxia (^b $p < .001$), and upon the interaction of sirt3 expression and hyperoxia ($p = .015$). The results are presented as fold-change \pm S.E., and normalized to control group. The fold-change in gene expression was calculated using the $2^{-\Delta\Delta CT}$ method. β -actin was used as the endogenous control. Experiments were repeated at least three times and representative data are shown. (B) Densitometry analysis of Sirt3 protein expression level in MCF-7C and MCF-7S3 cells in normoxia and hyperoxia. Data are presented as mean \pm S.D. Significant increase in Sirt3 expression was observed in normoxia (^a $p < .001$), hyperoxia (^b $p < .01$), and upon the interaction of Sirt3 expression and hyperoxia ($p = .008$). (C) Immunoblots of Sirt3 protein expression level. Amidoblack was used as a loading control. The experiments were repeated at least three times and representative blots are shown. (D,E) Sirt3 colocalizes with mitochondria and is enriched upon hyperoxia. Confocal image analysis of MCF-7 clones in normoxia and hyperoxia. Representative confocal image analysis of Sirt3 localization in normoxia and hyperoxia (Sirt3-FITC). Mitochondria and nuclei were detected with Mitotracker Deep Red or DAPI, respectively. Overlay image shows complete overlap of two staining patterns: fluorescence from the Sirt3 -FITC protein and fluorescence from the Mitotracker Deep Red stained mitochondria.

mitochondrial content in both clones, whereas the Sirt3 expression was increased exclusively in clone with *de novo* Sirt3 expression.

De novo Sirt3 expression enhances downregulation of proangiogenic and cancer-malignancy-related genes and proteins upon hyperoxic treatment

To assess the mechanism by which Sirt3 and hyperoxia influence tumorigenic characteristics and potential of MCF-7 cells, we surveyed the expression of genes involved in antioxidant protection (*sod2*, *cat*), metabolic regulation (*sirt1*), mitochondrial electron transfer (*mtND1*), angiogenesis (*vegfa* and *vegfr1*) and epithelial mesenchymal transition (EMT; *vimentin* and *slug*) (Figure 2(A)). We found that *de novo* Sirt3 expression in normoxia downregulated proangiogenic gene *vegfr1* involved in cell proliferation with having no effect on the expression of *vegfa*. In addition, strong downregulation of EMT markers – *vimentin* and *slug*, compared with control clones, was also observed. Hyperoxia induced proangiogenic genes (*vegfa*, *vimentin*) and *mtND1*, while having no significant effect on other genes. Interaction of *de novo* expressed Sirt3 and hyperoxia downregulated antioxidant defence genes *sod2* and *cat*, along with *sirt1*. In addition, *slug* and *vegfr1* were decreased as well. These results collectively demonstrate that suppressive effect of Sirt3 on proangiogenic and cancer-malignancy-related genes in normoxia is enhanced upon hyperoxic exposure.

Next we wanted to explore if this pattern of regulation was followed by changes in the expression of proteins involved in these processes. Therefore, we tested the expression of proteins involved in glycolysis (lactate dehydrogenase A; LdhA), antioxidant defense (Sod2 and Cat), cellular homeostasis (Sirt1) and mitochondrial biogenesis (peroxisome proliferator-activated receptor gamma coactivator 1-alpha; PGC1 α) of MCF-7 cells. LdhA, a marker of aerobic glycolysis, which is considered to be a key enzyme to glycolytic phenotype of tumor cells, was downregulated in MCF-7S3 cells. Hyperoxia significantly upregulated LdhA expression in MCF-7C compared with their normoxic group, while interaction of Sirt3 and hyperoxia abrogated this effect. Sod2 and Cat showed similar pattern of expression: the expression was reduced in MCF-7S3 cells, additionally reduced in hyperoxia, and almost completely absent in hyperoxic MCF-7S3 cells. Hyperoxia lowered Sirt1 level, regardless of Sirt3 expression. PGC1 α expression was markedly increased in MCF-7S3 cells, but reduced in hyperoxic MCF-7C, whereas interaction of hyperoxia and Sirt3 partially rescued its expression. Since hyperoxia is known to induce DNA

damage, we wanted to check the expression of a marker of DNA double strand breaks – phosphorylated gamma-H2A histone family, member X (p γ H2AX) and a major tumour suppressor, p53. In normoxic MCF-7C cells, the p γ H2AX was absent, whereas the expression of p53 was weak, but slightly increased upon Sirt3 expression. As expected, hyperoxia induced both p γ H2AX and p53, thus showing a clear sign of ROS-induced DNA damage which was even more pronounced upon interaction of Sirt3 and hyperoxia. These results collectively suggest that Sirt3 and hyperoxia may act in favour of the inhibiting the proliferation of cancer cells (Figure 2(B–I)).

De novo Sirt3 expression and hyperoxia decrease proliferation rate and metabolic activity of MCF-7 cells

Since we found that some of the proliferation and angiogenic factors crucial for tumorigenicity were downregulated upon *de novo* expression of Sirt3, we decided to test whether it plays a role in metabolic activity and proliferative potential (growth curve, clonogenic survival) of MCF-7 cells. The growth curve in normoxic conditions showed that MCF-7S3 cells grow more slowly than their corresponding controls (Figure 3(A)). MTT test showed that MCF-7S3 cells had small, but significantly decreased metabolic activity (88% of MCF-7C) (Figure 3(B)). Hyperoxia additionally decreased metabolic activity in both groups irrespective of Sirt3 expression. The drop in metabolic activity in normoxic MCF-7S3 was accompanied by decrease in the capacity to produce colonies, as showed with CFU assay (Figure 3(C,D)). As expected, hyperoxia dramatically decreased the capacity to produce colonies in both clones, irrespective of Sirt3 expression. These results collectively demonstrate the suppressive effect of either Sirt3 or hyperoxia alone on proliferation and metabolic activity of MCF-7 breast cancer cells.

De novo Sirt3 expression and hyperoxia increase cytosolic and mitochondrial ROS production

Hyperoxia has a well-known effect of increasing cellular ROS levels. Since Sirt3 is considered as a fidelity protein that particularly regulates production of mitochondrial ROS (mtROS), we tested whether *de novo* expression of Sirt3 would influence mitochondrial or cytosolic ROS production. By measuring cytosolic ROS production with H2DCFDA fluorescent probe, we showed that Sirt3 expression increased cytosolic oxidative stress in normoxia (Figure 4(A)). Hyperoxia *per se* increased cytosolic ROS in MCF-7C which was followed by additional increase in MCF-7S3. Similar pattern was observed for

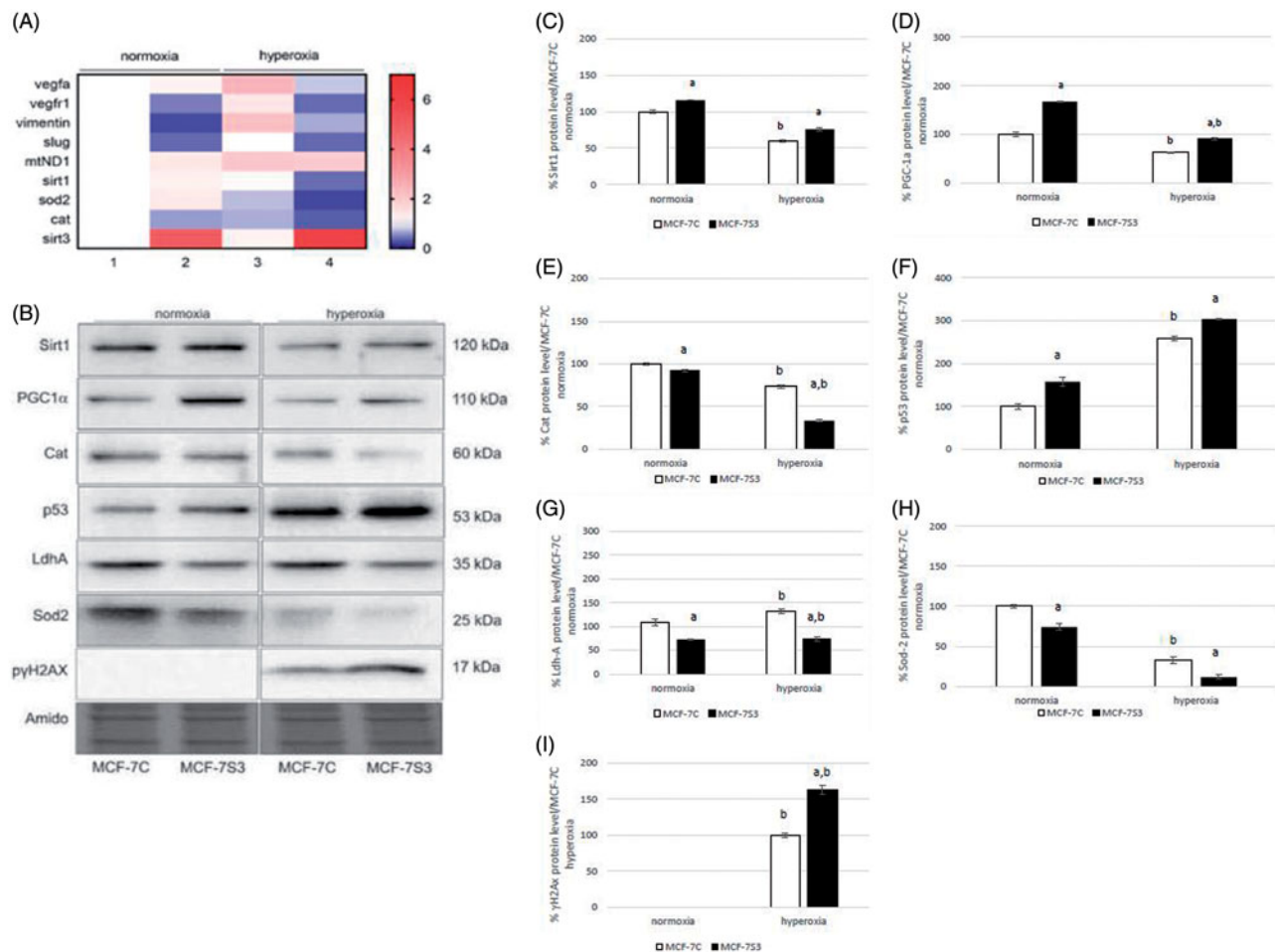


Figure 2. *De novo* Sirt3 expression enhances downregulation of proangiogenic and cancer-malignancy-related genes and proteins upon hyperoxia (A) Heatmap of differential gene expression as determined using real-time quantitative PCR method. The fold-change in gene expression was calculated using the $2^{-\Delta\Delta CT}$ method and β -actin as the endogenous control. Colour of the squares on the heatmap corresponds to the mean value of the log fold-change from three biological and three technical replicates. β -Actin was used for normalisation. Significant effect of sirt3 was found for *vegfr1* – fold change -2.0 , $p < .05$; *vimentin* – fold-change: -4.76 , $p < .001$; *slug* – fold-change: -2.70 , $p < .05$. Significant effect of hyperoxia was found for: *vegfa* – fold-change: $+2.0$, $p < .05$; *vimentin* – fold-change: $+2.17$, $p < .01$; *mtND1* – fold-change: $+2.0$, $p < .05$. Significant interaction of sirt3 and hyperoxia was found for *vegfr1* – fold-change: -2.43 , $p < .05$; *slug* – fold-change: -3.84 , $p < .01$; *sirt1* – fold-change: -2.38 , $p < .05$; *sod2* – fold-change: -4.34 , $p < 0.001$; *cat* – fold-change: -2.94 , $p < .01$. (B) Protein expression levels of Sirt1, PGC1 α , Cat, p53, LdhA, Sod2 and γ H2AX. Amido black was used as a loading control. The experiments were repeated three times and representative immunoblots are shown. (C–I) Graphical analysis of immunoblots of protein expression. Significant effect of Sirt3 ($^a p < .001$) on Sirt1 (C), PGC1 α (D), Cat (E), p53 (F), LdhA (G) and γ H2AX (I) was found, as well as on Sod2 ($^a p < .01$; H). Significant effect of hyperoxia ($^b p < .001$) on Sirt1 (C), PGC1 α (D), Cat (E), p53 (F), Sod2 (H) and γ H2AX (I) was found, as well as on LdhA ($^b p < .05$; G). Significant effect of Sirt3 and hyperoxia interaction ($p < .001$) on PGC1 α (D), Cat (E) and γ H2AX (I) was found, as well as on LdhA level ($p = .015$; G).

mtROS, ie Sirt3 expression and hyperoxia induced mtROS in both clones (Figure 4(B)). These results collectively demonstrate that *de novo* Sirt3 expression and hyperoxia increase ROS levels in both cytosolic and mitochondrial compartments.

Hyperoxia-induced alteration of mitochondrial function parameters is associated with *de novo* Sirt3 expression

It has been shown that Sirt3-increased mtROS have capacity to induce mtDNA damage, leading to potential

mitochondrial dysfunction [9]. Therefore, we wanted to determine whether *de novo* Sirt3 expression can influence mtDNA level, along with other mitochondrial parameters, such as mitochondrial mass, mitochondrial potential and oxygen consumption. First we examined the ratio of mitochondrial to nuclear DNA in all experimental groups and observed significant increase in mtDNA level in MCF-7S3 cells, which was also retained in hyperoxic conditions (Figure 5(A)). Although combination of hyperoxia and Sirt3 elevated mitochondrial mass, and hyperoxia substantially increased mitochondrial

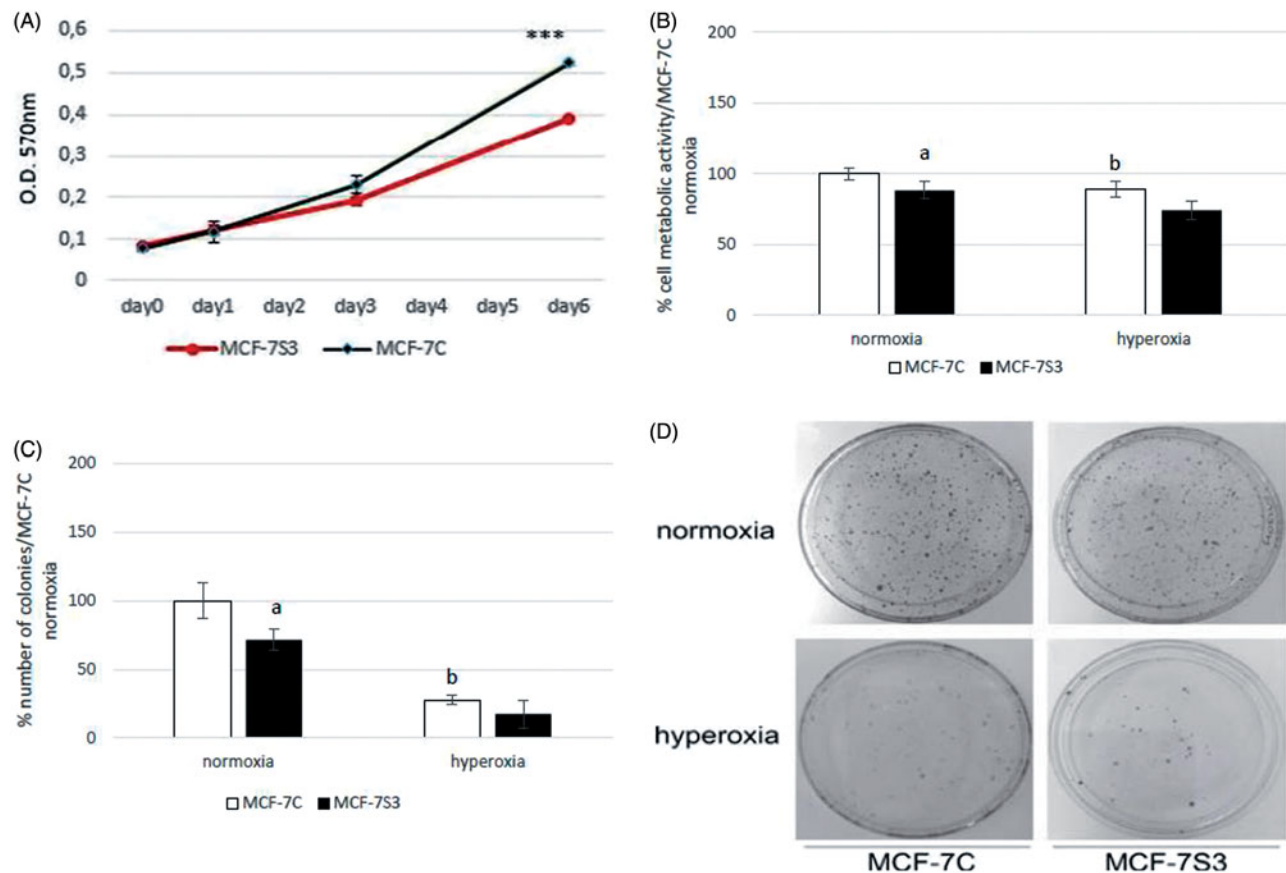


Figure 3. *De novo* Sirt3 expression and hyperoxia result in decrease of metabolic activity and survival. (A) Growth curves of MCF-7C and MCF-7S3 clones in high-glucose medium in normoxia. The representative experiment is shown. Results are presented as mean \pm SD *** $p < .001$, MCF-7C versus MCF-7S3 (two-tailed Student's *t*-test). (B) Percentage of metabolic activity of MCF-7S3 cells in normoxia and hyperoxia compared with MCF-7C cells. Significant effect of Sirt3 (^a $p < .001$) and hyperoxia (^b $p < .001$) on metabolic activity is observed. Results are shown as mean \pm SD (C) Graphical display of number of colonies (CFU assay) relative to normoxic MCF-7C. Significant effect of Sirt3 (^a $p < .005$) and hyperoxia (^b $p < .001$) on cellular clonogenic capacity is observed. The experiments were repeated at least three times. (D) Representative plates stained with crystal violet.

potential regardless of Sirt3 expression (Figure 5(B,C)), hyperoxic treatment significantly lowered O₂ consumption in both cell lines (Figure 5(D)).

De novo Sirt3 expression antagonises senescence

From the above results, it is evident that hyperoxia causes DNA damage that eventually results in cell death. However, we did not observe difference in rate of apoptosis as a result of Sirt3 expression or hyperoxia and Sirt3 (data not shown), thus we conclude that hyperoxia-induced cell death did not occur via apoptosis. Furthermore, the unchanged expressions of poly (ADP-ribose) polymerase one (PARP-1) imply that it also did not occur via PARP-1-dependent cell death, parthanatos (data not shown). Therefore, we tested whether hyperoxia-induced DNA damage influenced senescence-associated phenotype in both clones. SA- β -Gal activity assay showed that MCF-7S3 cells had lower ratio of SA- β -Gal positive cells compared with MCF-7C cells

(Figure 6(A,B)), whereas hyperoxia induced increase of SA- β -Gal positive cells in both groups. Similar to normoxia, the expression of Sirt3 inhibited hyperoxia-induced cellular senescence by 20% compared with hyperoxia-treated MCF-7C cells. Rotenone was used as a positive control for senescence induction [21].

Discussion

In this study, we demonstrated the potential of *de novo* Sirt3 expression to suppress proangiogenic and cancer-malignancy-related properties of human MCF-7 breast cancer cells, as well as to enhance their susceptibility to hyperoxic treatment. Sirt3 has bifunctional role, acting as both oncogene and tumour suppressor, depending on the tissue and cancer-type-specific metabolic programs [4]. Because breast cancer cells have strikingly reduced Sirt3 level, and 20% of them have almost no detectable Sirt3 protein [11], we developed *de novo* Sirt3 expressing transfectants to examine its effect on

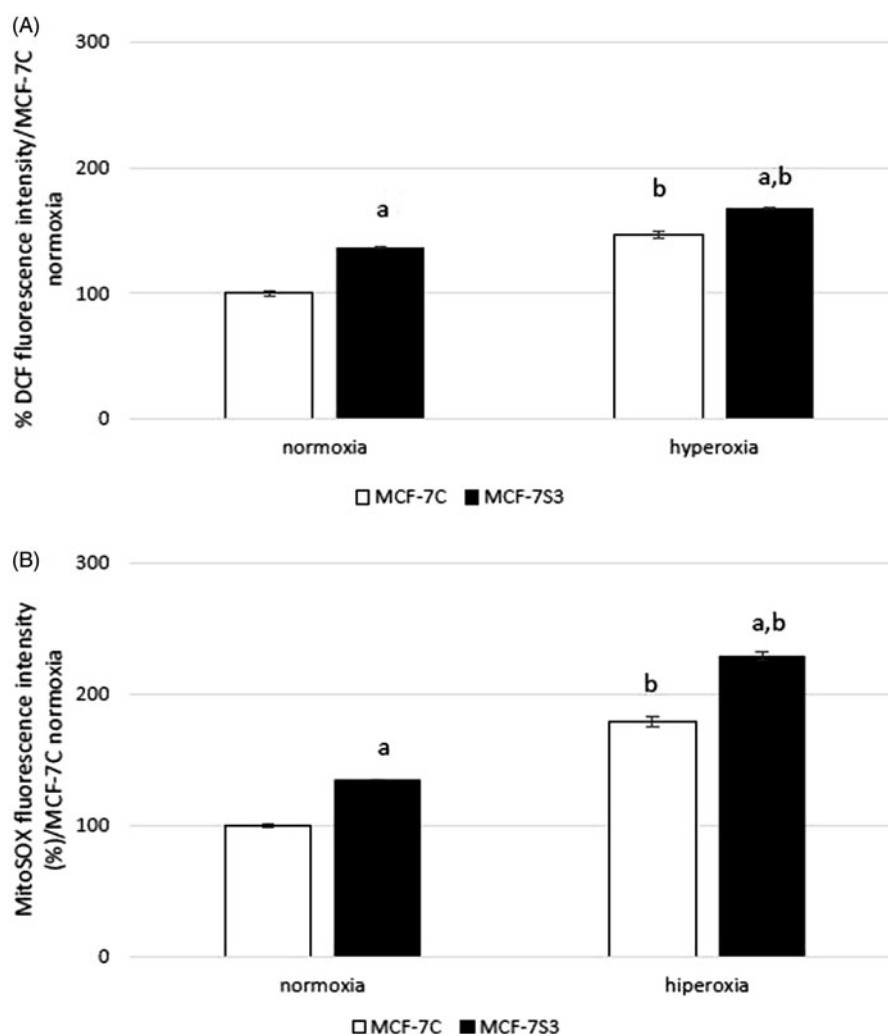


Figure 4. *De novo* Sirt3 expression and hyperoxia increase cytosolic and mitochondrial ROS production. (A) Cytosolic ROS levels were examined by H2DCFDA staining. Results are presented as mean \pm SD. The experiments were performed at least three times and representative data are shown. Significant effect of Sirt3 ($^ap < .001$) and hyperoxia ($^bp < .001$), and their interaction on cytosolic ROS production is observed ($p < .01$). (B) mtROS levels were measured with MitoSOX Red. Mean fluorescence intensity was compared with normoxic control clone. Significant effect of Sirt3 ($^ap < .001$) and hyperoxia ($^bp < .001$), and their interaction on mitochondrial ROS production is observed ($p = .01$).

characteristics of MCF-7 breast cancer cells, combined with hyperoxic treatment which has already shown to suppress the growth of certain mammary carcinoma cells [7].

A number of breast cancer cells, particularly MCF-7, depend on a mixture of glycolysis and OXPHOS to support their proliferation [22]. The faster growth rate of control MCF-7 clones in high-glucose medium (Figure 3(A)) implies the preferential use of glycolysis pathway to facilitate the uptake and incorporation of nutrients into the biomass thus supporting their faster proliferation [23]. It seems that Sirt3 induced the metabolic shift from glycolysis to OXPHOS, which involves the PGC1 α -induced mitochondrial regulation, therefore, causing decrease in fast supply of nutrients usually provided by glycolysis and, consequently, reduced

metabolic activity and clonogenic capacity of MCF-7 cells in normoxic conditions. Besides increasing PGC1 α , a master regulator of mitochondrial biogenesis [24], Sirt3 also reduced the expression of LdhA, a marker of glycolysis, thus confirming previous reports indicating that metabolic reprogramming mediated by Sirt3 contributes to its tumour-suppressive role in human breast cancer cell lines [11].

Sirt3 reduced *vegfr1* and two markers of EMT, vimentin and slug. Since vimentin contributes to cell polarity and motility and regulates the expression of slug to further enhance EMT phenotypes and cancer malignancy [25], the dramatic reduction of these genes suggests that Sirt3 indeed acts as a suppressor of EMT transition and malignant properties of the MCF-7 cells. In addition, Sirt3 reduced senescence of MCF-7 cells.

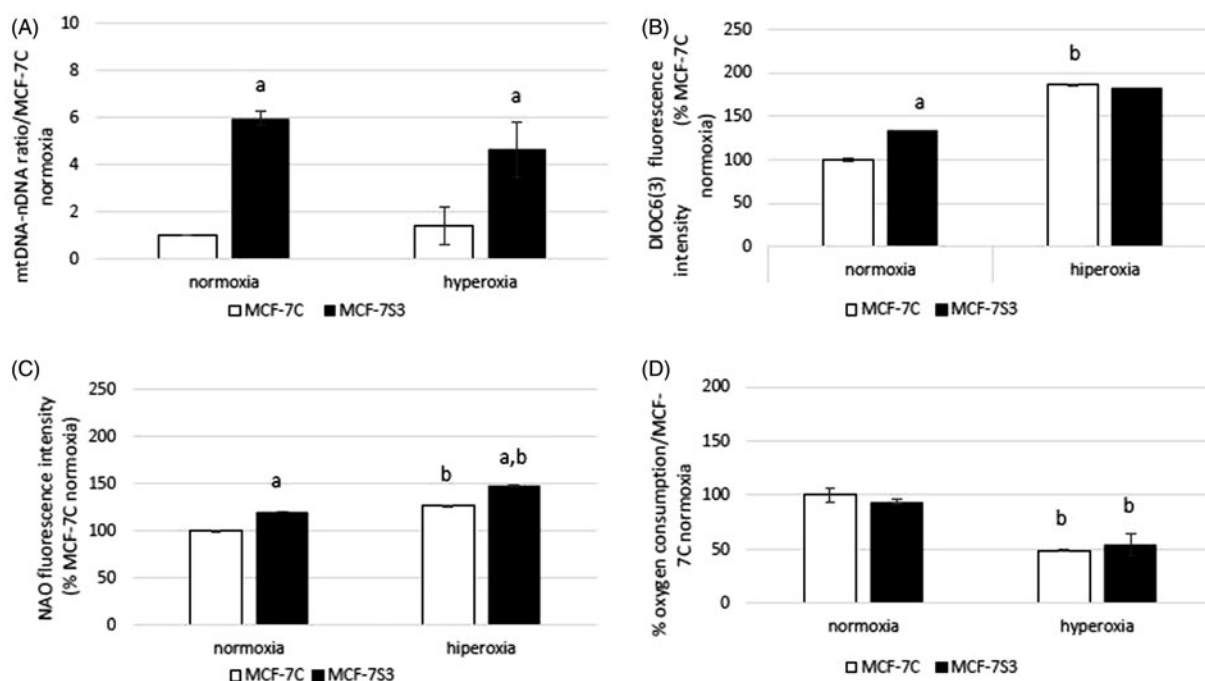


Figure 5. Hyperoxia-induced alteration in mitochondrial function parameters is associated with *de novo* Sirt3 expression (A) mtDNA content of MCF-7C and MCF-7S3 in normoxia and hyperoxia. Significant effect of Sirt3 ($^ap < .001$) and the interaction of Sirt3 and hyperoxia ($^bp < .05$) on mtDNA content is observed. (B) Significant effect of Sirt3 ($^ap < .05$) and hyperoxia ($^bp < .001$) on mitochondrial potential is observed. (C) Significant effect of Sirt3 ($^ap < .001$), hyperoxia ($^bp < .001$) and their interaction ($p < .05$) on mitochondrial mass is observed. Mean fluorescence intensity of all experimental groups was compared with the normoxic control clone. (D) Significant effect of hyperoxia ($^bp < .001$) on oxygen consumption is observed. Data are presented as percent of mean \pm SD. The experiments were performed at least three times and representative data are shown.

Although senescence is usually activated in a variety of premalignant steps to limit tumour progression [26], in certain contexts, it may create a pro-oncogenic tissue environment, thus leading to functional decline of tissues and the rise in cancer incidence [27]. Therefore, reduced senescence of MCF-7 cells may also contribute to the role of Sirt3 in inhibiting their tumourigenic properties. Another crucial tumour suppressor, p53, is often mutated or deregulated in many human cancers [28]. Since cells without a functional p53 lack the DNA-damage-sensing capability to induce the protective response [29], its slight increase upon the Sirt3 expression may have beneficial effect on suppression of tumourigenic potential. Taking all these factors in consideration, we conclude that Sirt3 inhibits the tumourigenic properties of MCF-7 cells in normoxia.

Although tumour cells often live in hypoxic conditions due to metabolic and structural abnormalities, their angiogenesis, growth and survival depend upon the sufficient supply of oxygen. The high ROS production and proangiogenic gene expression upon hyperoxic treatment at first suggest tumour-promoting effects of hyperoxia, since cells respond to elevated ROS levels by increasing the vegfa expression through the activation of signalling pathways usually involved in

tumourigenesis [30]. Hyperoxia also significantly up-regulated the EMT marker vimentin, as well as LdhA, an indicator of lactate generation, which initiates the vegf production [31] and contributes to aerobic glycolysis. This is also supported by a recent study showing higher uptake of glucose in the hyperoxia-treated MCF-7 cells [32]. However, hyperoxia initiated a number of events indicative of suppressing the tumourigenic properties, e.g. strong activation of p53, induction of senescence and mitochondrial dysfunction, as well as depleted PGC1 α , Sirt1 and Sod2 proteins abundance, which may finally be responsible for diminished cell proliferation and survival, as shown recently [12,33]. Moreover, hyperoxia increased mitochondrial potential and ROS production. Since even slight increase in mitochondrial potential may cause significant rise in ROS levels [34], this finding implies that tumour-suppressive effect of hyperoxia may be partially achieved through mitochondrial dysfunction. Excessive ROS are also important for establishing cellular senescence [35], which usually suppresses tumours in response to stress and is highly dependent on functional p53 [29]. Although one would expect that cells with a lot of DNA damage would undergo apoptosis pathway, MCF-7 cells rather become senescent than enter the apoptosis, probably due to

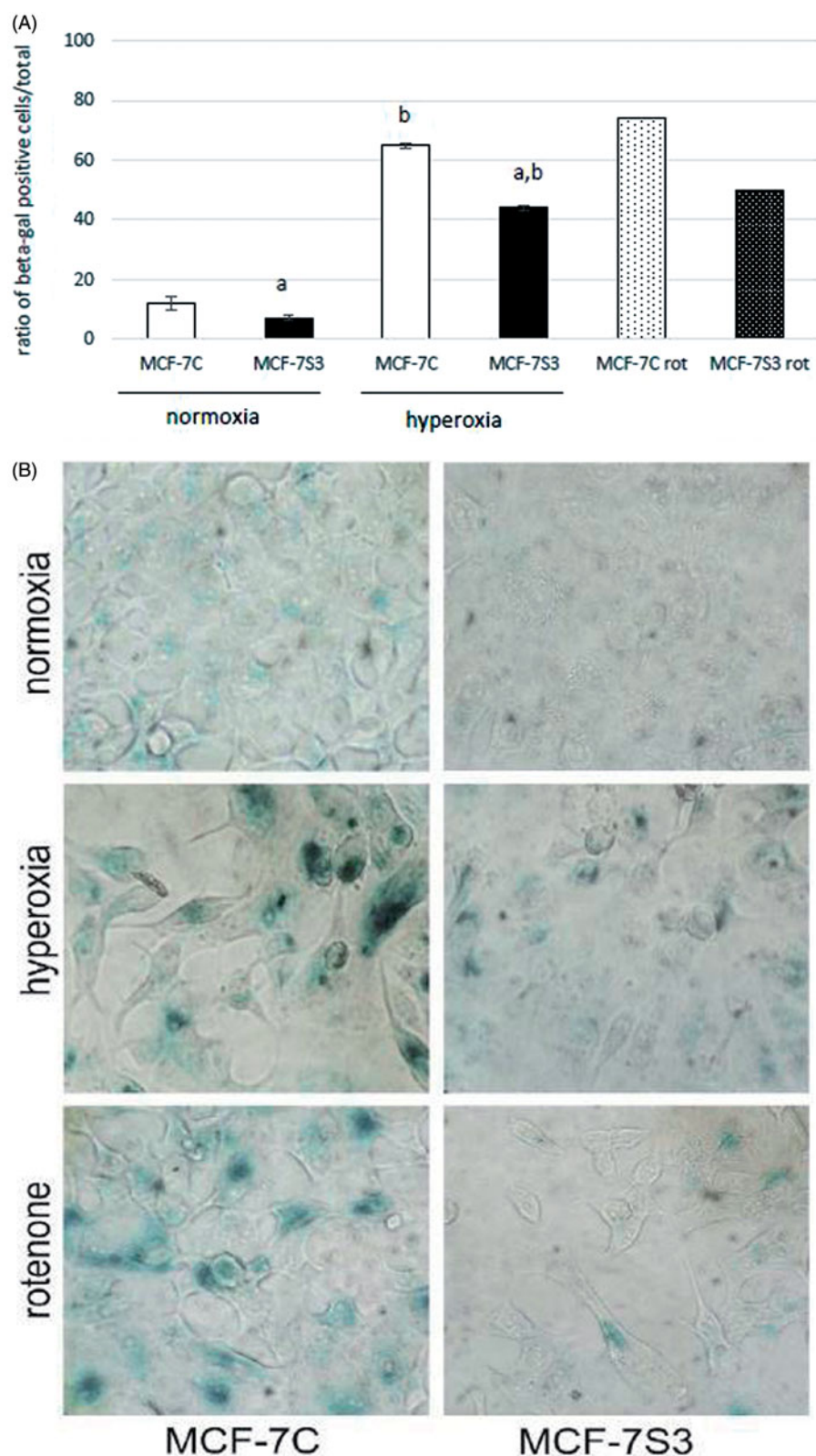


Figure 6. *De novo* Sirt3 expression antagonises senescence in both normoxia and hyperoxia (A) Graphical display of the ratio of β -gal positive cells in normoxic and hyperoxic conditions. Data present percentage of positive senescent cells analysed by β -galactosidase staining. The experiments were repeated three times and representative data are shown. Significant effect of Sirt3 ($^ap < .001$), hyperoxia ($^bp < .001$) and their interaction ($p < .01$) on senescence-associated β -galactosidase activity is observed. (B) Representative images of cells stained for senescence-associated β -galactosidase activity. Rotenone was used as a positive control for senescence induction.

the lack of functional caspase 3 expression [36]. This was also shown in previous studies where hyperbaric oxygen treatment lowered proliferation, but did not induce apoptosis in MCF-7 cells [37]. Collectively and in agreement with previous studies [37,38], these results show that hyperoxia inhibits proliferation and survival of cancer cells through the mitochondrial dysfunction and activation of p53 upon DNA damage and induction of senescence.

Under hyperoxic conditions, Sirt3 additionally down-regulated majority of genes involved in angiogenesis and tumour promotion, as well as EMT-inducing gene slug. Furthermore, increased DNA damage was accompanied with additional increase of ROS levels and consequent mitochondrial dysfunction and depletion of antioxidative enzymes. Sirt3 also antagonised senescence in both conditions, as expected [39].

The mitigation of tumourigenic properties and enhancement of the susceptibility of the MCF-7 breast cancer cells to the hyperoxic treatment upon the *de novo* Sirt3 expression, observed through their reduced survival, proliferation and mitochondrial function, as well as upregulation of the cells growth suppressors, indicates that both Sirt3 and hyperoxia, especially combined, have a potential to negatively modulate the properties of the cancer cells and that they should be further explored, *in vitro* and particularly *in vivo*, as an adjuvant tumour therapy in breast cancer malignancies.

Acknowledgements

The authors would like to thank Iva Pešun Medimorec and Marina Marš for their excellent technical contribution. SS is thankful to Dr Neda Slade for providing anti-p53 antibody and to Dr Dubravka Švob Štrac for advices and expertise regarding statistical analysis of the data.

Disclosure statement

No potential conflict of interest was reported by the authors.

Funding

This work was supported by the Croatian Science Foundation (HRZZ), Grant no. [IP-2014-09-4533] "SuMERA".

References

- [1] Giralt A, Villarroja F. SIRT3, a pivotal actor in mitochondrial functions: metabolism, cell death and aging. *Biochem J*. 2012;444(1):1–10.
- [2] Schwer B, North BJ, Frye RA, et al. The human silent information regulator (Sir)2 homologue hSIRT3 is a mitochondrial nicotinamide adenine dinucleotide-dependent deacetylase. *J Cell Biol*. 2002;158(4):647–657.
- [3] Brown K, Xie S, Qiu X, et al. SIRT3 reverses aging-associated degeneration. *Cell Rep*. 2013;3(2):319–327.
- [4] Torrens-Mas M, Oliver J, Roca P, et al. SIRT3: oncogene and tumor suppressor in cancer. *Cancers (Basel)*. 2017;9(7):90.
- [5] Yu L, Chen X, Wang L, et al. The sweet trap in tumors: aerobic glycolysis and potential targets for therapy. *Oncotarget*. 2016;7(25):38908–38926.
- [6] Kalliomäki T, Hill RP. Effects of tumour acidification with glucose + MIBG on the spontaneous metastatic potential of two murine cell lines. *Br J Cancer*. 2004;90(9):1842–1849.
- [7] Moen I, Stuhr LEB. Hyperbaric oxygen therapy and cancer – a review. *Target Oncol*. 2012;7(4):233–242.
- [8] Barja G. Updating the mitochondrial free radical theory of aging: an integrated view, key aspects, and confounding concepts. *Antioxid Redox Signal*. 2013;19(12):1420–1445.
- [9] Kim HS, Patel K, Muldoon-Jacobs K, et al. SIRT3 is a mitochondria-localized tumor suppressor required for maintenance of mitochondrial integrity and metabolism during stress. *Cancer Cell*. 2010;17(1):41–52.
- [10] Chen Y, Fu LL, Wen X, et al. Sirtuin-3 (SIRT3), a therapeutic target with oncogenic and tumor-suppressive function in cancer. *Cell Death Dis*. 2014;5:e1047.
- [11] Finley LWS, Carracedo A, Lee J, et al. SIRT3 opposes reprogramming of cancer cell metabolism through HIF1 α destabilization. *Cancer Cell*. 2011;19(3):416–428.
- [12] Resseguie EA, Staversky RJ, Brookes PS, et al. Hyperoxia activates ATM independent from mitochondrial ROS and dysfunction. *Redox Biol*. 2015;5:176–185.
- [13] Ferlay J, Soerjomataram I, Dikshit R, et al. Cancer incidence and mortality worldwide: sources, methods and major patterns in GLOBOCAN 2012. *Int J Cancer*. 2015;136(5):E359–E386.
- [14] Igci M, Kalender ME, Borazan E, et al. High-throughput screening of sirtuin family of genes in breast cancer. *Gene*. 2016;586(1):123–128.
- [15] Papa L, Germain D. SirT3 regulates the mitochondrial unfolded protein response. *Mol Cell Biol*. 2014;34(4):699–710.
- [16] North BJ, Marshall BL, Borra MT, et al. The human Sir2 ortholog, SIRT2, is an NAD⁺-dependent tubulin deacetylase. *Mol Cell*. 2003;11(2):437–444.
- [17] Šarić A, Crnolatac I, Bouillaud F, et al. Non-toxic fluorescent phosphonium probes to detect mitochondrial potential. *Methods Appl Fluoresc*. 2017;5(1):015007.
- [18] Sobočanec S, Balog T, Šarić A, et al. Cyp4a14 overexpression induced by hyperoxia in female CBA mice as a possible contributor of increased resistance to oxidative stress. *Free Radic Res*. 2010;44(2):181–190.
- [19] Venegas V, Wang J, Dimmock D, et al. Real-time quantitative PCR analysis of mitochondrial DNA content. *Curr Protoc Hum Genet*. 2011;Chapter(19):Unit 19.7.
- [20] R Development Core Team. R: A language and environment for statistical computing. Available from: <http://www.R-project.org>. Vienna, Austria: R Foundation for Statistical Computing. ISBN 3-900051-07-0; 2008.

- [21] Gonçalves AP, Máximo V, Lima J, et al. Involvement of p53 in cell death following cell cycle arrest and mitotic catastrophe induced by rotenone. *Biochim Biophys Acta*. 2011;1813(3):492–499.
- [22] Zheng JIE. Energy metabolism of cancer: glycolysis versus oxidative phosphorylation (Review). *Oncol Lett*. 2012;4(6):1151–1157.
- [23] Vander Heiden MG, Cantley LC, Thompson CB. Understanding the Warburg effect: the metabolic Requirements of cell proliferation. *Science*. 2009; 324(5930):1029–1033.
- [24] Antico Arciuch VG, Elguero ME, Poderoso JJ, et al. Mitochondrial regulation of cell cycle and proliferation. *Antioxid Redox Signal*. 2012;16(10):1150–1180.
- [25] Liu CY, Lin HH, Tang MJ, et al. Vimentin contributes to epithelial-mesenchymal transition cancer cell mechanics by mediating cytoskeletal organization and focal adhesion maturation. *Oncotarget*. 2015;6(18): 15966–15983.
- [26] Childs BG, Baker DJ, Kirkland JL, et al. Senescence and apoptosis: dueling or complementary cell fates? *EMBO Rep*. 2014;15(11):1139–1153.
- [27] Shay JW, Roninson IB. Hallmarks of senescence in carcinogenesis and cancer therapy. *Oncogene*. 2004; 23(16):2919–2933.
- [28] Murray-Zmijewski F, Slee EA, Lu X. A complex barcode underlies the heterogeneous response of p53 to stress. *Nat Rev Mol Cell Biol*. 2008;9(9):702–712.
- [29] Burkhardt DL, Sage J. Cellular mechanisms of tumour suppression by the retinoblastoma gene. *Nat Rev Cancer*. 2008;8(9):671–682.
- [30] Liu ZJ, Velazquez OC. Hyperoxia, endothelial progenitor cell mobilization, and diabetic wound healing. *Antioxid Redox Signal*. 2008;10(11):1869–1882.
- [31] Zabel DD, Feng JJ, Scheuenstuhl H, et al. Lactate stimulation of macrophage-derived angiogenic activity is associated with inhibition of poly(ADP-ribose) synthesis. *Lab Invest*. 1996;74(3):644–649.
- [32] Fernandez-Carrascal A, Garcia-Algar M, Nazareno M, et al. Metabolic pathway for the universal fluorescent recognition of tumor cells. *Oncotarget*. 2017;8(44): 76108–76115.
- [33] Moore RL, Faller DV. SIRT1 represses estrogen-signaling, ligand-independent ER α -mediated transcription, and cell proliferation in estrogen-responsive breast cells. *J Endocrinol*. 2013;216(3):273–285.
- [34] Suski JM, Lebiezinska M, Bonora M, et al. Relation between mitochondrial membrane potential and ROS Formation. In: Palmeira CM, Moreno AJ, eds. *Mitochondrial bioenergetics: methods and protocols*. Vol. 810. New York: Humana Press; 2012. p. 183–205.
- [35] Ziegler DV, Wiley CD, Velarde MC. Mitochondrial effectors of cellular senescence: beyond the free radical theory of aging. *Aging Cell*. 2015;14(1):1–7.
- [36] Kagawa S, Gu J, Honda T, et al. Deficiency of caspase-3 in MCF7 cells blocks Bax-mediated nuclear fragmentation but not cell death. *Clin Cancer Res* 2001;7(5):1474–1480.
- [37] Granowitz EV, Tonomura N, Benson RM, et al. Hyperbaric oxygen inhibits benign and malignant human mammary epithelial cell proliferation. *Anticancer Res*. 2005;25(6B):3833–3842.
- [38] Marinello PC, da Silva TNX, Panis C, et al. Mechanism of metformin action in MCF-7 and MDA-MB-231 human breast cancer cells involves oxidative stress generation, DNA damage, and transforming growth factor β 1 induction. *Tumour Biol*. 2016;37(4): 5337–5346.
- [39] Wiley CD, Velarde MC, Lecot P, et al. Mitochondrial dysfunction induces senescence with a distinct secretory phenotype. *Cell Metab*. 2016;23(2):303–314.



Article

Sirt3 Exerts Its Tumor-Suppressive Role by Increasing p53 and Attenuating Response to Estrogen in MCF-7 Cells

Marija Pinterić ^{1,†}, Iva I. Podgorski ^{1,†} , Marijana Popović Hadžija ¹ , Vedrana Filić ², Mladen Paradžik ^{2,3} , Bastien Lucien Jean Proust ¹, Ana Dekanić ¹ , Ivan Ciganek ¹, Denis Pleše ¹, Dora Marčinko ¹, Tihomir Balog ¹ and Sandra Sobočanec ^{1,*}

¹ Division of Molecular Medicine, Ruđer Bošković Institute, 10000 Zagreb, Croatia; mpinter@irb.hr (M.P.); iskrinj@irb.hr (I.I.P.); mhadzija@irb.hr (M.P.H.); Bastien.Lucien.Jean.Proust@irb.hr (B.L.J.P.); adekani@irb.hr (A.D.); iciganek@stud.biol.pmf.hr (I.C.); dplese@pharma.hr (D.P.); dora.marcinko@krka.biz (D.M.); balog@irb.hr (T.B.)

² Division of Molecular Biology, Ruđer Bošković Institute, 10000 Zagreb, Croatia; Vedrana.Filic.Mileta@irb.hr (V.F.); Mladen.Paradzik@irb.hr (M.P.)

³ Department Molecular Biotechnology and Health Sciences, Molecular Biotechnology Centre (MBC), University of Torino, 10124 Torino, Italy

* Correspondence: ssoboc@irb.hr; Tel.: +385-1-4561-172

† These authors contributed equally to this work.

Received: 25 February 2020; Accepted: 30 March 2020; Published: 1 April 2020



Abstract: Estrogen (E2) is a major risk factor for the initiation and progression of malignancy in estrogen receptor (ER) positive breast cancers, whereas sirtuin 3 (Sirt3), a major mitochondrial NAD⁺-dependent deacetylase, has the inhibitory effect on the tumorigenic properties of ER positive MCF-7 breast cancer cells. Since it is unclear if this effect is mediated through the estrogen receptor alpha (ER α) signaling pathway, in this study, we aimed to determine if the tumor-suppressive function of Sirt3 in MCF-7 cells interferes with their response to E2. Although we found that Sirt3 improves the antioxidative response and mitochondrial fitness of the MCF-7 cells, it also increases DNA damage along with p53, AIF, and ER α expression. Moreover, Sirt3 desensitizes cells to the proliferative effect of E2, affects p53 by disruption of the ER α –p53 interaction, and decreases proliferation, colony formation, and migration of the cells. Our observations indicate that these tumor-suppressive effects of Sirt3 could be reversed by E2 treatment only to a limited extent which is not sufficient to recover the tumorigenic properties of the MCF-7 cells. This study provides new and interesting insights with respect to the functional role of Sirt3 in the E2-dependent breast cancers.

Keywords: sirtuin 3; MCF-7; estrogen receptor; p53; breast cancer cells

1. Introduction

17 β -estradiol (E2) is a steroid hormone essential for the maintenance of the female reproductive system with important physiological functions in the immune, cardiovascular, and neural systems [1,2]. However, E2 is a major risk factor for initiation and progression of malignancy in estrogen receptor (ER) positive breast cancers [3]. E2 mainly exerts its effect through the classical genomic pathway involving estrogen receptors alpha (ER α) and beta (ER β) that function as transcription factors [4], with ER α being essential for proliferative signaling in both normal and breast cancer cells [5]. By binding to ER α , E2 promotes cellular proliferation through the upregulation of cell cycle regulating genes, and simultaneously triggers ER α proteasomal degradation required for the cellular response to environmental E2 levels [6].

Sirtuin 3 (Sirt3), NAD⁺ dependent deacetylase, is the only member of the sirtuin family that is linked to longevity in humans. In addition, important cellular and mitochondrial processes, including reactive oxygen species (ROS) generation, are integrated through Sirt3. It has been shown that Sirt3 has a bifunctional role in cancer, acting as both oncoprotein and tumor suppressor, depending on the tissue and cancer-type specific metabolic programs [7]. We have recently shown that Sirt3 has the inhibitory effect on tumorigenic properties of ER α positive breast cancer cells, particularly when combined with hyperoxic treatment [8]. However, it is not clear if this effect is mediated through the ER α signaling pathway.

While ER α plays an important role in the progression of breast cancer, p53 functions as a major tumor suppressor through induction of target genes for cell cycle arrest and DNA repair [9]. Given that p53 functions primarily as a tumor suppressor, any aberration in the p53 gene or dysfunction of p53-mediated signaling pathway leads to cellular proliferation and potential tumorigenesis [10]. Breast cancer cells usually have functional p53, although its activity is altered by various mechanisms [11]. In ER α positive breast cancer cells, the abrogation of the p53 signaling pathway is a major event towards cancer progression, where p53 is functionally repressed by interaction with ER α [12]. However, the mechanism underlying the inactivation of p53 function is not fully understood.

Although the elevated levels of ER α contribute to an increased risk of breast cancer [3], it has also been reported that ER α overexpression can be associated with reduced metabolic potential and invasiveness [13]. Earlier studies have shown that low Sirt3 expression is associated with reduced survival in all breast cancers and highlighted its potential role as a biomarker to assist in identifying high risk patients [14]. Furthermore, it was also shown that the full-length nuclear Sirt3 can indirectly activate and prevent degradation of p53 in MCF-7 cells through deacetylation of phosphatase PTEN [15]. Considering the tumor suppressive role of Sirt3, we hypothesized that E2/ER α signaling can be negatively affected by Sirt3. So far, it has not been shown that Sirt3 exerts its tumor-suppressive function in MCF-7 cells by interfering with their response to E2.

Here, we report that overexpressed Sirt3 reduces the response of MCF-7 cells to E2, affects p53 by disruption of the ER α –p53 interaction, and inhibits the clonogenic growth of MCF-7 cells. Thus, Sirt3 can be considered to reduce tumor-initiating capacity of these cells by attenuating response of the ER α positive breast cancer cells to the E2. These results provide new and interesting insights concerning the functional role of Sirt3 in breast cancer and its therapeutic potential in hormone-positive breast tumors.

2. Materials and Methods

2.1. Cell Lines, Transfection, Treatments

The MCF-7 cell line was obtained from Public Health England (London, UK; ECACC 86012803), tested for mycoplasma contamination, and was grown in high glucose Dulbecco's modified Eagle medium (DMEM, Sigma-Aldrich, St. Louis, MO, USA) with 10% fetal bovine serum (FBS, Capricorn Scientific, Germany), 1% nonessential amino acids (Sigma-Aldrich, St. Louis, MO, USA) and 1% antibiotic/antimycotic solution (Capricorn Scientific, Germany) at 37 °C with 5% CO₂ in a humidified atmosphere. Due to the commercial source of the cells, there was no need to authenticate them prior to the study. The MCF-7 cells were transfected with the FLAG-tagged Sirt3 (MCF-7S3) or empty pcDNA3.1 plasmid (MCF-7C), as described previously in [8]. To examine the E2 effect on the characteristics of E2-dependent cell growth, we used white DMEM medium with steroid free (charcoal treated) serum (Sigma-Aldrich, St. Louis, MO, USA), since it is known that phenol red can activate ER α gene regulation [16,17]. Therefore, in our study, both phenol red and white DMEM (Capricorn Scientific, Germany) were used, depending on the parameters examined. For the experiments in white DMEM, cells were grown in this media for one week before the experiments. In our research, we treated cells with 10 nM E2 (17 β -estradiol, Sigma-Aldrich, St. Louis, MO, USA) for 2 h and if we wanted to confirm that E2 effect was mediated by ER α , we treated cells with ER α inhibitor 100 nM ICI (ICI 182,780; Santa Cruz Biotechnology, Dallas, TX, USA) 2 h before adding E2.

2.2. RNA Isolation, Reverse Transcription, and qPCR Analysis

Total RNA was isolated from $\sim 10^6$ cells using TRIzol reagent (Invitrogen, Carlsbad, CA, USA) according to the manufacturer's instructions. Relative gene expression of *sirt-3* (Hs00953477_m1, TaqMan, Thermo Fisher Scientific, Waltham, MA, USA) and *esr-1* (Hs01046816_m1, TaqMan, Thermo Fisher Scientific, Waltham, MA, USA) were quantified by reverse transcription of total RNA and real-time quantitative PCR (qPCR) analysis. Data were analyzed using the $2^{-\Delta\Delta C_t}$ method and presented as the fold change in gene expression normalized to endogenous reference gene (β -actin; Hs01060665_g1, TaqMan, Thermo Fisher Scientific, Waltham, MA, USA) and relative to the control. All reactions were carried out in triplicate.

2.3. siRNA-Mediated Silencing of Sirt3 and ER α Expression

Silencing of Sirt3 and ER α expression was done using Lipofectamine2000 (Thermo Fisher Scientific, Waltham, MA, USA) according to the manufacturer's guidelines. Sirt3 siRNA (siSirt3), ER α siRNA (siER α), and scrambled control siRNA (siSCR) were obtained from Ambion (Thermo Fisher Scientific, Waltham, MA, USA). Cells (10^5) were seeded on a 24-well plate, and 24 h later transfected with 100 nM siRNA for 48 h, followed by protein collection and Western blot analysis for targeted proteins.

2.4. Fractionation, SDS-PAGE, and Western Blot Analysis

For fractionation analysis, 2×10^6 cells were seeded on 10 cm Petri dish and 24 h later treated with ICI and E2, followed by fractionation by Cell Fractionation Kit Standard (ab109719, Abcam, UK) according to the manufacturer's instructions. Proteins of obtained fractions were measured by Pierce™ BCA Protein Assay Kit (Thermo Fischer Scientific, Waltham, MA, USA) and prepared in SDS-PAGE sample buffer (100 mM Tris-HCl (pH 6.8), 2% SDS, 20% glycerol, 4% β -mercaptoethanol, 0.5% bromophenol blue dye) for Western blot analysis. Anti-GAPDH and anti-H3 antibodies were used as controls for purity of cytoplasmic and nuclear fractions, respectively [18,19]. Total cellular proteins for Western blot analysis were isolated in Ripa buffer with protease inhibitors (Roche, Basel, Switzerland). SDS-PAGE and Western blot analysis were carried out as described previously in [8]. Primary and secondary antibodies used in this study are listed in Supplementary Table S1.

2.5. Immunofluorescence, Micronucleated Cells and Confocal Microscopy

Immunofluorescence analysis was performed as described previously in [20]. When MitoTracker Deep Red (Thermo Fisher Scientific, Waltham, MA, USA) was used, cells were labelled with 100 nM MitoTracker for 20 minutes before the end of the E2 treatment. Primary and secondary antibodies used in this study are listed in Supplementary Table S2. DAPI (4,6-diamidino-2-phenylindol, Sigma-Aldrich, St. Louis, MO, USA) was used for nuclear staining. For detection of micronucleated cells, 10^4 cells/well were seeded on coverslips in a 24-well plate and were grown in white DMEM for 10 days, then fixed with 4% PFA, and stained with 5 μ M Hoechst 33342 (Sigma-Aldrich, St. Louis, MO, USA) for 10 min. As a positive control, formation of micronucleated cells in MCF-7C clone was induced with 400 μ M H₂O₂ for 4 h after which they were left to grow in fresh DMEM for the next 72 h, and then were further processed and analyzed as untreated cells. Confocal imaging was performed by sequential scanning using a Leica TCS SP8 X laser scanning microscope (Leica Microsystems, Germany), equipped with a HC PL APO CS2 63/1.40 oil immersion objective and a white light laser. The excitation wavelengths and emission detection ranges used were 350 nm and 412 to 460 nm for Hoechst 33342, 405 nm and 412 to 460 nm for DAPI, 488 nm and 495 to 550 nm for Alexa488, 594 nm and 601 to 644 nm for Alexa594, and 644 nm and 651 to 700 nm for MitoTracker Deep Red, respectively.

2.6. Cellular Proliferation, Metabolic Activity, Clonogenic Capacity

In order to determine the cell proliferation, EdU Click-iT® assay (Thermo Fisher Scientific, Waltham, MA, USA) was used according to the manufacturer's instructions [21]. Briefly, 4×10^5 cells

were seeded in six-well plates in both red and white DMEM, 24 h later they were treated with E2 and ICI, and left to grow for an additional 48 h. The samples were analyzed using FACS Calibur flow cytometer (BD Biosciences, Franklin Lakes, NJ, USA), while acquisition was made using the CellQuest software package (BD Biosciences, Franklin Lakes, NJ, USA). The analysis of the frequencies of proliferative (EdU positive) cells was performed using the FCS Express 3 software package (De Novo software, Pasadena, CA, USA). For the MTT(3-(4,5-dimethylthiazol-2-yl)-2,5-diphenyl tetrazolium bromide; tetrazolium dye) assay, 5×10^3 cells were seeded in a 96-well plate and 24 h later treated with ICI and E2 and processed as described previously in [8]. For the clonogenic capacity (CFU) assay, 2×10^3 cells were seeded in 5 cm Petri dishes, and 24 h later treated with ICI and E2. After that, the cells were incubated for 14 days until the visible colonies were observed and processed as previously described [8].

2.7. Migration Assay

For monitoring cell migration, 1×10^5 cells were treated for 2 h with E2 in serum-reduced DMEM, seeded in migration Transwell Cell Culture Inserts (pore size 8 mm; Corning, Corning, NY, USA), and left to migrate for 22 h towards 10% FBS in DMEM as a chemoattractant. Cells migrated to the underside of the filter were fixed with 4% PFA, stained with 1% crystal violet solution, photographed, and quantified using NIH ImageJ (v1.52a, U.S. National Institutes of Health, Bethesda, MD, USA).

2.8. Measurements of Mitochondrial Membrane Potential, Cytosolic, and Mitochondrial ROS Production

Quantitative analysis of mitochondrial membrane potential ($\Delta\Psi_m$), and mitochondrial superoxide production (mtROS) was carried out using 100 nM MitoTracker Deep Red and 5 μ M MitoSOX Red reagent (both from Thermo Fisher Scientific, Waltham, MA, USA), respectively. Cytosolic ROS production was measured with 20 μ M dihydroethidium (DHE) (Invitrogen Molecular Probes, Carlsbad, CA, USA). Sytox Red (500 nM, Thermo Fisher Scientific, Waltham, MA, USA) and PI (1.5 μ g/mL) were used for exclusion of dead cells dyed with MitoSOX Red or DHE, and MitoTracker Deep Red, respectively. The samples were analyzed using a FACS Calibur flow cytometer as described above.

2.9. Antioxidant Enzyme Activities

Superoxide dismutase (SOD) activity was assayed with a RANSOD kit (RANDOX Labs, UK) according to the manufacturer's protocol. The SOD-2 activity was determined under identical conditions with the addition of 4 mM KCN in the assay buffer for 30 min to inhibit SOD1. The SOD1 activity was obtained by subtracting the SOD2 activity from the total SOD activity. Lyophilized cells and standard solutions were used for the SOD assay. The absorbance was measured at 505 nm on a microplate reader (Bio-Tek Instruments, Inc., Winooski, VT, USA).

2.10. Immunoprecipitation and Coimmunoprecipitation

Cells were seeded in white DMEM and 24 h later treated with E2 for 2 h, followed by cell lysis in Co-IP buffer (250 mM NaCl, 0.1% NP-40, 50 mM HEPES). Since Sirt3 is FLAG-tagged, ANTI-FLAG M2 affinity gel (Sigma-Aldrich, St. Louis, MO, USA) was used for Sirt3 coimmunoprecipitation. For ER α , anti-ER α antibody (F-10, Santa Cruz Biotechnology, Dallas, TX, USA) was used and Pierce Crosslink Immunoprecipitation Kit (Thermo Fisher Scientific, Waltham, MA, USA) according to the manufacturer's guidelines, with the exception of the Co-IP buffer instead of IP Lysis/Wash Buffer from the kit.

2.11. Statistical Analysis

Statistical analysis of data was performed using R v2.15.3 (CRAN, <http://cran.r-project.org>) and RStudio for Windows, v0.97 (<http://www.rstudio.com/>) and SPSS for Windows (17.0, IBM, Armonk, NY, USA). Before all analyses, the samples were tested for normality of distribution using the Shapiro–Wilk

test. If the data followed a non-Gaussian distribution, the following nonparametric analyses were performed: Kruskal–Wallis non-parametric ANOVA for testing differences between groups that do not follow normal distribution, followed by Wilcoxon signed-rank test for testing differences between two related groups. In the case of normal distributions, the following parametric tests were performed: two-way ANOVA, followed by Bonferroni adjustments for the analysis of (simple) main effects. For comparisons of the two samples, the Student's t-test or Mann–Whitney U test were used, depending on the distribution of data. Significance was set at $p < 0.05$.

3. Results

3.1. Sirt3 Participates in Regulation of ER α Expression and Localization and Alters Its Response to E2 Treatment in MCF-7 Cells

To examine if and how Sirt3 affects ER α expression, first, we stably overexpressed Sirt3 in MCF-7 cells (hereafter MCF-7S3) since MCF-7 cells express Sirt3 at almost undetectable levels (Figure 1A,C and Figure 2). Then, we analyzed mRNA and protein expression level of ER α in both MCF-7S3 and MCF-7 cells transfected with empty plasmid as a negative control (hereafter MCF-7C) (Figure 1B,C). Because MCF-7 cells proliferate in an E2-dependent manner [22], we next tested how E2 addition affected its cognate receptor ER α in the absence and presence of Sirt3. We found a positive effect of Sirt3 on both *esr-1* gene transcript and protein expression level, with +2.1-fold change and 30% increase in the absence of E2, respectively (Figure 1B,C). In the absence of Sirt3, E2 addition increased ER α protein expression ($p < 0.01$), whereas in Sirt3 clones it caused reduction of already upregulated ER α protein level ($p < 0.01$). Antiestrogen ICI, which was added two hours prior to E2 addition, had an inhibitory effect on ER α expression in both cell lines (Figure 1C, $p < 0.001$). We also examined the effects of Sirt3 or ER α silencing on ER α and Sirt3 expression (Figure 1D) and showed that Sirt3 silencing lowers the expression of ER α ($p < 0.01$). Furthermore, we investigated the effect of Sirt3 on cellular localization of ER α . Using the fractionation method, we found that E2 treatment promoted nuclear accumulation of ER α in both cell lines ($p < 0.001$), whereas a lower signal observed in cells treated with ICI prior to E2 addition indicated degradation of ER α . Interestingly, Sirt3 overexpression slightly delocalizes ER α in the cytosol (Figure 1E, $p < 0.001$). Confocal microscopy confirmed the primary localization of ER α in the nucleus (Figure 2). These results collectively indicate, while E2 affects both localization and the abundance of ER α expression, Sirt3 only affects the amount of ER α expressed in the cell.

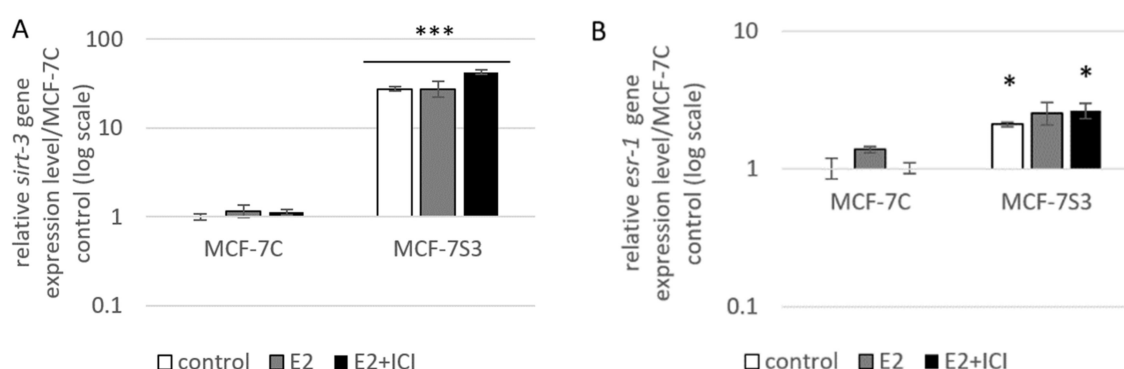


Figure 1. Cont.

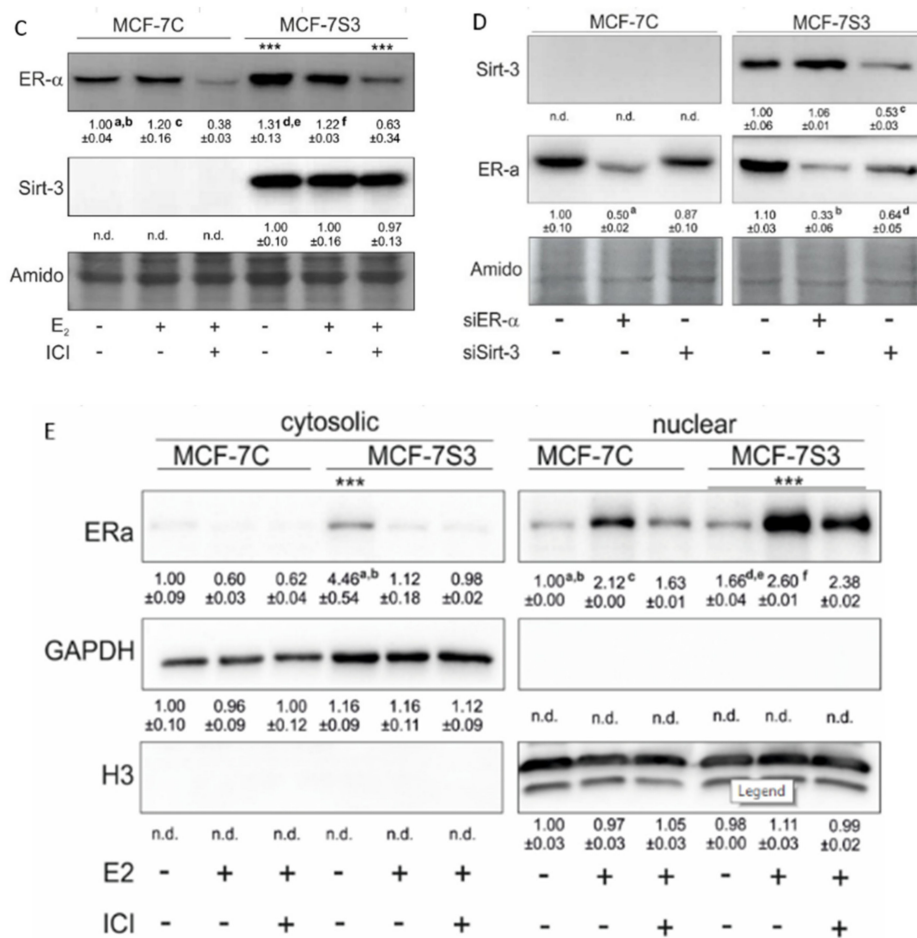


Figure 1. Sirt3 regulates ERα expression and localization. (A) Expression of *sirt-3* gene was significantly increased in MCF-7S3 clones as compared with MCF-7C ($*** p < 0.001$). The results are presented as fold change \pm SE on a log-scale, normalized to the control MCF-7C. Experiments were repeated at least three times (hereafter referred to as $n \geq 3$); (B) Expression of *esr-1* gene was significantly increased in the control and E2 + ICI-treated MCF-7S3 clones as compared with MCF-7C ($* p < 0.05$); (C) Immunoblots of ERα and Sirt3 protein expression level. Two-way ANOVA revealed significant interaction effect between Sirt3 and treatment on ERα $F(2,12) = 9.321, p = 0.004$, partial $\eta^2 = 0.608$; higher in the control ($*** p < 0.001$) and E2 + ICI-treated ($*** p < 0.001$) MCF-7S3 vs. MCF-7C. In MCF-7C, higher in E2 vs. the control ($^a p < 0.01$) and E2 + ICI-treated ($^c p < 0.001$) and in the control vs. E2 + ICI-treated ($^b p < 0.001$). In MCF-7S3, higher in the control vs. E2 ($^d p < 0.01$) and E2 + ICI-treated ($^e p < 0.001$) and in E2 vs. E2 + ICI-treated ($^f p < 0.001$); (D) Immunoblots of ERα and Sirt3 protein expression level in the cells transfected with scrambled (siSCR) control or siERα and siSirt3 RNA. Lower ERα in the siERα-treated vs. siSCR MCF-7C cells ($^a p < 0.05$) and MCF-7S3 cells ($^b p < 0.01$). In MCF-7S3, lower Sirt3 ($^c p < 0.05$) and ERα ($^d p < 0.01$) in the siSirt3-treated cells; (E) Immunoblots of ERα protein expression in cellular fractions. For cytosolic fraction, two-way ANOVA revealed a significant interaction effect between Sirt3 and treatment $F(2,12) = 54.61, p < 0.001$, partial $\eta^2 = 0.948$; higher cytosolic ERα in the control MCF-7S3 vs. MCF-7C ($*** p < 0.001$). In MCF-7S3, higher cytosolic ERα in the control vs. E2 ($^a p < 0.001$) and E2 + ICI-treated group ($^b p < 0.001$). For nuclear fraction, two-way ANOVA revealed significant interaction effect between Sirt3 and treatment $F(2,12) = 1054.57, p < 0.001$, partial $\eta^2 = 0.997$; higher nuclear ERα in MCF-7S3 vs. MCF-7C ($*** p < 0.001$). In MCF-7C, lower nuclear ERα in the control vs. E2 ($^a p < 0.001$) and E2 + ICI-treated group ($^b p < 0.001$); higher nuclear ERα in E2 vs. E2 + ICI-treated group ($^c p < 0.001$). In MCF-7S3, lower nuclear ERα in the control vs. E2 ($^d p < 0.001$) and E2 + ICI-treated group ($^e p < 0.001$) and higher nuclear ERα in E2 vs. E2 + ICI-treated group ($^f p < 0.001$). For (C), (D) and (E) results are shown as a ratio of the mean \pm SD normalized to the control MCF-7C ($n \geq 3$). AmidoBlack was used as a loading control.

3.2. Sirt3 Does Not Interact with ER α in MCF-7 Cells

Since the presence of ER α in mitochondria has been described by several studies [23,24], we next investigated the possibility that ER α resides inside mitochondria and interacts with Sirt3. Using both coimmunoprecipitation and confocal imaging, we found no interaction between ER α and Sirt3 (Supplementary Figure S1) or colocalization signal for ER α and Sirt3, respectively (Figure 2). These results collectively suggest that Sirt3 indirectly participates in the regulation of ER α expression.

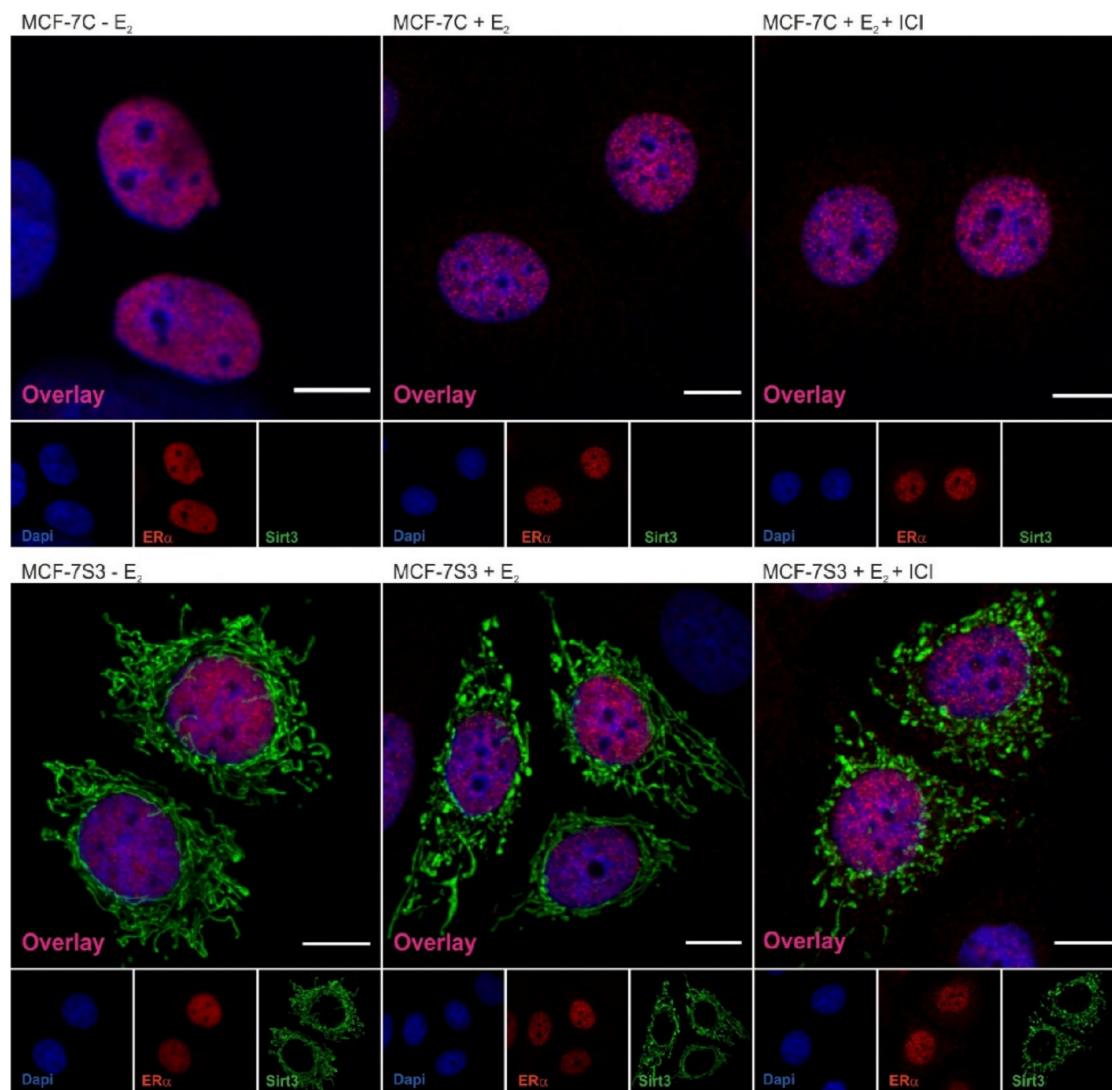


Figure 2. Sirt3 does not colocalize with ER α in MCF-7 cells. Confocal imaging of ER α localization in control, E2, and E2 + ICI-treated MCF-7C and MCF-7S3 cells. Bar represents 10 μ m.

3.3. Sirt3 Amplifies E2-Induced Metabolic Activity and Mitochondrial Fitness of MCF-7 Cells

To explore if Sirt3 plays a role in E2-induced metabolic activity of MCF-7 cells [25], we measured several parameters of mitochondrial function. First, we tested the effect of E2 and Sirt3 on metabolic activity of MCF-7 cells using MTT assay. The MTT salt is reduced to formazan in the metabolically active cells predominantly by mitochondrial complex-II subunit succinate dehydrogenase A (SDH-A) and is considered to be a marker of metabolic potential of the cell [26]. The Sirt3-overexpressing cells had significantly higher basal metabolic activity ($p < 0.001$) and Sirt3 further enhanced the inducing effect of E2 (Figure 3A), while ICI effectively abolished E2-induced metabolic activity to control levels in both cell lines. This result was confirmed with the observed protein expression levels of SDH-A

(Figure 3B), indicating the combined effect of E2 and Sirt3 and involvement of ER α in the regulation of metabolic activity in MCF-7 cells. Furthermore, the expression levels of respiratory complex I (NDUFA9) and III (UQCRC2) were also elevated in Sirt3 overexpressors ($p < 0.001$), although with no significant effect of E2 (Figure 3B). Another marker of mitochondrial functionality is the mitochondrial membrane potential ($\Delta\Psi_m$) which plays a key role in mitochondrial homeostasis [27]. While in the absence of Sirt3, $\Delta\Psi_m$ remained unaffected by E2 or ICI addition, the MCF-7S3 cells exhibited increased basal $\Delta\Psi_m$ ($p = 0.003$), which was further enhanced by E2 addition and abolished by ICI (Figure 3C, $p < 0.001$). These results collectively suggest that (a) Sirt3 acts synergistically with E2 to induce metabolic activity, (b) E2-induced rise in mitochondrial potential is Sirt3 dependent, and (c) ER α is involved in Sirt3-mediated mitochondrial fitness of MCF-7 cells.

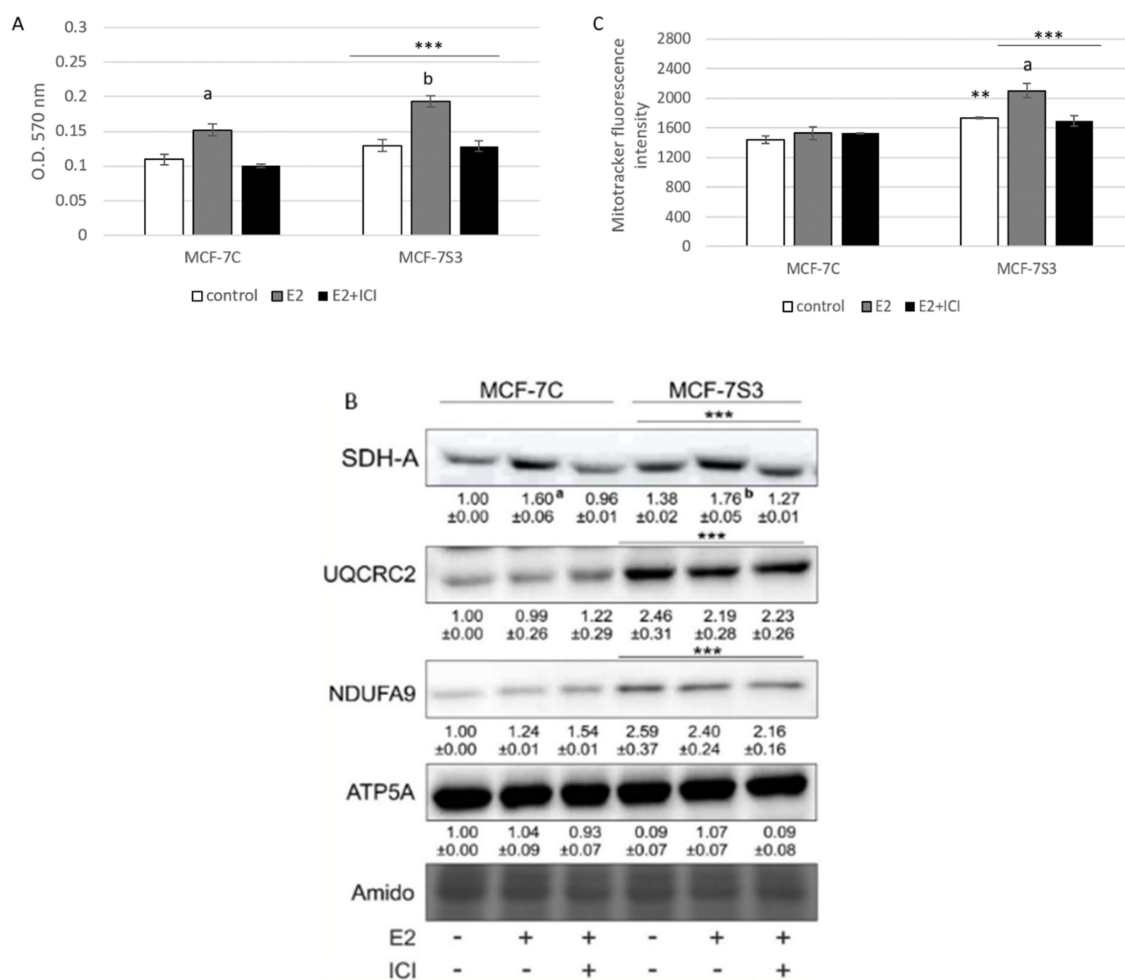


Figure 3. Sirt3 amplifies E2-induced metabolic activity and mitochondrial fitness of MCF-7 cells. (A) Metabolic activity measured with MTT assay. Two-way ANOVA revealed significant interaction effect between Sirt3 and treatment on metabolic activity $F(2,34) = 7.051$, $p = 0.003$, partial $\eta^2 = 0.293$; *** $p < 0.001$ MCF-7S3 vs. MCF-7C. In MCF-7C, higher in E2 vs. other groups (^a $p < 0.001$). In MCF-7S3, higher in E2-treated vs. other groups (^b $p < 0.001$). Results are shown as mean \pm SD ($n \geq 3$); (B) Immunoblots of mitochondrial respiration complexes. Two-way ANOVA revealed significant interaction effect between Sirt3 and treatment on SDH-A expression $F(2,6) = 10.846$, $p = 0.010$, partial $\eta^2 = 0.783$; *** $p < 0.001$ MCF-7C vs. MCF-7S3 cells. In MCF-7C, higher SDH-A expression in E2-treated vs. other groups (^a $p < 0.001$). In MCF-7S3, higher SDH-A expression in E2-treated vs. other groups (^b $p < 0.001$). Higher UQCRC2 and NDUFA9 protein expression in MCF-7S3 cells as compared with

MCF-7C (** $p < 0.001$). Results are shown as mean \pm SD normalized to the control MCF-7C ($n \geq 3$). Amidoblack was used as a loading control and representative immunoblots are shown; (C) Mitochondrial membrane potential ($\Delta\Psi_m$) measured with MitoTracker Deep Red dye using flow cytometry. Two-way ANOVA revealed significant interaction effect between Sirt3 and treatment $F(2,12) = 11,019$, $p = 0,010$, partial $\eta^2 = 0.786$; higher $\Delta\Psi_m$ in the control (** $p = 0.003$), E2, and E2 + ICI-treated (** $p < 0.001$) MCF-7S3 vs. MCF-7C. In MCF-7S3, higher $\Delta\Psi_m$ in E2 vs. the control and E2 + ICI-treated ($p < 0.001$). Results are shown as mean \pm S.D ($n \geq 3$).

3.4. Sirt3 Enhances Antioxidative Enzyme Activities and Cytosolic ROS, but Opposes E2-Induced Cytosolic and mtROS Production

Since it is known that Sirt3 mediates mitochondrial oxidative pathways and regulates production of ROS (reviewed by [28]), we aimed to analyze the antioxidant enzyme system in MCF-7S3 cells. We found that MCF-7S3 cells exhibited significantly increased activities of two major antioxidative enzymes, mitochondrial manganese-dependent superoxide dismutase MnSOD (SOD2, Figure 4A, $p < 0.001$) and cytosolic copper zinc-dependent superoxide dismutase CuZnSOD (SOD1, Figure 4B, $p < 0.001$), which was also confirmed by decreased expression level of inactive, acetylated form of MnSOD, AcSOD2 (Figure 4C, $p < 0.001$). Moreover, protein levels of the catalase (Cat) and transcription nuclear factor erythroid 2-related factor 2 (Nrf2), a major activator of antioxidant response, were also upregulated in Sirt3-overexpressing cells (Figure 4C, $p < 0.001$). Next, we examined the role of E2 in the activation of antioxidant enzyme system. While having a positive effect on the activation of CuZnSOD ($p < 0.001$), Cat ($p < 0.001$), and Nrf2 ($p < 0.01$) in the control cells, in Sirt3 overexpressors, E2 failed to further increase their already elevated levels (Figure 4B,C). Collectively, these results indicate that Sirt3-overexpressing cells exhibit a higher antioxidative response regardless of the E2 treatment. Due to the elevated antioxidant enzyme system in the MCF-7S3 cells, we aimed to investigate the effect of Sirt3 and E2 on cellular ROS levels and, on the one hand, found that E2 promoted mitochondrial ROS (mtROS) production in MCF-7C cells ($p < 0.001$), and this effect was inhibited by ICI (Figure 4E, $p < 0.001$). On the other hand, both cytosolic and mtROS levels were significantly reduced in E2-treated MCF-7S3 cells as compared with their controls (Figure 4D,E and $p < 0.001$). However, without E2 treatment, MCF-7S3 cells exhibited a significant rise in cytosolic ROS ($p < 0.001$) with a parallel decline in mtROS levels ($p = 0.002$). These results indicate that Sirt3 increases cytosolic ROS but abolishes E2-induced increase of both cytosolic and mtROS levels.

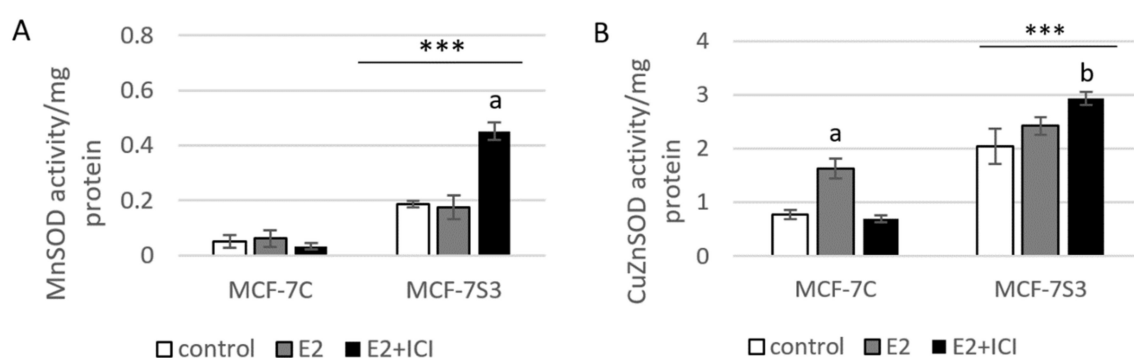


Figure 4. Cont.

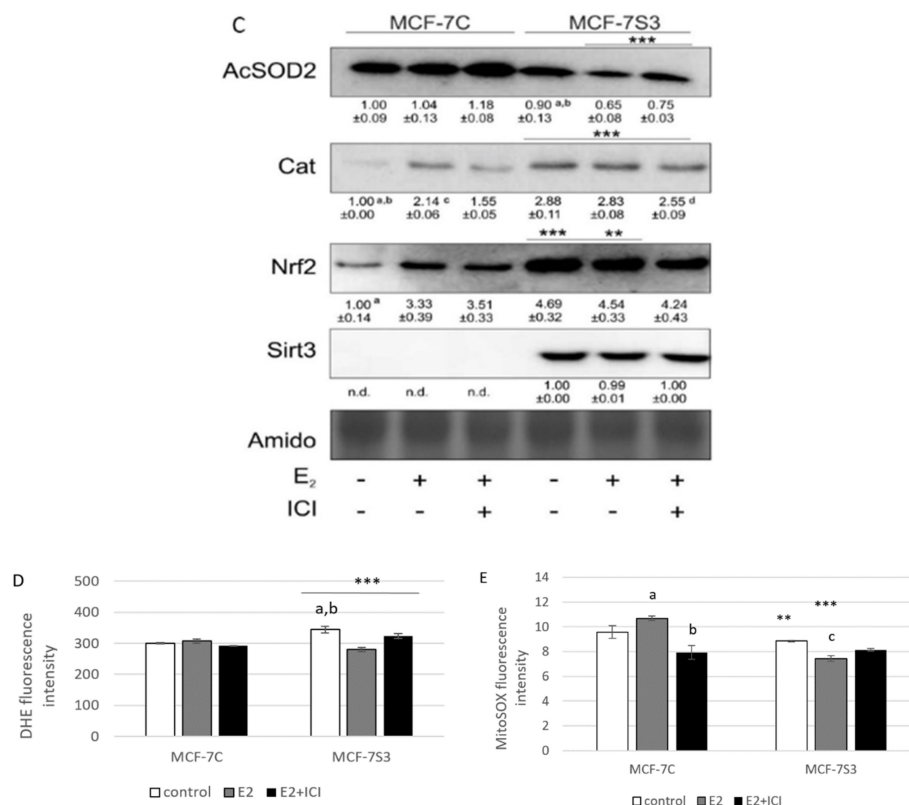


Figure 4. Sirt3 enhances antioxidative enzyme activities and cytosolic ROS but opposes E2-induced cytosolic and mtROS production. (A) For MnSOD activity, two-way ANOVA revealed a significant interaction effect between Sirt3 and treatment $F(2,12) = 53,853$, $p < 0.001$, partial $\eta^2 = 0.900$; *** $p < 0.001$ MCF-7S3 vs. MCF-7C. In MCF-7S3, higher activity in the E2 + ICI-treated vs. the other groups (^a $p < 0.001$); (B) For CuZnSOD activity, two-way ANOVA revealed a significant interaction effect between Sirt3 and treatment $F(2,12) = 75,435$, $p < 0.001$, partial $\eta^2 = 0.952$; *** $p < 0.001$ MCF-7S3 vs. MCF-7C. In MCF-7C, higher activity in the E2-treated vs. the other groups (^a $p < 0.001$). In MCF-7S3, higher activity in E2 + ICI vs. other groups (^b $p < 0.001$). Results are shown as mean \pm SD ($n \geq 3$); (C) For immunoblots of proteins of antioxidative response, two-way ANOVA revealed significant interaction effect between Sirt3 and treatment on AcSOD2 $F(2,12) = 11,691$; $p < 0.01$, partial $\eta^2 = 0.916$; E2 and E2 + ICI-treated MCF-7S3 vs. MCF-7C (*** $p < 0.001$). In MCF-7S3, higher AcSOD2 in the control vs. the E2 (^a $p < 0.01$) and E2 + ICI-treated (^b $p < 0.05$). Two-way ANOVA revealed significant interaction effect between Sirt3 and treatment on Cat $F(2,12) = 69,293$, $p < 0.001$, partial $\eta^2 = 0.959$; *** $p < 0.001$ MCF-7S3 vs. MCF-7C. In MCF-7C, lower Cat in the control vs. E2 (^a $p < 0.001$) and E2 + ICI-treated (^b $p < 0.01$); higher Cat in the E2 vs. E2 + ICI-treated (^c $p < 0.01$). In MCF-7S3, lower Cat in the E2 + ICI-treated vs. other groups (^d $p < 0.01$). Two-way ANOVA revealed significant interaction effect between Sirt3 and treatment on Nrf2 $F(2,12) = 14,011$, $p = 0.005$, partial $\eta^2 = 0.955$; the control (*** $p < 0.001$) and E2-treated (** $p < 0.01$) MCF-7S3 vs. MCF-7C. In MCF-7C, lower Nrf2 in the control vs. the other groups (^a $p < 0.01$). Results are shown as mean \pm SD normalized to the control MCF-7C ($n \geq 3$). Amidoblack was used as a loading control; (D) For cytosolic ROS levels measured with DHE, two-way ANOVA revealed a significant interaction between Sirt3 and treatment $F(2,12) = 805,710$, $p < 0.001$, partial $\eta^2 = 0.996$; *** $p < 0.001$ MCF-7C vs. MCF-7S3 cells. In MCF-7S3, lower cytosolic ROS in E2 (^a $p < 0.001$) and E2 + ICI-treated (^b $p < 0.01$) vs. the control cells; (E) For MitoROS levels measured with MitoSOX Red, two-way ANOVA revealed a significant interaction effect between Sirt3 and treatment $F(2,12) = 94.860$, $p < 0.001$, partial $\eta^2 = 0.941$; the control (** $p = 0.002$) and E2-treated (*** $p < 0.001$) MCF-7S3 vs. MCF-7C. In MCF-7C, higher mtROS in E2-treated vs. the control (^a $p < 0.001$); lower mtROS in E2 + ICI-treated vs. other groups (^b $p < 0.001$). In MCF-7S3, lower mtROS in E2-treated vs. other groups (^c $p < 0.01$). Results show the relative fluorescence intensity as the average geometric mean \pm SD ($n \geq 3$).

3.5. Sirt3 Abolishes the Proliferative Effect of E2 on Colony Forming Capacity by Diminishing the E2-Induced DNA Synthesis of MCF-7 Cells

Our previous results showed that Sirt3 has an inhibitory role on several tumorigenic parameters of MCF-7 cells [8], therefore, we wanted to analyze its effect on the colony forming capacity in the presence or absence of E2. Since the MCF-7S3 cells were not able to produce colonies in white DMEM, we also performed this experiment in red DMEM with the addition of E2 and ICI. The observed difference in clonogenic capacity of the cells in red and white DMEM is not surprising, since it is well known that ER α -positive breast cancer cells grow slower in phenol red-depleted media [17]. We observed a significant decrease in the colony forming ability of the MCF-7S3 cells in red DMEM as compared with the MCF-7C cells (Figure 5A,B and $p < 0.001$). As expected for the red DMEM, in which the phenol red mimics the action of E2 and renders cells unresponsive to the proliferative effect of physiological concentrations of E2 [29], E2 addition failed to show any difference in the number of colonies as compared with the untreated cells. In white DMEM, the colony forming capacity of the MCF-7C cells was reduced to 5% of their counterparts in red DMEM (Figure 5C,D). While E2 addition potentiated the growing capacity of the MCF-7C cells to nearly 70% of the cells in red DMEM, the MCF-7S3 cells completely failed to form colonies, even with the addition of E2. The number of colonies treated with ICI declined in both media as compared with their corresponding controls ($p < 0.001$). Collectively, these results indicate that Sirt3 attenuates the colony forming capacity of MCF-7 cells and abolishes the proliferative effect of E2 on MCF-7 cells.

Due to the observed reduced capacity of Sirt3-overexpressing cells to divide and form colonies, we investigated if Sirt3 affects cellular growth by inhibition of DNA synthesis using EdU Click-IT[®] assay (Thermo Fisher Scientific, USA). In white DMEM, E2 significantly promoted DNA synthesis in MCF-7C cells only (Figure 5E and $p < 0.05$), whereas the ICI treatment effectively inhibited DNA synthesis in both cell lines ($p < 0.05$). These data collectively indicate that Sirt3 abolishes cellular proliferation by inhibiting E2-induced DNA synthesis.

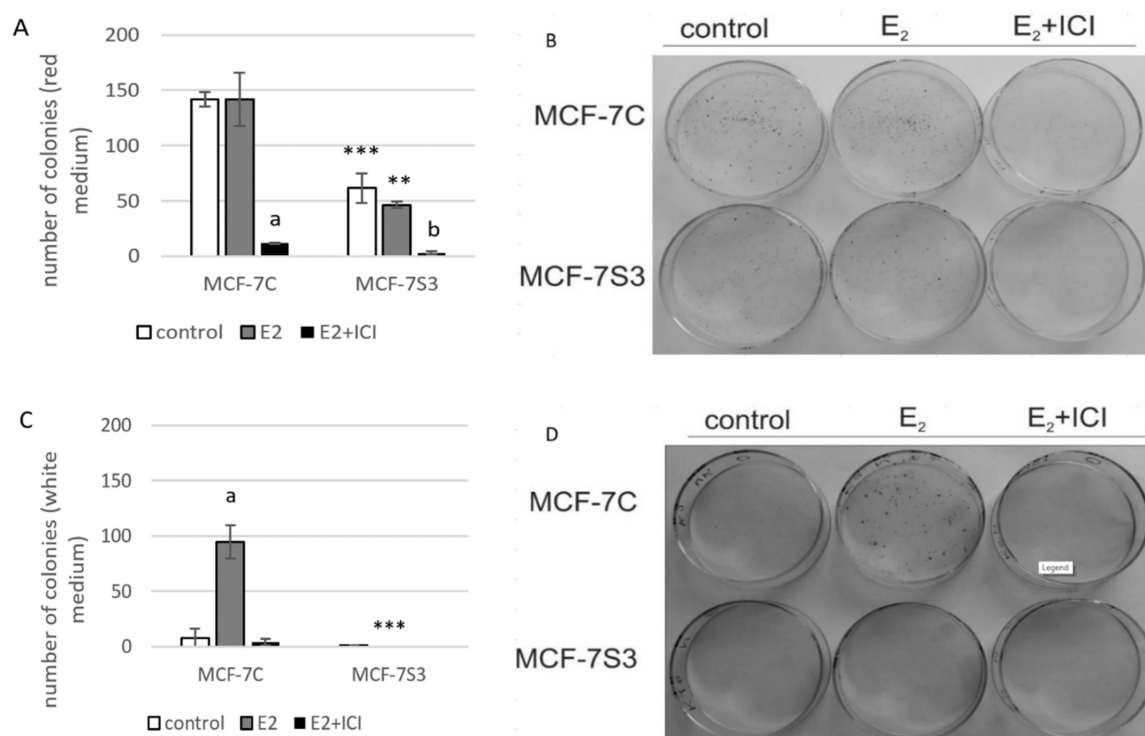


Figure 5. Cont.

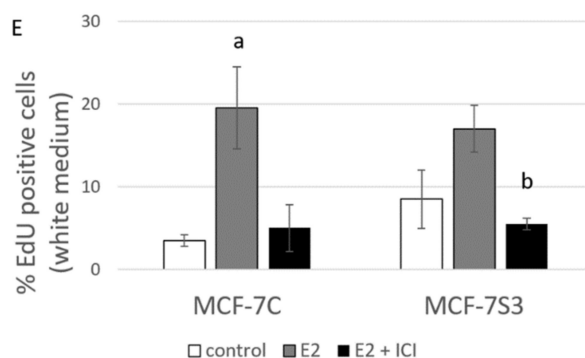


Figure 5. Sirt3 abolishes the proliferative effect of E2 on colony forming capacity by diminishing the E2-induced DNA synthesis of MCF-7 cells. (A) Histogram showing the number of colonies in red DMEM (CFU assay). Two-way ANOVA revealed significant interaction effect between Sirt3 and treatment on cellular clonogenic capacity $F(2,15) = 26,780$; $p < 0.001$; partial $\eta^2 = 0.856$; the control ($*** p < 0.001$) and E2-treated ($** p < 0.01$) MCF-7S3 vs. MCF-7C. In MCF-7C, lower E2 + ICI-treated vs. other groups ($^a p < 0.001$). In MCF-7S3, the lower E2 + ICI-treated vs. the other groups ($^b p < 0.001$). Results are shown as mean \pm SD ($n \geq 3$); (B) Representative plates of colonies grown in red DMEM stained with crystal violet; (C) Histogram showing the number of colonies in white DMEM (CFU assay). Two-way ANOVA revealed a significant interaction effect between Sirt3 and treatment on cellular clonogenic capacity $F(2,6) = 52.397$, $p < 0.001$, partial $\eta^2 = 0.946$, E2-treated ($*** p < 0.001$) MCF-7S3 vs. MCF-7C. In MCF-7C, higher in the E2-treated vs. the other groups ($^a p < 0.001$). Results are shown as mean \pm SD ($n \geq 3$); (D) Representative plates of colonies grown in white DMEM stained with crystal violet; (E) DNA synthesis as a sign of proliferation in white DMEM measured with Click-iT[®] assay using flow cytometry. In MCF-7C, higher in the E2-treated vs. other groups ($^a p < 0.05$). In MCF-7S3, lower in the E2 + ICI-treated vs. the E2-treated group ($^b p < 0.05$). Results are shown as mean \pm SD ($n \geq 3$).

3.6. Sirt3 Induces Tumor-Suppressive Markers in MCF-7 Cells

Since in our earlier study we observed higher levels of p53 in Sirt3-overexpressing cells [8], in this study, we investigated the level of p53 expression upon E2 treatment along with the expression of other p53-related proteins, such as apoptosis-inducing factor (AIF) and marker of DNA double strand breaks (phospho- γ H2AX). Consistent with our previous results, the p53 level was elevated in MCF-7S3 cells ($p < 0.001$). However, E2 and ICI had the opposite effect on the p53 expression level in Sirt3-overexpressed and control cells; while both treatments decreased p53 expression in MCF-7S3 cells ($p < 0.01$), they elevated the expression in the control MCF-7C cells (Figure 6A, $p < 0.05$ for E2 and $p < 0.001$ for E2 + ICI). AIF was significantly increased by both E2 and Sirt3 ($p < 0.001$), whereas DNA damage showed to be higher in the presence of Sirt3 ($p < 0.001$), however, was lowered by E2 addition ($p < 0.001$). This was confirmed by confocal microscopy which clearly demonstrated more DNA damage in the Sirt3-overexpressed cells, and less in the E2-treated groups of both cell lines (Figure 6B). In addition, we also noticed a higher number of micronucleated cells in the Sirt3-overexpressed line (Figure 6C), which is considered to be an indicator of genomic instability and usually predisposes cells to apoptosis [30]. The MCF-7S3 line displayed a higher frequency of micronucleated cells than the controls, with values similar to the H_2O_2 -treated cells, which were used as a positive control for the induction of apoptosis [31]. Since earlier studies showed that upon both DNA damage and p53 activation, cell migration is decreased [32–34], we also checked the migration of the cells. The migration rate was reduced in the MCF-7S3 cells as compared with the controls ($p = 0.007$). Moreover, while migration was not affected by E2 in the control cells, E2 administration only slightly increased migration in the Sirt3 overexpressors (Figure 6D and Supplementary Figure S2). These data collectively demonstrate the tumor-suppressive role of Sirt3 in MCF-7 cells, which is partially restored by E2 treatment.

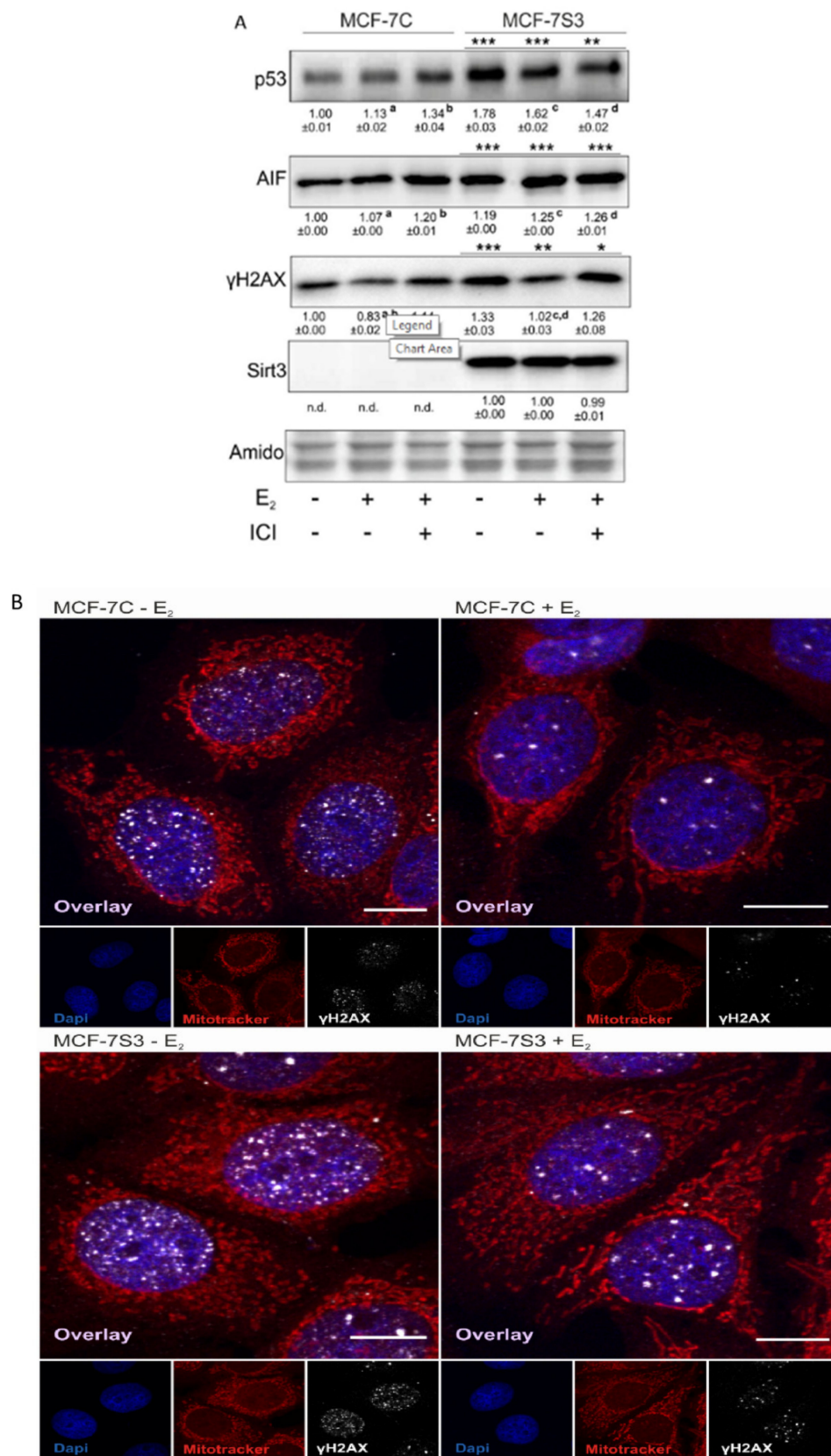


Figure 6. Cont.

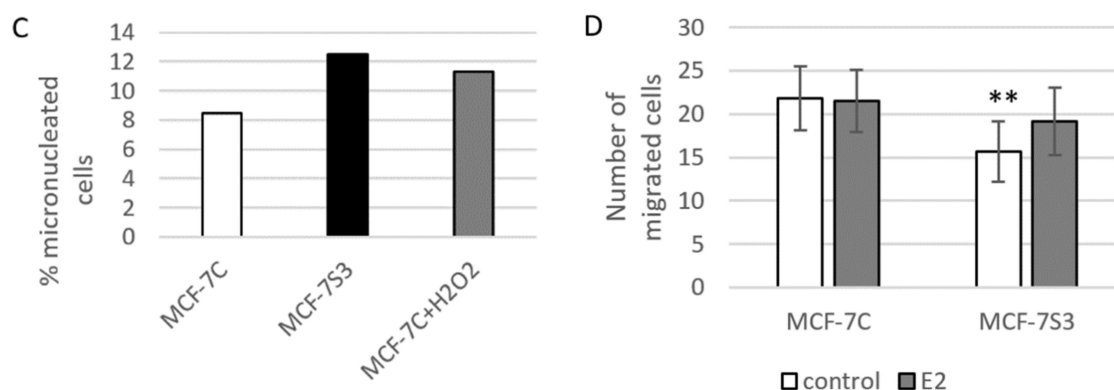


Figure 6. Sirt3 induces tumor-suppressive markers in MCF-7 cells. **(A)** Western blot analysis of proteins associated with tumor-suppressive function. Two-way ANOVA revealed a significant interaction effect between Sirt3 and treatment on the p53 level $F(2,12) = 118.1$, $p < 0.001$, partial $\eta^2 = 0.975$; higher in the MCF-7S3 control and E2-treated ($*** p < 0.001$) and E2 + ICI-treated ($** p < 0.01$) vs. MCF-7C. In MCF-7C, higher in the E2 ($^a p < 0.05$) and E2 + ICI-treated ($^b p < 0.001$) vs. the control. In MCF-7S3, lower in the E2 and E2 + ICI-treated vs. the control ($^{c,d} p < 0.01$). For AIF, two-way ANOVA revealed a significant interaction effect between Sirt3 and treatment $F(2,12) = 187.56$, $p < 0.001$, partial $\eta^2 = 0.984$; $*** p < 0.001$ MCF-7S3 vs. MCF-7C. In MCF-7C, higher in the E2 and E2 + ICI-treated vs. the control ($^{a,b} p < 0.001$). In MCF-7S3, higher in the E2 and E2 + ICI-treated vs. the control ($^{c,d} p < 0.001$). For phospho- γ H2AX, two-way ANOVA revealed significant interaction effect between Sirt3 and treatment $F(2,12) = 5.39$, $p < 0.05$, partial $\eta^2 = 0.642$; the MCF-7S3 control ($*** p < 0.001$), E2 ($** p < 0.01$), and E2 + ICI-treated ($* p < 0.05$) vs. MCF-7C. In MCF-7C, lower in E2 vs. the control ($^a p < 0.05$) and E2 + ICI-treated ($^b p < 0.01$). In MCF-7S3, lower in E2 vs. the control ($^c p < 0.001$) and E2 + ICI-treated ($^d p < 0.01$). Results are shown as mean \pm SD ($n \geq 3$). Amidoblack was used as a loading control; **(B)** Confocal imaging of phospho- γ H2AX signal abundance as a marker of DNA damage in MCF-7C and MCF-7S3 cells with or without E2 treatment. Bar represents 10 μ m; **(C)** Graphical chart of frequency of micronucleated cells in MCF-7C and MCF-7S3 cells, as well as in MCF-7C cells treated with H₂O₂ as a positive control. The experiments were repeated at least three times and representative data are shown; **(D)** Graphical chart of number of migrated MCF-7C and MCF-7S3 cells with or without E2 treatment. Two-way ANOVA revealed a significant effect of Sirt3 on migration rate $F(1,23) = 1.812$, $p = 0.007$, partial $\eta^2 = 0.279$; lower in MCF-7S3 vs. MCF-7C cells ($** p = 0.007$). Results are shown as mean \pm SD ($n \geq 3$).

3.7. Sirt3 Induces Disruption of ER α –p53 Interaction in MCF-7 Cells

Due to the observed higher expression of p53 in MCF-7S3 cells, we hypothesized that Sirt3 can contribute to the lower proliferative capacity of the cells by increasing the p53 level. It is known that ER α binds p53 and represses its function [35]. Since we observed no interaction between Sirt3 and p53 (Supplementary Figure S1), we tested to determine if Sirt3 affects p53 indirectly by altering the crosstalk between ER α and p53. Using coimmunoprecipitation, we demonstrated that in the MCF-7S3 cells ER α binding to p53 was markedly reduced as compared with the MCF-7C cells ($p < 0.001$) and E2 addition partially reverted this interaction (Figure 7). These results indicate that Sirt3-induced disruption of the ER α –p53 interaction is partially reverted by E2 addition.

Collectively, on the one hand, the results show that Sirt3 improved the antioxidative response and mitochondrial fitness of the MCF-7 cells. On the other hand, it increased cytosolic ROS, DNA damage, along with p53, AIF, and ER α expression. Moreover, Sirt3 disrupted the p53–ER α interaction resulting in attenuation of tumor-promoting properties and proliferative effect of E2 in MCF-7 cells.

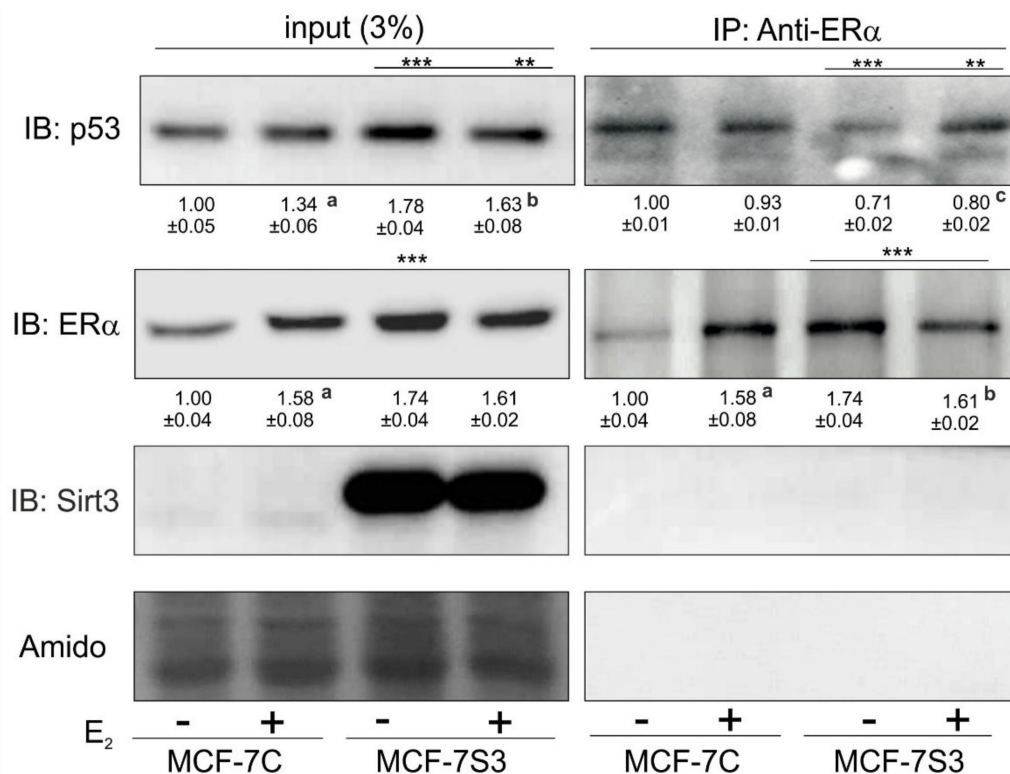


Figure 7. Sirt3 induces disruption of the ER α –p53 interaction in MCF-7 cells. Western blot analysis of coimmunoprecipitation experiment of ER α and its interacting partners using anti-ER α and anti-p53 antibody. For input p53, MCF-7C + E2 vs. MCF-7C (^a $p < 0.001$), MCF-7S3 + E2 vs. MCF-7S3 (^b $p < 0.01$), the MCF-7S3 control vs. MCF-7C (^{***} $p < 0.001$), MCF-7S3 + E2 vs. MCF-7C (^{**} $p < 0.01$). For input ER α , MCF-7C + E2 vs. MCF-7C (^a $p < 0.01$), MCF-7S3 vs. MCF-7C (^{***} $p < 0.001$). For IP-ER α , a control that IP was successful (MCF-7C + E2 vs. MCF-7C (^a $p < 0.001$, MCF-7S3 + E2 vs. MCF-7S3 (^b $p < 0.001$, and MCF-7S3 vs. MCF-7C (^{***} $p < 0.001$). For IP-Sirt3, a confirmation that there is no interaction between ER α and Sirt3. For IP-p53, two-way ANOVA revealed a significant interaction effect between Sirt3 and treatment on the p53 level $F(1,4) = 64.47$, $p = 0.001$, partial $\eta^2 = 0.942$; lower in the control (^{***} $p < 0.001$) and the E2-treated (^{**} $p < 0.01$) MCF-7S3 vs. MCF-7C. In MCF-7S3, lower in the control vs. the E2-treated cells (^c $p = 0.003$). Representative blots are shown ($n \geq 3$).

4. Discussion

The significance of Sirt3 in breast cancer cells lies in the fact that only 23% of normal breast tissue shows to be negative for Sirt3 expression, whereas even up to 72% of in situ breast lesions and 74% of invasive lesions are negative for the expression of Sirt3 [14]. Previously, we showed the tumor-suppressive role of overexpressed Sirt3 in human MCF-7 breast cancer cells, which are characterized by low Sirt3 expression [8]. In this study, we investigated if the tumor-suppressive effect of Sirt3 is mediated through the ER α signaling pathway in MCF-7 cells [3]. In this study, we report that a mitochondrial protein Sirt3, despite improving the mitochondrial function, induces DNA damage and tumor-suppressive factors, affects p53 by disruption of the ER α –p53 interaction, reduces response of the MCF-7 cells to E2 treatment, and consequently inhibits the migration and clonogenic capacity of the cells.

The expression of ER α can be regulated by different cellular factors and mechanisms (reviewed by [36]) and, in our study, we found that there is significant upregulation of ER α expression in Sirt3-overexpressing cells (Figure 1B,C). Furthermore, Sirt3 silencing caused downregulation of ER α expression (Figure 1D), indicating the involvement of Sirt3 in the ER α expression level. Since Sirt3 is a mitochondrial protein and ER α is mostly localized in the nucleus [37,38], it is unlikely that they interact. Some earlier studies proposed the regulation of a small fraction of ER α by estrogen in mitochondria

(reviewed by [39]), but these claims are still controversial. We were also not able to confirm interaction between Sirt3 and ER α (Supplementary Figure S1). Moreover, confocal microscopy confirmed, in our model, that ER α , indeed, does not reside inside mitochondria, and Sirt3 does not reside in the nucleus (Figure 2) or cytoplasm, as was already shown in our previous study [8]. Thus, we hypothesized that overexpressed Sirt3 indirectly regulates the expression of ER α in MCF-7 breast cancer cells. It is known that ER α contains a nuclear localization signal for the transport into the nucleus, which happens 10 to 30 min after E2 stimulation (reviewed by [40]). Therefore, we investigated the nuclear level of ER α as an indicator of its E2-stimulated activation. The fractionation experiments indicated that both MCF-7C and MCF-7S3 cells have functional ER α because it was successfully shuttled into the nucleus upon E2 treatment (Figure 1E). ICI, a compound that impairs the dimerization of ER- α , an event that takes place after E2 binding and is essential for the nuclear localization of the receptor [41], led to receptor degradation (Figure 1C,E) and partially depleted its nuclear localization as judged by more cytoplasmic ER α (Figure 2). Altogether, these data confirmed that ER α in our system is activated by E2 and that ICI is a good control for analysis of the ER-dependent pathways.

Several studies have shown that E2 has the ability to increase mitochondrial function and biogenesis (reviewed in [42]), therefore, we explored whether Sirt3 plays a role in E2-induced metabolic fitness of MCF-7 cells. As observed in Figure 3A,C, Sirt3 potentiated this inducing effect of E2 leading to increased metabolic activity, primarily as a result of the induced rise in SDH-A expression (Figure 3B) [26]. This is not surprising, considering that ER α is an essential estrogen receptor for most E2-mediated increases in respiratory chain proteins and antioxidant enzymes [43,44]. Furthermore, Sirt3 also induced expression of complex I (NDUFA9) and III (UQCRC2) and elevated mitochondrial potential (Figure 3C). The latter was further enhanced upon E2 addition, indicating that the E2-induced rise in mitochondrial potential is Sirt3 dependent.

Elevated ROS is a common hallmark of cancer progression and can activate oncogenic signals involved in cell proliferation [45,46], hence, we wanted to check the ROS status of our cell lines. In agreement with others [47], our results showed that E2 promoted mtROS production in MCF-7C cells, while ICI abolished this effect (Figure 4E), suggesting the involvement of the ER α receptor in the E2-induced production of mtROS. This is not surprising, since E2 plays a critical role in the development of breast cancer by altering the mitochondrial function and causing a shift towards higher mtROS levels [48]. Sirt3 is a mitochondrial protein involved in the regulation of mitochondrial oxidative pathways [28] and we tested to determine if it regulates E2-induced proliferation by affecting ROS levels. In Sirt3-overexpressing cells, we observed lower mtROS levels (Figure 4E) and hypothesized that this could be the result of a more efficient mitochondrial antioxidant enzyme system induced by Sirt3. The oxidative stress response is manifested through upregulated antioxidative enzymes such as SOD and Cat that are under the control of Nrf2, which is activated upon oxidative stress or increased ROS production (reviewed by [49]). Our results showed a significant increase of Nrf2, Cat, and SOD in the MCF-7S3 cells (Figure 4A–C), indicating that the Sirt3-induced antioxidative response is associated with enhanced metabolic activity of the cells. Contrary to the MCF-7C cells, the E2-treated Sirt3-overexpressed cells showed lowered levels of both cytosolic and mtROS (Figure 4D,E), suggesting that the E2-generation of ROS is attenuated by Sirt3. Since numerous data postulate that an increase in ROS generated after exposure to E2 contributes to the development of human breast cancer [50,51], our findings propose that Sirt3 can function as a tumor suppressor by activating antioxidative enzymes and attenuating the E2-induced ROS levels from both cytosolic and mitochondrial compartments.

Although the Sirt3-overexpressing cells demonstrated improved mitochondrial function and antioxidative enzyme system response, the opposite effect was observed on their proliferation and migration. Control of proliferation by estrogens is a very complex process based on E2 binding to ER α and subsequent regulation of target genes and concomitant activation of G1 to S phase progression [16]. In the case of non-invasive ER α -positive MCF-7 cells that otherwise display reduced expression of Sirt3 protein [52], the overexpression of Sirt3 diminished their growth, suggesting that Sirt3 inhibits their tumorigenic properties [8]. Furthermore, this inhibitory effect of Sirt3 is enhanced in the white

DMEM regardless of E2 treatment (Figure 5A–D), indicating again that Sirt3 attenuates the proliferative effect of E2 on these cells. Interestingly, the observation that Sirt3-overexpressing cells have higher metabolic activity (Figure 3A) seems opposite to the fact that they show lower proliferation (Figure 5). However, cell cycle arrest does not necessarily result in metabolic dysfunction. On the contrary, some stressors can even increase the metabolic activity [53]. The Sirt3-mediated inhibitory effect on E2-induced proliferation was also supported by the analysis of DNA synthesis where we showed that E2 promotes DNA synthesis to a lesser extent in the MCF-7S3 cells as compared with the MCF-7C cells (Figure 5E). ICI decreases BrdU incorporation irrespective of Sirt3, confirming previous findings of the anti-proliferative effect of ICI by inhibition of DNA synthesis [53].

The mechanism of the Sirt3 effect on the reduction of clonogenic capacity is still not clear but involves DNA damage accumulation observed as an increase in γ H2AX phosphorylation. The increased DNA damage was accompanied by a higher frequency of micronucleated cells in Sirt3-overexpressed cells, which are characterized by small, extra-nuclear chromatin bodies that arise in dividing cells due to chromosome aberrations or genome mutations (reviewed by [30]), and therefore are used as an indicator of genomic instability. In addition to the observed higher DNA damage and more micronucleated cells, the Sirt3-overexpressed cells also showed lower migration capacity. Some of these effects were partially rescued by E2 addition (Figure 6 and Supplementary Figure S2). These observations indicate that Sirt3 overexpression is associated with excessive genomic instability of MCF-7 cells, which can be alleviated by E2 treatment but only to a limited extent. However, this is not sufficient to rescue tumorigenic properties of these cells.

Since, in our earlier study, we observed higher levels of p53 in MCF-7S3 cells [8], we hypothesized that Sirt3 contributes to lower cellular proliferative capacity by increasing the p53 level. The upregulation of p53 and the tumor-suppressive effect of Sirt3 was shown also in other types of cancers [54,55]. The p53 protein is a transcriptional regulator and tumor suppressor that activates target genes for cell cycle arrest, apoptosis, and DNA repair, and is stabilized within the nucleus upon DNA damage or oncogenic signals (reviewed by [56]). Furthermore, p53 balances mitochondrial respiration by inhibiting the glycolysis and promoting OXPHOS. Our results showed that p53 is indeed upregulated in Sirt3-overexpressing cells (Figure 6A), but not through the interaction between Sirt3 and p53 (Supplementary Figure S1). Consistently, the apoptosis inducing factor (AIF), known to be transcriptionally upregulated by p53 [57], was also upregulated in Sirt3 clones. AIF is a mitochondrial flavoprotein harboring numerous functions for efficient oxidative phosphorylation and cytoprotective role in the mitochondria [58,59]. However, it has the opposite effect on cell survival upon translocation to the nucleus, where it serves as a potent pro-apoptotic trigger [60], resulting in large-scale DNA fragmentation [61]. This is also in line with the observed higher frequency of micronucleated cells in Sirt3-overexpressing cells (Figure 6C). Studies have shown that ER α directly binds to p53 and represses its function, thus, affecting p53-mediated cell cycle arrest [62]. Since ER α binding to p53 results in inactivation of p53, disruption of this interaction by Sirt3 indicates the possible mechanism of the tumor suppressive role of Sirt3 in breast cancer. Our results suggest that this disruption of the ER α –p53 interaction is partially rescued upon E2 addition (Figure 7). However, these E2-mediated effects are not sufficient for MCF-7S3 cells to reach the proliferation capacity of the control cells (Figure 5A–D). Furthermore, the observed overexpression of ER α (Figure 1C) correlates well with the increased level of p53 (Figure 6A), which is associated with inhibition of cellular growth [63]. Finally, while p53 can enhance metabolic activity by promoting OXPHOS [56], at the same time it inhibits cell cycle progression and causes a suppressive effect on growth of cancer cells.

5. Conclusions

In conclusion, based on the results from this study, we report that Sirt3, despite improving the mitochondrial function of MCF-7 breast cancer cells, reduces their response to E2, affects p53 by disruption of the ER α –p53 interaction, and inhibits clonogenic cell growth. Furthermore, the tumor suppressive effects of Sirt3 could be partially reversed by E2 treatment, but this is not sufficient to

rescue the full tumorigenic potential of these cells. Therefore, because the majority of breast cancers are negative for the expression of Sirt3, we conclude that by reverting its expression in MCF-7 cells, breast cancer cell normalization could be induced. Thus, Sirt3 should be considered to be a potential therapeutic measure for treating E2-dependent breast cancers.

Supplementary Materials: The following are available online at <http://www.mdpi.com/2076-3921/9/4/294/s1>, Table S1: Antibodies used in this study for Western blot analyses, Table S2: Antibodies used in this study for immunofluorescence analyses, Figure S1: Sirt3 does not interact with p53 or ER α in MCF-7 cells, Figure S2: E2 partially rescues reduced migration of MCF-7S3 cells.

Author Contributions: Conceptualization, M.P. (Marija Pinteric), I.I.P., and S.S.; Formal analysis, M.P. (Marija Pinteric), I.I.P., M.P.H., V.F., M.P. (Mladen Paradzik), B.L.J.P., A.D., I.C., and S.S.; Funding acquisition, T.B.; Investigation, M.P. (Marija Pinteric), I.I.P., M.P.H., D.P., D.M., and S.S.; Methodology, M.P. (Marija Pinteric), I.I.P., M.P.H., M.P. (Mladen Paradzik), B.L.J.P., A.D., I.C., D.P., D.M., T.B. and S.S.; Project administration, T.B.; Resources, T. B.; Software, I.I.P. and S.S.; Supervision, T.B. and S.S.; Validation, S.S.; Visualization, V.F.; Writing—original draft, M.P. (Marija Pinteric), I.I.P. and S.S.; Writing—review and editing, M.P. (Marija Pinteric), I.I.P., M.P.H., V.F., M.P. (Mladen Paradzik), B.L.J.P., A.D., I.C., D.P., D.M., T.B., and S.S. All authors have read and agreed to the published version of the manuscript.

Funding: This research was funded by the Croatian Science Foundation (HRZZ), grant no. IP-2014-09-4533 “SuMERA”, and with the support of the Marie Curie Alumni Association.

Acknowledgments: The authors would like to thank Iva Pešun Medimorec and Marina Marš for their excellent technical contribution.

Conflicts of Interest: The authors declare no conflict of interest. The funders had no role in the design of the study; in the collection, analyses, or interpretation of data; in the writing of the manuscript, or in the decision to publish the results.

References

1. Zárate, S.; Stevnsner, T.; Gredilla, R. Role of estrogen and other sex hormones in brain aging. Neuroprotection and DNA repair. *Front. Aging Neurosci.* **2017**, *9*, 430. [[CrossRef](#)] [[PubMed](#)]
2. Trenti, A.; Tedesco, S.; Boscaro, C.; Trevisi, L.; Bolego, C.; Cignarella, A. Estrogen, angiogenesis, immunity and cell metabolism: solving the puzzle. *Int. J. Mol. Sci.* **2018**, *19*, 859. [[CrossRef](#)] [[PubMed](#)]
3. Holst, F.; Stahl, P.R.; Ruiz, C.; Hellwinkel, O.; Jehan, Z.; Wendland, M.; Lebeau, A.; Terracciano, L.; Al-Kuraya, K.; Jänicke, F.; et al. Estrogen receptor alpha (ESR1) gene amplification is frequent in breast cancer. *Nat. Genet.* **2007**, *39*, 655–660. [[CrossRef](#)] [[PubMed](#)]
4. Klinge, C.M.; Jernigan, S.C.; Mattingly, K.A.; Risinger, K.E.; Zhang, J. Estrogen response element-dependent regulation of transcriptional activation of estrogen receptors α and β by coactivators and corepressors. *J. Mol. Endocrinol.* **2004**, *33*, 387–410. [[CrossRef](#)]
5. Musgrove, E.A.; Sutherland, R.L. Biological determinants of endocrine resistance in breast cancer. *Nat. Rev. Cancer* **2009**, *9*, 631–643. [[CrossRef](#)]
6. Reid, G.; Hübner, M.R.; Métivier, R.; Brand, H.; Denger, S.; Manu, D.; Beaudouin, J.; Ellenberg, J.; Gannon, F. Cyclic, Proteasome-mediated turnover of unliganded and liganded ER α on responsive promoters is an integral feature of estrogen signaling. *Mol. Cell* **2003**, *11*, 695–707. [[CrossRef](#)]
7. Torrens-Mas, M.; Pons, D.G.; Sastre-Serra, J.; Oliver, J.; Roca, P. SIRT3 silencing sensitizes breast cancer cells to cytotoxic treatments through an increment in ROS production. *J. Cell. Biochem.* **2016**, *118*, 397–406. [[CrossRef](#)]
8. Pinterić, M.; Skrinjar, I.; Sobočanec, S.; Hadžija, M.P.; Paradzik, M.; Dekanić, A.; Marinović, M.; Halasz, M.; Belužić, R.; Davidović, G.; et al. De novo expression of transfected sirtuin 3 enhances susceptibility of human MCF-7 breast cancer cells to hyperoxia treatment. *Free. Radic. Res.* **2018**, *52*, 672–684. [[CrossRef](#)]
9. Li, T.; Kon, N.; Jiang, L.; Tan, M.; Ludwig, T.; Zhao, Y.; Baer, R.; Gu, W. Tumor suppression in the absence of p53-mediated cell-cycle arrest, apoptosis, and senescence. *Cell* **2012**, *149*, 1269–1283. [[CrossRef](#)]
10. Oren, M.; Damalas, A.; Gottlieb, T.; Michael, D.; Taplick, J.; Leal, J.F.M.; Maya, R.; Moas, M.; Seger, R.; Taya, Y.; et al. Regulation of p53. *Ann. N. Y. Acad. Sci.* **2002**, *973*, 374–383. [[CrossRef](#)]
11. Lacroix, M.; Toillon, R.-A.; Leclercq, G. p53 and breast cancer, an update. *Endocr-Relat. Cancer* **2006**, *13*, 293–325. [[CrossRef](#)] [[PubMed](#)]

12. Konduri, S.D.; Medisetty, R.; Liu, W.; Kaiparettu, B.; Srivastava, P.; Brauch, H.; Fritz, P.; Swetzig, W.M.; Gardner, A.E.; Khan, S.A.; et al. Mechanisms of estrogen receptor antagonism toward p53 and its implications in breast cancer therapeutic response and stem cell regulation. *Proc. Natl. Acad. Sci. USA* **2010**, *107*, 15081–15086. [[CrossRef](#)]
13. Rochefort, H.; Platet, N.; Hayashido, Y.; Derocq, D.; Lucas, A.; Cunaat, S.; Garcia, M. Estrogen receptor mediated inhibition of cancer cell invasion and motility: An overview. *J. Steroid Biochem. Mol. Biol.* **1998**, *65*, 163–168. [[CrossRef](#)]
14. Desouki, M.M.; Doubinskaia, I.; Gius, D.; Abdulkadir, S.A. Decreased mitochondrial SIRT3 expression is a potential molecular biomarker associated with poor outcome in breast cancer. *Hum. Pathol.* **2014**, *45*, 1071–1077. [[CrossRef](#)]
15. Zhao, K.; Zhou, Y.; Qiao, C.; Ni, T.; Li, Z.; Wang, X.; Guo, Q.; Lu, N.; Wei, L. Oroxyn A promotes PTEN-mediated negative regulation of MDM2 transcription via SIRT3-mediated deacetylation to stabilize p53 and inhibit glycolysis in wt-p53 cancer cells. *J. Hematol. Oncol.* **2015**, *8*, 41. [[CrossRef](#)] [[PubMed](#)]
16. Dalvai, M.; Bystricky, K. Cell cycle and anti-estrogen effects synergize to regulate cell proliferation and ER target gene expression. *PLoS ONE* **2010**, *5*, e11011. [[CrossRef](#)] [[PubMed](#)]
17. Węsierska-Gądek, J.; Schreiner, T.; Maurer, M.; Waringer, A.; Ranftler, C. Phenol red in the culture medium strongly affects the susceptibility of human MCF-7 cells to roscovitine. *Cell. Mol. Biol. Lett.* **2007**, *12*, 280–293. [[CrossRef](#)]
18. Tristan, C.; Shahani, N.; Sedlak, T.W.; Sawa, A. The diverse functions of GAPDH: Views from different subcellular compartments. *Cell. Signal.* **2010**, *23*, 317–323. [[CrossRef](#)]
19. DiMauro, I.; Pearson, T.; Caporossi, D.; Jackson, M.J. A simple protocol for the subcellular fractionation of skeletal muscle cells and tissue. *BMC Res. Notes* **2012**, *5*, 513. [[CrossRef](#)]
20. Šarić, A.; Crnolatac, I.; Bouillaud, F.; Sobočanec, S.; Mikecin, A.-M.; Šafranko, Ž.M.; Delgeorgiev, T.; Piantanida, I.; Balog, T.; Petit, P.X.; et al. Non-toxic fluorescent phosphonium probes to detect mitochondrial potential. *Methods Appl. Fluoresc.* **2017**, *5*, 15007. [[CrossRef](#)]
21. Chehrehasa, F.; Meedeniya, A.C.; Dwyer, P.; Abrahamsen, G.; Mackay-Sim, A. EdU, a new thymidine analogue for labelling proliferating cells in the nervous system. *J. Neurosci. Methods* **2009**, *177*, 122–130. [[CrossRef](#)] [[PubMed](#)]
22. Totta, P.; Pesiri, V.; Marino, M.; Acconcia, F. Lysosomal function is involved in 17 β -estradiol-induced estrogen receptor α degradation and cell proliferation. *PLoS ONE* **2014**, *9*, e94880. [[CrossRef](#)]
23. Chen, J.Q.; Delannoy, M.; Cooke, C.; Yager, J.D. Mitochondrial localization of ER α and ER β in human MCF7 cells. *Am. J. Physiol. Metab.* **2004**, *286*, E1011–E1022. [[CrossRef](#)] [[PubMed](#)]
24. Yaşar, P.; Ayaz, G.; User, S.D.; Güpür, G.; Muyan, M. Molecular mechanism of estrogen-estrogen receptor signaling. *Reprod. Med. Biol.* **2016**, *16*, 4–20. [[CrossRef](#)] [[PubMed](#)]
25. Ko, B.H.; Paik, J.Y.; Jung, K.H.; Lee, K.H. 17 β -estradiol augments 18 F-FDG uptake and glycolysis of T47D breast cancer cells via membrane-initiated rapid PI3K-Akt activation. *J. Nucl. Med.* **2010**, *51*, 1740–1747. [[CrossRef](#)]
26. Rai, Y.; Pathak, R.; Kumari, N.; Sah, D.K.; Pandey, S.; Kalra, N.; Soni, R.; Dwarakanath, B.S.; Bhatt, A.N. Mitochondrial biogenesis and metabolic hyperactivation limits the application of MTT assay in the estimation of radiation induced growth inhibition. *Sci. Rep.* **2018**, *8*, 1531. [[CrossRef](#)]
27. Zorova, L.D.; Popkov, V.A.; Plotnikov, E.Y.; Silachev, D.N.; Pevzner, I.B.; Jankauskas, S.S.; Babenko, V.A.; Zorov, S.D.; Balakireva, A.V.; Juhaszova, M.; et al. Mitochondrial membrane potential. *Anal. Biochem.* **2018**, *552*, 50–59. [[CrossRef](#)]
28. Singh, C.K.; Chhabra, G.; Ndiaye, M.A.; Garcia-Peterson, L.M.; Mack, N.J.; Ahmad, N. The role of sirtuins in antioxidant and redox signaling. *Antioxid. Redox Signal.* **2018**, *28*, 643–661. [[CrossRef](#)]
29. Węsierska-Gądek, J.; Schreiner, T.; Gueorgieva, M.; Ranftler, C. Phenol red reduces ROSC mediated cell cycle arrest and apoptosis in human MCF-7 cells. *J. Cell. Biochem.* **2006**, *98*, 1367–1379. [[CrossRef](#)]
30. Hintzsche, H.; Hemmann, U.; Poth, A.; Utesch, D.; Lott, J.; Stopper, H.; Working Group “In vitro micronucleus test”; Gesellschaft für Umwelt-Mutationsforschung (GUM, German-speaking section of the European Environmental Mutagenesis and Genomics Society EEMGS). Fate of micronuclei and micronucleated cells. *Mutat. Res. Mutat. Res.* **2017**, *771*, 85–98. [[CrossRef](#)]

31. Fenech, M.; Crott, J.; Turner, J.; Brown, S. Necrosis, apoptosis, cytostasis and DNA damage in human lymphocytes measured simultaneously within the cytokinesis-block micronucleus assay: Description of the method and results for hydrogen peroxide. *Mutagenesis* **1999**, *14*, 605–612. [\[CrossRef\]](#) [\[PubMed\]](#)
32. Hsu, F.-F.; Lin, T.-Y.; Chen, J.-Y.; Shieh, S.-Y. p53-Mediated transactivation of LIMK2b links actin dynamics to cell cycle checkpoint control. *Oncogene* **2010**, *29*, 2864–2876. [\[CrossRef\]](#) [\[PubMed\]](#)
33. Herraiz, C.; Calvo, F.; Pandya, P.; Cantelli, G.; Rodriguez-Hernandez, I.; Orgaz, J.; Kang, N.; Chu, T.; Sahai, E.; Sanz-Moreno, V. Reactivation of p53 by a cytoskeletal sensor to control the balance between DNA damage and tumor dissemination. *J. Natl. Cancer Inst.* **2015**, *108*, 289. [\[CrossRef\]](#) [\[PubMed\]](#)
34. Roger, L.; Gadea, G.; Roux, P. Control of cell migration: A tumour suppressor function for p53? *Boil. Cell* **2006**, *98*, 141–152. [\[CrossRef\]](#) [\[PubMed\]](#)
35. Liu, W.; Konduri, S.D.; Bansal, S.; Nayak, B.K.; Rajasekaran, S.A.; Karuppayil, S.M.; Rajasekaran, A.K. Estrogen receptor- α binds p53 tumor suppressor protein. *J. Biol. Chem.* **2006**, *281*, 9837–9840. [\[CrossRef\]](#)
36. Hua, H.; Zhang, H.; Kong, Q.; Jiang, Y. Mechanisms for estrogen receptor expression in human cancer. *Exp. Hematol. Oncol.* **2018**, *7*, 24. [\[CrossRef\]](#)
37. Gourdy, P.; Guillaume, M.; Fontaine, C.; Adlanmerini, M.; Montagner, A.; Laurell, H.; Lenfant, F.; Arnal, J.-F. Estrogen receptor subcellular localization and cardiometabolism. *Mol. Metab.* **2018**, *15*, 56–69. [\[CrossRef\]](#)
38. Levin, E.R.; Hammes, S.R. Nuclear receptors outside the nucleus: Extranuclear signalling by steroid receptors. *Nat. Rev. Mol. Cell Biol.* **2016**, *17*, 783–797. [\[CrossRef\]](#)
39. Klinge, C.M. Estrogens regulate life and death in mitochondria. *J. Bioenerg. Biomembr.* **2017**, *49*, 307–324. [\[CrossRef\]](#)
40. Cruz, A.C.T.; Pérez-Alvarado, I.A.; Ramírez-Jarquín, J.O.; Rocha-Zavaleta, L. Nucleo-cytoplasmic transport of estrogen receptor α in breast cancer cells. *Cell. Signal.* **2017**, *34*, 121–132. [\[CrossRef\]](#)
41. Avendaño, C.; Menéndez, J.C. Anticancer drugs that inhibit hormone action. In *Medicinal Chemistry of Anticancer Drugs*; Elsevier BV: Amsterdam, The Netherlands, 2008; pp. 53–91.
42. Klinge, C.M. Estrogenic control of mitochondrial function and biogenesis. *J. Cell. Biochem.* **2008**, *105*, 1342–1351. [\[CrossRef\]](#) [\[PubMed\]](#)
43. O’Lone, R.; Knorr, K.; Schaffer, M.E.; Martini, P.G.; Mendelsohn, M.E.; Jaffe, I.Z.; Karas, R.H.; Bienkowska, J.; Hansen, U. Estrogen receptors α and β mediate distinct pathways of vascular gene expression, including genes involved in mitochondrial electron transport and generation of reactive oxygen species. *Mol. Endocrinol.* **2007**, *21*, 1281–1296. [\[CrossRef\]](#) [\[PubMed\]](#)
44. Chen, J.-Q.; Cammarata, P.R.; Baines, C.P.; Yager, J.D. Regulation of mitochondrial respiratory chain biogenesis by estrogens/estrogen receptors and physiological, pathological and pharmacological implications. *Biochim. et Biophys. Acta (BBA)-Bioenerg.* **2009**, *1793*, 1540–1570. [\[CrossRef\]](#) [\[PubMed\]](#)
45. Kumari, S.; Badana, A.K.; Malla, R. Reactive oxygen species: a key constituent in cancer survival. *Biomark. Insights* **2018**, *13*, 1–9. [\[CrossRef\]](#)
46. Schieber, M.; Chandel, N.S. ROS function in redox signaling and oxidative stress. *Curr. Biol.* **2014**, *24*, R453–R462. [\[CrossRef\]](#)
47. Parkash, J.; Felty, Q.H.; Roy, D. Estrogen exerts a spatial and temporal influence on reactive oxygen species generation that precedes calcium uptake in high-capacity mitochondria: implications for rapid nongenomic signaling of cell growth. *Biochemistry* **2006**, *45*, 2872–2881. [\[CrossRef\]](#)
48. Felty, Q.H.; Roy, D. Estrogen, mitochondria, and growth of cancer and non-cancer cells. *J. Carcinog.* **2005**, *4*, 1. [\[CrossRef\]](#)
49. Vomund, S.; Schäfer, A.; Parnham, M.J.; Brüne, B.; Von Knethen, A. Nrf2, the master regulator of anti-oxidative responses. *Int. J. Mol. Sci.* **2017**, *18*, 2772. [\[CrossRef\]](#)
50. Penney, R.; Roy, D. Thioredoxin-mediated redox regulation of resistance to endocrine therapy in breast cancer. *Biochim. et Biophys. Acta (BBA)-Bioenerg.* **2013**, *1836*, 60–79. [\[CrossRef\]](#)
51. Okoh, V.O.; Garba, N.A.; Penney, R.B.; Das, J.; Deoraj, A.; Singh, K.P.; Sarkar, S.; Felty, Q.; Yoo, C.; Jackson, R.M.; et al. Redox signalling to nuclear regulatory proteins by reactive oxygen species contributes to oestrogen-induced growth of breast cancer cells. *Br. J. Cancer* **2015**, *112*, 1687–1702. [\[CrossRef\]](#)
52. Finley, L.W.; Carracedo, A.; Lee, J.; Souza, A.; Egia, A.; Zhang, J.; Teruya-Feldstein, J.; Moreira, P.I.; Cardoso, S.M.; Clish, C.; et al. SIRT3 opposes reprogramming of cancer cell metabolism through HIF1 α destabilization. *Cancer Cell* **2011**, *19*, 416–428. [\[CrossRef\]](#) [\[PubMed\]](#)

53. McGowan, E.; Alling, N.; Jackson, E.A.; Yagoub, D.; Haass, N.K.; Allen, J.D.; Martiniello-Wilks, R. Evaluation of cell cycle arrest in estrogen responsive MCF-7 breast cancer cells: pitfalls of the MTS assay. *PLoS ONE* **2011**, *6*, e20623. [[CrossRef](#)]
54. Zhang, Y.-Y.; Zhou, L.-M. Sirt3 inhibits hepatocellular carcinoma cell growth through reducing Mdm2-mediated p53 degradation. *Biochem. Biophys. Res. Commun.* **2012**, *423*, 26–31. [[CrossRef](#)] [[PubMed](#)]
55. Xiao, K.; Jiang, J.; Wang, W.; Cao, S.; Zhu, L.; Zeng, H.; Ouyang, R.; Zhou, R.; Chen, P. Sirt3 is a tumor suppressor in lung adenocarcinoma cells. *Oncol. Rep.* **2013**, *30*, 1323–1328. [[CrossRef](#)] [[PubMed](#)]
56. Moulder, D.E.; Hatoum, D.; Tay, E.; Lin, Y.; McGowan, E. The roles of p53 in mitochondrial dynamics and cancer metabolism: the pendulum between survival and death in breast cancer? *Cancers* **2018**, *10*, 189. [[CrossRef](#)] [[PubMed](#)]
57. Stambolsky, P.; Weisz, L.; Shats, I.; Klein, Y.; Goldfinger, N.; Oren, M.; Rotter, V. Regulation of AIF expression by p53. *Cell Death Differ.* **2006**, *13*, 2140–2149. [[CrossRef](#)]
58. Vahsen, N.; Cande, C.; Brière, J.-J.; Bénit, P.; Joza, N.; Larochette, N.; Mastroberardino, P.G.; Pequignot, M.O.; Casares, N.; Lazar, V.; et al. AIF deficiency compromises oxidative phosphorylation. *EMBO J.* **2004**, *23*, 4679–4689. [[CrossRef](#)]
59. Urbano, A.; Lakshmanan, U.; Choo, P.H.; Kwan, J.C.; Ng, P.Y.; Guo, K.; Dhakshinamoorthy, S.; Porter, A. AIF suppresses chemical stress-induced apoptosis and maintains the transformed state of tumor cells. *EMBO J.* **2005**, *24*, 2815–2826. [[CrossRef](#)]
60. Cregan, S.P.; Dawson, V.L.; Slack, R. Role of AIF in caspase-dependent and caspase-independent cell death. *Oncogene* **2004**, *23*, 2785–2796. [[CrossRef](#)]
61. Susin, S.A.; Lorenzo, H.K.; Zamzami, N.; Marzo, I.; Brenner, C.; Larochette, N.; Prévost, M.-C.; Boyko, A.; Kroemer, G. Mitochondrial release of caspase-2 and -9 during the apoptotic process. *J. Exp. Med.* **1999**, *189*, 381–394. [[CrossRef](#)]
62. Berger, C.E.; Qian, Y.; Liu, G.; Chen, H.; Chen, X. p53, a target of estrogen receptor (ER) α , modulates DNA damage-induced growth suppression in ER-positive breast cancer cells*. *J. Biol. Chem.* **2012**, *287*, 30117–30127. [[CrossRef](#)] [[PubMed](#)]
63. Fernandez-Cuesta, L.; Anaganti, S.; Hainaut, P.; Olivier, M. Estrogen levels act as a rheostat on p53 levels and modulate p53-dependent responses in breast cancer cell lines. *Breast Cancer Res. Treat.* **2010**, *125*, 35–42. [[CrossRef](#)] [[PubMed](#)]



© 2020 by the authors. Licensee MDPI, Basel, Switzerland. This article is an open access article distributed under the terms and conditions of the Creative Commons Attribution (CC BY) license (<http://creativecommons.org/licenses/by/4.0/>).

Sirt3 Exerts Its Tumor-Suppressive Role by Increasing p53 and Attenuating Response to Estrogen in MCF-7 Cells

**Marija Pinterić^{1,†}, Iva I. Podgorski^{1,†}, Marijana Popović Hadžija¹, Vedrana Filić²
Mladen Paradžik^{2,3}, Bastien Lucien Jean Proust¹, Ana Dekanić¹, Ivan Ciganek¹, Denis Pleše¹,
Dora Marčinko¹, Tihomir Balog¹ and Sandra Sobočanec^{1,*}**

¹ Division of Molecular Medicine, Ruđer Bošković Institute, 10000 Zagreb, Croatia; mpinter@irb.hr (M. Pinterić); iskrinj@irb.hr (I.I.P.); mhadzija@irb.hr (M.P.H.); Bastien.Lucien.Jean.Proust@irb.hr (B.L.J.P.); adekanic@irb.hr (A.D.); iciganek@stud.biol.pmf.hr (I.C.); dplese@pharma.hr (D.P.); dora.marcinko@krka.biz (D.M.); balog@irb.hr (T.B.)

² Division of Molecular Biology, Ruđer Bošković Institute, 10000 Zagreb, Croatia; Vedrana.Filic.Mileta@irb.hr (V.F.); Mladen.Paradzic@irb.hr (M. Paradzik)

³ Department Molecular Biotechnology and Health Sciences, Molecular Biotechnology Centre (MBC), University of Torino, 10124 Torino, Italy

* Correspondence: ssoboc@irb.hr; Tel.: +385-1-4561-172

† These authors contributed equally to this work

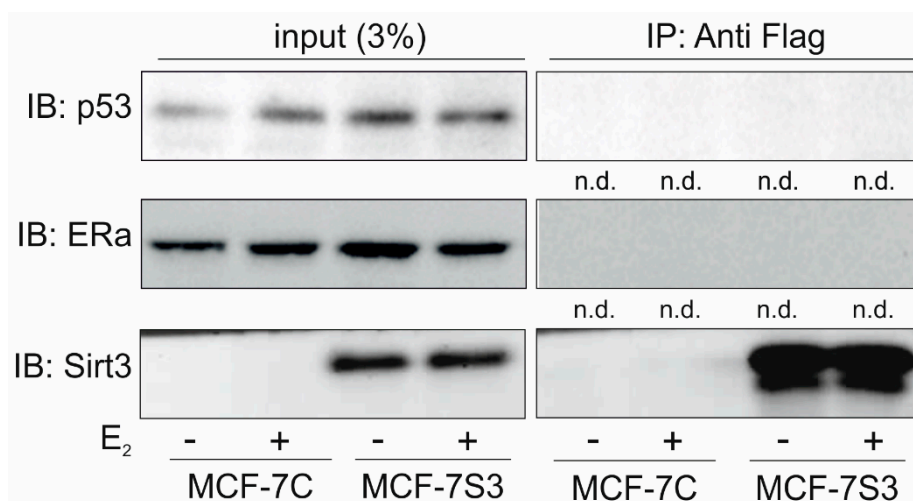
Received: 25 February 2020; Accepted: 30 March 2020; Published: date

Table S1. Antibodies used in this study for Western blot analyses.

Antibody	Dilution	Host	Manufacturer
Sirt3 (F-10, sc-365175)	1:500	Mouse	Santa Cruz Biotechnology, USA
ER- α (F-10, sc-8002)	1:500	Mouse	Santa Cruz Biotechnology, USA
GAPDH (ab9485)	1:5000	Mouse	Abcam, UK
H3 (ab1791)	1:3000	Rabbit	Abcam, UK
NDUFA9 (ab14713)	1:1000	Mouse	Abcam, UK
UQCRC (ab14745)	1:1000	Mouse	Abcam, UK
ATP5A (ab14748)	1:1000	Mouse	Abcam, UK
SDHA (ab14715)	1:1000	Mouse	Abcam, UK
AcSOD2 (ab137037)	1:1000	Rabbit	Abcam, UK
Catalase (ab1877)	1:1000	Rabbit	Abcam, UK
Nrf2 (ab31163)	1:1000	Rabbit	Abcam, UK
p53 (DO-1, sc-126)	1:2000	Mouse	Santa Cruz Biotechnology, USA
AlF (B-9, sc-55519)	1:500	Mouse	Santa Cruz Biotechnology, USA
gamma H2AX (phospho S139, ab11174)	1:8000	Rabbit	Abcam, UK
Anti-mouse (170-6516)	1:5000	Goat	Bio-rad, USA
Anti-rabbit (NA934)	1:5000	Goat	GE Healthcare, USA

Table S2. Antibodies used in this study for immunofluorescence analyses.

Antibody	Dilution	Host	Manufacturer
Sirt3 (F-10, sc-365175)	1:100	Mouse	Santa Cruz Biotechnology, USA
ER- α (ab16660)	1:500	Rabbit	Abcam, UK
gamma H2AX (phospho S139, ab11174)	1:5000	Rabbit	Abcam, UK
Alexa 488 (A-11001)	1:2000	Mouse	Thermo Fisher Scientific, USA
Alexa 594 (A-11012)	1:1000	Rabbit	Thermo Fisher Scientific, USA

**Figure S1.** Sirt3 does not interact with p53 or ER- α in MCF-7 cells. Western blot analysis of coimmunoprecipitation experiment showing no interaction between Sirt3 and ER- α or p53.

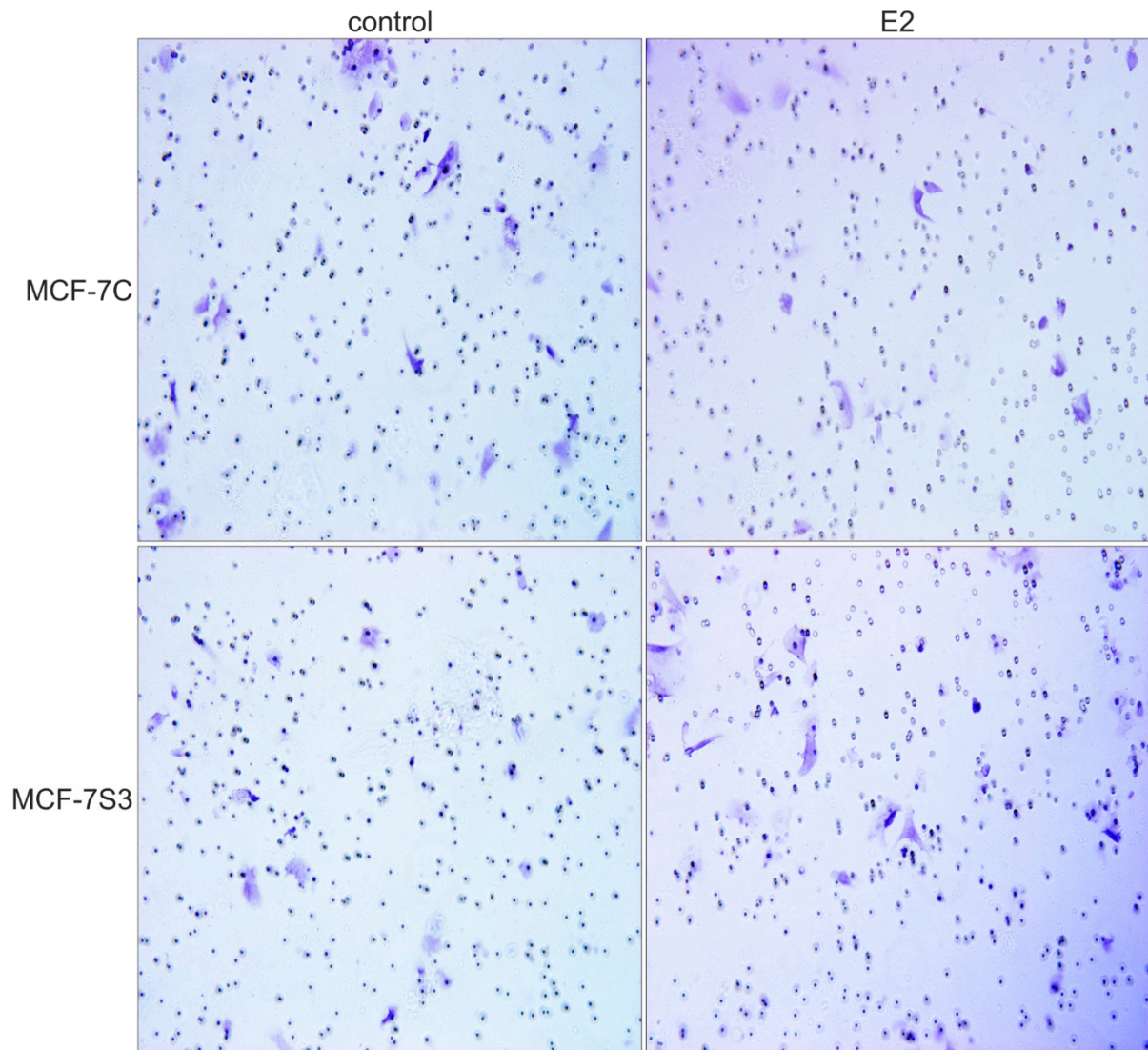


Figure S2. E2 partially rescues reduced migration of MCF-7S3 cells. Representative photographs of migrated MCF-7C and MCF-7S3 cells treated with E2. Samples are stained with crystal violet.



Article

Role of Sirt3 in Differential Sex-Related Responses to a High-Fat Diet in Mice

Marija Pinterić ^{1,†}, Iva I. Podgorski ^{1,†}, Marijana Popović Hadžija ¹, Ivana Tartaro Bujak ³, Ana Dekanić ¹, Robert Bagarić ², Vladimir Farkaš ², Sandra Sobočanec ^{1,*} and Tihomir Balog ¹

¹ Division of Molecular Medicine, Ruđer Bošković Institute, 10000 Zagreb, Croatia; mpinter@irb.hr (M.P.); iskrinj@irb.hr (I.I.P.); mhadzija@irb.hr (M.P.H.); adekani@irb.hr (A.D.); balog@irb.hr (T.B.)

² Division of Experimental Physics, Ruđer Bošković Institute, 10000 Zagreb, Croatia; robert.bagaric@irb.hr (R.B.); vladimir.farkas@irb.hr (V.F.)

³ Division of Materials Chemistry, Ruđer Bošković Institute, 10000 Zagreb, Croatia; itartaro@irb.hr

* Correspondence: ssoboc@irb.hr; Tel.: +385-1-4561-172

† These authors contributed equally to this work.

Received: 7 February 2020; Accepted: 18 February 2020; Published: 20 February 2020

Abstract: Metabolic homeostasis is differently regulated in males and females. Little is known about the mitochondrial Sirtuin 3 (Sirt3) protein in the context of sex-related differences in the development of metabolic dysregulation. To test our hypothesis that the role of Sirt3 in response to a high-fat diet (HFD) is sex-related, we measured metabolic, antioxidative, and mitochondrial parameters in the liver of Sirt3 wild-type (WT) and knockout (KO) mice of both sexes fed with a standard or HFD for ten weeks. We found that the combined effect of Sirt3 and an HFD was evident in more parameters in males (lipid content, glucose uptake, *ppary*, *cyp2e1*, *cyp4a14*, Nrf2, MnSOD activity) than in females (protein damage and mitochondrial respiration), pointing towards a higher reliance of males on the effect of Sirt3 against HFD-induced metabolic dysregulation. The male-specific effects of an HFD also include reduced Sirt3 expression in WT and alleviated lipid accumulation and reduced glucose uptake in KO mice. In females, with a generally higher expression of genes involved in lipid homeostasis, either the HFD or Sirt3 depletion compromised mitochondrial respiration and increased protein oxidative damage. This work presents new insights into sex-related differences in the various physiological parameters with respect to nutritive excess and Sirt3.

Keywords: sirtuin 3; high fat diet; sex differences; mice; oxidative stress; metabolic stress

1. Introduction

The metabolic syndrome is metabolic derangement involving a cluster of risk factors primarily associated with obesity, type two diabetes, and a high risk of cardiovascular events, but also with the development of inflammation, atherosclerosis, renal, liver and respiratory disease, cancer, and premature aging [1], [2]. The prevalence of metabolic syndrome is dramatically on the rise in low- and mid-income countries and is one of the leading risks for global deaths representing serious threat to public health. The increase in caloric food intake or consumption of diets high in both fat and carbohydrates (also known as a “western diet”) along with physical inactivity leads to increased obesity, a key factor in the development of metabolic syndrome. Human metabolic syndrome can be effectively mimicked in rodent models using dietary intervention, such as high-fat diets (HFDs) [3]. The nutrient overload generated by an HFD in mice leads to a chronic increase in reactive oxygen species (ROS) production, which leads to oxidative stress (rev. in [1]). Oxidative stress is associated with the metabolic syndrome, but whether it is the cause or the consequence is a matter of debate. Nevertheless, an HFD is capable of functioning as a metabolic stressor causing mitochondrial

dysfunction and other metabolic changes that contribute to pathological state and may mimic age-related pathology [4].

In most mammals, including humans, life expectancy differs between sexes. Females show lower incidence of some age-related pathologies linked with oxidative stress conditions and this sex-difference disappears after menopause, which led to the conclusion that this protection is attributed to the effect of sex hormones (rev in [5]). The important approach to study ageing and age-linked pathologies is to investigate sex dimorphism in defense to metabolic stressors. Historically, the impact of sex on metabolic status in mouse models has been neglected [6]. Indeed, most *in vivo* studies are focused on male mice. One of the reasons for a strong male sex bias is the belief that female mammals are intrinsically more variable than males due to the estrogen cycle. However, this has been disproven and without foundation [7]. While numerous papers examined the metabolic profiles of inbred mouse strain 129 [8–10], little attention has been paid to the impact of sex on the development of metabolic syndrome caused by HFD.

Sirtuin 3 (Sirt3) is the only member of sirtuin family that has been linked to longevity in humans [11]. In addition, Sirt3 integrates cellular energy metabolism and various mitochondrial processes including ROS generation. The excessive production of ROS leads to oxidative stress, a crucial event that contributes to mitochondrial dysfunction and age-related pathologies [12]. Sirt3 plays a role in preventing metabolic syndrome [10], and is found to be upregulated in response to caloric restriction and exercise [13], while being downregulated with age, upon an HFD, and in diabetes [14]. Sirt3 is dispensable at a young age under homeostatic conditions but is essential under stress conditions or at an old age, making it a potential regulator of aging process. Although Sirt3 mediates oxidative stress suppression during caloric restriction [15], it remains to be elucidated whether Sirt3 may alleviate chronic oxidative stress initiated by excessive caloric intake in the form of an HFD. Many mitochondrial proteins are targets for deacetylation and activation by Sirt3, including proteins of oxidative phosphorylation, fatty acid oxidation, and the citric acid (TCA) cycle [16]. These data suggest that fatty acid metabolism and the TCA cycle are among the pathways that are tightly regulated by Sirt3. Moreover, Sirt3 is found to be regulated by a redox-sensitive, Keap1/Nrf2/ARE signaling axis, which facilitates transcription of Sirt3 and other antioxidant-response genes under stress conditions [17].

Little is currently known about Sirt3 expression in the context of sex-related differences in the development of metabolic syndrome. The understanding of sex differences in physiology and disease is of fundamental importance with regard to preventing metabolic disease. Therefore, our aim was to determine the role of Sirt3 in sex-related responses to a high-fat diet in 129S mice. In this study, we found that an HFD reduces hepatic Sirt3 expression only in wild-type (WT) males, while HFD-induced lipid accumulation is alleviated in Sirt3 knockout (KO) males, with impaired glucose uptake and increased reliance on fatty acids. Moreover, females had more efficient lipid metabolism but also displayed higher oxidative stress following an HFD in both genotypes with compromised mitochondrial respiration and increased protein oxidative damage. These data present new insights into sex-related differences in the metabolic parameters with respect to nutritive excess and Sirt3.

2. Materials and Methods

2.1. Animal Model and Experimental Design

Sirt3 WT (hereafter WT) and Sirt3 KO (hereafter KO) mice on a 129/SV background (stock no. 027975) were purchased from the Jackson Laboratory (Bar Harbor, ME, USA). WT and KO mice of both sexes at of 8 weeks of age, were fed with either a standard fat diet (SFD, 11.4% fat, 62.8% carbohydrates, 25.8% proteins; Mucedola, Settimo Milanese, Italy) or a high fat diet (HFD, 58% fat, 24% carbohydrates, 18% proteins; Mucedola, Settimo Milanese, Italy) during 10 weeks. The mice were age-matched and housed in standard conditions (3 mice per cage, 22 °C, 50–70% humidity, and a cycle of 12 h light and 12 h darkness). The animals were divided into 8 groups (6 mice per group): SFD-fed WT males, HFD-fed WT males, SFD-fed KO males, HFD-fed KO males, SFD-fed WT females, HFD-fed WT females, SFD-fed KO females, and HFD-fed KO females. Body weight was measured

once a week, as well as glucose level, which was measured by glucometer (StatStrip Xpress-I, Nova Biomedical, GmbH, Mörfelden-Walldorf, Germany) in a blood drop taken from the tail vein. Before glucose measurements, mice were fasted for 6 h. After 10 weeks, mice were anesthetized by intraperitoneal injection of ketamine/xylazine (Ketamidol 10%, Richter pharma Ag, Wels, Austria; Xylazine 2%, Alfasan International, Woerden, Netherlands) and organs of interest were obtained and stored in liquid nitrogen until analysis. Animal experiments were done within the project funded by Croatian Science Foundation, project ID: IP-014-09-4533, approved on 01/09/2015. All procedures were approved by the Ministry of Agriculture of Croatia, (No: UP/I-322-01/15-01/25 525-10/0255-15-2 from 20 July 2015) and carried out in accordance with the associated guidelines EU Directive 2010/63/EU.

2.2. Histology and Oil Red O Staining

A histological analysis of the liver sections from all experimental groups was performed in order to determine lipid accumulation caused by HFD. At the end of the feeding period, the anesthetized animals were perfused via the left ventricle of the heart with ice-cold phosphate-buffered saline (PBS; 137 mM NaCl, 2.7 mM KCl, 8 mM Na₂HPO₄, and 2 mM K₂PO₄, pH 7.4) for 2–3 min (to remove blood via the incised abdominal vena cava). Liver tissue was fixed by immersion in 4% paraformaldehyde in 0.1 M PBS (pH 7.4), left overnight at 4 °C, and was then washed with 1× PBS and cryoprotected in 30% sucrose in PBS until the sectioning on cryomicrotome at 8 µm. Fat vacuoles in hepatocytes of frozen sections were visualized by Oil Red O dye (Sigma Aldrich, St. Louis, MO, USA) prepared in propylene glycol (0.5% Oil Red O solution) according to the following protocol. The slides were dried for 60 min at room temperature (RT) and then fixed in ice-cold 10% formalin for 10 min followed by another 60 min of drying. The slides were then incubated for 5 min in absolute propylene glycol followed by staining in pre-warmed (60 °C) Oil Red O solution for 10 min and incubation for 5 min in 85% propylene glycol. Before staining with hematoxylin for 30 s, the slides were rinsed 2× in distilled water. After hematoxylin, the stained slides were thoroughly washed in running tap water followed by distilled water and mounted in mounting medium. An analysis of the stained liver sections was done using an Olympus BX51 microscope (Tokyo, Japan) with associated software analysis. The quantification of the lipid accumulation signal was done using ImageJ software (U.S. National Institutes of Health, Bethesda, MD, USA).

2.3. Total Lipid Extraction

Total lipids were extracted from liver tissue according to a modified Folch procedure [18]. Briefly, 0.1 g of liver tissue was homogenized in MeOH, followed by the addition of 2 mL of CHCl₃ and vigorous shaking. The mixture was filtered, and the remaining mixture was resuspended in CHCl₃-MeOH (2:1). The mixture was filtered and washed again with fresh solvent, followed by washing the solution with 1.5 mL of 0.88% KCl and drawing off the aqueous layer using a Pasteur pipette. The washing step was repeated with 1.5 mL of KCl/MeOH (4:1, *v/v*), and the organic layer containing lipids was carefully transferred to a glass tube. A rotary evaporator (IKA Rotary evaporator RV 10 digital, Staufen, Germany) was used to remove the solvent, and the total lipids were determined by gravimetric analysis.

2.4. RNA Isolation and Quantitative Real-Time PCR Analysis

The TRIzol reagent (Invitrogen, Waltham, MA, USA) was used for total RNA extraction from a mouse liver (5% extract). The isolated RNA was treated with DNase (TURBO DNA-free Kit, Thermo Fisher Scientific, Waltham, MA, USA) followed by reverse transcription using a High-Capacity cDNA Reverse Transcription Kit (Thermo Fisher Scientific) according to the manufacturer's recommendations. For real-time PCR analysis, an ABI 7300 sequence detection system was used. To quantify the relative mRNA expression of *cyp2a4*, *cyp2e1*, *cyp4a14*, *hnf4α*, *ppara*, and *ppary* in the livers of mice, the comparative C_T ($\Delta\Delta C_T$) method according to the Taqman® Gene Expression Assays Protocol (Applied Biosystems, Foster City, CA, USA) was used. The assays' ID used for the analyses

are shown in Supplementary Table S1. The data on the graphs are shown as the fold-change in gene expression, which is normalized to the endogenous reference gene (β -actin) and relative to the Sirt3 WT males fed with a SFD.

2.5. Protein Carbonylation

Protein carbonylation experiments were performed with an ELISA-based assay. Liver homogenates (5%) were prepared in PBS with protease inhibitors (Roche, Basel, Switzerland) and incubated for 1 h at RT with a lipid removal agent (13360-U, Sigma Aldrich, St. Louis, MO, USA), followed by centrifugation for 20 min at 16,000 g. A Pierce™ BCA Protein Assay Kit (Thermo Fischer Scientific) was used to determine the protein concentration, and 100 μ L of 1 μ g/ μ L lysate was incubated overnight at 4 °C using Maxisorb wells (Sigma Aldrich). 2,4-dinitrophenylhydrazine (DNPH; 12 μ g/mL) was used for derivatization of adsorbed proteins, and rabbit anti-DNP primary (D9656, Sigma Aldrich) followed by goat anti-rabbit secondary antibody conjugated to HRP (NA934, GE Healthcare, Chicago, IL, USA) were used to detect the derivatized dinitrophenol (DNP)-carbonyl. Enzyme substrate 3,3',5,5'-tetramethylbenzidine (Sigma Aldrich) was added into samples and incubated until color developed, followed by stopping the reaction using 0.3 M H₂SO₄. The absorbance was measured at 450 nm on a microplate reader (Bio-Tek Instruments, Winooski, VT, USA).

2.6. Analysis of Antioxidative Enzyme Activities

Antioxidative enzyme activities were analyzed in liver tissue lysates homogenized in PBS supplemented with protease inhibitors (Roche, Basel, Switzerland) using an ice-jacketed Potter-Elvehjem homogenizer (Thomas Scientific, Swedesboro, NJ, USA), at 1300 rpm. Superoxide dismutase (SOD) activities were determined measuring inhibition of the xanthine/xanthine oxidase-mediated reduction of 2-(4-iodophenyl)-3-(4-nitrophenyl)-5-phenyltetrazolium chloride (I.N.T.) using a Ransod kit (Randox Laboratories, Crumlin, UK) according to the manufacturer's recommendations. This reaction is inhibited by the conversion of the superoxide radical to hydrogen peroxide and oxygen as a consequence of SOD activity. A total of 4 mM of KCN for 30 min was used to selectively inhibit CuZnSOD activity and obtain the MnSOD activity. CuZnSOD activity was obtained by subtracting the MnSOD activity from the total SOD activity. The Catalase (Cat) activity was done, as previously described [19], by measuring the change in absorbance (at 240 nm) in the reaction mixture during the interval of 30 s following sample addition. The final concentrations of 10 mM H₂O₂ and 50 mM PBS (pH 7.0) were used. Glutathione peroxidase (Gpx) activity was measured at 340nm, as previously described [20], using a RANSEL kit (Randox Laboratories). In kit, a decrease in absorbance at 340 nm is accompanied by NADPH oxidation to NADP⁺ as an indirect measure of Gpx activity.

2.7. Protein Isolation and Western Blot Analysis

Liver samples were homogenized in an ice-cold lysis buffer (RIPA buffer supplemented with protease inhibitors (Roche)) using an ice-jacketed Potter-Elvehjem homogenizer (1300 rpm). Liver homogenates (5%) were centrifuged at 2000× g for 15 min at 4 °C, and the supernatant was sonicated (3 × 30 s) and centrifuged at 16,000× g for 20 min at 4 °C. The resulting lysate was transferred to a new tube and the protein concentration was estimated by the Pierce™ BCA Protein Assay Kit (Thermo Fischer Scientific). Proteins (40 μ g/ μ L) were resolved by SDS-PAGE and were electrotransferred onto a PVDF membrane (Roche, Basel, Switzerland). Membranes were blocked in a I-Block™ Protein-Based Blocking Reagent (Invitrogen, Waltham, MA, USA) for 1 h at RT and were incubated with primary polyclonal or monoclonal antibodies overnight at 4 °C. For chemiluminescence detection, an appropriate horseradish peroxidase (HRP)-conjugated secondary antibody was used. The list of primary and secondary antibodies is in Supplementary Table S2. AmidoBlack (Sigma Aldrich) was used for total protein normalization. The Alliance 4.7 Imaging System (UVITEC, Cambridge, UK)

was used for the detection of immunoblots using an enhanced chemiluminescence kit (Thermo Fischer Scientific).

2.8. Mitochondria Isolation and Oxygen Consumption

Mice liver mitochondria were isolated by differential centrifugation as described previously [21], with the following modification: liver was homogenized at a ratio of 100 mg tissue/mL of isolation buffer (10% liver homogenate). Isolated mitochondria were kept in the isolation buffer (250 mM sucrose, 2 mM EGTA, 0.5% fatty acid-free BSA, 20 mM Tris-HCl, pH 7.4) until the experiment on the Clark-type electrode (Oxygraph, Hansatech Instruments Ltd, Pentney, UK) in an airtight 1.5 mL chamber at 35°C. The protein concentration was determined with a Pierce™ BCA Protein Assay Kit. For the determination of oxygen consumption, mitochondria (800 µg protein) were resuspended in a 500 µL respiration buffer (200 mM sucrose, 20 mM TrisHCl, 50 mM KCl, 1 mM MgCl₂·6H₂O, 5 mM KH₂PO₄, pH 7.0). Complex I assessment samples were incubated with 2.5 mM glutamate and 1.25 mM malate. Mitochondrial respiration was accelerated by the addition of 2 mM ADP for state 3 respiration measurements. Then, ATP synthesis was terminated by adding 5 µg/mL of oligomycin to achieve state 4 rate. To inhibit the mitochondrial respiration, 2 µM antimycin A was used. Oxygen uptake is calculated in nmol/min/mg protein.

2.9. PET Analysis

For ¹⁸FDG-microPET imaging, animals have been anesthetized in induction chamber with 4% isoflurane (Forane, Abbott Laboratories, Chicago, IL, USA) and intraperitoneally injected with 100–200 µL of solution containing 25 MBq of radiotracer [¹⁸F] fluoro-2-deoxy-2-D-glucose (¹⁸FDG). To avoid the influence of warming on ¹⁸FDG biodistribution in mice injected intravenously, in our experiments we used the model of intraperitoneal FDG administration described in [22]. ¹⁸FDG-microPET imaging, along with ¹⁸FDG liver uptake data analysis, was performed according to our previous model [23]. The co-registration of PET images was made in PMOD FUSION software mode (PMOD Technologies LLC, Zürich, Switzerland). The final result is given in standardized uptake value units (SUV).

2.10. Statistical Analysis

For the statistical analysis of data, SPSS for Windows (17.0, IBM, Armonk, NY, USA) was used. A Shapiro–Wilk test was used before all analyses to test the samples for normality of distribution. Since all data followed normal distribution, parametric tests for multiple comparisons were performed: a student's *t*-test for comparisons between males and females, and a two-way ANOVA for the interaction effect of Sirt3 × diet within each sex. If a significant interaction was observed, all pairwise comparisons were made between groups, using Tukey's post-hoc test with Bonferroni's correction. Significance was set at *p* < 0.05. On graphical displays, the indicator of the differences between males and females was marked as x; the indicator of differences between SFD and HFD (the effect of diet) was marked as a letter (a,b, etc.); the indicator of differences between WT and KO (the effect of Sirt3) was marked as *.

3. Results

3.1. HFD Reduces Hepatic Sirt3 Protein Expression in Males Only

To investigate if the hepatic expression of Sirt3 was altered in a sex- or diet-dependent manner, we first detected Sirt3 protein expression in all groups. Expectedly, in KO mice, Sirt3 protein level was undetectable. In WT mice, HFD partially (24%) reduced Sirt3 protein expression in males but did not affect Sirt3 in females. Therefore, HFD-fed males had lower Sirt3 expression than females (Figure 1A,B). These data suggest that ten weeks of HFD feeding reduces Sirt3 protein expression in a male-specific manner.

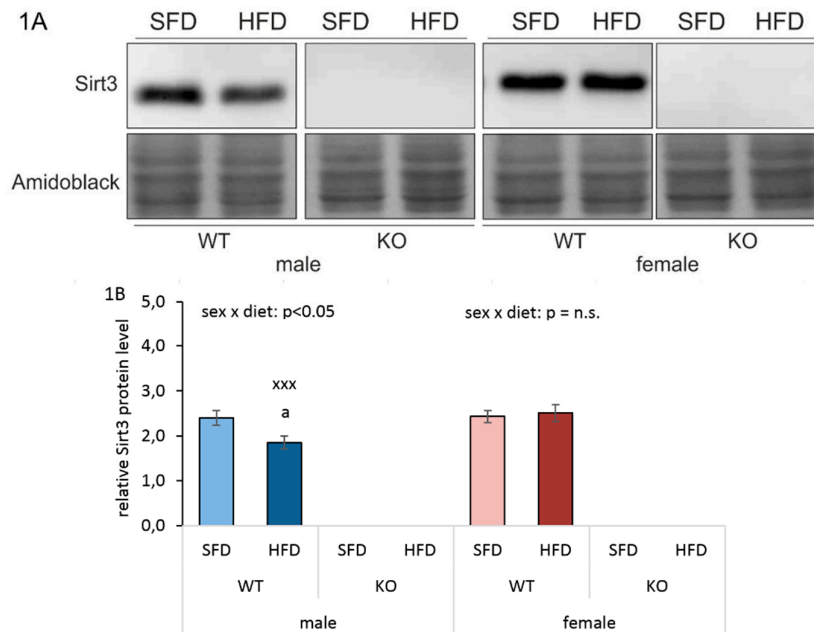


Figure 1. Hepatic Sirtuin 3 (Sirt3) protein expression in Sirt3 wild-type (WT) and knockout (KO) mice fed with a standard fat diet (SFD) or a high fat diet (HFD) for 10 weeks. **(A)** A representative immunoblot of the hepatic Sirt3 protein expression level. **(B)** A graphical display of the averaged densitometry values of immunoblots in Figure 1A. Males: HFD-fed vs. SFD-fed WT mice ($p < 0.001$); Females: no changes. Males vs. females: HFD-fed WT mice ($^{xxx}p < 0.001$). The data are shown as mean \pm SD. $n = 6$. Amidoblack was used as a loading control.

3.2. HFD Has no Influence on Body Weight and Glucose Level

It has been shown that the decreased level of Sirt3 contributes to impaired glucose metabolism [24], and since we noticed reduced Sirt3 expression upon HFD in WT males, we next tested whether differential Sirt3 expression and HFD would affect body weight and fasting glucose levels. After 10 weeks of feeding, treatment with an HFD did not affect whole body weight or glucose level in either sex, irrespective of Sirt3 (Figure 2A,B, Figure S1A,B). However, at the end of the 10th week, males had a higher body weight and glucose level compared to female mice (Figure 2A,B).

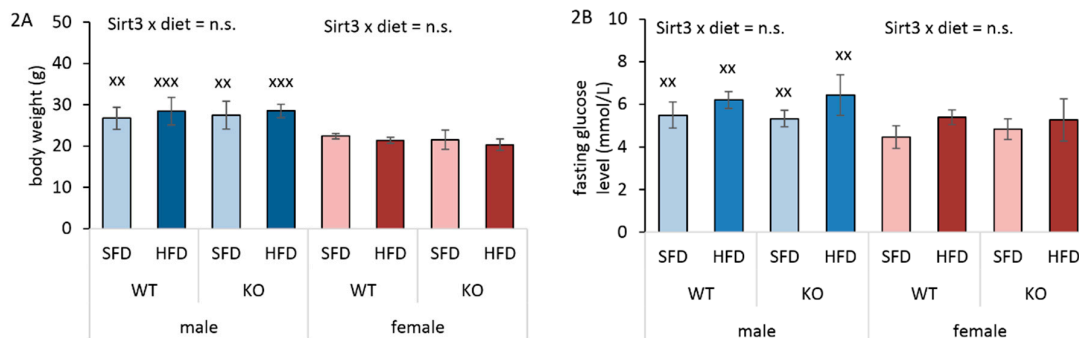


Figure 2. Body weight and fasting glucose level in Sirt3 wild-type (WT) and knockout (KO) mice fed with a standard fat diet (SFD) or a high fat diet (HFD) for 10 weeks. **(A)** A graphical display of body weight. Males: no changes. Females: no changes. Males vs. females: SFD-fed mice ($^{xx}p < 0.01$); HFD-fed mice ($^{xxx}p < 0.001$). **(B)** A graphical display of fasting glucose levels. Males: no changes. Females: no changes. Males vs. females: $^{xx}p < 0.01$. The data are shown as mean \pm SD. $n = 6$ per group.

3.3. Differential Hepatic Fat Accumulation in Males Upon HFD Depends on Sirt3

While glucose levels showed a male-specific pattern, the interesting fact was that the HFD failed to cause weight gain compared to SFD in both sexes. To investigate whether HFD-fed mice developed a fatty liver, we determined the hepatic accumulation of lipids. Expectedly, fat vacuoles were predominately present in the livers of HFD-fed mice of both genotypes, confirming that HFD treatment caused lipid accumulation in mice livers (Figure 3A–H, Supplementary Figure S2). Folch extraction was performed to measure lipid content in larger parts of liver tissue. In males, an HFD caused significant lipid accumulation in both WT and KO mice. In SFD conditions, WT males had less, and, in HFD conditions, WT males had more hepatic lipids than KO males. In females, an HFD also induced significant lipid accumulation regardless of Sirt3. While in WT mice there were no differences in lipid content between males and females, more lipids were observed in SFD-fed, and less in HFD-fed KO males compared to KO females (Figure 3I). These results suggest that, in males, the hepatic lipid accumulation was partially influenced by Sirt3.

3.4. HFD Reduces Hepatic Glucose Uptake in Sirt3 KO Males

Because the presence of non-alcoholic fatty liver disease (NAFLD) is closely associated with decreased glucose metabolism, we determined hepatic glucose uptake using ^{18}F -FDG PET. In KO males, an HFD significantly reduced glucose uptake. Also, HFD-fed KO males had lower glucose uptake than WT mice. On the contrary, in females, an HFD had no effect on glucose uptake across groups. Reduced hepatic glucose uptake in HFD-fed KO males resulted in significantly lower values compared to HFD-fed KO females. These data indicate the importance of Sirt3 in the maintenance of hepatic glucose uptake following HFD, but only in males (Figure 3J).

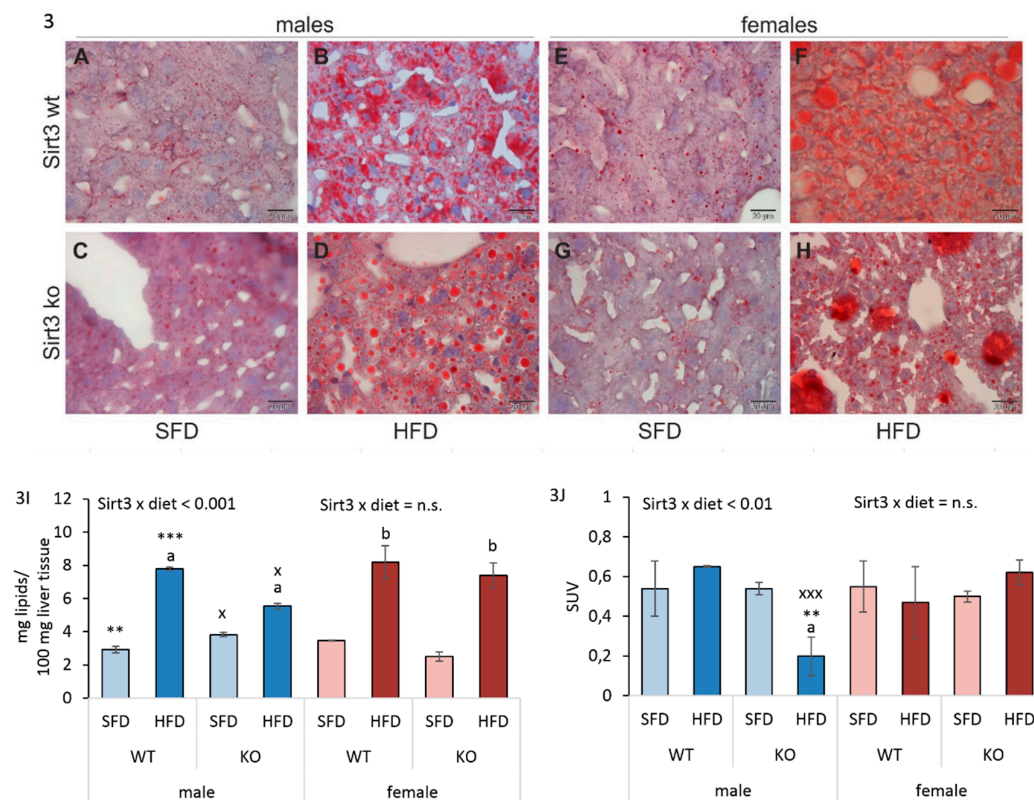


Figure 3. Sex-related differences in hepatic lipid accumulation and glucose (^{18}F FDG) uptake in Sirt3 wild-type (WT) and knockout (KO) mice of both sexes fed with a standard fat diet (SFD) or a high fat diet (HFD) for 10 weeks. (A–H) Liver cryo-sections stained with Oil Red O. Representative images show lower fat content in mice fed with a SFD (A, C, E, G), and promoted lipid accumulation in HFD-

fed mice of both sexes and genotypes (B, D, F, H). (I) A graphical display of total lipid content in liver samples. Males: HFD-fed vs. SFD-fed mice ($^a p < 0.001$); SFD-fed WT vs. KO mice ($^{**} p < 0.01$); HFD-fed WT vs. KO mice ($^{***} p < 0.001$). Females: HFD-fed vs. SFD-fed mice ($^b p < 0.001$). Males vs. females: SFD-fed KO mice ($^c p < 0.05$); HFD-fed KO mice ($^c p < 0.05$). (J) A graphical display of hepatic glucose uptake expressed as standardized uptake value (SUV). Males: SFD-fed vs. HFD-fed KO mice ($^a p < 0.001$); HFD-fed WT vs. KO mice ($^{**} p < 0.01$). Females: no changes. Males vs. females: HFD-fed KO mice ($^{xxx} p < 0.001$). Data are shown as mean \pm SD. $n = 3$ –4 per group. scale bar = 20 μ m.

3.5. HFD Further Suppresses the Male-Specific Reduction of Hepatic *hnf4a*, *ppara*, *ppary*, and *cyp2a4* mRNA Level

Since it was observed that an HFD causes lipid accumulation in liver, we wanted to investigate several important genes involved in the lipid metabolism that are known to be expressed in sex-related manner and may be responsible for the observed phenotype, such as *hnf4a*, *ppara*, *ppary*, *cyp2a4*, *cyp2e1*, and *cyp4a14*.

Hepatocyte nuclear factor 4 α (*hnf4a*) is a master regulator of many genes involved in lipid, glucose, and drug metabolism. In our study, no change in *hnf4a* transcript level was found either within the male or female group of mice. The only differences were found between WT males and females, where males had less *hnf4a* transcript compared to females (Figure 4A,C).

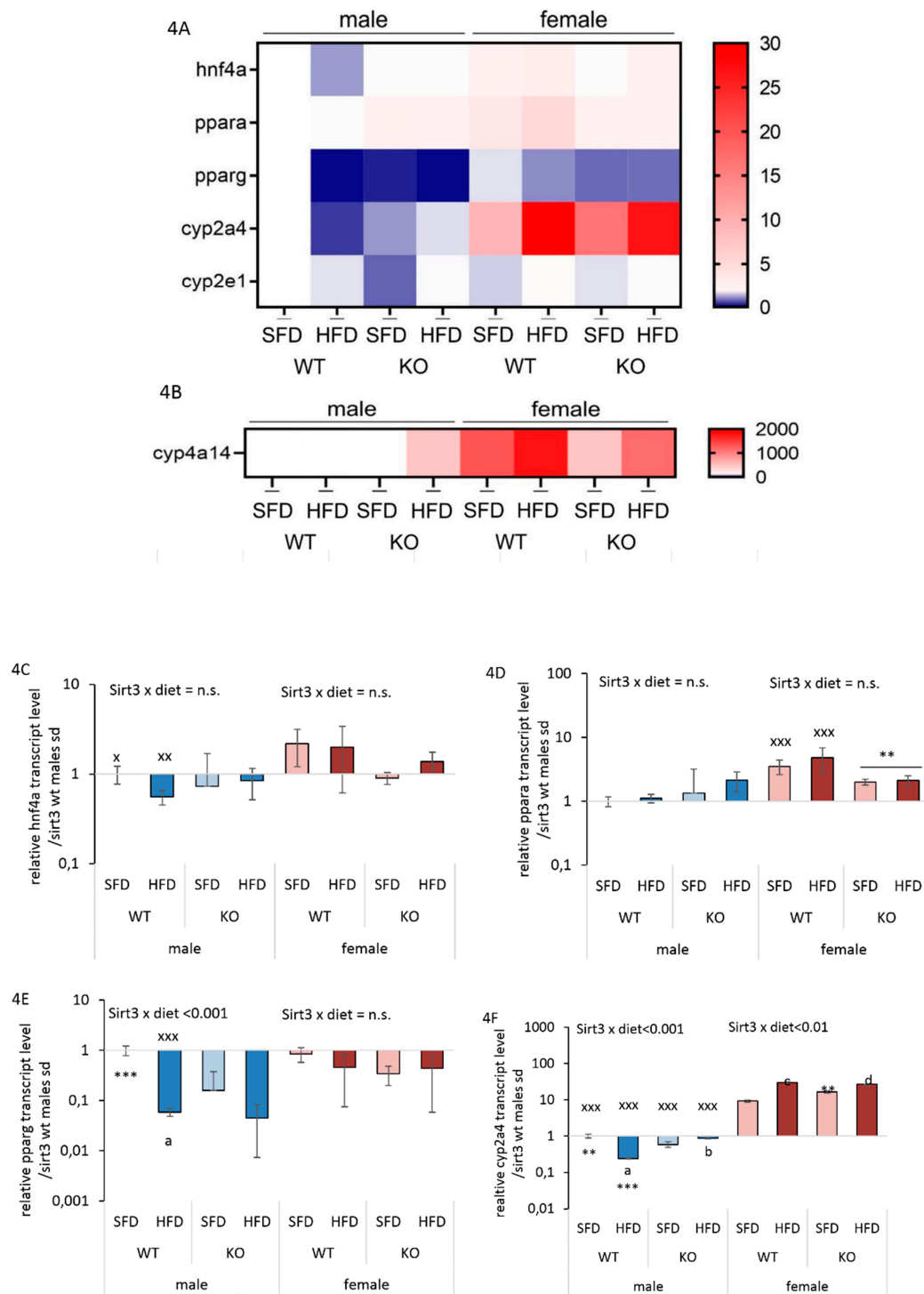
The peroxisome proliferator-activated receptor α (*ppara*) is shown to be upregulated during HFD as it serves as a ligand for free fatty acids [25]. In males, we observed no change in the transcription level of *ppara*, while in females, *ppara* was reduced in the absence of Sirt3. Interestingly, HFD had no effect on the *ppara* in any sex. WT females had higher *ppara* than males. These data indicate sex-related differences in *ppara* gene expression that are lost in the absence of Sirt3 (Figure 4A,D).

Hepatic *ppary* gene expression is upregulated in animal models of severe obesity and lipoatrophy [26]. Since in our study HFD-fed mice did not have increased weight gain compared to SFD, we checked whether this was associated with the altered expression of *ppary* in liver. In WT males, an HFD strongly reduced *ppary*, which was maintained in KO males as well. On the contrary, females exhibited no change in *ppary*. Overall, HFD-fed WT males had reduced *ppary* compared to females. These data indicate that both HFD and Sirt3 depletion reduce *ppary* only in males (Figure 4A,E).

Cyp2a4 (steroid 15 α -hydroxylase) is the enzyme that is constitutively expressed in the livers of female mice while in males its expression is hormonally regulated [27]. Considering its sex-related expression and regulation, we wanted to check whether lack of Sirt3 or change in diet affects the expression of this gene. In WT males, an HFD reduced *cyp2a4*, whereas in KO mice, an HFD rescued the reduced *cyp2a4* observed in SFD-fed mice. In SFD conditions, WT males had more *cyp2a4*, and in HFD conditions less than KO males. In females, HFD induced *cyp2a4*. Additionally, higher *cyp2a4* was observed in SFD-fed KO females compared to WT. Overall, males had lower *cyp2a4* than females across all groups (Figure 4A, 4F).

Cyp2e1 expression and activity in the liver are increased in humans and in animal models of NAFLD [7,10,11]. Similar to *cyp2a4*, in WT males, an HFD reduced *cyp2e1*, whereas in KO mice an HFD rescued reduced *cyp2e1* observed in SFD-fed mice. SFD-fed KO males displayed lower *cyp2e1* than WT mice. In females, HFD induced *cyp2e1*. The differences in *cyp2e1* between males and females were observed only in SFD-fed KO mice, with lower *cyp2e1* expression in males (Figure 4A,G).

Mouse Cyp4a14 catalyzes the omega-hydroxylation of saturated and unsaturated fatty acids in mice and shows female-predominant expression in liver, where it is induced by *ppara* [28]. In WT males, HFD strongly increased otherwise very low *cyp4a14* by 51-fold, and in KO males by almost 400-fold. In females, HFD upregulated *cyp4a14* by 2.5-fold in KO mice. Overall, females displayed higher *cyp4a14* expression than males, except in HFD-fed KO mice (Figure 4B,H).



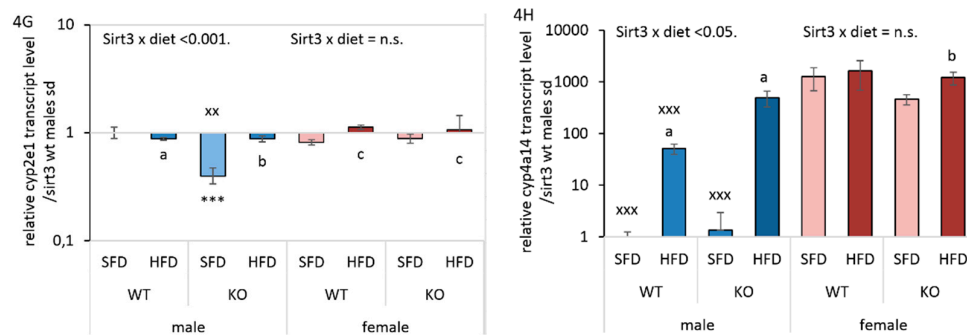


Figure 4. Gene expression of *hnf4a*, *ppara*, *ppary*, *cyp2a4*, *cyp2e1*, and *cyp4a14* in the livers of Sirt3 wild-type (WT) and knockout (KO) mice fed with a standard fat diet (SFD) or a high fat diet (HFD) for 10 weeks. (A) A heatmap of the mRNA levels of *hnf4a*, *ppara*, *ppary*, *cyp2a4*, *cyp2e1*, and (B) *cyp4a14* genes. The color of the squares on the heat map corresponds to the mean value of the log fold change from three biological and three technical replicates. (C) A graphical display of *hnf4a* mRNA level. Males: no changes. Females: no changes. Males vs. females: SFD-fed ($*p < 0.05$) and HFD-fed ($^{**}p < 0.01$). (D) A graphical display of *ppara* mRNA levels. Males: no changes. Females: KO vs. WT mice ($^{**}p < 0.01$). Males vs. females: WT mice ($^{xxx}p < 0.001$). (E) A graphical display of *ppary* mRNA levels. Males: HFD-fed vs. SFD-fed WT mice ($^{*}p < 0.001$); SFD-fed WT vs. KO mice ($^{***}p < 0.001$). Females: no changes. Males vs. females: HFD-fed WT mice ($^{xxx}p < 0.001$). (F) A graphical display of *cyp2a4* mRNA levels. Males: HFD-fed vs. SFD-fed WT mice ($^{*}p < 0.001$); HFD-fed vs. SFD-fed KO mice ($^{b}p < 0.01$); SFD-fed WT vs. KO mice ($^{**}p < 0.01$) and HFD-fed WT vs. KO mice ($^{***}p < 0.001$); Females: HFD-fed vs. SFD-fed WT ($^{c}p < 0.001$) and KO mice ($^{d}p < 0.01$); SFD-fed KO vs. WT mice ($^{**}p < 0.01$); Males vs. females: $^{xxx}p < 0.001$. (G) A graphical display of *cyp2e1* mRNA levels. Males: HFD-fed vs. SFD-fed WT mice ($^{*}p < 0.05$); HFD-fed vs. SFD-fed KO mice ($^{b}p < 0.001$); SFD-fed KO vs. WT mice ($^{***}p < 0.001$). Females: HFD-fed vs. SFD-fed mice ($^{c}p < 0.01$). Males vs. females: SFD-fed KO mice ($^{xx}p < 0.01$). (H) A graphical display of *cyp4a14* mRNA levels. Males: HFD-fed vs. SFD-fed mice ($^{*}p < 0.001$). Females: HFD-fed vs. SFD-fed KO mice ($^{b}p < 0.01$). Males vs. females: WT mice and SFD-fed KO mice ($^{xxx}p < 0.001$). β -actin was used for normalization. The data are shown as mean \pm SD. $n = 3$ per group in technical triplicates.

3.6. Sirt3 KO Mice Exhibit Increased Protein Oxidative Damage and Upregulated Keap1-Nrf2-Ho1 Axis in Liver

Following the observed differences between males and females in lipid accumulation and the genes involved in lipid homeostasis, along with the fact that sensitivity towards the oxidative stress is sex-related as well [29,30], we next examined sensitivity to oxidative stress with respect to Sirt3 or diet by measuring protein carbonylation (PC), a marker of protein oxidative damage. In males, higher PC levels were observed in the absence of Sirt3. Contrary to that, in WT females, an HFD increased PC, resulting in levels similar to KO females in both diets. Moreover, SFD-fed KO females had higher PC than WT mice. Overall, the sex-specific differences evident in HFD-fed WT mice were abrogated in the KO mice, where similar PC levels were observed in both sexes (Figure 5A). These data indicate that, besides protein oxidative damage caused by the absence of Sirt3 in both sexes, females are also susceptible to protein damage caused by an HFD only.

We next aimed to investigate whether major proteins involved in antioxidative response pathway, such as Keap1/Nrf2/Ho1, were altered. Nrf2 is a transcription factor that induces the gene expression of antioxidant enzymes and many other cytoprotective enzymes. Upon oxidative stress, the interaction between Keap1 and Nrf2 is disrupted, which induces Nrf2-dependent gene expression [31]. WT males had higher Keap1 compared to KO mice and HFD partially rescued Keap1 in KO mice. Likewise, in females, Keap1 was also reduced in KO mice. There were no differences in Keap1 between males and females (Figure 5C). In WT males, HFD reduced Nrf2. Moreover, Nrf2 was higher in KO mice compared to WT mice of both sexes, which is in accordance with reduced Keap1. Differences between males and females were evident only in SFD-fed WT mice, where males had

higher Nrf2 (Figure 5D). In males, an HFD had the opposite effect on Ho1 expression, where it decreased the expression of the Ho1 protein in WT and increased it in KO males. In WT females, an HFD increased Ho-1 protein level, which remained higher in KO mice, irrespective of diet. Differences in Ho1 between males and females were only observable in WT mice, with higher Ho1 in SFD-fed and lower in HFD-fed males (Figure 5E). This finding indicates the presence of the adaptive stress response in conditions of nutritional excess only in the absence of Sirt3.

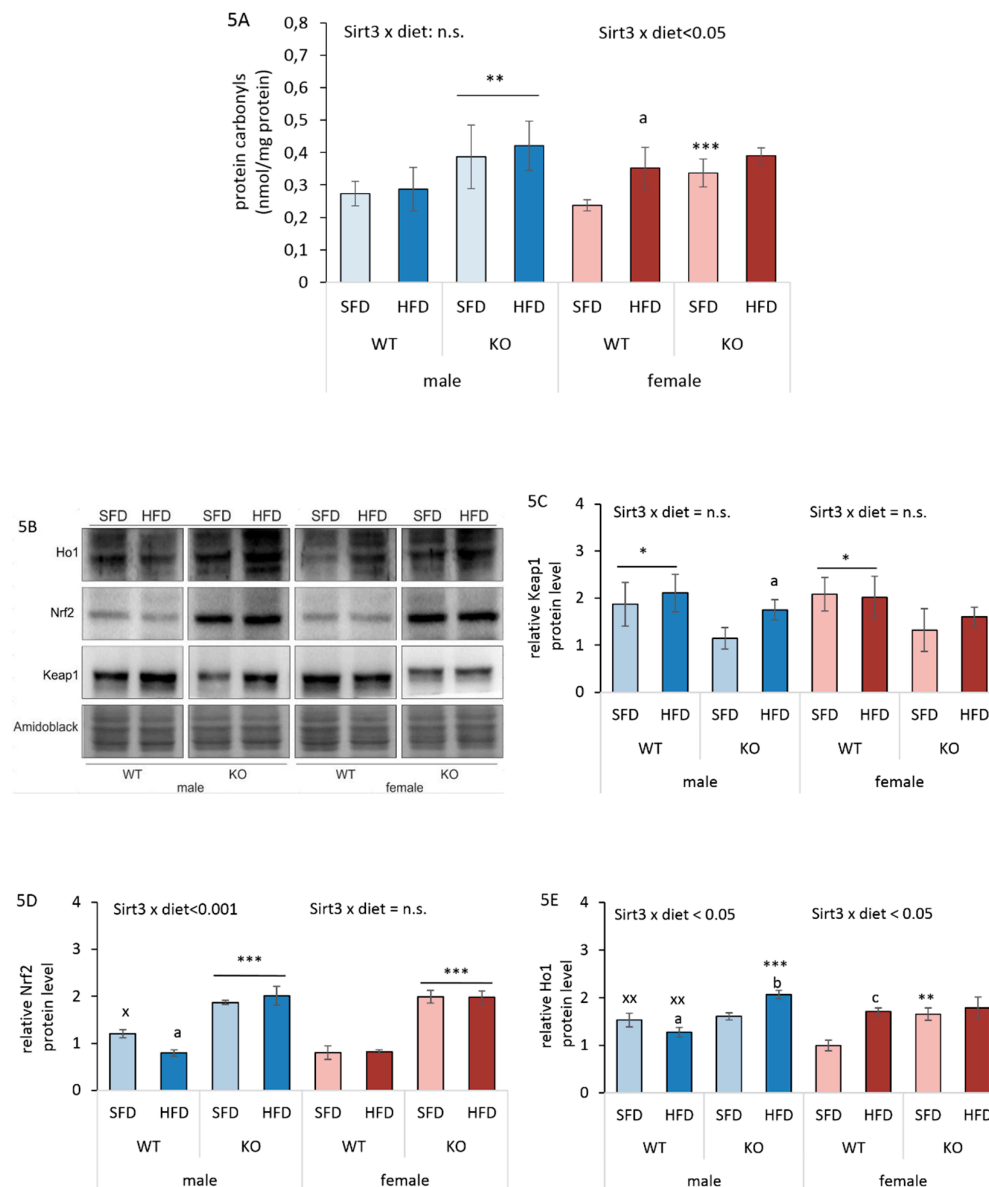


Figure 5. Protein oxidative damage and antioxidant response in the livers of Sirt3 wild-type (WT) and knockout (KO) mice fed with a standard fat diet (SFD) or a high fat diet (HFD) for 10 weeks. **(A)** The total amount of protein carbonyls (PC) measured with an ELISA-based assay at 450 nm. Males: KO vs. WT mice ($**p < 0.01$). Females: HFD-fed vs. SFD-fed WT mice ($^ap < 0.01$); SFD-fed KO vs. WT mice ($***p < 0.001$). Males vs. females: no changes. The data are shown as mean \pm SD. $n = 6$ per group. **(B)** The representative immunoblots of hepatic Keap1, Nrf2, and Ho1 protein expression. Amidoblack was used as a loading control. **(C)** A graphical display of the averaged densitometry values for Keap-1 protein expression. Males: HFD-fed vs. SFD-fed KO mice ($^ap < 0.05$); WT vs. KO mice ($^ap < 0.05$).

Females: WT vs. KO mice ($^*p < 0.05$). Males vs. females: no changes. (D) A graphical display of the averaged densitometry values for Nrf-2 protein expression. Males: HFD-fed vs. SFD-fed WT mice ($^ap < 0.001$); KO vs. WT mice ($^{**}p < 0.001$). Females: KO vs. WT mice ($^{***}p < 0.001$). Males vs. females: SFD-fed WT mice ($^sp < 0.05$). (E) A graphical display of averaged densitometry values of Ho-1 protein expression. Males: HFD-fed vs. SFD-fed WT mice ($^ap < 0.05$); HFD-fed vs. SFD-fed KO mice ($^bp < 0.01$); HFD-fed KO vs. WT mice ($^{***}p < 0.001$). Females: HFD-fed vs. SFD-fed WT mice ($^cp = 0.002$); SFD-fed KO vs. WT mice ($^{**}p < 0.01$). Males vs. females: WT mice ($^{xp} < 0.05$). The data are shown as mean \pm SD. $n = 6$.

3.7. HFD-Induced Reduction in Sirt3/MnSOD Axis is Male-Specific

Sirt3 mediates the reduction of oxidative and metabolic damage, while exposure to HFD leads to reduced Sirt3 expression, consequent hyper acetylation of manganese superoxide dismutase (AcSOD2), and the reduction of SOD2 activity (hereafter MnSOD) [32]. Since we found that an HFD reduced Sirt3 protein level only in males, we further examined whether this pattern affects AcSOD2 protein and MnSOD activity in the same way. HFD-fed WT males displayed increased AcSOD2 protein levels along with decreased MnSOD activity. SFD-fed WT males had reduced AcSOD2 protein and higher MnSOD activity than KO mice. HFD-fed WT females also displayed increased AcSOD2 protein, but without change in MnSOD activity. SFD-fed WT females had reduced AcSOD2 protein but higher MnSOD activity on both diets compared to KO mice (Figure 6A–D). This suggests that the acetylation status of MnSOD acetyl-K68 that regulates MnSOD activity in males under HFD conditions, does not contribute to alteration of MnSOD activity in females. Both KO males and females had similar AcSOD2 levels, with reduced MnSOD activity, thus confirming the importance of Sirt3 in regulation of MnSOD activity.

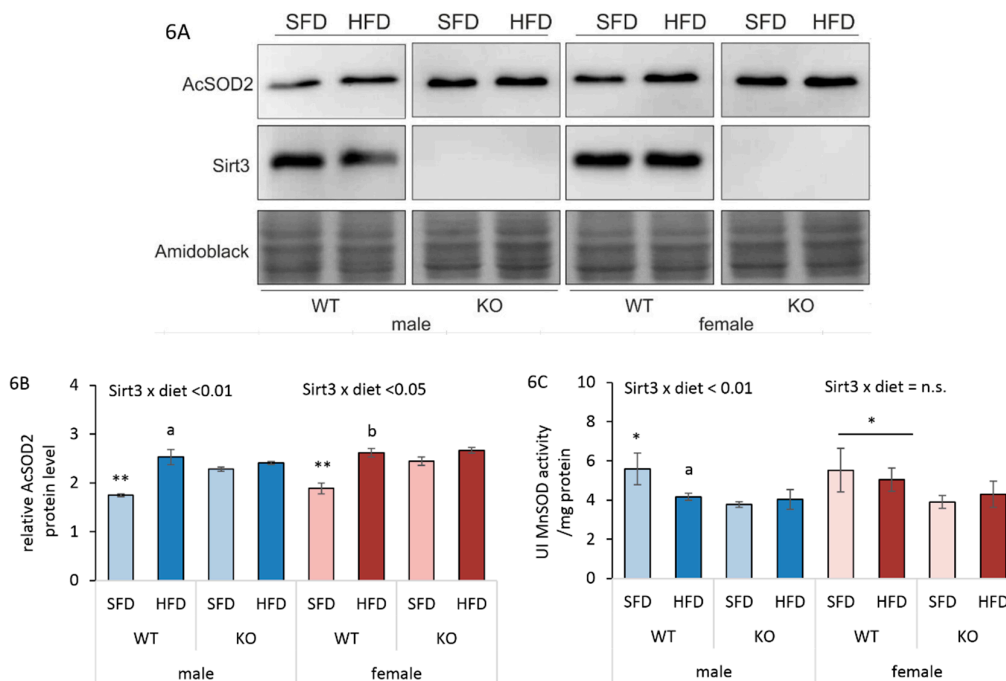


Figure 6. Sirt3/MnSOD axis in liver of Sirt3 wild-type (WT) and knockout (KO) mice fed with a standard fat diet (SFD) or a high fat diet (HFD) for 10 weeks. (A) A representative immunoblot of hepatic Sirt3 and AcSOD2 protein expression. Amidoblack was used as a loading control. (B) A graphical display of averaged densitometry values for AcSOD2 protein expression. Males: HFD-fed vs. SFD-fed WT mice ($^ap < 0.01$); SFD-fed WT vs. KO mice ($^{**}p < 0.01$). Females: HFD-fed vs. SFD-fed WT mice ($^bp < 0.01$); SFD-fed WT vs. KO mice ($^{**}p < 0.01$). Males vs. females: no change. (C) MnSOD activity. Males: HFD-fed vs. SFD-fed WT mice ($^ap < 0.01$); SFD-fed WT vs. KO mice ($^sp < 0.05$). Females:

WT vs. KO mice ($*p < 0.05$). Males vs. females: no change. The data are shown as mean \pm SD. $n = 6$ per group.

3.8. HFD Affects Antioxidant Enzyme Activities Differently in Males and Females

Beside major mitochondrial antioxidant enzyme MnSOD, we also determined other antioxidant enzymes, such as copper zinc superoxide dismutase (CuZnSOD, SOD1), catalase (Cat), and glutathione peroxidase (Gpx1) at protein level (Supplementary Figure S3) and their activities (Figure 7a–c). We observed a discrepancy between protein expression and antioxidant enzyme activity, indicating the complex regulatory mechanisms of enzyme activities. Therefore, the results of enzyme activities are more informative and are shown here. In males, an HFD reduced very mildly CuZnSOD activity in both WT (14%) and KO (10%) mice. Additionally, SFD-fed WT mice had marginally higher CuZnSOD activity compared to KO mice (14.2%). On the contrary, females displayed no changes in CuZnSOD activity (Figure 7A). Cat activity was increased following an HFD in both sexes and genotypes (Figure 7B). The inducing effect of HFD on Cat activity in both genotypes and sexes suggests that increased Cat activity is needed to effectively degrade excess of H_2O_2 produced by increased lipid metabolism, irrespective of sex or Sirt3. Gpx is a cytosolic enzyme that also functions in the detoxification of H_2O_2 , specifically by catalyzing the reduction of hydrogen peroxide to water. In WT males, HFD increased Gpx activity to levels of KO mice. SFD-fed WT males also displayed lower Gpx activity compared to KO mice. In females, Gpx activity was lower in WT mice compared to KO mice. The differences in Gpx activity between males and females were evident only in HFD-fed WT mice, where males had higher Gpx activity (Figure 7C). These results point toward differential sex-related effect of HFD on antioxidant enzyme activities.

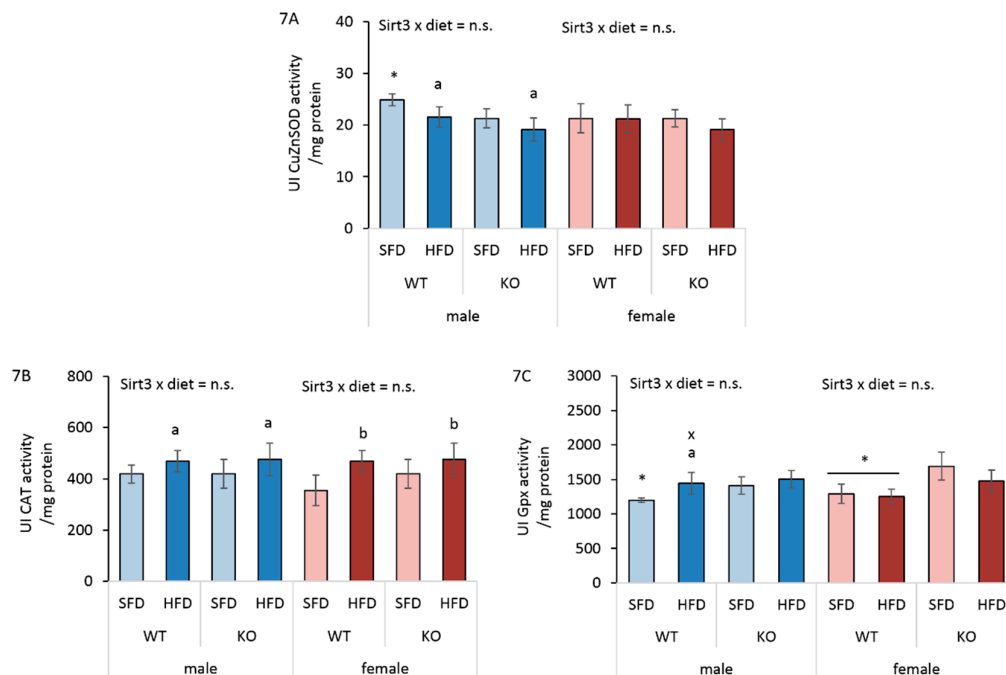


Figure 7. Analysis of CuZnSOD, Cat, and Gpx1 activities in the livers of Sirt3 wild-type (WT) and knockout (KO) mice of both sexes fed with a standard fat diet (SFD) or a high fat diet (HFD) for 10 weeks. **(A)** CuZnSOD activity. Males: HFD-fed vs. SFD-fed mice ($*p < 0.05$); SFD-fed WT vs. KO mice ($*p < 0.05$); Females: no changes. Males vs. females: no changes. **(B)** Cat activity. Males: HFD-fed vs. SFD-fed mice ($*p < 0.05$). Females: HFD-fed vs. SFD-fed mice ($*p < 0.01$). Males vs. females: no changes. **(C)** Gpx1 activity. Males: HFD-fed vs. SFD-fed WT mice ($*p < 0.05$); SFD-fed WT vs. KO mice ($*p < 0.05$). Females: WT vs. KO mice ($*p < 0.05$). Males vs. females: HFD-fed WT mice ($*p < 0.05$). The data are shown as mean \pm SD. $n = 6$ per group.

3.9. HFD and Sirt3 Depletion Affect Mitochondrial Respiration Differently in Males and Females

Sirt3 is an important regulator of mitochondrial respiration, and its targets include subunits of the respiratory chain complexes. Studies showed that KO mice display decreased oxygen consumption in liver [33] and reduced glucose tolerance when placed on an HFD [10]. To examine whether the loss of Sirt3 would impair respiration in a sex- and diet-dependent manner, we measured oxygen consumption in mitochondria from liver using a Clark type electrode.

WT males had higher malate/glutamate (MG) + ADP respiration than KO males, suggesting defective CI-driven respiration in the absence of Sirt3. Interestingly, an HFD partially restored low CI-driven respiration in KO males. In WT females, an HFD significantly decreased CI-driven respiration, which remained low in the absence of Sirt3. Finally, we observed that females had higher CI-driven respiration compared to males, except in HFD-fed WT mice, where this difference was reversed in favor of males (Figure 8A).

The respiratory control ratio (RCR) is defined as the ratio of the state 4 respiratory rate (termination of ATP synthesis by addition of oligomycin) to the state 3 (ADP-stimulated respiration) respiratory rate and indicates how well the electron transport system is coupled to ATP synthesis. WT males had higher RCR than KO males on a SFD, while an HFD partially restored low the RCR observed in the absence of Sirt3. In WT females, an HFD decreased RCR, which remained low in the absence of Sirt3. Females had higher RCR than males in SFD-fed conditions, while the opposite was found in HFD-fed WT mice. These results collectively indicate that the effective CI respiration in both sexes depends on Sirt3. Moreover, both CI-driven respiration and RCR display a sex-specific effect of HFD and Sirt3, with an inducing effect of HFD in KO males and a suppressive effect in WT females.

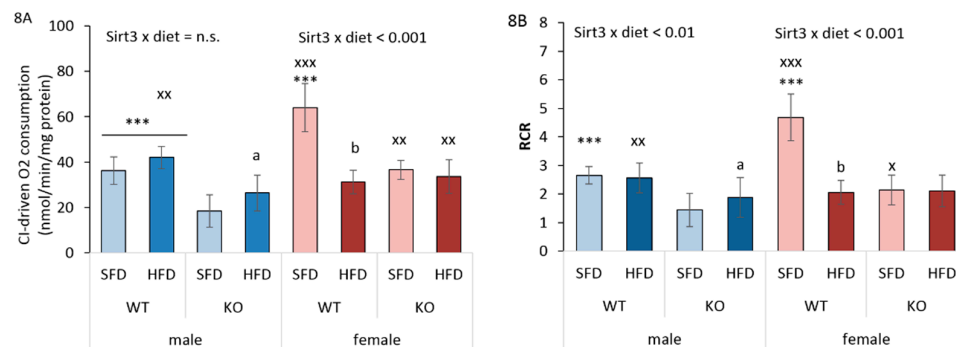


Figure 8. Complex I (CI)-driven respiration and the respiratory control ratio (RCR) of liver mitochondria of Sirt3 wild-type (WT) and knockout (KO) mice of both sexes fed with a standard fat diet (SFD) or a high fat diet (HFD) for 10 weeks. **(A)** CI-driven respiration. Males: HFD-fed vs. SFD-fed KO mice ($^a p < 0.05$); WT vs. KO mice ($^{***} p < 0.001$). Females: HFD-fed vs. SFD-fed WT mice ($^b p < 0.001$); SFD-fed WT vs. KO mice ($^{***} p < 0.001$). Males vs. females: SFD-fed WT mice ($^{xxx} p < 0.001$); HFD-fed WT mice ($^{xx} p < 0.01$); KO mice ($^{xx} p < 0.01$). **(B)** The respiratory control ratio (RCR). Males: HFD-fed vs. SFD-fed KO mice ($^a p < 0.001$); SFD-fed WT vs. KO mice ($^{***} p < 0.001$). Females: HFD-fed vs. SFD-fed WT mice ($^b p < 0.001$); SFD-fed WT vs. KO mice ($^{***} p < 0.001$). Males vs. females: SFD-fed WT mice ($^{xxx} p < 0.001$); HFD-fed WT mice ($^{xx} p < 0.01$); SFD-fed KO mice ($^x p < 0.05$). The data are shown as mean \pm SD. $n = 4$ per group.

4. Discussion

Sexual dimorphism exists in various physiological processes, with males and females differing with respect to their regulation of energy homeostasis, metabolic rate, or body weight gain [34]. For example, HFD feeding leads to larger body weight gain in male rats/mice than in females [35]. In this study, we report the following novel observations in conditions of HFD feeding and Sirt3 depletion in liver of 129S mice: (a) HFD reduces hepatic Sirt3 expression solely in males, but only partially; (b)

HFD-induced lipid accumulation is alleviated in the absence of Sirt3 only in males, which may be attributed to impaired glucose uptake and an increased reliance on fatty acids; (c) in females, either an HFD or the absence of Sirt3 compromised mitochondrial respiration and increased protein oxidative damage, which could be associated with more efficient lipid metabolism.

Sirt3 plays an important role in regulating lipid homeostasis by ameliorating HFD-induced inflammation, liver fibrosis, and steatosis. Reports show that HFD feeding in WT male mice results in a reduction of Sirt3 expression in the liver [36] and that deleterious effects of HFD feeding are exacerbated in male mice lacking Sirt3 [10]. Accordingly, we found that Sirt3 was reduced upon HFD feeding in male mice, however, without any change in females (Figure 1A, 1B). This result suggests that the regulation of Sirt3 in a sexually dimorphic manner following HFD in males may contribute to the observed sex-related differences in the development of metabolic dysregulation.

It has been shown that a decreased level of Sirt3 contributes to impaired glucose metabolism [24]. However, in our study, we did not observe the effect of Sirt3 on differences in glucose levels, only the effect of sex, where females had lower fasting glucose levels compared to males (Figure 2B), suggesting a possible role of female sex hormones in maintaining low glucose in females [37]. The interesting fact is that we did not observe gained weight in mice fed with an HFD (Figure 2A). The observed phenotype upon HFD feeding comes from the specific characteristics of this particular strain of mice (129S), which are not prone to the development of obesity when fed with an HFD [38]. However, despite the fact that mice did not gain weight following HFD feeding, both sexes displayed excessive hepatic lipid accumulation (Figure 3), indicating a fatty liver phenotype after ten weeks of an HFD.

Sirt3 deficiency reduces fatty acid oxidation and results in the accumulation of hepatic lipids in SFD-fed male mice [39], which is confirmed in our study. On the contrary, this effect was not evident in Sirt3-depleted females, which showed less accumulation of lipids than males in SFD conditions (Figure 3I). Thus, disturbances in fatty acid oxidation in standard conditions and upon the depletion of Sirt3 may result in elevated lipids and impaired metabolism, thus supporting the critical role of Sirt3 in the maintenance of metabolic homeostasis in males. Studies have shown that an HFD acts as a metabolic stressor causing mitochondrial dysfunction and other metabolic changes that contribute to pathological conditions [4]. In HFD conditions, Sirt3-depleted males displayed the lowest total lipid content in liver along with the lowest hepatic glucose uptake (Figure 3I, 3J). These results indicate that in the absence of Sirt3 in males, HFD may cause impairments in hepatic glucose uptake, creating an increased reliance on fatty acids. This was previously also shown in the skeletal muscles of Sirt3 KO male mice [33]. Again, the observed differences in males were not evident in Sirt3-depleted females. The absence of these effects in WT mice indicates that sex-related differences in lipid accumulation and glucose uptake are present only in Sirt3-depleted mice.

In tissues that have a high fatty acid uptake, such as adipocytes and liver tissue, the capacity for the β oxidation of fatty acids, the major lipid catabolic pathways, is regulated at the level of gene expression in response to various physiologic stimuli [28]. Moreover, the maintenance of lipid homeostasis relies on cytochrome P450 (P450) enzymes, the majority of which are regulated in a sex-dependent manner [40]. To test if hepatic P450 enzymes are involved in sex-related differences in lipid accumulation in the absence of Sirt3, we measured the expression of several genes involved in fatty acid oxidation and lipid homeostasis (Figure 4). One important factor is *ppary*, which is predominantly expressed in adipose tissue but also in the liver and muscle, and promotes the storage of lipids [41]. Since in our study HFD-fed mice did not have increased weight compared to SFD-fed mice, we tested whether this was due to the altered expression of *ppary*, which is essential for adipogenesis [42]. Indeed, both sexes displayed downregulated levels of *ppary* (Figure 4E), allowing us to hypothesize that the downregulation of hepatic *ppary* may be related to the fact that mice did not gain weight after feeding with HFD. Furthermore, we observed sex-related differences in *cyp2e1*, *cyp2a4*, and *cyp4a14* transcripts of P450 genes involved in the maintenance of lipid homeostasis (Figure 4A, 4F–H). Females generally responded to an HFD with an upregulated expression of these involved genes, while males had a different response to an HFD with respect to Sirt3. Considering their role in lipid metabolism, the downregulation of *cyp2a4* and *cyp2e1* in male KO mice fed with

SFD may be associated with their tendency towards accumulating more hepatic fat than females. In HFD conditions, these genes tend to be upregulated in KO males, therefore suggesting more effective lipid metabolism in association with lower accumulation of total lipids in liver.

Since we found sex-related differences in several parameters involved in lipid homeostasis upon different types of diet, we next investigated whether they reflected sex-related sensitivity to oxidative stress under the same conditions. Protein carbonylation (PC) is considered to be an important marker of oxidative stress resulting from HFD-induced oxidative damage to proteins [43,44]. Here, we show that an HFD induced a female-specific increase in the PC of WT mice (Figure 5A) as a possible consequence of the upregulated expression of genes involved in fatty acid oxidation, that is associated with the generation of hydrogen peroxide [45] involved in protein oxidative damage. Unlike WT males, HFD-fed WT females also displayed increased Ho1 protein expression (Figure 5B, 5E), which is an indicator of the presence of oxidative stress [46]. However, they failed to counteract oxidative damage by the activation of an antioxidative response, since no induction of the Keap1/Nrf2 axis (Figure 5C, 5D) and major antioxidative enzyme activities (MnSOD, CuZnSOD, Gpx1) was observed (Figure 6C, 7A, 7C), resulting in greater protein oxidative damage (Figure 5A). On the other hand, higher PC levels in KO mice of both sexes were associated with upregulated Keap1/Nrf2 axis, but with no response in antioxidant enzyme activities. This shows that in WT mice, an HFD induces oxidative stress only in females, pointing at their increased susceptibility towards the oxidative stress in conditions of nutritive stress. Furthermore, Sirt3 deficiency increases susceptibility to protein oxidative damage equally in both sexes, indicating that Sirt3 is important for protection against the oxidative damage of proteins.

Several studies demonstrated that lipid metabolism has a potential to generate ROS [47,48]. For example, both peroxisomal and mitochondrial β -oxidation produce H_2O_2 and O_2^- as byproducts of fatty acid degradation. During nutritional excess, the imbalance in lipid metabolism along with upregulated key genes involved in fatty acid β -oxidation, such as *ppara*, contributes to increased ROS and oxidative stress [45]. Catalase (Cat), a peroxisomal enzyme, has also been found in cardiac mitochondria with significantly increased activity during HFD feeding [48]. We observed the inducing effect of HFD on Cat activity in both genotypes and sexes (Figure 7B), suggesting that increased Cat activity is needed to effectively degrade excess of H_2O_2 produced by increased fat metabolism in HFD-fed mice.

Mitochondrial function is tightly associated with the activity of the respiratory chain complexes, and depends on the degree of coupling of oxidative phosphorylation [49]. Fatty acids are metabolic fuels and β -oxidation represents their main degradation pathway in mitochondria [50]. Sirt3 WT females had significantly higher CI-driven respiration and RCR than Sirt3 WT males in standard conditions, suggesting a more efficient function of Complex I in the electron transport chain of hepatic mitochondria in females. Contrary to males, in WT females, HFD feeding dramatically decreased MG-ADP state respiration, indicating female-specific impairment in CI-driven respiration and RCR following an HFD (Figure 8A, 8B). The observed defective CI-driven respiration in HFD-fed females could be due to their higher fatty acid oxidation, in synchronization with upregulated genes involved in the lipid oxidation process (*ppara*, *cyp2a4*, *cyp2e1*, *cyp4a14*), resulting in increased oxidative damage of mitochondrial proteins, thereby affecting mitochondrial respiration. Indeed, fatty acids can act as inhibitors of mitochondrial respiration, either by the partial inhibition of electron transport within CI or III, or by a decrease in proton motive force [51,52]. Based on this result, we hypothesize that in conditions of nutritive excess, more efficient lipid metabolism in WT females may cause higher oxidative stress in association with reduced mitochondrial function.

Sirt3 KO male mice display decreased CI-driven oxygen consumption [33], which is in agreement with our results. In addition, we show for the first time that, despite reduced respiration in Sirt3-depleted mice, females have higher respiration than males. However, since in KO males an HFD increased respiration, we hypothesize that they compensate impaired glucose uptake by increasing their reliance on fatty acids to provide substrates for the respiratory chain. This is in accordance to [53] and [54], where HFD-fed male rodents exhibited increased mitochondrial capacity and respiration [55]. Our results collectively indicate that the CI-driven respiration displays a sex-

specific effect with respect to both HFD and Sirt3, with an inducing effect of HFD on respiration in KO males and a suppressive effect in WT females.

Sexual dimorphism exists in various physiological processes, which also includes sex-related prevalence towards metabolic dysregulation. In this study, we found significant sex differences at the level of metabolic, oxidant/antioxidant, and mitochondrial parameters. In addition, this study points towards a different role of Sirt3 in males and females under the conditions of nutritive stress. This is an important step that adds to previous knowledge that can be studied to prevent metabolic dysfunction, improve preclinical research, and allow for the development of sex-related therapeutic agents for obesity and diabetes.

Supplementary Materials: The following are available online at www.mdpi.com/xxx/s1, Figure S1: Body weight gain of Sirt3 WT and KO mice fed with standard fat diet (SFD) or high fat diet (HFD) for 10 weeks. Figure S2: Quantification of hepatic lipid accumulation signal (from Figure 2A–H) in Sirt3 WT and KO mice of both sexes fed with standard fat diet (SFD) or high fat diet (HFD) for 10 weeks. Figure S3: Western blot analysis of antioxidative enzymes in Sirt3 WT and KO mice of both sexes fed with standard fat diet (SFD) or high fat diet (HFD) for 10 weeks. Table S1: Assays (Taqman® Applied Biosystems, Foster City, CA, USA) used for real time quantitative PCR analyses, Table S2: Antibodies used in this study for the Western blot analyses.

Author Contributions: Conceptualization, M.P., I.I.P. and S.S.; Data curation, M.P., I.I.P., M.P.H. and S.S.; Formal analysis, I.I.P., I.T.B., A.D., R.B., V.F. and S.S.; Funding acquisition, T.B.; Investigation, S.S.; Methodology, M.P., I.I.P., M.P.H., I.T.B., A.D., R.B., V.F. and S.S.; Software, R.B. and V.F.; Supervision, T.B.; Validation, I.I.P.; Visualization, M.P.H.; Writing – original draft, M.P., I.I.P. and S.S.; Writing – review & editing, M.P., I.I.P., M.P.H., I.T.B., A.D., R.B., V.F., S.S. and T.B. All authors have read and agreed to the published version of the manuscript.

Funding: This work was supported by the Croatian Science Foundation (HRZZ), Grant no. [IP-2014-09-4533] “SuMERA”.

Acknowledgments: The authors would like to thank Iva Pešun Međimorec and Marina Marš for their excellent technical contribution.

Conflicts of Interest: The authors declare no conflict of interest.

References

1. Bonomini, F.; Rodella, L.F.; Rezzani, R. Metabolic syndrome, aging and involvement of oxidative stress. *Aging Dis.* **2015**, *6*, 109–120.
2. Nunn, A.V.; Guy, G.W.; Brodie, J.S.; Bell, J.D. Inflammatory modulation of exercise salience: using hormesis to return to a healthy lifestyle. *Nutr. Metab. (Lond)*. **2010**, *7*, 87.
3. Kakimoto, P.A.; Kowaltowski, A.J. Effects of high fat diets on rodent liver bioenergetics and oxidative imbalance. *Redox Biol.* **2016**, *8*, 216–225.
4. Guarner-Lans, V.; Rubio-Ruiz, M.E.; Pérez-Torres, I.; Baños de MacCarthy, G. Relation of aging and sex hormones to metabolic syndrome and cardiovascular disease. *Exp. Gerontol.* **2011**, *46*, 517–523.
5. Lejri, I.; Grimm, A.; Eckert, A. Mitochondria, Estrogen and Female Brain Aging. *Front. Aging Neurosci.* **2018**, *10*, 124.
6. Beery, A.K.; Zucker, I. Sex bias in neuroscience and biomedical research. *Neurosci. Biobehav. Rev.* **2011**, *35*, 565–572.
7. Meziane, H.; Ouagazzal, A.-M.; Aubert, L.; Wietrzyk, M.; Krezel, W. Estrous cycle effects on behavior of C57BL/6J and BALB/cByJ female mice: Implications for phenotyping strategies. *Genes Brain Behav.* **2007**, *6*, 192–200.
8. Kahle, M.; Horsch, M.; Fridrich, B.; Seelig, A.; Schultheiß, J.; Leonhardt, J.; Irmeler, M.; Beckers, J.; Rathkolb, B.; Wolf, E.; et al. Phenotypic comparison of common mouse strains developing high-fat diet-induced hepatosteatosis. *Mol. Metab.* **2013**, *2*, 435–446.
9. Narvik, J.; Vanaveski, T.; Innos, J.; Philips, M.-A.; Ottas, A.; Haring, L.; Zilmer, M.; Vasar, E. Metabolic profile associated with distinct behavioral coping strategies of 129Sv and B6 mice in repeated motility test. *Sci. Rep.* **2018**, *8*, 3405.
10. Hirschey, M.D.; Shimazu, T.; Jing, E.; Grueter, C.A.; Collins, A.M.; Aouizerat, B.; Stančáková, A.; Goetzman, E.; Lam, M.M.; Schwer, B.; et al. SIRT3 Deficiency and Mitochondrial Protein Hyperacetylation Accelerate the Development of the Metabolic Syndrome. *Mol. Cell* **2011**, *44*, 177–190.

11. Bellizzi, D.; Rose, G.; Cavalcante, P.; Covello, G.; Dato, S.; De Rango, F.; Greco, V.; Maggiolini, M.; Feraco, E.; Mari, V.; et al. A novel VNTR enhancer within the SIRT3 gene, a human homologue of SIR2, is associated with survival at oldest ages. *Genomics* **2005**, *85*, 258–263.
12. Barja, G. Updating the Mitochondrial Free Radical Theory of Aging: An Integrated View, Key Aspects, and Confounding Concepts. *Antioxid. Redox Signal.* **2013**, *19*, 1420–1445.
13. Vargas-Ortiz, K.; Pérez-Vázquez, V.; Macías-Cervantes, H.M. Exercise and Sirtuins: A Way to Mitochondrial Health in Skeletal Muscle. *Int. J. Mol. Sci.* **2019**, *20*, 2717.
14. Brown, K.; Xie, S.; Qiu, X.; Mohrin, M.; Shin, J.; Liu, Y.; Zhang, D.; Scadden, D.T.T.; Chen, D. SIRT3 Reverses Aging-Associated Degeneration. *Cell Rep.* **2013**, *3*, 319–327.
15. Qiu, X.; Brown, K.; Hirschey, M.D.; Verdin, E.; Chen, D. Calorie Restriction Reduces Oxidative Stress by SIRT3-Mediated SOD2 Activation. *Cell Metab.* **2010**, *12*, 662–667.
16. Hebert, A.S.; Dittenhafer-Reed, K.E.; Yu, W.; Bailey, D.J.; Selen, E.S.; Boersma, M.D.; Carson, J.J.; Tonelli, M.; Balloon, A.J.; Higbee, A.J.; et al. Calorie Restriction and SIRT3 Trigger Global Reprogramming of the Mitochondrial Protein Acetylome. *Mol. Cell* **2013**, *49*, 186–199.
17. Calabrese, V.; Cornelius, C.; Cuzzocrea, S.; Iavicoli, I.; Rizzarelli, E.; Calabrese, E.J. Hormesis, cellular stress response and vitagenes as critical determinants in aging and longevity. *Mol. Aspects Med.* **2011**, *32*, 279–304.
18. Ways, P.; Hanahan, D.J. Characterization and quantification of red cell lipids in normal man. *J. Lipid Res.* **1964**, *5*, 318–328.
19. Aebi, H.B.T.-M. in E. [13] Catalase in vitro. In *Oxygen Radicals in Biological Systems*; Academic Press:Cambridge, MA, USA, 1984; Volume 105, pp. 121–126 ISBN 0076-6879.
20. Paglia, D.E.; Valentine, W.N. Studies on the quantitative and qualitative characterization of erythrocyte glutathione peroxidase. *J. Lab. Clin. Med.* **1967**, *70*, 158–169.
21. Šarić, A.; Crnolatac, I.; Bouillaud, F.; Sobočanec, S.; Mikecin, A.M.; Mačak Šafranko, Ž.; Delgeorgiev, T.; Piantanida, I.; Balog, T.; Petit, P.X. Non-toxic fluorescent phosphonium probes to detect mitochondrial potential. *Methods Appl. Fluoresc.* **2017**, *5*, 15007.
22. Fueger, B.J.; Czernin, J.; Hildebrandt, I.; Tran, C.; Halpern, B.S.; Stout, D.; Phelps, M.E.; Weber, W.A. Impact of Animal Handling on the Results of 18F-FDG PET Studies in Mice. *J. Nucl. Med.* **2006**, *47*, 999–1006.
23. Šarić, A.; Sobočanec, S.; Mačak Šafranko, Ž.; Popović Hadžija, M.; Bagarić, R.; Farkaš, V.; Švarc, A.; Marotti, T.; Balog, T. Diminished Resistance to Hyperoxia in Brains of Reproductively Senescent Female CBA/H Mice. *Med. Sci. Monit. Basic Res.* **2015**, *21*, 191–199.
24. Jing, E.; Emanuelli, B.; Hirschey, M.D.; Boucher, J.; Lee, K.Y.; Lombard, D.; Verdin, E.M.; Kahn, C.R. Sirtuin-3 (Sirt3) regulates skeletal muscle metabolism and insulin signaling via altered mitochondrial oxidation and reactive oxygen species production. *Proc. Natl. Acad. Sci. USA* **2011**, *108*, 14608–14613.
25. Patsouris, D.; Reddy, J.K.; Müller, M.; Kersten, S. Peroxisome Proliferator-Activated Receptor α Mediates the Effects of High-Fat Diet on Hepatic Gene Expression. *Endocrinology* **2006**, *147*, 1508–1516.
26. Liss, K.H.H.; Finck, B.N. PPARs and nonalcoholic fatty liver disease. *Biochimie* **2017**, *136*, 65–74.
27. Waxman, D.J.; Holloway, M.G. Sex differences in the expression of hepatic drug metabolizing enzymes. *Mol. Pharmacol.* **2009**, *76*, 215–228.
28. Kersten, S.; Rakhshandehroo, M.; Knoch, B.; Müller, M. Peroxisome proliferator-activated receptor alpha target genes. *PPAR Res.* **2010**, *2010*, 612089.
29. Sobočanec, S.; Šarić, A.; Mačak Šafranko, Ž.; Popović Hadžija, M.; Abramić, M.; Balog, T. The role of 17 β -estradiol in the regulation of antioxidant enzymes via the Nrf2-Keap1 pathway in the livers of CBA/H mice. *Life Sci.* **2015**, *130*, 57–65.
30. Kander, M.C.; Cui, Y.; Liu, Z. Gender difference in oxidative stress: A new look at the mechanisms for cardiovascular diseases. *J. Cell. Mol. Med.* **2017**, *21*, 1024–1032.
31. Tu, W.; Wang, H.; Li, S.; Liu, Q.; Sha, H. The Anti-Inflammatory and Anti-Oxidant Mechanisms of the Keap1/Nrf2/ARE Signaling Pathway in Chronic Diseases. *Aging Dis.* **2019**, *10*, 637–651.
32. Tyagi, A.; Nguyen, C.U.; Chong, T.; Michel, C.R.; Fritz, K.S.; Reisdorph, N.; Knaub, L.; Reusch, J.E.B.; Pugazhenth, S. SIRT3 deficiency-induced mitochondrial dysfunction and inflammasome formation in the brain. *Sci. Rep.* **2018**, *8*, 1–16.
33. Lantier, L.; Williams, A.S.; Williams, I.M.; Yang, K.K.; Bracy, D.P.; Goelzer, M.; James, F.D.; Gius, D.; Wasserman, D.H. SIRT3 is crucial for maintaining skeletal muscle insulin action and protects against severe insulin resistance in high-fat-fed mice. *Diabetes* **2015**, *64*, 3081–3092.

34. Shi, H.; Seeley, R.J.; Clegg, D.J. Sexual differences in the control of energy homeostasis. *Front. Neuroendocrinol.* **2009**, *30*, 396–404.
35. Yang, Y.; Smith Jr., D.L.; Keating, K.D.; Allison, D.B.; Nagy, T.R. Variations in body weight, food intake and body composition after long-term high-fat diet feeding in C57BL/6J mice. *Obesity* **2014**, *22*, 2147–2155.
36. Bao, J.; Scott, I.; Lu, Z.; Pang, L.; Dimond, C.C.; Gius, D.; Sack, M.N. SIRT3 is regulated by nutrient excess and modulates hepatic susceptibility to lipotoxicity. *Free Radic. Biol. Med.* **2010**, *49*, 1230–1237.
37. Mauvais-Jarvis, F. Gender differences in glucose homeostasis and diabetes. *Physiol. Behav.* **2018**, *187*, 20–23.
38. Ussar, S.; Griffin, N.W.; Bezy, O.; Fujisaka, S.; Vienberg, S.; Softic, S.; Deng, L.; Bry, L.; Gordon, J.I.; Kahn, C.R. Interactions between Gut Microbiota, Host Genetics and Diet Modulate the Predisposition to Obesity and Metabolic Syndrome. *Cell Metab.* **2015**, *22*, 516–530.
39. Chen, T.; Liu, J.; Li, N.; Wang, S.; Liu, H.; Li, J.; Zhang, Y.; Bu, P. Mouse SIRT3 attenuates hypertrophy-related lipid accumulation in the heart through the deacetylation of LCAD. *PLoS ONE* **2015**, *10*, e0118909–e0118909.
40. Yang, L.; Li, Y.; Hong, H.; Chang, C.-W.; Guo, L.-W.; Lyn-Cook, B.; Shi, L.; Ning, B. Sex Differences in the Expression of Drug-Metabolizing and Transporter Genes in Human Liver. *J. Drug Metab. Toxicol.* **2012**, *3*, 1000119.
41. Sugii, S.; Olson, P.; Sears, D.D.; Saberi, M.; Atkins, A.R.; Barish, G.D.; Hong, S.H.; Castro, G.L.; Yin, Y.Q.; Nelson, M.C.; et al. PPAR γ activation in adipocytes is sufficient for systemic insulin sensitization. *Proc. Natl. Acad. Sci. USA* **2009**, *106*, 22504–22509.
42. Rosen, E.D.; Sarraf, P.; Troy, A.E.; Bradwin, G.; Moore, K.; Milstone, D.S.; Spiegelman, B.M.; Mortensen, R.M. PPAR γ is required for the differentiation of adipose tissue in vivo and in vitro. *Mol. Cell* **1999**, *4*, 611–617.
43. Krisko, A.; Radman, M. Phenotypic and genetic consequences of protein damage. *PLoS Genet.* **2013**, *9*, e1003810.
44. Rincón-Cervera, M.A.; Valenzuela, R.; Hernandez-Rodas, M.C.; Marambio, M.; Espinosa, A.; Mayer, S.; Romero, N.; Barrera Cynthia, M.S.; Valenzuela, A.; Videla, L.A. Supplementation with antioxidant-rich extra virgin olive oil prevents hepatic oxidative stress and reduction of desaturation capacity in mice fed a high-fat diet: Effects on fatty acid composition in liver and extrahepatic tissues. *Nutrition* **2016**, *32*, 1254–1267.
45. Chen, Q.; Tang, L.; Xin, G.; Li, S.; Ma, L.; Xu, Y.; Zhuang, M.; Xiong, Q.; Wei, Z.; Xing, Z.; et al. Oxidative stress mediated by lipid metabolism contributes to high glucose-induced senescence in retinal pigment epithelium. *Free Radic. Biol. Med.* **2019**, *130*, 48–58.
46. Kamalvand, G.; Pinard, G.; Ali-Khan, Z. Heme-oxygenase-1 response, a marker of oxidative stress, in a mouse model of AA amyloidosis. *Amyloid* **2003**, *10*, 151–159.
47. Flor, A.C.; Wolfgeher, D.; Wu, D.; Kron, S.J. A signature of enhanced lipid metabolism, lipid peroxidation and aldehyde stress in therapy-induced senescence. *Cell Death Discov.* **2017**, *3*, 17075.
48. Tahara, E.B.; Navarete, F.D.T.; Kowaltowski, A.J. Tissue-, substrate-, and site-specific characteristics of mitochondrial reactive oxygen species generation. *Free Radic. Biol. Med.* **2009**, *46*, 1283–1297.
49. Crescenzo, R.; Bianco, F.; Mazzoli, A.; Giacco, A.; Liverini, G.; Iossa, S. Alterations in proton leak, oxidative status and uncoupling protein 3 content in skeletal muscle subsarcolemmal and intermyofibrillar mitochondria in old rats. *BMC Geriatr.* **2014**, *14*, 79.
50. Aon, M.A.; Bhatt, N.; Cortassa, S. Mitochondrial and cellular mechanisms for managing lipid excess. *Front. Physiol.* **2014**, *5*, 282.
51. Schönfeld, P.; Reiser, G. Rotenone-like Action of the Branched-chain Phytanic Acid Induces Oxidative Stress in Mitochondria. *J. Biol. Chem.* **2006**, *281*, 7136–7142.
52. Schönfeld, P.; Wojtczak, L. Fatty acids decrease mitochondrial generation of reactive oxygen species at the reverse electron transport but increase it at the forward transport. *Biochim. Biophys. Acta-Bioenerg.* **2007**, *1767*, 1032–1040.
53. Hoeks, J.; Briedé, J.J.; de Vogel, J.; Schaart, G.; Nabben, M.; Moonen-Kornips, E.; Hesselink, M.K.C.; Schrauwen, P. Mitochondrial function, content and ROS production in rat skeletal muscle: Effect of high-fat feeding. *FEBS Lett.* **2008**, *582*, 510–516.

54. Turner, N.; Bruce, C.R.; Beale, S.M.; Hoehn, K.L.; So, T.; Rolph, M.S.; Cooney, G.J. Excess Lipid Availability Increases Mitochondrial Fatty Acid Oxidative Capacity in Muscle. *Diabetes* **2007**, *56*, 2085–2092.
55. Crescenzo, R.; Bianco, F.; Mazzoli, A.; Giacco, A.; Liverini, G.; Iossa, S. Mitochondrial efficiency and insulin resistance. *Front. Physiol.* **2015**, *5*, 512.



© 2020 by the authors. Licensee MDPI, Basel, Switzerland. This article is an open access article distributed under the terms and conditions of the Creative Commons Attribution (CC BY) license (<http://creativecommons.org/licenses/by/4.0/>).



Table S1. Assays (Taqman® Applied Biosystems, Foster City, CA, USA) used for real time quantitative PCR analyses.

Gene	Assay ID	Product Size (bp)
<i>β-actin</i>	Mm00607939_s1	115
<i>cyp2a4</i>	Mm00487248_m1	75
<i>cyp2e1</i>	Mm00491127_m1	83
<i>cyp4a14</i>	Mm00484132_m1	71
<i>hnf4α</i>	Mm00433964_m1	114
<i>ppara</i>	Mm00627559_m1	86
<i>ppary</i>	Mm00440940_m1	63

Table S2. Antibodies used in this study for the Western blot analyses.

Antibody	Dilution	Host	Manufacturer
Sirt3 (D22A3)	1:1000	Rabbit	Cell Signaling Technology, Danvers, MA, USA
Ho-1 (ab52947)	1:700	Rabbit	Abcam, Cambridge, UK
Nrf2 (ab31163)	1:2000	Rabbit	Abcam, Cambridge, UK
Keap1 (60027-1-Ig)	1:1000	Mouse	Proteintech, Rosemont, IL, USA
AcSOD2 (ab137037)	1:1000	Rabbit	Abcam, Cambridge, UK
CuZnSOD (ab 16831)	1:3000	Rabbit	Abcam, Cambridge, UK
Cat (ab1877)	1:4000	Rabbit	Abcam, Cambridge, UK
Gpx1 (ab16798)	1:2000	Rabbit	Abcam, Cambridge, UK
Anti-mouse (170-6516)	1:5000	Goat	Bio-rad, Hercules, CA, USA
Anti-rabbit (NA934)	1:5000	Goat	GE Healthcare, Chicago, IL, USA

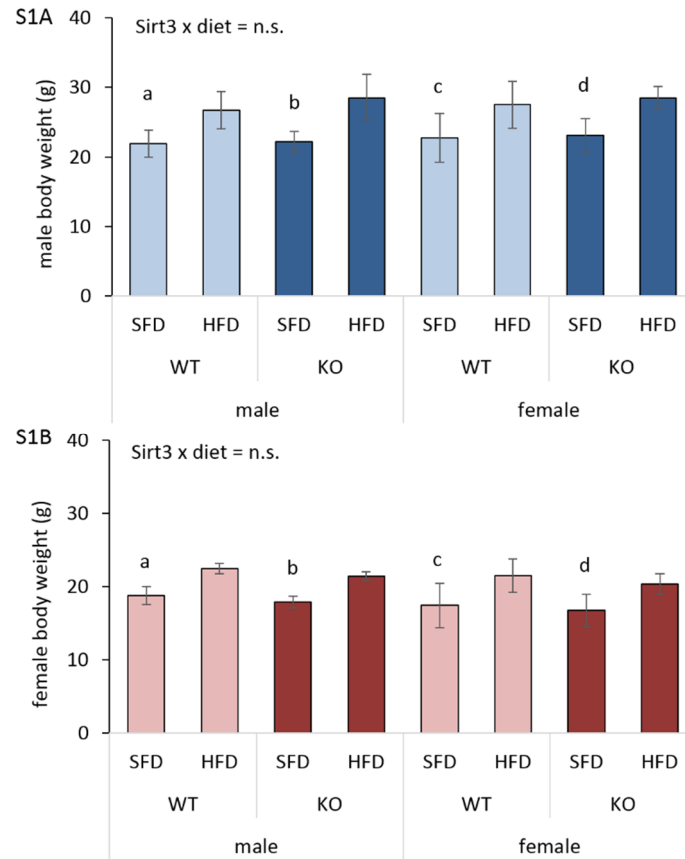


Figure S1. Body weight gain of Sirt3 WT and KO mice fed with standard fat diet (SFD) or high fat diet (HFD) for 10 weeks. **(A)** Body weight of male mice. Week 1 vs. week 10 in SFD-fed WT (^a $p < 0.01$), HFD-fed WT (^b $p < 0.001$), SFD-fed KO (^c $p < 0.05$) and HFD-fed KO mice (^d $p < 0.001$). **(B)** Body weight of female mice. Week 1 vs. week 10 in SFD-fed WT (^a $p < 0.001$), HFD-fed WT (^b $p < 0.001$), SFD-fed KO (^c $p < 0.05$) and HFD-fed KO mice (^d $p < 0.01$). Data are shown as mean \pm SD. N=6 per group.

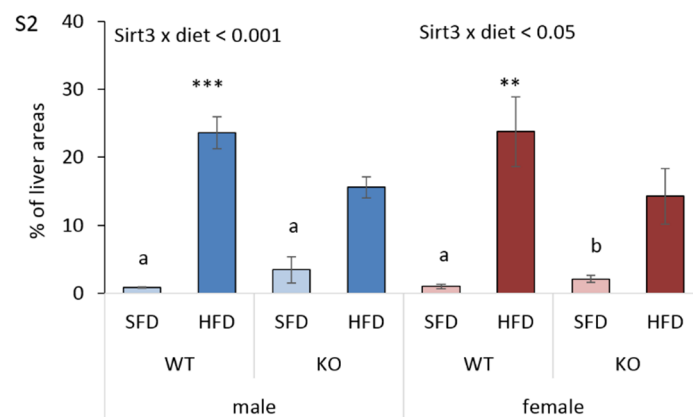


Figure S2. Quantification of hepatic lipid accumulation signal (from Figure 2A-H) in Sirt3 WT and KO mice of both sexes fed with standard fat diet (SFD) or high fat diet (HFD) for 10 weeks. **Males:** WT and KO mice ($a_{p < 0.001}$); HFD-fed WT vs. KO mice ($***p < 0.001$). **Females:** SFD-fed vs. HFD-fed WT mice ($a_{p < 0.001}$); SFD-fed vs. HFD-fed KO mice ($b_{p < 0.01}$); HFD-fed WT vs. KO mice ($**p < 0.01$). **Males vs. females:** no changes. Data are shown as mean \pm SD. N=3 per group.

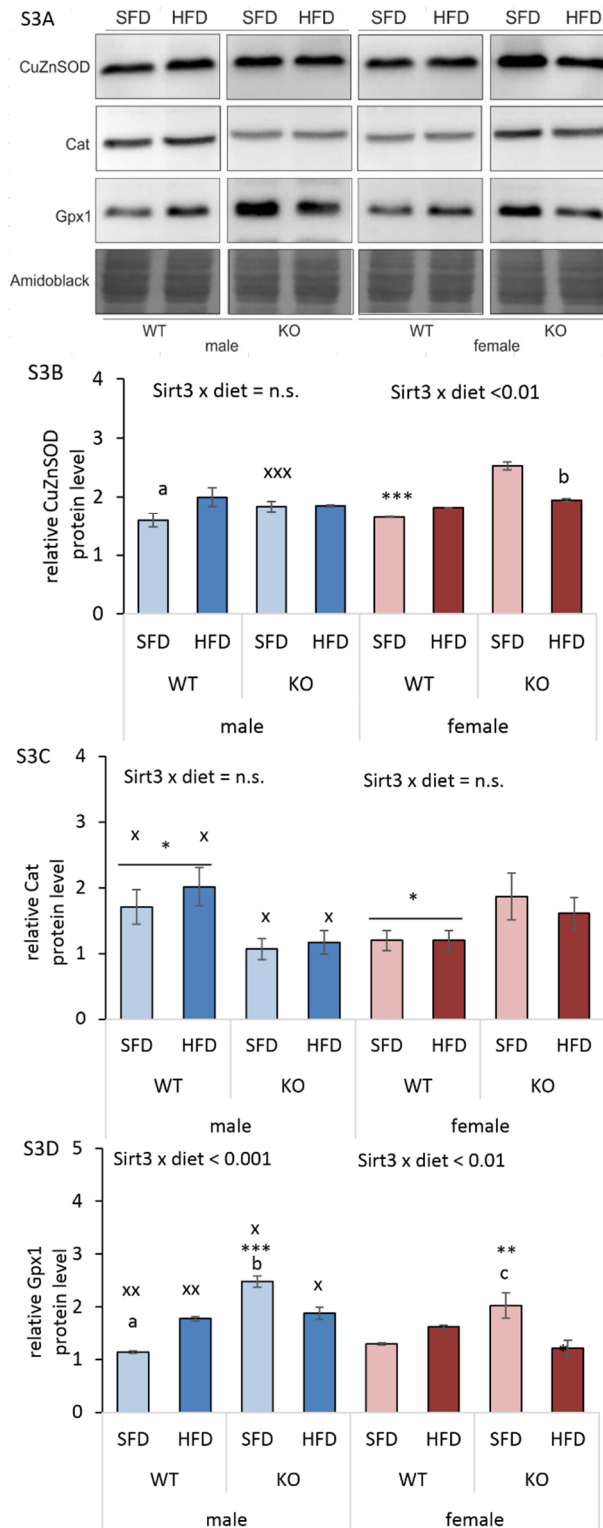


Figure S3. Western blot analysis of antioxidative enzymes in Sirt3 WT and KO mice of both sexes fed with standard fat diet (SFD) or high fat diet (HFD) for 10 weeks. **(A)** Representative immunoblot of hepatic CuZnSOD, Cat and Gpx1 protein expression. Amidoblack was used as a loading control. **(B)** Graphical display of averaged densitometry values of CuZnSOD protein expression. **Males:** SFD-fed vs. HFD-fed WT mice ($^a p < 0.05$). **Females:** HFD-fed vs. SFD-fed KO mice ($^b p < 0.001$); SFD-fed WT vs. KO mice ($^{xxx} p < 0.001$). **Males vs. females:** SFD-fed KO mice ($^{xxx} p < 0.001$). **(C)** Graphical display of averaged densitometry values of Cat protein expression. **Males:** WT vs. KO mice ($^* p < 0.05$). **Females:** WT vs. KO mice ($^* p < 0.05$). **Males vs. females:** WT mice ($^x p < 0.05$) and KO mice ($^* p < 0.05$). **(D)** Graphical display of averaged densitometry values of Gpx1 protein expression. **Males:** SFD-fed vs. HFD-fed

WT mice (^a $p < 0.001$); SFD-fed vs. HFD-fed KO mice (^b $p < 0.01$); SFD-fed KO vs. WT mice (^{***} $p < 0.001$). **Females:** SFD-fed vs. HFD-fed KO mice (^c $p < 0.01$); SFD-fed KO vs. WT mice (^{**} $p < 0.01$); HFD-fed KO vs. WT mice (^{*} $p < 0.05$). **Males vs. females:** SFD-fed WT mice (^{xx} $p < 0.01$); HFD-fed WT (^{xx} $p < 0.01$), SFD-fed KO (^x $p < 0.05$) and HFD-fed KO mice (^x $p < 0.05$). Data for B), C) and D) are shown as mean \pm SD. N=4 per group.



Article

Chronic High Fat Diet Intake Impairs Hepatic Metabolic Parameters in Ovariectomized Sirt3 KO Mice

Marija Pinterić ^{1,†} , Iva I. Podgorski ^{1,†} , Marijana Popović Hadžija ¹ , Ivana Tartaro Bujak ² , Ana Tadijan ¹ , Tihomir Balog ¹ and Sandra Sobočanec ^{1,*}

¹ Division of Molecular Medicine, Ruđer Bošković Institute, 10000 Zagreb, Croatia; mpinter@irb.hr (M.P.); iskrinj@irb.hr (I.I.P.); mhadzija@irb.hr (M.P.H.); Ana.Tadijan@irb.hr (A.T.); balog@irb.hr (T.B.)

² Division of Materials Chemistry, Ruđer Bošković Institute, 10000 Zagreb, Croatia; itartaro@irb.hr

* Correspondence: ssoboc@irb.hr; Tel.: +385-1-4561-172

† Equal contribution.

Abstract: High fat diet (HFD) is an important factor in the development of metabolic diseases, with liver as metabolic center being highly exposed to its influence. However, the effect of HFD-induced metabolic stress with respect to ovary hormone depletion and sirtuin 3 (Sirt3) is not clear. Here we investigated the effect of Sirt3 in liver of ovariectomized and sham female mice upon 10 weeks of feeding with standard-fat diet (SFD) or HFD. Liver was examined by Folch, gas chromatography and lipid hydroperoxide analysis, histology and oil red staining, RT-PCR, Western blot, antioxidative enzyme and oxygen consumption analyses. In SFD-fed WT mice, ovariectomy increased Sirt3 and fatty acids synthesis, maintained mitochondrial function, and decreased levels of lipid hydroperoxides. Combination of ovariectomy and Sirt3 depletion reduced *ppara*, *Scd-1* ratio, MUFA proportions, CII-driven respiration, and increased lipid damage. HFD compromised CII-driven respiration and activated peroxisomal ROS scavenging enzyme catalase in sham mice, whereas in combination with ovariectomy and Sirt3 depletion, increased body weight gain, expression of NAFLD- and oxidative stress-inducing genes, and impaired response of antioxidative system. Overall, this study provides evidence that protection against harmful effects of HFD in female mice is attributed to the combined effect of female sex hormones and Sirt3, thus contributing to preclinical research on possible sex-related therapeutic agents for metabolic syndrome and associated diseases.

Keywords: sirtuin 3; ovariectomy; high fat diet; fatty liver



Citation: Pinterić, M.; Podgorski, I.I.; Popović Hadžija, M.; Tartaro Bujak, I.; Tadijan, A.; Balog, T.; Sobočanec, S. Chronic High Fat Diet Intake Impairs Hepatic Metabolic Parameters in Ovariectomized Sirt3 KO Mice. *Int. J. Mol. Sci.* **2021**, *22*, 4277. <https://doi.org/10.3390/ijms22084277>

Academic Editor: Muriel Le Romancer

Received: 25 March 2021

Accepted: 16 April 2021

Published: 20 April 2021

Publisher's Note: MDPI stays neutral with regard to jurisdictional claims in published maps and institutional affiliations.



Copyright: © 2021 by the authors. Licensee MDPI, Basel, Switzerland. This article is an open access article distributed under the terms and conditions of the Creative Commons Attribution (CC BY) license (<https://creativecommons.org/licenses/by/4.0/>).

1. Introduction

The metabolic syndrome is a cluster of risk factors responsible for the development of cardiovascular diseases and many other health problems, and as such is one of the leading risks for global deaths representing a serious threat to public health [1]. A high fat diet (HFD) is an important factor in the development of many metabolic diseases, with liver as a metabolic center being highly exposed to its influence [2]. Metabolic syndrome can be effectively mimicked and studied in rodent models using various dietary interventions, including HFD [3], which then lead to mitochondrial dysfunction and other metabolic changes induced by oxidative stress (reviewed in [1]). Feeding mice with HFD results in one of the diet-induced models of non-alcoholic fatty liver disease (NAFLD), which is accompanied by liver inflammation and steatosis [4]. Indeed, hepatic steatosis occurs when high concentrations of circulatory fatty acids (FAs) reaching the liver and de novo lipogenesis are not counterbalanced by FA oxidation or lipid export as lipoproteins [5].

In most mammals, including humans, life expectancy is female-biased [6,7]. Females show lower incidence of some age-related pathologies linked with oxidative stress and this sex-difference disappears after menopause, which leads to the conclusion that this protection is attributed to sex hormones (reviewed in [8]). Thus, one approach to study age-linked pathologies is to investigate hormone-depleted or -augmented animals and their defense

from metabolic stressors. Estradiol (E2) is an important regulator of energy homeostasis, thus making it a potential target for preventing or treating metabolic disorders. Previous studies established the association of metabolic syndrome and E2 loss during menopause in women (reviewed in [9]) and reported that E2 can alter hepatic proteins involved in de novo lipid synthesis [10]. However, the mechanism behind those observations, especially how the fat-lowering action of E2 is modulated in the liver, remains elusive, especially in a sex-related manner.

Sirtuin 3 (Sirt3) is a mitochondrial protein that integrates cellular energy metabolism and plays an important role in preventing metabolic syndrome [4]. Although Sirt4 and Sirt5 are also present in mitochondria, Sirt3 is the main mitochondrial deacetylase because only Sirt3-knockout mice show hyperacetylation of mitochondrial proteins and less effective mitochondria. In addition, Sirt3 is involved in the regulation of all mitochondrial functions, including the tricarboxylic acid (TCA), the urea cycle, amino acid metabolism, fatty acid oxidation, oxidative phosphorylation (OXPHOS), ROS detoxification, mitochondrial dynamics, and the mitochondrial unfolded protein response (UPR) [11,12]. It promotes mitochondrial oxidative metabolism via deacetylation of numerous metabolic enzymes, including those involved in FA catabolism, as demonstrated earlier by an abnormal accumulation of FA oxidation intermediates in Sirt3 KO mice [4]. It was also shown that Sirt3 expression is reduced during chronic HFD in male mice [4,13]. Although E2-dependent protection includes improvement of mitochondrial function [14], it is not clear whether Sirt3, as a pivotal factor regulating mitochondrial biogenesis and reactive oxygen species (ROS) management, participates in these events.

In our recent study, we found significant sex differences in mice at the level of metabolic, oxidant, antioxidant, and mitochondrial parameters upon HFD. Also, we pointed towards a different role of Sirt3 in males and females under the conditions of nutritive stress, with higher reliance of males than females to the effect of Sirt3 against HFD-induced metabolic dysregulation [13]. These observations led us to the hypothesis that females' protection from HFD-induced metabolic dysregulation *in vivo* could be attributed to the complementary beneficial effect of Sirt3 and ovary hormones. However, the mechanism by which this combination operates still needs to be elucidated. Therefore, this study explored the metabolic, mitochondrial, oxidative, and antioxidative parameters following HFD and ovarian hormone deprivation in young adult Sirt3 WT and Sirt3 KO female mice.

2. Results

2.1. Ovariectomy Increases Sirt3 and *pgc1-α* Expression in the Liver of Female Mice

Since ovaries are the main source of female sex hormones' production in the body [15], we performed ovariectomy (ovx) to assess the effect of ovary hormones in our experiments. Loss of ovarian hormones was confirmed by reduced uterus size and by cytological examination of vaginal smears, showing estrous phase in control (sham) and anestrus phase in ovx mice (Supplemental Figure S1A–C). To assess the functional role of hepatic Sirt3 with respect to ovx and HFD, we examined gene and protein expression in female sham and ovx Sirt3 WT and KO mice after 10 weeks of feeding with SFD or HFD. OvX increased *sirt3* gene (** $p < 0.001$) and protein (* $p < 0.05$) expression in both SFD and HFD conditions (Figure 1A–C). Thus, ovx upregulated Sirt3 irrespective of type of diet in WT female mice. A similar pattern was observed with peroxisome proliferator-activated receptor-γ coactivator-1 α (*pgc1-α*), a master regulator of mitochondrial function [16]. OvX upregulated *pgc1-α* gene expression regardless of Sirt3 in SFD conditions (* $p < 0.05$) (Figure 1D). Following HFD, KO normalized ovx-induced (** $p < 0.01$) *pgc1-α* gene expression (^a $p < 0.01$). These data indicate that ovx induces both *pgc1-α* and Sirt3 in WT mice irrespective of diet and that expression of the *pgc1-α* in ovx KO mice depends on the type of diet.

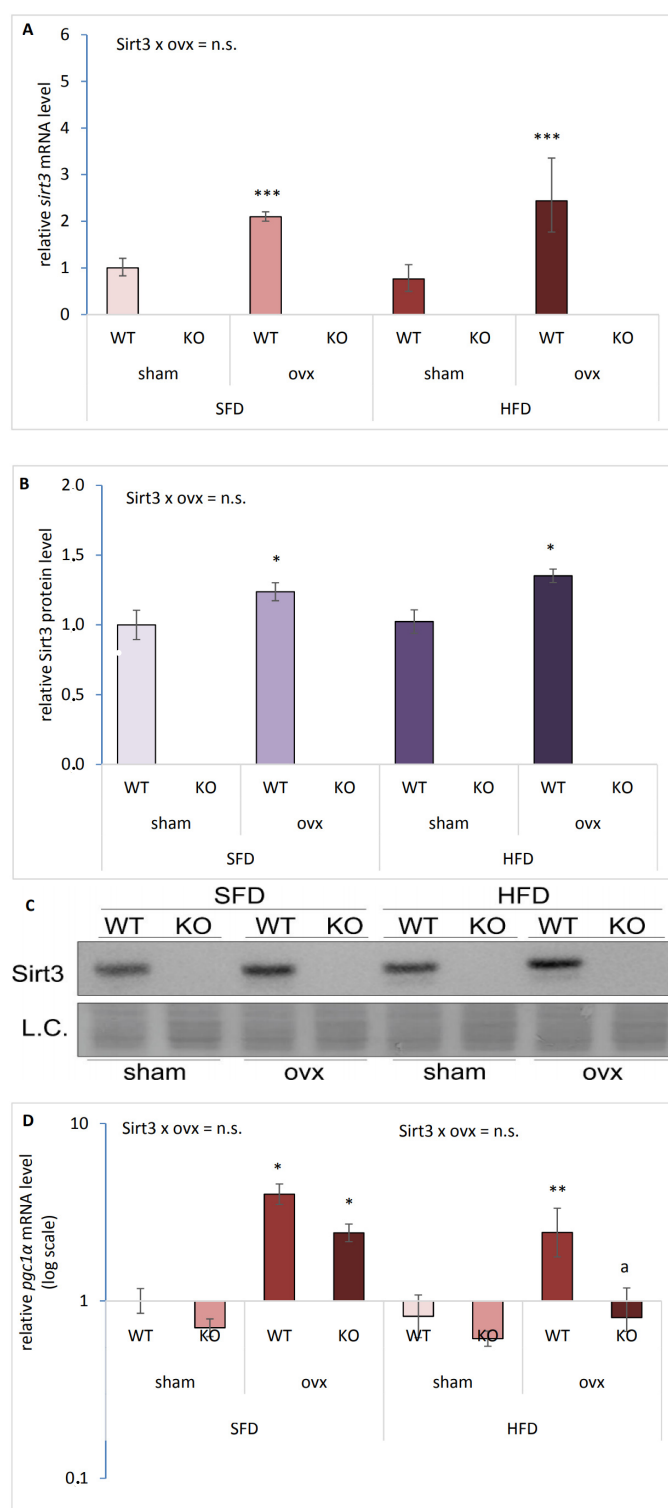


Figure 1. Ovariectomy (ovx) increases Sirt3 and *pgc1-α* in liver of female mice. **(A)** *sirt3* gene expression in sham and ovx Sirt3 WT and KO mice. SFD: WT sham vs. ovx (** $p < 0.001$). HFD: WT sham vs. ovx (** $p < 0.001$). SFD vs. HFD: no changes. **(B)** Graphical display of averaged densitometry values for Sirt3 protein expression in sham and ovx Sirt3 WT and KO mice. SFD: WT sham vs. ovx (* $p < 0.05$). HFD: WT sham vs. ovx (* $p < 0.05$). SFD vs. HFD: no changes. **(C)** Immunoblot of Sirt3 protein expression. Amidoblack was used as a loading control (L.C.). **(D)** *pgc1-α* gene expression in sham and ovx Sirt3 WT and KO mice. SFD: sham vs. ovx (* $p < 0.05$). HFD: WT sham vs. ovx (** $p < 0.01$); ovx WT vs. KO (^a $p < 0.01$). SFD vs. HFD: no changes. Data are shown as mean \pm SD. $n = 3$ mice per group. The representative image is displayed.

2.2. The Effect of Sirt3 and Ovx on Body Weight Gain Depends on the Type of Diet

Fasting glucose level remained unchanged by either ovx or Sirt3 depletion in both SFD and HFD-fed mice (Figure 2A). In agreement with our previous observations [13], we found no change in body weight in SFD- and HFD-fed sham mice (data not shown). However, body weight gain was affected differently in ovx KO mice, depending on type of diet: SFD-fed KO ovx mice gained less weight than WT ovx (^a $p < 0.05$) or sham KO mice (^{**} $p < 0.01$) (Figure 2B). Contrary to SFD conditions, upon HFD, KO ovx mice gained more weight than WT ovx (^b $p < 0.01$) or sham KO mice (^{**} $p < 0.01$). Also, HFD-fed ovx KO mice were the only group that had increased body weight gain compared to their SFD littermates (^{xxx} $p < 0.001$). These data indicate that ovary hormone deficiency in the absence of Sirt3 makes these mice most resistant towards gaining weight on SFD but also most sensitive towards gaining weight upon HFD.

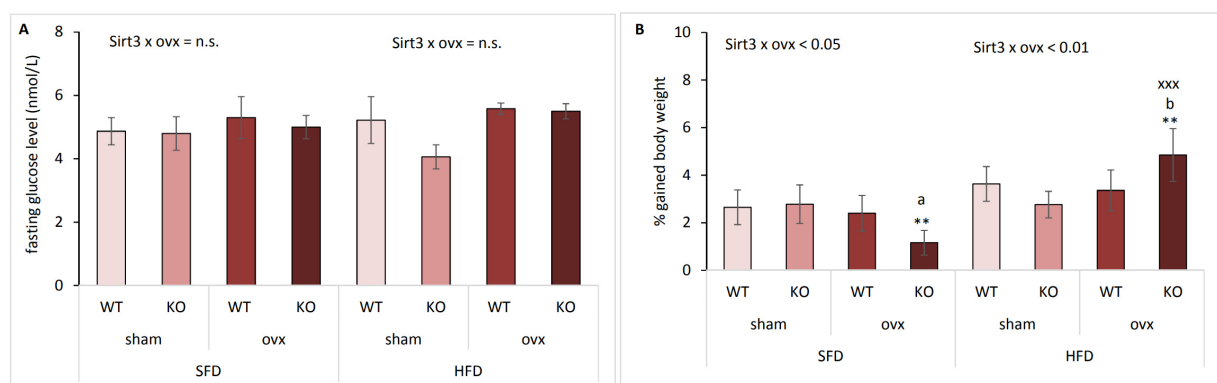


Figure 2. The effect of Sirt3 and ovariectomy (ovx) on body weight gain is diet dependent. (A) Fasting blood glucose in sham and ovx Sirt3 WT and KO mice. SFD: no changes. HFD: no changes. SFD vs. HFD: no changes. (B) Gained body weight (%) in sham and ovx Sirt3 WT and KO mice. SFD: ovx WT vs. KO (^a $p < 0.05$); KO sham vs. ovx (^{**} $p < 0.01$). HFD: ovx WT vs. KO (^b $p < 0.01$); KO sham vs. ovx (^{**} $p < 0.01$). SFD vs. HFD: KO ovx (^{xxx} $p < 0.001$). Data are shown as mean \pm SD. $n = 6$ mice per group.

2.3. Sirt3 and Ovx have Combined Effect on the Expression of Genes Responsible for Lipid Metabolism and Oxidative Stress

Due to significant differences in body weight gain with respect to Sirt3 and ovx in SFD and HFD, we investigated whether combination of Sirt3 depletion and ovx affected genes involved in the lipid metabolism and oxidative stress, i.e., peroxisome proliferator-activated receptor alpha (*pparα*) [17], cytochrome P450 4a14 (*cyp4a14*), *cyp2e1* [18], and heme oxygenase-1 (*ho-1*) [19]. In SFD-fed mice, ovx affected *pparα* expression differently depending on Sirt3: ovx increased *pparα* only in WT mice (^{***} $p < 0.001$), without affecting KO mice (^a $p < 0.01$) (Figure 3A). In HFD-fed mice, *pparα* was also increased only in ovx WT compared to sham WT mice (^{*} $p < 0.05$). HFD generally increased levels of *pparα* in all groups (^x $p < 0.05$) except in ovx WT. In SFD conditions, *cyp4a14* expression was increased in ovx KO mice compared to both ovx WT (^a $p < 0.01$) and sham KO mice (^{*} $p < 0.05$) (Figure 3B). In HFD-fed conditions, ovx increased *cyp4a14* expression only in KO mice (^{**} $p < 0.001$). Also, *cyp4a14* expression was higher in all HFD-fed mice compared to the respective SFD-fed groups (^x $p < 0.05$, ^{xx} $p < 0.01$). In SFD-fed mice, ovx increased *cyp2e1* expression in both WT (^{*} $p < 0.05$) and KO mice (^{**} $p < 0.01$) (Figure 3C). Sirt3 depletion reverted upregulated *cyp2e1* expression in ovx mice (^a $p < 0.05$). Changes in *cyp2e1* expression between SFD and HFD-fed mice were observed in sham KO (^{xx} $p < 0.01$) and ovx KO group (^x $p < 0.05$), whereas HFD increased or decreased *cyp2e1* in these groups, respectively. *Ho-1* gene expression level remained unchanged in SFD conditions (Figure 3D). Following HFD, in WT mice ovx increased *ho-1* gene expression level compared to WT sham mice (^{*} $p < 0.05$), but Sirt3 depletion reverted it (^a $p < 0.05$). These data indicate that ovx induces *pparα*, *cyp2e1*, and *ho-1* genes in WT mice, and Sirt3 depletion mostly reverses this effect.

On the other hand, *cyp4a14* is induced by HFD, and additionally by the combination of ovx and Sirt3 depletion.

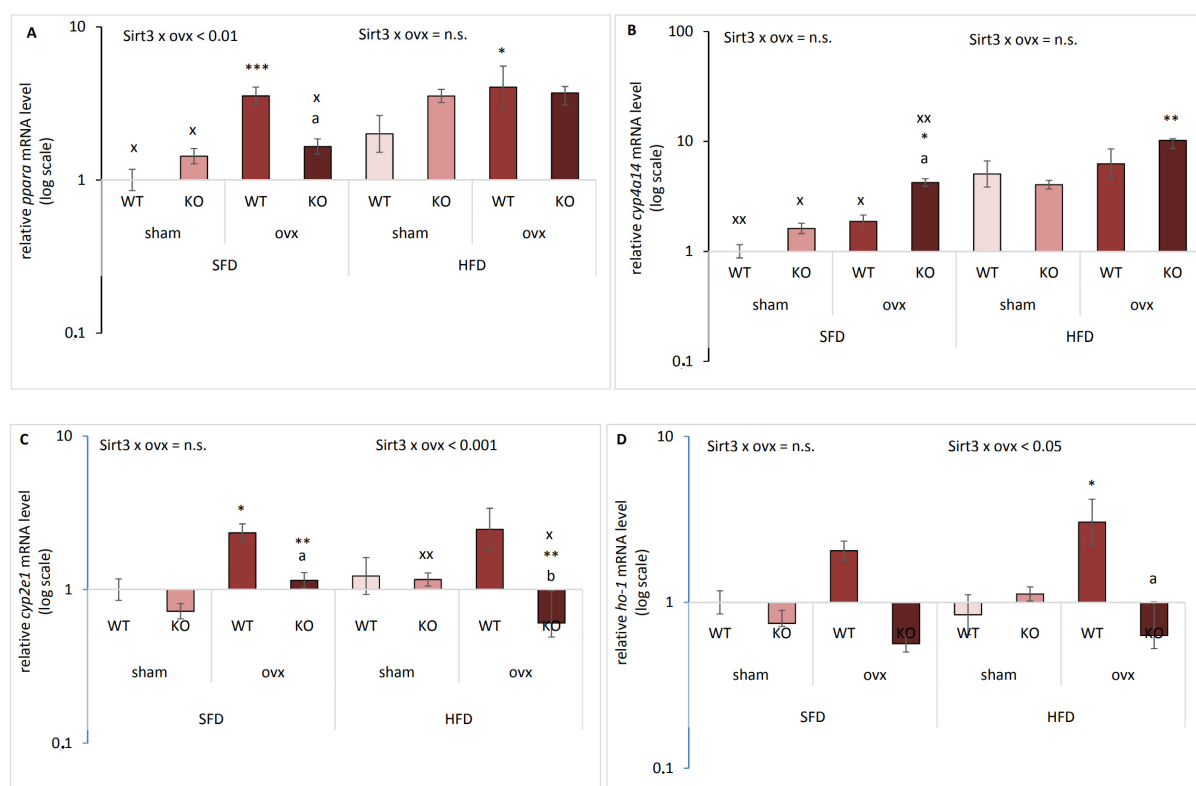


Figure 3. Sirt3 and ovx have a combined effect on the expression of genes involved in lipid metabolism and oxidative stress. Graphical displays of gene expression levels in sham and ovx Sirt3 WT and KO mice after 10 weeks of feeding with SFD or HFD. (A) *ppara*. SFD: ovx WT vs. KO (^a $p < 0.01$); WT sham vs. ovx (^{***} $p < 0.001$). HFD: WT sham vs. ovx (^{*} $p < 0.05$). SFD vs. HFD: sham (^x $p < 0.05$), ovx KO (^x $p < 0.05$). (B) *cyp4a14*. SFD: ovx WT vs. KO (^a $p < 0.05$). HFD: KO sham vs. ovx (^{**} $p < 0.01$). SFD vs. HFD: sham WT (^{xx} $p < 0.01$); sham KO, ovx WT (^x $p < 0.05$); ovx KO (^{xx} $p < 0.01$). (C) *cyp2e1*. SFD: ovx WT vs. KO (^a $p < 0.01$); WT sham vs. ovx (^{*} $p < 0.05$); KO sham vs. ovx (^{**} $p < 0.01$). HFD: ovx WT vs. KO (^b $p < 0.01$); KO sham vs. ovx (^{**} $p < 0.01$). SFD vs. HFD: sham KO (^{xx} $p < 0.01$); ovx KO (^x $p < 0.05$). (D) *ho-1*. SFD: no changes. HFD: WT sham vs. ovx (^{*} $p < 0.05$); ovx WT vs. KO (^a $p < 0.05$). SFD vs. HFD: no changes. β -actin was used for normalization. Data are shown as mean \pm SD. $n = 3$ mice per group in technical triplicates.

2.4. Sirt3 KO Ovz Mice Have Reduced Lipid Accumulation in SFD Conditions

To determine whether the increase in expression of genes involved in lipid metabolism was associated with hepatic lipid accumulation with respect to Sirt3 and ovx in SFD and HFD conditions, we measured lipid content using Folch extraction and performed the immunohistochemical (IHC) analysis of hepatic tissue using oil red staining. In SFD conditions, ovx reduced lipid content in Sirt3-depleted mice (^{**} $p < 0.01$) (Figure 4A). Expectedly, HFD-fed mice had more lipid content than SFD-fed (^{xxx} $p < 0.001$), while ovx decreased lipid content in HFD conditions, irrespective of Sirt3 (^{*} $p < 0.05$). IHC analysis showed interaction between Sirt3 and ovx in SFD-fed conditions: sham KO mice accumulated more lipids than WT (^a $p < 0.01$), and ovx WT mice accumulated more lipids than sham (^{*} $p < 0.05$). Similar to Folch, oil red staining showed that SFD-fed mice depleted of both Sirt3 and ovary hormones accumulated less lipids compared to either ovx WT (^b $p < 0.001$) or sham KO mice (^{***} $p < 0.001$) (Figure 4B,C). In HFD conditions, all groups had higher lipid accumulation compared to their SFD-fed littermates (^{xxx} $p < 0.001$).

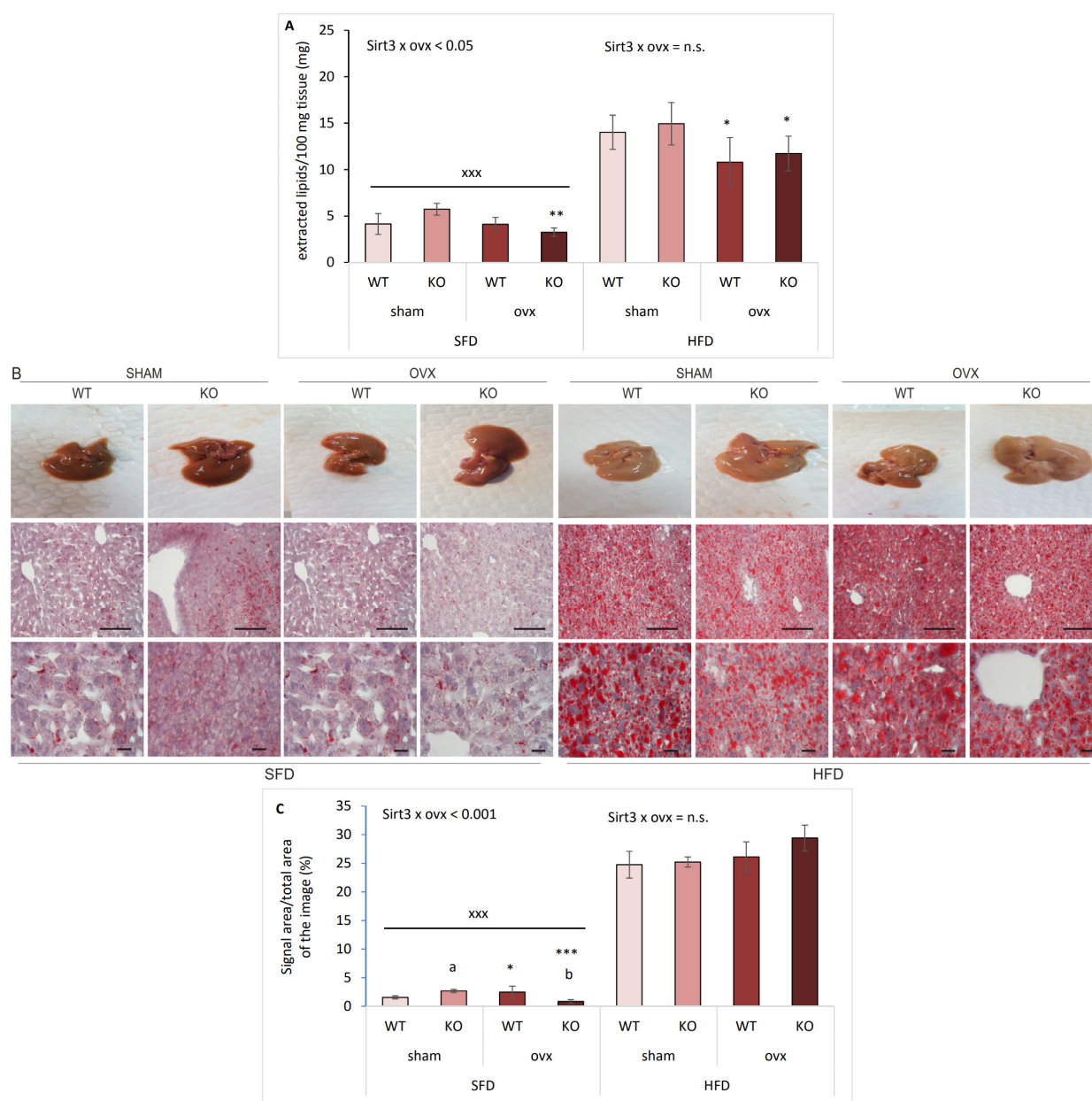


Figure 4. Sirt3 KO ovx mice have reduced lipid accumulation in SFD conditions. **(A)** Graphical display of hepatic total lipid content in sham and ovx Sirt3 WT and KO mice. SFD: KO ovx vs. sham ($** p < 0.01$). HFD: sham vs. ovx ($* p < 0.05$). HFD vs. SFD: $^{xxx} p < 0.001$. **(B)** Representative macroscopic photographs of liver (upper panel) and histological analysis of liver sections with oil red staining (middle and lower panel). Scale bars: 100 μ m (middle panel) and 20 μ m (bottom panel). **(C)** Quantification of oil red signal in IHC samples using Image J. SFD: sham KO vs. WT ($^a p < 0.05$); WT sham vs. ovx ($* p < 0.05$); KO sham vs. ovx ($^{***} p < 0.001$); ovx WT vs. KO ($^b p < 0.001$). HFD: no change. SFD vs. HFD: $^{xxx} p < 0.001$. Data are shown as mean \pm SD. $n = 4$ mice per group.

2.5. Sirt3 KO OvX Mice Have Reduced Scd-1 Ratio and Less MUFA in SFD Conditions

To determine global changes in FAs composition, we determined total hepatic saturated FAs (SFA), monounsaturated FAs (MUFA), and polyunsaturated FAs (PUFA) by gas chromatography (GC). SFD-fed mice had a higher proportion of SFA compared to HFD-fed mice only in KO groups, irrespective of ovx ($^{xx} p < 0.01$) (Figure 5A). Proportions of MUFA were lowest in SFD-fed ovx KO mice, compared to both sham KO ($** p < 0.01$) and WT ovx mice ($^a p < 0.01$) (Figure 5B). HFD-fed mice had significantly higher proportions of MUFAs than SFD-fed mice ($^{xxx} p < 0.001$). The highest proportions of PUFAs were detected

in SFD-fed ovx KO mice, compared to both sham KO ($** p < 0.01$) and WT ovx mice ($^a p < 0.01$) (Figure 5C). HFD-fed mice had lower PUFAs than SFD-fed mice ($^{xxx} p < 0.001$). These results indicate that in SFD-fed mice the depletion of Sirt3 and ovary hormones was associated with more hepatic PUFA than MUFA content and that HFD markedly shifted the dominant FAs in the liver from PUFAs to MUFAs following ten weeks of HFD feeding.

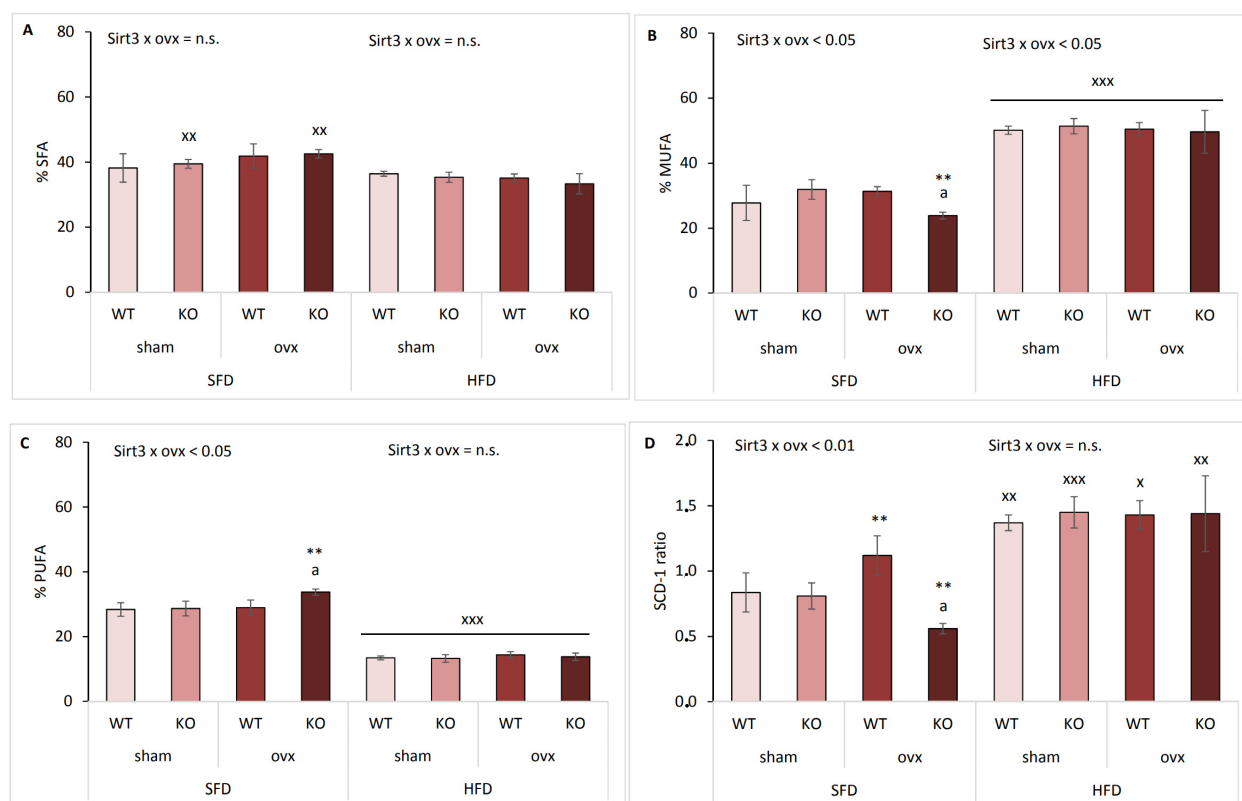


Figure 5. Sirt3 KO ovx mice have reduced Scd-1 ratio and MUFA in SFD conditions. Graphical display of hepatic fatty acid profile in sham and ovx Sirt3 WT and KO mice after 10 weeks of feeding with SFD or HFD. (A) % SFA. SFD: no changes. HFD: no changes. SFD vs. HFD: KO sham and ovx ($^{xx} p < 0.01$). (B) % MUFA. SFD: ovx WT vs. KO ($^a p < 0.01$); KO ovx vs. sham ($^{**} p < 0.01$). HFD: no changes. SFD vs. HFD: $^{xxx} p < 0.001$. (C) % PUFA. SFD: ovx WT vs. KO ($^a p < 0.01$); KO ovx vs. sham ($^{**} p < 0.01$). HFD: no changes. SFD vs. HFD: $^{xxx} p < 0.001$. (D) Scd-1 ratio. SFD: ovx WT vs. KO ($^a p < 0.01$); ovx vs. sham ($^{**} p < 0.01$). HFD: no changes. SFD vs. HFD: KO sham ($^{xxx} p < 0.001$); WT sham and KO ovx ($^{xx} p < 0.01$); WT ovx ($^x p < 0.05$). Data are shown as mean \pm SD. $n = 4$ mice per group.

The most abundant SFAs were palmitate (C16:0), followed by stearate (C18:0) (Supplemental Figure S2A,B). SFD-fed ovx KO mice displayed accumulation of stearate compared to WT ovx mice ($^a p < 0.001$). Moreover, stearate was increased in all groups of SFD-fed mice compared to HFD-fed mice ($^{xxx} p < 0.001$) but did not influence the total SFA content in WT SFD mice compared to HFD, as observed in Figure 5A. Since mice depleted of both ovary hormones and Sirt3 on SFD had lower MUFA and higher PUFA levels, we wanted to explore which FAs contributed to the increase in PUFA to MUFA ratio. The main FAs in MUFA were palmitoleic, oleic, and vaccenic acid (Supplemental Figure S3A–C). Oleic acid, which is the main product of Scd-1 reaction and associates Scd-1 with the development of obesity and the metabolic syndrome [20], was significantly decreased in SFD-fed ovx KO mice ($^* p < 0.05$), making all three main MUFAs reduced upon Sirt3 and ovary hormone deficiency. Furthermore, oleic acid levels were higher in all HFD-fed groups compared to SFD-fed groups ($^{xxx} p < 0.001$) which suggests that oleic acid is responsible for higher MUFA proportions after HFD feeding. The most abundant PUFA were linoleic acid (LNA), followed by arachidonic (AA) and docosahexaenoic acid (DHA)

(Supplemental Figure S4A–C). Generally, lower total PUFAs in HFD-fed mice are the result of reduced levels of LNA, AA, and DHA.

Stearoyl-CoA desaturase-1 (Scd-1) plays the important role in lipogenesis and is expressed in metabolically active tissues, such as liver and adipose tissue [21]. Desaturation index (DI), the ratio of product to precursor FAs, is an indirect marker for tissue Scd-1 activity, which is decreased in conditions of inhibited Scd-1 activity [4]. In our study, DI was determined for palmitoleic/palmitic acid. In SFD conditions, Sirt3 depletion significantly attenuated (^a $p < 0.001$) ovx-mediated increase in Scd-1 ratio (^{**} $p < 0.01$) (Figure 5D). HFD-fed mice displayed a similar Scd-1 ratio across all groups, which was significantly higher than SFD-fed groups (^x $p < 0.05$, ^{xx} $p < 0.01$, ^{xxx} $p < 0.001$). Higher Scd-1 ratio in HFD-fed mice that indicates higher Scd-1 activity may be due to higher MUFA content in HFD rather than direct product of Scd-1 activity.

2.6. Combination of Ovx and Sirt3 Depletion Increases Lipid Damage in SFD Conditions

Since ovx induces oxidative stress and Sirt3 ameliorates oxidative damage, we also determined by lipid hydroperoxide (LOOH) analysis the effect of ovx and Sirt3 depletion on oxidative damage to lipids with respect to type of diet. In SFD-fed sham mice no changes were observed in LOOH level, whereas upon ovx, KO mice displayed higher LOOH than WT mice (^a $p < 0.01$) indicating that combination of ovx and Sirt3 depletion resulted in increased lipid damage (Figure 6). Also, SFD-fed ovx WT mice had lower LOOH than sham WT (^{*} $p < 0.05$). Within the HFD group, sham KO mice displayed lower LOOH than WT mice (^b $p < 0.01$). OvX significantly reduced LOOH levels in WT mice (^{**} $p < 0.01$), without the effect of Sirt3. SFD-fed KO mice had significantly higher lipid damage than HFD-fed KO mice, irrespective of ovx (^x $p < 0.05$, ^{xx} $p < 0.01$). Together, these data confirm that both Sirt3- and ovary hormone-depletion are associated with increased lipid damage only in SFD conditions.

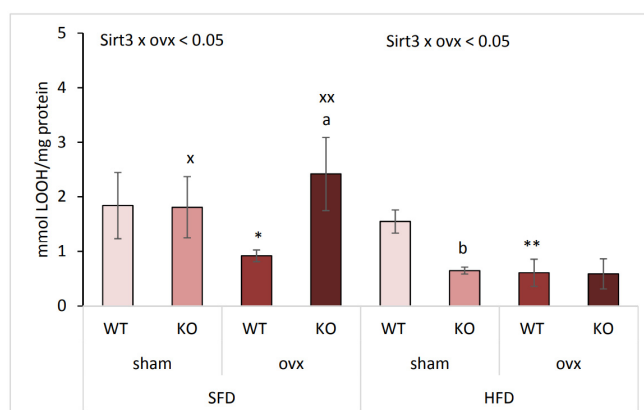


Figure 6. The combination of ovx and Sirt3 depletion increases lipid damage in SFD conditions. Graphical display of lipid hydroperoxide levels (LOOH) in sham and ovx Sirt3 WT and KO mice after 10 weeks of feeding with SFD or HFD. SFD: ovx WT vs. KO (^a $p < 0.05$); WT sham vs. ovx (^{*} $p < 0.05$). HFD: sham KO vs. WT (^b $p < 0.01$); WT sham vs. ovx (^{**} $p < 0.01$). SFD vs. HFD: KO sham (^x $p < 0.05$), KO ovx (^{xx} $p < 0.01$). Data are shown as mean \pm SD. $n = 4$ mice per group.

2.7. Ovariectomized Females Maintain Mitochondrial CII-Driven Respiration in HFD Conditions

To determine if mitochondrial function was affected by ovx and/or Sirt3 depletion, we measured CI-driven (malate + glutamate, ADP added) and CII-driven (succinate + rotenone, ADP added) active mitochondrial respiration by Clark-type electrode. In SFD conditions, KO mice exhibited lower CI-driven respiration than WT mice irrespective of ovx (^a $p < 0.01$) (Figure 7A). A similar effect was observed in HFD-fed mice (^b $p < 0.001$), indicating the importance of Sirt3 in active mitochondrial respiration. CII-driven respiration showed a similar trend as CI considering Sirt3 in SFD conditions, with KO mice having lower

respiration than WT mice in both sham ($^a p < 0.05$) and to a greater extent in ovx group ($^b p < 0.001$) (Figure 7B). Following HFD, KO mice also showed lower CII-driven respiration than WT mice ($^c p < 0.001$). HFD generally decreased CII-driven respiration in both sham WT ($^{xx} p < 0.01$) and KO mice ($^{xxx} p < 0.001$) compared to their SFD-fed littermates. Surprisingly, CII-driven respiration was maintained in HFD-fed ovx mice, being higher than in HFD-fed sham mice ($^{***} p < 0.001$). These data indicate that mitochondrial CI-driven respiration depends only on Sirt3. Mitochondrial CII-driven respiration is also dependent on Sirt3, but is also diet and ovary hormone-dependent, with nutritional stress repressing CII-driven respiration only in sham mice.

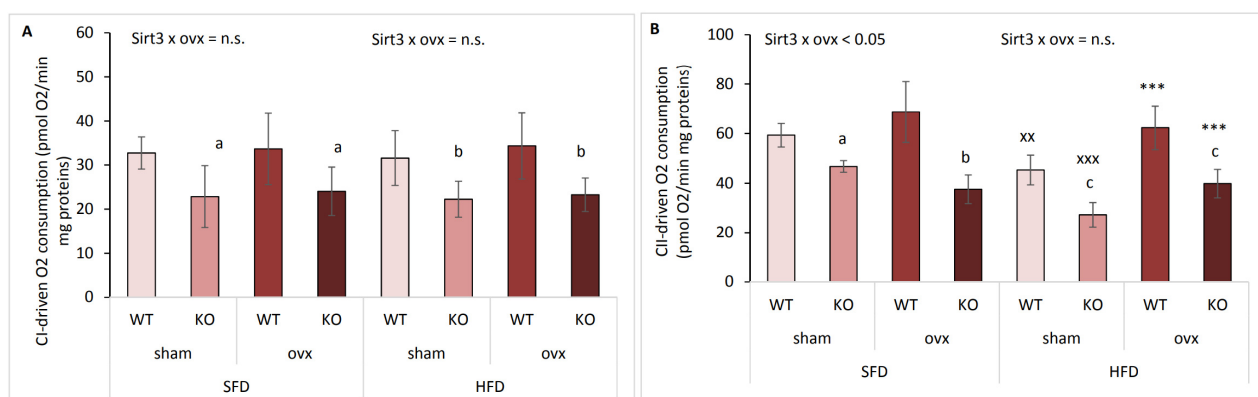


Figure 7. Ovariectomized females maintain mitochondrial CII-driven respiration in HFD conditions. Graphical displays of CI- and CII-driven mitochondrial respiration in sham and ovx Sirt3 WT and KO mice after 10 weeks of feeding with SFD or HFD. **(A)** CI-driven respiration. SFD: WT vs. KO ($^a p < 0.01$). HFD: WT vs. KO ($^b p < 0.001$). SFD vs. HFD: no changes. **(B)** CII-driven respiration. SFD: sham WT vs. KO ($^a p < 0.01$); ovx WT vs. KO ($^b p < 0.001$). HFD: WT vs. KO ($^c p < 0.001$); ovx vs. sham ($^{***} p < 0.001$). SFD vs. HFD: WT sham ($^{xx} p < 0.01$); KO sham ($^{xxx} p < 0.001$). Data are shown as mean \pm SD. $n = 4$ –6 mice per group.

2.8. Antioxidative Enzyme Activities Are Affected by OvX and Type of Diet

Since we previously found that the antioxidative enzyme system was affected in a sex-related manner with respect to the type of diet [13], we analyzed the activities of major antioxidant enzymes: catalase (Cat), manganese superoxide dismutase (MnSod), and copper-zinc superoxide dismutase (CuZnSod). Expectedly, Cat activity was unchanged within SFD-fed mice (Figure 8A). Within HFD, ovx mice had lower Cat activity than sham mice irrespective of Sirt3 ($^* p < 0.05$), but it was still significantly increased compared to SFD-fed groups, indicating increased activity of Cat following HFD in all groups ($^x p < 0.05$, $^{xx} p < 0.01$). Interestingly, in the case of MnSod activity, hormone depletion increased it in SFD conditions ($^{**} p < 0.01$) regardless of Sirt3 (Figure 8B). HFD-fed mice had no change in MnSod activity between groups, and only WT sham mice had increased activity compared to their SFD-fed littermates ($^{xx} p < 0.01$). Similar to Cat activity, CuZnSod activity remained unchanged within SFD-fed mice, but also decreased in ovx mice compared to sham mice ($^{**} p < 0.01$) following HFD (Figure 8C). This indicates that hormone depletion decreases both Cat and CuZnSod activity in HFD-fed mice. Overall, the activities of antioxidant enzymes were not affected by Sirt3, only by ovx and type of diet.

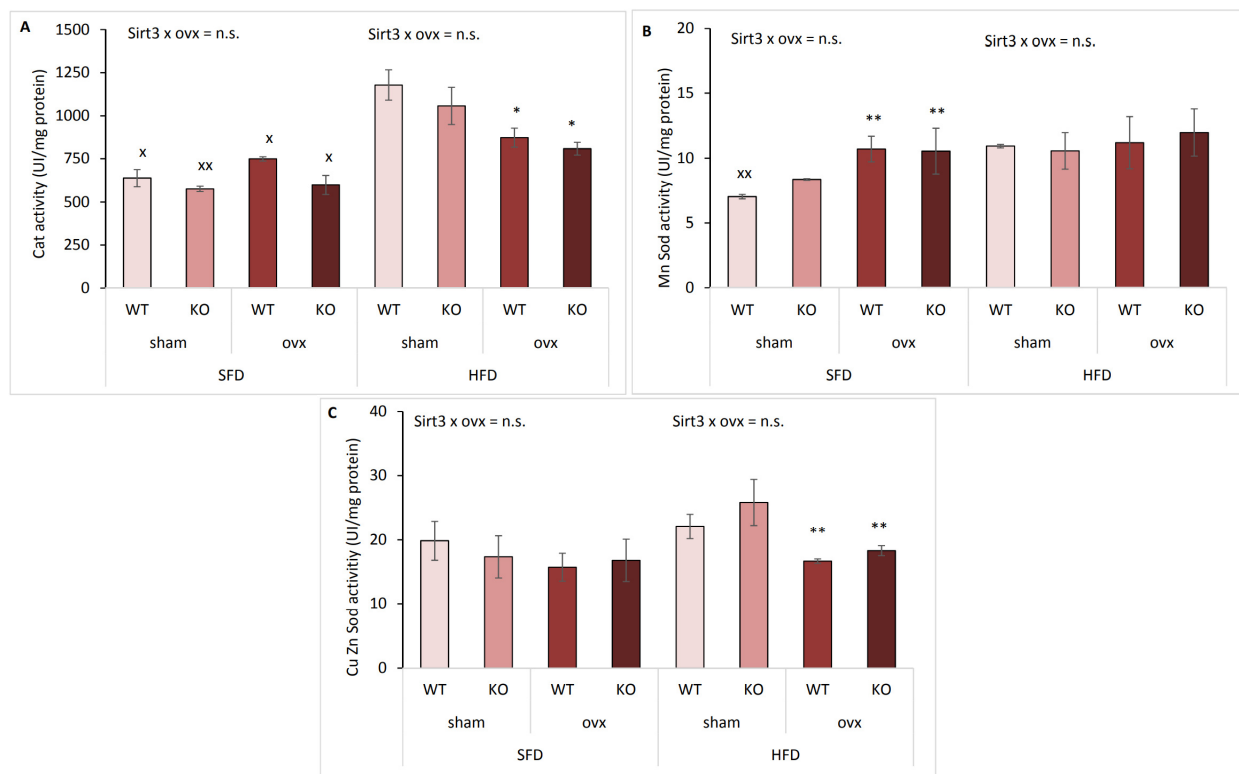


Figure 8. Antioxidative enzyme activities are affected by ovx and type of diet. Graphical display of antioxidant enzyme activities in sham and ovx Sirt3 WT and KO mice after 10 weeks of feeding with SFD or HFD. **(A)** Catalase activity. SFD: no changes. HFD: ovx vs. sham (* $p < 0.05$). SFD vs. HFD: WT sham, ovx WT and KO (x $p < 0.05$), KO sham (xx $p < 0.01$). **(B)** MnSod activity. SFD: ovx vs. sham (** $p < 0.01$). HFD: no changes. SFD vs. HFD: WT sham (xx $p < 0.01$). **(C)** CuZnSod activity. SFD: no changes. HFD: ovx vs. sham (** $p < 0.01$). SFD vs. HFD: no changes. Data are shown as mean \pm SD. $n = 4$ mice per group.

3. Discussion

Obesity and metabolic syndrome represent major health problems worldwide [22], development of which is associated with metabolic and hormonal changes occurring during the lifespan in both sexes. Since diet can additionally favor the disease progression, understanding these disorders and their causes in both sexes has one of the highest priorities. Although many studies showed that females have better protection against HFD-induced metabolic stress than males [23–26], the combined effect of main mitochondrial deacetylase Sirt3 and ovary hormones in regulating metabolic stress in vivo has not yet been investigated. To test our hypothesis that females' protection from HFD was attributed to the synergistic effect of female sex hormones and Sirt3, we investigated the effects of Sirt3 depletion and ovarian hormone deficiency (ovx) on metabolic parameters, mitochondrial function, antioxidant system, and lipid profile in the liver of SFD- and HFD-fed female 129S mice.

Our results indicate that in SFD-fed Sirt3 WT mice, ovx resulted in a following compensatory response to stress: increased *pgc1- α* and its downstream target Sirt3, accompanied with maintained mitochondrial function, increased FAs synthesis (higher Scd-1 activity [27]), and MnSod activity coupled with lower levels of LOOH. OvX also induced *ppara* expression, known for upregulation of hepatic lipid metabolism proteins [28]. Although it has been reported that Sirt3 downregulates Scd-1 in male mice [29], here the ovx in females caused upregulation of Sirt3 and increased Scd-1. However, ovary hormone and Sirt3 depletion caused downregulation of Scd-1, indicating that Sirt3 participates in the regulation of Scd-1 in the absence of ovary hormones. It could be possible that Sirt3 increases Scd-1 by deacetylation and inhibition of its negative regulator STAT3 [21], however, this needs

to be confirmed in future studies. We suggest that, although in SFD conditions ovx mice have increased FA synthesis, the upregulation of Sirt3 compensates for the loss of ovary hormones by maintaining mitochondrial metabolism and preventing oxidative damage. Consistent with previous reports indicating that increased Sirt3 expression is in association with decreased oxidative stress [30,31], these results show that in SFD conditions Sirt3 protects from mitochondrial dysfunction and oxidative damage in ovx females.

Previous studies showed that the genetic background of mice strain plays a significant role in the progression of disease under the same conditions of HFD. Although 129S mice develop features of metabolic syndrome with lower severity compared to some other strains [32–36], 129S Sirt3 KO mice are extremely useful in studying the role of FA oxidation in diabetes, steatosis, and life span [4,37]. However, the conducted metabolism-associated studies involved male mice only. Although our strain of mice develops obesity with lower severity, weight gain was significantly affected in KO ovx mice: these females were most resistant towards gaining weight on SFD but most sensitive upon HFD. Decreased body weight gain in SFD conditions was associated with reduced *pparα* expression, lower Scd-1 activity, and lowest hepatic lipid content. The inhibition of Scd-1 is found to shift FA metabolism towards increased FA oxidation pathway [38], which participates in alleviation of obesity by burning off excessive accumulated lipids [39]. Thus, this may explain their resistance towards gaining weight under SFD conditions. Other parameters that indicate reduced Scd-1 activity are lowered content of oleic in favor of stearic acid, and elevated PUFAs, known as powerful inhibitors of Scd-1 gene expression, specifically AA and DHA (reviewed in [21]). Also, ovx KO females have more compromised CII-driven mitochondrial respiration associated with the highest lipid oxidative damage. In conclusion, we propose that combined loss of both Sirt3 and ovary hormones in SFD conditions results in the lowest body weight gain as a consequence of reduced *pparα* expression and Scd-1 activity, compromised CII-driven respiration, and higher lipid oxidative damage, thus pointing towards unquestionable protective effect of combined Sirt3 and ovary hormones in maintaining metabolic and oxidative homeostasis in female mice.

HFD-fed ovx mice usually exhibit an obese phenotype with decreased energy expenditure, referring to the importance of the estrogen signaling pathway in the maintenance of energy homeostasis [40]. However, the role of Sirt3 in these processes is not clear. In agreement with previous data regarding the protective role of Sirt3 and ovary hormones in obesity [11,41], HFD-fed ovx KO females displayed the highest body weight gain, but interestingly, lower lipid accumulation than sham mice. This is consistent with our previous study if we compare ovx KO females to male KO mice, which also showed to have the lowest lipid accumulation on HFD, indicating their increased reliance on FAs which probably compensated for their impaired glucose uptake [13]. At the time, we assumed that the observed sex-related differences in lipid accumulation are present only in Sirt3 KO mice, but now we demonstrate the same effect in both ovx WT and KO females, suggesting the important role of ovary hormones in these processes. In addition, HFD-fed ovx mice maintained their CII-driven respiration, possibly due to increased MUFAs (palmitoleic and vaccenic acids) known for enhancing FA oxidation, i.e., energy consumption by raising mitochondrial respiratory complexes and ATP production [42]. Whilst mitochondria are the primary site of β -oxidation for energy production in the form of ATP, peroxisomal β -oxidation is involved in biosynthesis pathways with the end product acetyl CoA and H_2O_2 [43]. Based on observed lower mitochondrial CII-driven respiration in HFD-fed sham mice, as well as higher Cat, a common peroxisomal ROS scavenging enzyme, we propose that these females depend more on peroxisomal FA oxidation. This indicates that HFD aggravates their metabolic parameters by compromising mitochondrial function and activating ROS-induced upregulation of antioxidant enzymes.

Although ovx females on HFD have lower lipid accumulation, depletion of either ovary hormones or both ovary hormones and Sirt3 changes the expression of *cyp2e1* and *cyp4a14*. Higher expression of either of these genes indicates that these mice are prone to NAFLD since it is known that both of them induce hepatosteatosis, with an increase in

ROS and oxidative stress [18,44]. In addition, the expression level of the *ho-1* gene, which has been reported to attenuate oxidative stress and prevent nonalcoholic steatohepatitis (NASH) [45], is upregulated in WT and decreased in KO ovx mice. Thus, in ovx females, Sirt3 may protect from NASH by upregulation of *ho-1*, while in the absence of Sirt3 the expression of *ho-1* is abolished, making these mice more susceptible to the development of NASH caused by HFD. From the two analyzed *cyp* genes, *cyp4a14* showed to be more involved in the induction of NAFLD [46] and *cyp2e1* in alcoholic hepatitis [47]. This may be the reason that *cyp4a14* has higher expression in all HFD groups, and highest in KO ovx groups in either SFD or HFD conditions. Overall, the expression of these genes indicates that, despite lower lipid accumulation in ovx females which may be due to differential dependence on peroxisomal and mitochondrial β -oxidation of FA, mice lacking ovary hormones and especially in combination with Sirt3 depletion are more prone to NAFLD.

The limitation of the study is that parameters such as Scd-1 which are derived from the ratio of particular FAs may not be fully reliable indicators of Scd-1 activity in HFD conditions because their levels highly depend on fat composition in the diet. Several authors stated that lipogenesis was reduced in mouse models of HFD feeding (reviewed in [48]). In addition, in this study, we included only young adult females, and ovx might not have such adverse effects as it would have in older females. Further studies in senescent mice are needed to compare parameters involved in lipid metabolism, mitochondrial function, and antioxidant system, which we plan to conduct in near future.

Despite these limitations, this research adds to our previous studies and confirms our hypothesis that protection against harmful effects of HFD in female mice is attributed to the combined effect of female sex hormones and Sirt3. With this, we add to the knowledge on the prevention of metabolic dysfunction, thus contributing to preclinical research and supporting future studies for the development of sex-related therapeutic agents for metabolic syndrome and associated diseases.

4. Materials and Methods

4.1. Animal Model and Experimental Design

129S1/SvImJ WT (Stock No: 002448) and Sirt3 KO (Stock No: 012755, Jackson Laboratory, Bar Harbor, ME, USA) female mice were housed in standard conditions (three females per cage, 22 °C, 50–70% humidity, 12 h light / 12 h darkness cycle). Ovariectomy (ovx) and sham surgery were performed at 7 weeks of age under ketamine/xylazine anesthesia (Ketamidol 10%, Richter pharma Ag, Wels, Austria; Xylazine 2%, Alfasan International, Woerden, Netherlands). Since low levels of E2 are normally detected in ovariectomized females due to other endogenous E2 sources (reviewed in [49]), plasma E2 levels were not used as an indicator of the efficiency of ovx. Instead, the success of ovx was checked by analyzing vaginal smear during five consecutive days after the surgery [50]. After recovery, mice were placed on either a standard fat diet (SFD, 11.4% fat, 62.8% carbohydrates, 25.8% proteins; Mucedola, Settimo Milanese, Italy) or a high fat diet (HFD, 58% fat, 24% carbohydrates, 18% proteins; Mucedola, Settimo Milanese, Italy) for 10 weeks. Body weight was measured once a week, as well as glucose level (glucometer StatStrip Xpress-I, Nova Biomedical, GmbH, Mörfelden-Walldorf, Germany) after 6 h of fasting, in a blood drop from the tail vein. After 10 weeks of feeding, mice were sacrificed and liver was used either fresh or was stored in liquid nitrogen or at -80°C , depending on the analysis. Animal experiments were done within the project funded by the Croatian Science Foundation, project ID: IP-014-09-4533, approved on 01/09/2015. All procedures were approved by the Ministry of Agriculture of Croatia (No: UP/I-322-01/15-01/25 525-10/0255-15-2 from 20th July 2015) and carried out following the EU Directive 2010/63/EU-associated guidelines.

4.2. Histology and Oil Red O Staining

A histological analysis of samples taken from the right liver lobe for all experimental groups was performed as described previously [13]. Fat vacuoles in hepatocytes of frozen sections were visualized by Oil Red O dye (Sigma Aldrich, St. Louis, MO, USA) according to

the previous protocol [13], with the following modifications: Oil Red O dye was prepared in isopropanol (0.5% Oil Red O solution), the sections (8 μm) of tissues embedded in Optimal Cutting Temperature medium (O.C.T 4583, Sakura Finetek, Torrance, CA, USA) were air-dried for 1 h and the tissue was fixed in ice-cold 10% formalin for 5 min, washed with dH_2O , and conditioned for staining by brief dipping of slides in 60% isopropanol. The tissue sections were stained with Oil Red O dye in the dark, at room temperature for 15 min, and then washed by rinsing in 60% isopropanol, and incubated for 5 min in dH_2O , followed by staining with Mayer's hematoxylin (Dako, Histological staining reagent S3309, Santa Clara, CA, USA) for 1 min and washing with tap water and dH_2O , and were finally mounted in aqueous mounting medium (Dako Faramount Aqueous Mounting Medium S3025, Agilent Technologies, Santa Clara, CA, USA). An analysis of the stained liver sections was done using an Olympus BX51 microscope (Tokyo, Japan) with associated software analysis.

4.3. Total Lipid Extraction and GC Lipid Analysis

Liver samples were snap-frozen and stored at $-80\text{ }^\circ\text{C}$ until analysis. Total lipids were extracted from liver tissue according to a modified Folch procedure as described previously [13,51]. The lipid extract was treated with 0.5 M KOH/MeOH for 20 min at room temperature, and the corresponding FA methyl esters (FAMES) were formed and analyzed by gas chromatography (GC). GC analyses of total FAs were performed by Varian 450-GC equipped with a flame ionization detector (Varian Medical Systems, Houten, Netherlands). A Stabilwax column (crossbond carbowax polyethylene glycol, 60 m \times 0.25 mm) was used as a stationary phase at a programmed temperature with helium as the carrier gas. The heating was carried out at a temperature of $150\text{ }^\circ\text{C}$ for 1 min followed by an increase of $1\text{ }^\circ\text{C}/\text{min}$ up to $250\text{ }^\circ\text{C}$. Methyl esters were identified by comparison with the retention times of commercially available standard mixtures (Marine oil FAME mix, Restek Corporation, Bellefonte, PA, USA).

4.4. Lipid Hydroperoxide Analysis

Liver samples were snap-frozen and stored at $-80\text{ }^\circ\text{C}$ until analysis. Lipids were extracted according to the modified method previously described [52]. Briefly, 0.1 g of liver tissue was cut and homogenized in PBS. Lipid extraction started by adding 2.5 mL of CHCl_3 to the homogenate, followed by vigorous shaking. The solution was washed with 0.75 mL of 0.034% MgCl_2 and centrifuged (2 min, $3000\times g$) and the aqueous layer was drawn off by aspiration using a Pasteur pipette. The washing procedure was repeated with 1.25 mL of 2 M KCl/MeOH (4:1, v/v) to eliminate all proteins and non-lipid contaminants. CHCl_3 layer was finally washed with $\text{CHCl}_3/\text{MeOH}$ (2:1, v/v) and centrifuged (5 min, $3000\times g$). The organic layer containing lipids was carefully transferred to a glass tube and solvent was removed on a rotary evaporator. After weighing, the lipids were stored at $-20\text{ }^\circ\text{C}$ until the analysis of lipid hydroperoxides (LOOH). Spectrophotometric ferric thiocyanate assay was used for the determination of LOOH concentration. The analyzed samples were prepared by diluting with a deaerated mixture of $\text{CH}_2\text{Cl}_2/\text{MeOH}$ (2:1, v/v). The concentrations of LOOH were calculated by using the molar absorptivity of the complex $[\text{FeNCS}]^{2+}$ formed per mol of LOOH, $58\,440\text{ dm}^3\text{ mol}^{-1}\text{ cm}^{-1}$, at 500 nm [53].

4.5. RNA Isolation and Quantitative Real-Time PCR Analysis

Liver samples were snap-frozen and stored in liquid nitrogen until analysis. Total RNA from liver samples was isolated using TRIzol reagent (Invitrogen, Waltham, MA, USA). RNA was treated with DNase (TURBO DNA-free Kit, Thermo Fisher Scientific, Waltham, MA, USA) followed by reverse transcription using a High-Capacity cDNA Reverse Transcription Kit (Thermo Fisher Scientific, Waltham, MA, USA). For real-time PCR analysis, an ABI 7300 sequence detection system (Foster City, CA, USA) was used. To quantify the relative mRNA expression of *cyp2e1*, *cyp4a14*, *ppara*, *pgc1- α* , and *ho-1* (Supplementary Table S1) the comparative CT ($\Delta\Delta\text{CT}$) method according to the Taqman[®] Gene

Expression Assays Protocol (Applied Biosystems, Foster City, CA, USA) was used. The data on the graphs are shown as the fold-change in gene expression, which is normalized to the endogenous reference gene (β -actin) and relative to SFD-fed sham WT females.

4.6. Protein Isolation and Western Blot Analysis

Liver samples were snap-frozen and stored in liquid nitrogen until analysis. Liver proteins were prepared in Ripa buffer (supplemented with cOmplete™, EDTA-free Protease Inhibitor Cocktail tablets (Roche, Basel, Switzerland)) using an ice-jacketed Potter-Elvehjem homogenizer (1300 rpm; Thomas Scientific, Swedesboro, NJ, USA) according to our standard protocol [13]. Proteins (15 μ g/ μ L) were resolved by SDS-PAGE and transferred onto a PVDF membrane (Roche, Basel, Switzerland). Membranes were blocked and incubated with primary antibodies (Supplementary Table S2) overnight at 4°C. For chemiluminescence detection, an appropriate horseradish peroxidase (HRP)-conjugated secondary antibody was used. AmidoBlack (Sigma Aldrich, St. Louis, MO, USA) was used for total protein normalization. The Alliance 4.7 Imaging System (UVITEC, Cambridge, UK) was used for the detection of immunoblots using an enhanced chemiluminescence kit (Thermo Fischer Scientific, Waltham, MA, USA).

4.7. Analysis of Antioxidative Enzyme Activities

Liver samples were snap-frozen and stored in liquid nitrogen until analysis. Antioxidative enzyme activities were analyzed in liver homogenates prepared in PBS supplemented with cOmplete™, EDTA-free Protease Inhibitor Cocktail tablets (Roche, Basel, Switzerland) using an ice-jacketed Potter-Elvehjem homogenizer (1300 rpm; Thomas Scientific, Swedesboro, NJ, USA). Superoxide dismutase (Sod) activities were determined using a Ransod kit (Randox Laboratories, Crumlin, UK) according to the manufacturer's recommendations. The catalase (Cat) activity was done as previously described [54], by measuring the change in absorbance (at 240 nm) in the reaction mixture (10 mM H₂O₂ and 50 mM PBS (pH 7.0)) during the interval of 30 s following sample addition.

4.8. Mitochondria Isolation and Oxygen Consumption

Mice liver mitochondria were isolated from fresh liver by differential centrifugation as described previously [13]. Isolated mitochondria were kept in the isolation buffer (250 mM sucrose, 2 mM EGTA, 0.5% fatty acid-free BSA, 20 mM Tris-HCl, pH 7.4) until the experiment on the Clark-type electrode (Oxygraph, Hansatech Instruments Ltd., Pentney, UK) in an airtight 1.5 mL chamber at 35°C. Mitochondria (800 μ g protein) were resuspended in a 500 μ L respiration buffer (200 mM sucrose, 20 mM Tris-HCl, 50 mM KCl, 1 mM MgCl₂·6H₂O, 5 mM KH₂PO₄, pH 7.0) for the determination of oxygen consumption. Complex I assessment samples were incubated with 2.5 mM glutamate and 1.25 mM malate. Complex II assessment samples were incubated with 2 μ M rotenone and 10 mM succinate. Mitochondrial respiration was accelerated by the addition of ADP (2 mM final concentration) for state 3 respiration measurements. Then, ATP synthesis was terminated by adding oligomycin (6.25 nM final concentration) to achieve state 4 rate. To inhibit mitochondrial respiration, 2 μ M antimycin A was used. Oxygen consumption is calculated in nmol/min/mg protein.

4.9. Statistical Analysis

For the statistical analysis of data, SPSS for Windows (v.17.0, IBM, Armonk, NY, USA) was used. A Shapiro–Wilk test was used before all analyses to test the samples for normality of distribution. Since all data followed a normal distribution, parametric tests for multiple comparisons were performed: an unpaired Student's t-test for comparisons between SFD and HFD, and a two-way ANOVA for the interaction effect of Sirt3 and ovx within each diet. If a significant interaction was observed, all pairwise comparisons were made between groups, using Tukey's post-hoc test with Bonferroni's correction. Significance was set at $p < 0.05$. On graphical displays, the indicator of the differences between SFD and HFD

was marked as x; the indicator of differences between WT and KO (the effect of Sirt3) was marked as a letter (a, b, etc.); the indicator of differences between sham and ovx (the effect of ovx) was marked as *.

Supplementary Materials: The following are available online at <https://www.mdpi.com/article/10.3390/ijms22084277/s1>, Figure S1: Observations of uterus deterioration and vaginal smears of control (sham) and ovariectomized (ovx) mice. Figure S2: Graphical display of hepatic SFA content in sham and ovx Sirt3 WT and KO mice after 10 weeks of feeding with SFD or HFD. Figure S3: Graphical display of hepatic MUFA content in sham and ovx Sirt3 WT and KO mice after 10 weeks of feeding with SFD or HFD. Figure S4: Graphical display of hepatic PUFA content in sham and ovx Sirt3 WT and KO mice after 10 weeks of feeding with SFD or HFD. Table S1: Assays (Taqman[®] Applied Biosystems, UK) used for the real time quantitative PCR. Table S2: Antibodies used in this study for the Western blot analyses.

Author Contributions: Conceptualization, M.P., I.I.P., and S.S.; data curation, M.P., I.I.P., M.P.H., and S.S.; formal analysis, I.I.P., I.T.B., A.T., and S.S.; funding acquisition, T.B.; investigation, S.S.; Methodology, M.P., I.I.P., M.P.H., I.T.B., A.T., and S.S.; supervision, T.B.; validation, M.P., I.I.P., and S.S.; visualization, M.P.H.; writing—original draft, M.P., I.I.P., and S.S.; writing—review and editing, M.P., I.I.P., M.P.H., I.T.B., A.T., T.B., and S.S. All authors have read and agreed to the published version of the manuscript.

Funding: This research was funded by the Croatian Science Foundation (HRZZ), Grant no. [IP-2014-09-4533] “SuMERA”.

Institutional Review Board Statement: The study was conducted according to the EU Directive 2010/63/EU-associated guidelines, and approved by the Ministry of Agriculture of Croatia (No: UP/I-322-01/15-01/25 525-10/0255-15-2 from 20/07/2015) within the project funded by the Croatian Science Foundation, project ID: IP-014-09-4533, approved on 01/09/2015.

Data Availability Statement: The data presented in this study are available on request from the corresponding author.

Acknowledgments: The authors would like to thank Iva Pešun Međimorec and Marina Marš for their excellent technical contribution. The authors would like to thank Maro Bujak and Mladen Paradžik for their valuable discussions and critical reviews of the manuscript.

Conflicts of Interest: The authors declare no conflict of interest. The funders had no role in the design of the study; in the collection, analyses, or interpretation of data; in the writing of the manuscript, or in the decision to publish the results.

References

1. Bonomini, F.; Rodella, L.F.; Rezzani, R. Metabolic syndrome, aging and involvement of oxidative stress. *Aging Dis.* **2015**, *6*, 109–120. [CrossRef]
2. Rui, L. Energy metabolism in the liver. *Compr. Physiol.* **2014**, *4*, 177–197. [PubMed]
3. Kakimoto, P.A.; Kowaltowski, A.J. Effects of high fat diets on rodent liver bioenergetics and oxidative imbalance. *Redox Biol.* **2016**, *8*, 216–225. [CrossRef]
4. Hirschey, M.D.; Shimazu, T.; Jing, E.; Grueter, C.A.; Collins, A.M.; Aouizerat, B.; Stančáková, A.; Goetzman, E.; Lam, M.M.; Schwer, B.; et al. SIRT3 deficiency and mitochondrial protein hyperacetylation accelerate the development of the metabolic syndrome. *Mol. Cell* **2011**, *44*, 177–190. [CrossRef] [PubMed]
5. Haas, J.T.; Francque, S.; Staels, B. Pathophysiology and mechanisms of nonalcoholic fatty liver disease. *Annu. Rev. Physiol.* **2016**, *78*, 181–205. [CrossRef]
6. Austad, S.N. Why women live longer than men: Sex differences in longevity. *Gend. Med.* **2006**, *3*, 79–92. [CrossRef]
7. Kruger, D.J.; Nesse, R.M. An evolutionary life-history framework for understanding sex differences in human mortality rates. *Hum. Nat.* **2006**, *17*, 74–97. [CrossRef] [PubMed]
8. Mauvais-Jarvis, F.; Bairey Merz, N.; Barnes, P.J.; Brinton, R.D.; Carrero, J.J.; DeMeo, D.L.; De Vries, G.J.; Epperson, C.N.; Govindan, R.; Klein, S.L.; et al. Sex and gender: Modifiers of health, disease, and medicine. *Lancet* **2020**, *396*, 565–582. [CrossRef]
9. Ko, S.H.; Kim, H.S. Menopause-associated lipid metabolic disorders and foods beneficial for postmenopausal women. *Nutrients* **2020**, *12*, 202. [CrossRef]
10. Palmisano, B.T.; Zhu, L.; Stafford, J.M. Role of estrogens in the regulation of liver lipid metabolism. *Adv. Exp. Med. Biol.* **2017**, *1043*, 227–256.

11. Zhang, J.; Xiang, H.; Liu, J.; Chen, Y.; He, R.R.; Liu, B. Mitochondrial Sirtuin 3: New emerging biological function and therapeutic target. *Theranostics* **2020**, *10*, 8315–8342. [\[CrossRef\]](#)
12. Lombard, D.B.; Alt, F.W.; Cheng, H.L.; Bunkenborg, J.; Streeper, R.S.; Mostoslavsky, R.; Kim, J.; Yancopoulos, G.; Valenzuela, D.; Murphy, A.; et al. Mammalian Sir2 homolog SIRT3 regulates global mitochondrial lysine acetylation. *Mol. Cell Biol.* **2007**, *27*, 8807–8814. [\[CrossRef\]](#)
13. Pinteric, M.; Podgorski, I.I.; Hadzija, M.P.; Bujak, I.T.; Dekanic, A.; Bagaric, R.; Farkas, V.; Sobocanec, S.; Balog, T. Role of sirt3 in differential sex-related responses to a high-fat diet in mice. *Antioxidants* **2020**, *9*, 174. [\[CrossRef\]](#) [\[PubMed\]](#)
14. Simpkins, J.W.; Yi, K.D.; Yang, S.H.; Dykens, J.A. Mitochondrial mechanisms of estrogen neuroprotection. *Biochim. Biophys. Acta Gen. Subj.* **2010**, *1800*, 1113–1120. [\[CrossRef\]](#) [\[PubMed\]](#)
15. Gruber, C.J.; Tschugguel, W.; Schneeberger, C.; Huber, J.C. Production and Actions of Estrogens. *N. Engl. J. Med.* **2002**, *346*, 340–352. [\[CrossRef\]](#)
16. Liang, H.; Ward, W.F. PGC-1 α : A key regulator of energy metabolism. *Adv. Physiol. Educ.* **2006**, *30*, 145–151. [\[CrossRef\]](#)
17. Brandt, J.M.; Djouadi, F.; Kelly, D.P. Fatty acids activate transcription of the muscle carnitine palmitoyltransferase I gene in cardiac myocytes via the peroxisome proliferator-activated receptor α . *J. Biol. Chem.* **1998**, *273*, 23786–23792. [\[CrossRef\]](#)
18. Leclercq, I.A.; Farrell, G.C.; Field, J.; Bell, D.R.; Gonzalez, F.J.; Robertson, G.R. CYP2E1 and CYP4A as microsomal catalysts of lipid peroxides in murine nonalcoholic steatohepatitis. *J. Clin. Invest.* **2000**, *105*, 1067–1075. [\[CrossRef\]](#) [\[PubMed\]](#)
19. Chung, H.T.; Ryter, S.W.; Kim, H.P. Heme oxygenase-1 as a novel metabolic player. *Oxid. Med. Cell. Longev.* **2013**, *2013*, 814058. [\[CrossRef\]](#)
20. Jeffcoat, R. Obesity—A perspective based on the biochemical interrelationship of lipids and carbohydrates. *Med. Hypotheses* **2007**, *68*, 1159–1171. [\[CrossRef\]](#)
21. Mauvoisin, D.; Mounier, C. Hormonal and nutritional regulation of SCD1 gene expression. *Biochimie* **2011**, *93*, 78–86. [\[CrossRef\]](#)
22. Saklayen, M.G. The global epidemic of the metabolic syndrome. *Curr. Hypertens. Rep.* **2018**, *20*, 12. [\[CrossRef\]](#) [\[PubMed\]](#)
23. Hwang, L.L.; Wang, C.H.; Li, T.L.; Chang, S.D.; Lin, L.C.; Chen, C.P.; Chen, C.T.; Liang, K.C.; Ho, I.K.; Yang, W.S.; et al. Sex differences in high-fat diet-induced obesity, metabolic alterations and learning, and synaptic plasticity deficits in mice. *Obesity* **2010**, *18*, 463–469. [\[CrossRef\]](#)
24. Dorfman, M.D.; Krull, J.E.; Douglass, J.D.; Fasnacht, R.; Lara-Lince, F.; Meek, T.H.; Shi, X.; Damian, V.; Nguyen, H.T.; Matsen, M.E.; et al. Sex differences in microglial CX3CR1 signalling determine obesity susceptibility in mice. *Nat. Commun.* **2017**, *8*, 14556. [\[CrossRef\]](#) [\[PubMed\]](#)
25. Yang, Y.; Smith, D.L., Jr.; Keating, K.D.; Allison, D.B.; Nagy, T.R. Variations in body weight, food intake and body composition after long-term high-fat diet feeding in C57BL/6J mice. *Obesity* **2014**, *22*, 2147–2155. [\[CrossRef\]](#)
26. Lainez, N.M.; Jonak, C.R.; Nair, M.G.; Ethell, I.M.; Wilson, E.H.; Carson, M.J.; Coss, D. Diet-induced obesity elicits macrophage infiltration and reduction in spine density in the hypothalamus of male but not female mice. *Front. Immunol.* **2018**, *11*, 1992. [\[CrossRef\]](#) [\[PubMed\]](#)
27. Miller, C.W.; Ntambi, J.M. Peroxisome proliferators induce mouse liver stearoyl-CoA desaturase 1 gene expression. *Proc. Natl. Acad. Sci. USA* **1996**, *93*, 9443–9448. [\[CrossRef\]](#)
28. Kersten, S. Integrated physiology and systems biology of PPAR α . *Mol. Metab.* **2014**, *3*, 354–371. [\[CrossRef\]](#)
29. Zhang, T.; Liu, J.; Shen, S.; Tong, Q.; Ma, X.; Lin, L. SIRT3 promotes lipophagy and chaperon-mediated autophagy to protect hepatocytes against lipotoxicity. *Cell Death Differ.* **2020**, *27*, 329–344. [\[CrossRef\]](#)
30. Liu, J.; Li, D.; Zhang, T.; Tong, Q.; Ye, R.D.; Lin, L. SIRT3 protects hepatocytes from oxidative injury by enhancing ROS scavenging and mitochondrial integrity. *Cell Death Dis.* **2017**, *8*, e3158. [\[CrossRef\]](#)
31. Zheng, J.; Shi, L.; Liang, F.; Xu, W.; Li, T.; Gao, L.; Sun, Z.; Yu, J.; Zhang, J. Sirt3 ameliorates oxidative stress and mitochondrial dysfunction after intracerebral hemorrhage in diabetic rats. *Front. Neurosci.* **2018**, *12*, 414. [\[CrossRef\]](#) [\[PubMed\]](#)
32. Biddinger, S.B.; Almind, K.; Miyazaki, M.; Kokkotou, E.; Ntambi, J.M.; Kahn, C.R. Effects of diet and genetic background on sterol regulatory element-binding protein-1c, stearoyl-CoA desaturase 1, and the development of the metabolic syndrome. *Diabetes* **2005**, *54*, 1314–1323. [\[CrossRef\]](#) [\[PubMed\]](#)
33. Almind, K.; Kahn, C.R. Genetic determinants of energy expenditure and insulin resistance in diet-induced obesity in mice. *Diabetes* **2004**, *53*, 3274–3285. [\[CrossRef\]](#) [\[PubMed\]](#)
34. Ussar, S.; Griffin, N.W.; Bezy, O.; Fujisaka, S.; Vienberg, S.; Softic, S.; Deng, L.; Bry, L.; Gordon, J.I.; Kahn, C.R. Interactions between gut microbiota, host genetics and diet modulate the predisposition to obesity and metabolic syndrome. *Cell Metab.* **2015**, *22*, 516–530. [\[CrossRef\]](#) [\[PubMed\]](#)
35. Asgharpour, A.; Cazanave, S.C.; Pacana, T.; Seneshaw, M.; Vincent, R.; Banini, B.A.; Kumar, D.P.; Daita, K.; Min, H.K.; Mirshahi, F.; et al. A diet-induced animal model of non-alcoholic fatty liver disease and hepatocellular cancer. *J. Hepatol.* **2016**, *65*, 579–588. [\[CrossRef\]](#)
36. Sabidó, E.; Wu, Y.; Bautista, L.; Porstmann, T.; Chang, C.Y.; Vitek, O.; Stoffel, M.; Aebersold, R. Targeted proteomics reveals strain-specific changes in the mouse insulin and central metabolic pathways after a sustained high-fat diet. *Mol. Syst. Biol.* **2013**, *9*, 681. [\[CrossRef\]](#)
37. Hirschey, M.D.; Shimazu, T.; Goetzman, E.; Jing, E.; Schwer, B.; Lombard, D.B.; Grueter, C.A.; Harris, C.; Biddinger, S.; Ilkayeva, O.R.; et al. SIRT3 regulates mitochondrial fatty-acid oxidation by reversible enzyme deacetylation. *Nature* **2010**, *464*, 121–125. [\[CrossRef\]](#)

38. Flowers, M.T.; Ntambi, J.M. Role of stearoyl-coenzyme A desaturase in regulating lipid metabolism. *Curr. Opin. Lipidol.* **2008**, *19*, 248–256. [[CrossRef](#)]
39. Vijayakumar, R.S.; Lin, Y.; Shia, K.-S.; Yeh, Y.-N.; Hsieh, W.-P.; Hsiao, W.-C.; Chang, C.-P.; Chao, Y.-S.; Hung, M.-S. Induction of fatty acid oxidation resists weight gain, ameliorates hepatic steatosis and reduces cardiometabolic risk factors. *Int. J. Obes.* **2012**, *36*, 999–1006. [[CrossRef](#)]
40. Heine, P.A.; Taylor, J.A.; Iwamoto, G.A.; Lubahn, D.B.; Cooke, P.S. Increased adipose tissue in male and female estrogen receptor- α knockout mice. *Proc. Natl. Acad. Sci. USA* **2000**, *97*, 12729–12734. [[CrossRef](#)]
41. Leeners, B.; Geary, N.; Tobler, P.N.; Asarian, L. Ovarian hormones and obesity. *Hum. Reprod. Update* **2017**, *23*, 300–321. [[CrossRef](#)]
42. Cruz, M.M.; Lopes, A.B.; Crisma, A.R.; de Sá, R.C.C.; Kuwabara, W.M.T.; Curi, R.; de Andrade, P.B.M.; Alonso-Vale, M.I.C. Palmitoleic acid (16:1n7) increases oxygen consumption, fatty acid oxidation and ATP content in white adipocytes. *Lipids Health Dis.* **2018**, *17*, 55. [[CrossRef](#)]
43. Demarquoy, J.; Le Borgne, F. Crosstalk between mitochondria and peroxisomes. *World J. Biol. Chem.* **2015**, *6*, 301–309. [[CrossRef](#)]
44. Abdelmegeed, M.A.; Banerjee, A.; Yoo, S.H.; Jang, S.; Gonzalez, F.J.; Song, B.J. Critical role of cytochrome P450 2E1 (CYP2E1) in the development of high fat-induced non-alcoholic steatohepatitis. *J. Hepatol.* **2012**, *57*, 860–866. [[CrossRef](#)] [[PubMed](#)]
45. Nan, Y.; Wang, R.; Zhao, S.; Han, F.; Wu, W.J.; Kong, L.; Fu, N.; Kong, L.; Yu, J. Heme oxygenase-1 prevents non-alcoholic steatohepatitis through suppressing hepatocyte apoptosis in mice. *Lipids Health Dis.* **2010**, *9*, 124. [[CrossRef](#)] [[PubMed](#)]
46. Zhang, X.; Li, S.; Zhou, Y.; Su, W.; Ruan, X.; Wang, B.; Zheng, F.; Warner, M.; Gustafsson, J.Å.; Guan, Y. Ablation of cytochrome P450 omega-hydroxylase 4A14 gene attenuates hepatic steatosis and fibrosis. *Proc. Natl. Acad. Sci. USA* **2017**, *114*, 3181–3185. [[CrossRef](#)] [[PubMed](#)]
47. Leung, T.M.; Nieto, N. CYP2E1 and oxidant stress in alcoholic and non-alcoholic fatty liver disease. *J. Hepatol.* **2013**, *58*, 395–398. [[CrossRef](#)]
48. Duarte, J.A.G.; Carvalho, F.; Pearson, M.; Horton, J.D.; Browning, J.D.; Jones, J.G.; Burgess, S.C. A high-fat diet suppresses de novo lipogenesis and desaturation but not elongation and triglyceride synthesis in mice. *J. Lipid Res.* **2014**, *55*, 2541–2553. [[CrossRef](#)] [[PubMed](#)]
49. Cui, J.; Shen, Y.; Li, R. Estrogen synthesis and signaling pathways during aging: From periphery to brain. *Trends Mol. Med.* **2013**, *19*, 197–209. [[CrossRef](#)]
50. Mačak Šafranko, Ž.; Sobočanec, S.; Šarić, A.; Jajčanin-Jozić, N.; Krsnik, Ž.; Aralica, G.; Balog, T.; Abramić, M.; Šafranko, Ž.M.; Sobočanec, S.; et al. The effect of 17 β -estradiol on the expression of dipeptidyl peptidase III and heme oxygenase 1 in liver of CBA/H mice. *J. Endocrinol. Invest.* **2015**, *38*, 471–479. [[CrossRef](#)]
51. Ways, P.; Hanahan, D.J. Characterization and quantification of red cell lipids in normal man. *J. Lipid Res.* **1964**, *5*, 318–328. [[CrossRef](#)]
52. Bujak, M.; Bujak, I.T.; Sobočanec, S.; Mihalj, M.; Novak, S.; Cosić, A.; Levak, M.T.; Kopačin, V.; Mihaljević, B.; Balog, T.; et al. Trefoil Factor 3 Deficiency Affects Liver Lipid Metabolism. *Cell. Physiol. Biochem.* **2018**, *47*, 827–841. [[CrossRef](#)]
53. Mihaljević, B.; Katušin-Ražem, B.; Ražem, D. The reevaluation of the ferric thiocyanate assay for lipid hydroperoxides with special considerations of the mechanistic aspects of the response. *Free Radic. Biol. Med.* **1996**, *21*, 53–63. [[CrossRef](#)]
54. Aebi, H. Catalase in vitro. *Methods Enzymol.* **1984**, *105*, 121–126. [[PubMed](#)]

Supplementary material

Chronic High Fat Diet Intake Impairs Hepatic Metabolic Parameters in Ovariectomized Sirt3 KO Mice

Marija Pinterić ^{1†}, Iva I. Podgorski ^{1†}, Marijana Popović Hadžija ¹, Ivana Tartaro Bujak ², Ana Tadijan ¹, Tihomir Balog ¹, Sandra Sobočanec ^{1*}

¹ Division of Molecular Medicine, Ruđer Bošković Institute, 10000 Zagreb, Croatia

² Division of Materials Chemistry, Ruđer Bošković Institute, 10000 Zagreb, Croatia

[†] Equal contribution

*Correspondence: ssoboc@irb.hr; tel.+385-1-4561-172

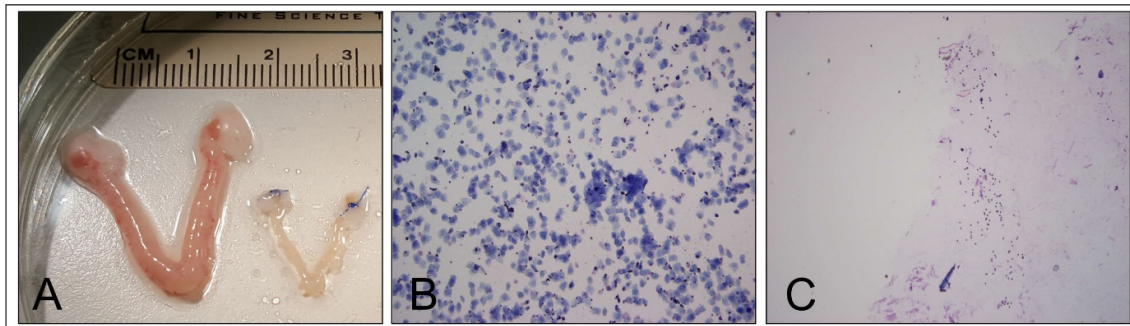


Figure S1. Observations of uterus deterioration and vaginal smears of control (sham) and ovariectomized (ovx) mice. **(A)** The uteri of sham and ovx mice. Vaginal smears from sham **(B)** and ovx **(C)** mice.

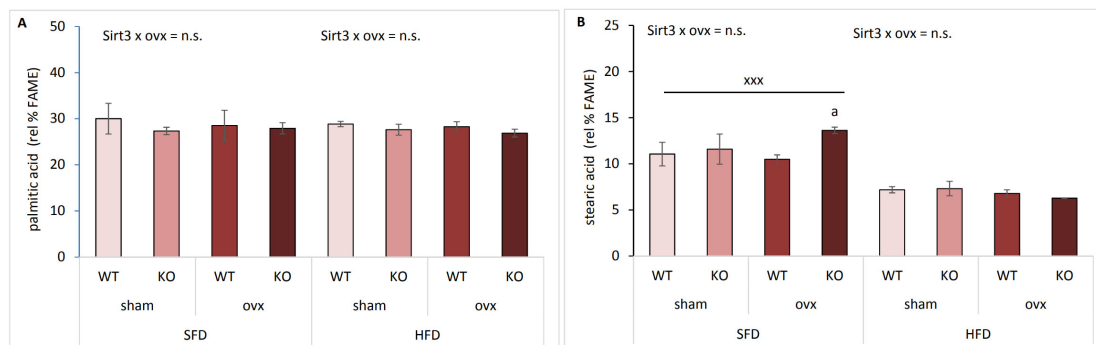


Figure S2. Graphical display of hepatic SFA content in sham and ovx Sirt3 WT and KO mice after 10 weeks of feeding with SFD or HFD. **(A) Palmitic acid.** SFD: no changes. HFD: no changes. SFD vs. HFD: no changes. **(B) Stearic acid.** SFD: ovx WT vs. KO ($^ap < 0.001$). HFD: no changes. SFD vs. HFD: $^{xxx}p < 0.001$. Data are shown as mean \pm SD. N=4 mice per group.

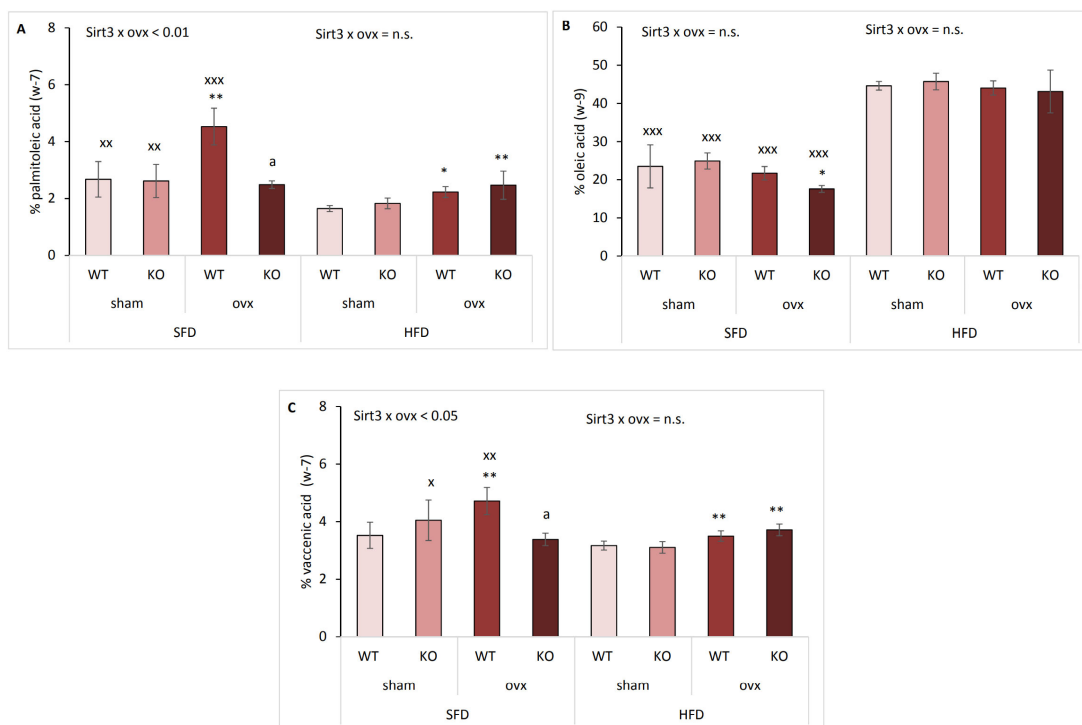


Figure S3. Graphical display of hepatic MUFA content in sham and ovx Sirt3 WT and KO mice after 10 weeks of feeding with SFD or HFD. **(A) Palmitoleic acid.** SFD: ovx WT vs. KO ($^ap<0.01$); WT sham vs. ovx ($^{**}p<0.01$). HFD: WT ovx vs. sham ($^*p<0.05$); KO ovx vs. sham ($^{**}p<0.01$). SFD vs. HFD: sham ($^{xx}p<0.01$); WT ovx ($^{xxx}p<0.001$). **(B) Oleic acid.** SFD: KO ovx vs. sham ($^*p<0.05$). HFD: no changes. SFD vs. HFD: $^{xxx}p<0.001$. **(C) Vaccenic acid.** SFD: ovx WT vs. KO ($^ap<0.01$); WT sham vs. ovx ($^{**}p<0.01$). HFD: ovx vs. sham ($^{**}p<0.01$). SFD vs. HFD: KO sham ($^x p<0.05$); WT ovx ($^{xx}p<0.01$). Data are shown as mean \pm SD. N=4 mice per group.

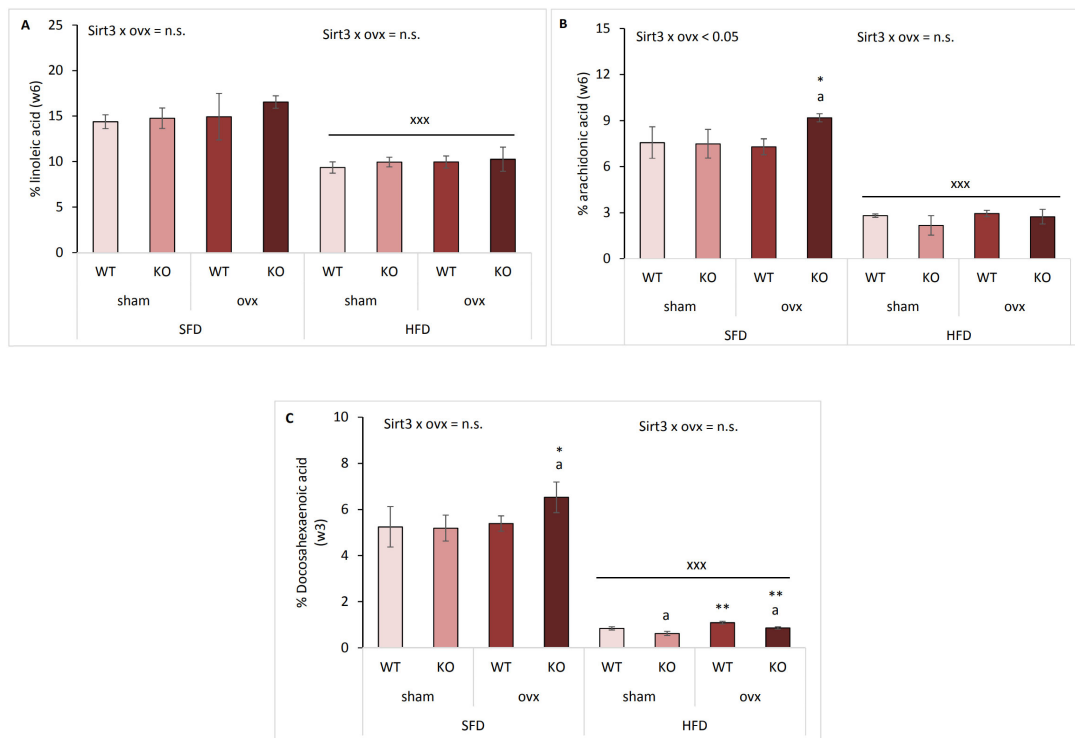


Figure S4. Graphical display of hepatic PUFA content in sham and ovx Sirt3 WT and KO mice after 10 weeks of feeding with SFD or HFD. **(A) Linoleic acid.** SFD: no changes. HFD: no changes. SFD vs. HFD: $^{xxx}p<0.001$. **(B) Arachidonic acid.** SFD: ovx WT vs. KO ($^ap<0.01$); KO sham

vs. ovx (* $p<0.05$). HFD: no changes. SFD vs. HFD: ^{xxx} $p<0.001$. **(C) Docosahexaenoic acid.** SFD: KO sham vs. ovx (* $p<0.05$); ovx WT vs. KO (^a $p<0.05$). HFD: KO vs. WT (^a $p<0.05$); ovx vs. sham (** $p<0.01$). SFD vs. HFD: ^{xxx} $p<0.001$. Data are shown as mean \pm SD. N=4 mice per group.

Table S1. Assays (Taqman® Applied Biosystems, UK) used for the real time quantitative PCR analyses

Gene	Assay ID	Product size (bp)
<i>β-actin</i>	Mm00607939_s1	115
<i>sirt3</i>	Mm00452131_m1	68
<i>cyp2e1</i>	Mm00491127_m1	83
<i>cyp4a14</i>	Mm00484132_m1	71
<i>ppara</i>	Mm00627559_m1	86
<i>pgc1α</i>	Mm00447183_m1	104
<i>ho-1</i>	Mm00516007_m1	92

Table S2. Antibodies used in this study for the Western blot analyses

Antibody	Dilution	Host	Manufacturer
Sirt3 (D22A3)	1:1000	Rabbit	Cell Signaling Technology, USA
Anti-rabbit (NA934)	1:5000	Goat	GE Healthcare, USA